PHOTOPHYSICAL BEHAVIOUR OF SOME MOLECULAR SYSTEMS AND A PROTEIN IN DEEP EUTECTIC SOLVENTS

A Thesis Submitted for the Degree of

DOCTOR OF PHILOSOPHY

by

Sk Saddam Hossain

School of Chemistry

University of Hyderabad

(P.O.) Central University, Gachibowli

Hyderabad- 500 046, India

December 2020

PHOTOPHYSICAL BEHAVIOUR OF SOME MOLECULAR SYSTEMS AND A PROTEIN IN DEEP EUTECTIC SOLVENTS

A Thesis Submitted for the Degree of

Doctor of Philosophy

by

Sk Saddam Hossain

School of Chemistry
University of Hyderabad
Hyderabad – 500 046
INDIA

December 2020

Dedicated

to

my 'Amma' & 'Abba'

"Learning never exhausts the mind"

Leonardo Da Vinci (1452-1519)

"A positive mind finds opportunity in everything"

A. P. J. Abdul Kalam (1931-2015)

Contents

Declaration

I, **Sk Saddam Hossain,** hereby declare that the matter embodied in the thesis entitled ***"Photophysical Behaviour of Some Molecular Systems and a Protein in Deep Eutectic Solvents"*** is the result of investigations carried out by me in the School of Chemistry, University of Hyderabad, India under the supervision of **Professor Anunay Samanta.**

In keeping with the general practice of reporting scientific investigations, the acknowledgements have been made wherever the work described is based on the findings of other investigators. Any omission or error that might have crept in is regretted.

Afsani
18/12/2020

Sk Saddam Hossain

University of Hyderabad
India
December 2020

UNIVERSITY OF HYDERABAD
HYDERABAD-500 046, INDIA

Phone: (work) +91 40 2313 4813, +91 40 2301 2341
(lab): +91 40 2313 4913
Fax: +91 40 2301 1594
Email: anunay@uohyd.ac.in OR anunay.samanta@gmail.com
URL: http://chemistry.uohyd.ac.in/~as/

Professor Anunay Samanta
School of Chemistry

Certificate

This is to certify that the thesis entitled ***"Photophysical Behaviour of Some Molecular Systems and a Protein in Deep Eutectic Solvents"*** submitted by **Mr. Sk Saddam Hossain** bearing the registration number 15CHPH04 in partial fulfilment of the requirements for the award of Doctor of Philosophy (Ph.D.) in the School of Chemistry, University of Hyderabad, India under my supervision and guidance. This thesis is free from plagiarism and has not been submitted previously in part or full to this or other University/Institution for any degree or diploma. Further, the student has following publications before submission of the thesis for adjudication and has produced evidences for the same in the form of reprints.

Parts of the thesis have been published in the following publications:

1. **S. S. Hossain** and A. Samanta, Solute Rotation and Translation Dynamics in an Ionic Deep Eutectic Solvent Based on Choline Chloride. *J. Phys. Chem. B,* **2017**, 121, 10556-10565. **(*Chapter 3*)**

2. **S. S. Hossain** and A. Samanta, How Do the Hydrocarbon Chain Length and Hydroxyl Group Position Influence the Solute Dynamics in Alcohol-Based Deep Eutectic Solvents? *Phys. Chem. Chem. Phys.,* **2018**, 20, 24613-24622. **(*Chapter 4*)**

3. **S. S. Hossain**, S. Paul and A. Samanta, Liquid Structure and Dynamics of Tetraalkylammonium Bromide-Based Deep Eutectic Solvents: Effect of Cation Chain Length. *J. Phys. Chem. B,* **2019**, 123, 6842-6850. **(*Chapter 5*)**

4. **S. S. Hossain**, S. Paul and A. Samanta, Complete Solvation Dynamics of Coumarin 153 in Tetraalkylammonium Bromide-Based Deep Eutectic Solvents. *J. Phys. Chem. B,* **2020**, 124, 12, 2473-2481. **(*Chapter 6*)**

5. **S. S. Hossain**, S. Paul and A. Samanta, Structural Stability and Conformational Dynamics of Cytochrome c in Deep Eutectic Solvents. ***(To be communicated)*** **(*Chapter 7*)**

The student has made presentation in the following conferences:

1. "Conventional and Single-Molecule Fluorescence Studies of Neutral and Charged Solutes in Choline Chloride Based Deep Eutectic Solvents", **Newton Bhabha Researcher Links Workshop (NMSB-2017),** IISER-Kolkata, India, December14-16, 2017. **(Poster *Presentation*)**

2. "Solute Rotation and Translation Dynamics in an Ionic Deep Eutectic Solvent Based on Choline Chloride", **14thTrombay Symposium on Radiation and Photochemistry (TSRP-2018),** BARC-Mumbai, India, January 03-07, 2018. **(Poster *Presentation*)**

3. "Effect of Hydrocarbon Chain Length and Hydroxyl Group Positioning at Hydrogen Bond Donor on the Rotational and Translational Dynamics of Solutes in Alcohol-Based Deep Eutectic Solvents", **15thAnnual In-House Symposium of the School of Chemistry (Chemfest-2018),** University of Hyderabad, Hyderabad, India, March 09-10, 2018. **(Poster *Presentation*)**

4. "Exploring the Liquid Structure and Dynamics of Alcohol-Based Deep Eutectic Solvents Using Ensemble and Single-Molecule Studies", **National Conference on Emerging trends in Chemical Sciences (ETCS-2019),** Aligarh Muslim University, Aligarh, India, February 23-24, 2019. **(*Oral Presentation*)**

5. "Effect of Deep Eutectic Solvents on the Structural Stability and Conformational Dynamics of a Protein", **National Workshop on Fluorescence and Raman Spectroscopy (FCS-2019),** TIFR-Hyderabad, Hyderabad, India, December 16-21, 2019. **(Poster *Presentation*)**

6. "Microscopic Structure and Dynamics of Ionic Deep Eutectic Solvents as Revealed by Single-Molecule and Ultrafast Fluorescence Techniques", **17thAnnual In-House Symposium of the School of Chemistry (Chemfest-2020),** University of Hyderabad, Hyderabad, India, February 27-28, 2020. **(*Oral Presentation*)**

The student has passed the following courses towards the fulfilment of the coursework requirement for Ph.D. degree:

Sl. No.	Course Code	Title	Credits	Status
1	CY801	Research Proposal	3	Pass
2	CY805	Instrumental Method-A	3	Pass
3	CY806	Instrumental Method-B	3	Pass
4	CY453	Molecular Spectroscopy	4	Pass

Anunay Samanta

Thesis Supervisor

PROF. ANUNAY SAMANTA
SCHOOL OF CHEMISTRY
UNIVERSITY OF HYDERABAD
HYDERABAD - 500 046

Dean 18.12.2020

School of Chemistry
University of Hyderabad

Dear
School of Chemistry
University of Hyderabad
Hyderabad 500 046

Acknowledgements

It is a pleasant task to express my thanks to all those who contributed in many ways to made this thesis possible.

It gives me immense pleasure and satisfaction to express my heartfelt and sincere gratitude to Sir, Prof. Anunay Samanta, for his continuous cooperation, encouragement and kind guidance. I am highly indebted to him for giving me the opportunity to work under his supervision and for providing complete freedom to express my thoughts and explore the area I wanted. Since the day I joined at the School of Chemistry (SoC), he has not only been my research guide, but also a guardian who has always been quite helpful to me in both academic and personal fronts. My special thanks are also to Sonali mam, Ani da and Boni for their close association with me which made me feel comfortable like home.

Financial support from the Department of Science and Technology (DST) and research fellowship (JRF & SFR) from the University Grant Commission (UGC), New Delhi, India is greatly acknowledged.

I extend my thanks to the former and present Dean(s), SoC, for their constant support, cooperation and providing the available facilities. I sincerely take the opportunity to thank my doctoral committee members, Prof. Samar K Das and Prof. Samudranil Pal for their valuable suggestions and encouragement at various stages of the PhD journey. I am extremely thankful to all the faculty members of the school for their timely help and encouragement, especially for interesting courses they taught me as a part of the course work.

I thank all the non-teaching staff of the SoC for being very helpful and supportive, Mr. Durga Prasad, Mr. Mahender, Mr. Abraham and Mr. Anandam in particular.

I would like to acknowledge Radhika, Shiva, Srinivas, and Naresh for their help in various occasions. They had all been quite amazing.

I am thankful to all my colleagues in the SoC for helping me time-to-time both academically and personally. I particularly thank Sarada, Ramesh and Ankit for their valuable help in different times. I also value my association with Akram, Junaid bhai, Irfan, Saukat bhai, Ishfaq, Surya anna, Anil anna and Satish anna.

I express thanks to my collaborators for the fruitful collaborative work which taught me many interesting aspects different from my research.

I would like to thank Dr. Maqbool Ahmed and Mr. Rajesh from Central Instrumental Laboratory, University of Hyderabad (UoH) for their assistance and cooperation during various experiments.

I value my association with my former lab seniors, Soujanya mam, Satyen da, Prasun da, Moloy da, Ravi anna, Dinesh da, Satyajit da and Soumya akka, and thank them for their valuable suggestions and discussion. My life inside the lab has always been an unforgettable journey with my colleagues, who have always been very much kind to me. I am grateful to have the opportunity to work with such talented people. I have enjoyed a lot working with each one of them. I sincerely thank my former lab-mates Shalini di, Ashok anna, Chandu anna, Navendu da, Sudipta da, Sneha di and Alila from whom I have learned many valuable aspects of research either through fruitful scientific discussions in group meeting or in various other occasions. I am extremely thankful to Shalini di with whom I started working for the first time in the lab. My special thanks go in particular to Sneha di, Navendu da and Sudipta da for their kind help in learning instruments. I sincerely acknowledge my present lab-mates Apurba, Tasnim, Somnath, Sumanta, Rajesh and Ramavath anna for maintaining a friendly, cheerful and cooperative atmosphere in the lab. I am extremely thankful to Sneha di, Apurba and Tasnim for clearing my doubts either on chemistry or far beyond that. I thank Apurba and Somnath for not only helping me academically but also whenever I needed. I offer my heartfelt thanks to all of them for tolerating me for last 5 years. I would also like to thank my project student, Prajit, who helped me in my research by asking many interesting question.

Since the day I joined UoH, I have been blessed with many caring and affectionate Bengali friends. I would like to express my sincere thanks to all my seniors; Santanu da, Arpita di, Rudra da, Sugata da, Suman da, Sajjad da, Abu Saleh da, Intaj da, Raja da, Arif da, Mahmud da, Kaushik da, Debparna di, Olivia di, Arpita di (from Chemistry), Subha da, Pati da, Sunanda di, Moumita di, Rahamat da, Hasan da, Kallol da and Sabari di. I will cherish each and every moments I have spent with them throughout my life. I am very much thankful to all my junior friends, Subham, Soutrick, Suman, Tausif, Liton, Sarada, Anupam, Mujahid, Nilanjan, Olivia, Debika, Sokina, Alam, Mainul, Debu, Pabitra, Joydev, Nasir and many others, with whom I have shared many unforgettable moments in this campus.

I am quite thankful to my dear friends, Apurba, Bappa, Arijit and Kuntal, with whom I have spent lots of memorable moments and whose company I have enjoyed always.

I value my close association with some good friends from the NRS hostel (D & F-wings) which includes Golu, Raj bhai, Prashant ji, Kailash, Kali da, Dhirendra and Dilip.

I am extremely thankful to Alim, Ankit, Hafijur and Taher. Without their cheerful company, the campus life would have been really boring with full of difficulties. Ailm is more than a friend to me; his love and care for me is not less than a family member. It's very difficult to get a friend like him. Very Special thanks to Hafijur bhai for making delicious food every Sunday and for giving me company in various occasions. I am grateful to Ankit for always offering me helping hands in my ups and downs.

I thank all 2015 batch-mates from SoC, in particular Senthil, Venky, Shankar, Tanmay, Basha, Arun, Ramesh, Harilal, Mou, Sameeta, Sipra, Sandeep, Anif, Manish, Manzoor, Chandni and Joycy, for their support and care.

During my stay at various hostels for more than 12 years, I met some amazing people: Gulfishan bhai, Alam, Irshad bhai, Ankit and Mahi. I had spent a wonderful time with them. I am really lucky to have had them as my room-mates.

I really don't know how to describe what I got from 'Aligarh Muslim University'. This place was and will always remain very close to my heart. I still enjoy the happy moments and unforgettable memories that I had with my Alig-friends. I sincerely thank my batch-mates, Rabiul, Mefta, Nirshad, Aslam, Akhi, Zulfikar, Wasikul, Bittu, Selim, Atiur, Aminul, Sahid, Ishrat, Nazia, Zeenat, Kanchan, Sakil, Munna, Ishtiyak, Yousuf along with my seniors, Samima apa, Tahasin da, Shamim da, Ifthekar da, Ashraful da, Saigal da, Ejaj da, Rauf da, Ismail da, Sahabuddin da, Musheer da (from UP), Sabbir da (MM hall), Mushir da and juniors, Sabir, Javed, Wahid, Mafizur, Kamal, Milon, Badsah and many more for encouraging me to do better and better always. I must acknowledge my two 'Alig Musketeers', Alim and Riyaz, for the valued friendship they offered and still maintained. I will cherish the time I spent there, throughout my life.

Thanks are also to my friends from 'Al-Ameen Mission', Shahjahan, Iqbal, Minaruddin, Sayeed and Sakib for making me feel happy whenever we met.

Friends from 'Mahachanda Vivekananda Siksha Pratisthan', particularly Saheli, Raj, Tanmay, Arindam, Arghya, Makhon, Chandrani, Keya, Banani, Monsura, Sultan, Ratan, Giyas, Bappa, Mujaffar, Habiba, Asmina, Riya, Fultusi, Anubha, Pravat and many more deserve a very warm acknowledge for sharing very crucial years with me and being with me afterwards. I always go nostalgic remembering those beautiful days of my life.

I might not forget my childhood buddies; Saiful, Saifuddin, Reshma, Sagar and Mujibur. I am very much fortunate to have had them in my life, who always stood by my side in my difficult times.

I express my heartfelt thanks to Fatema apa, Rabi bhai, Hela kaka, Makhon kaka, Amanullah sir, Kabita apa, Hafijul bhai and Basir bhai for their good wishes and blessings.

I am extremely grateful to all my gurus (teachers) who taught me ever since I started speaking for the first time. I would like to acknowledge the valuable contribution of all my gurus that I got at different stages of my life: Jibinnesa di, Milon da, Biman sir, Debashish sir, Sushanta sir, Ramkrishna sir, Surajit sir, Dadu, Subrata babu, Naren babu, Nihar babu, Ghoshal babu, Ashish sir(Math), Ashish sir (Chemistry), Pushpendu sir, Partha sir, Besra sir, Ajay sir, Sarbessar sir, Anima mam, Sudeshna mam, Sajal sir, Garai sir, Nurul sir (Secretary of AAM), Azijul sir, Hasibul sir, Sofikul sir, Rafikul sir, Monirul sir, Ashraf sir, Aminul sir, Suhail Sabir sir, Riyajuddin sir, Shakir sir, Musawwer sir, Jigyanshu bhai and Azam bhai. It is indeed their selfless help, lessons, encouragements, dedication and hard work which actually made my path easier over the years. I cannot thank enough Debashish sir for his unconditional love, care and support for me.

I would have not reached at this stage of life without the never ending support, love and contribution of my mother, father, brother (Firoj) and sister (Firdousi). They have always been source of tireless motivation and inspiration for me. The endless struggle, sacrifices and effort of my parents and brother to my journey can never be express in words. I owe everything to them. I am blessed with two very special people in my life, my sister-in-law (Rimpa) and sweetest nephew (Farhan), without them life would have been so color-less. I would like to thank all my relatives for their valuable support, love and encouragement since my childhood. I am very much grateful to my mejo mama (Ansar) and Taher mama for their special care and love for me. I also express sincere thanks to my father-in-law, mother-in-law and Sunny, Priyanka di, Samol da, Nahid, Alisha, Ehan and Insiya for their love and support.

It's extremely difficult to forget the love of my life, Kamrunnesa (my wife and a good friend). She is very special to me. I am highly grateful to her for the amount of unparalled love, support and patience she has offered me. Very special thanks to her for being an important part of my life.

I sincerely apologize if I forget to mention your name. I honestly want to thank all the people who have been directly or indirectly played a role in my life, yes, I really mean it.

Thanks a lot to each and all once again!!!

Saddam

List of Publications

Publications included in the thesis:

1. **S. S. Hossain** and A. Samanta, Solute Rotation and Translation Dynamics in an Ionic Deep Eutectic Solvent Based on Choline Chloride. ***J. Phys. Chem. B,*** **2017**, 121, 10556-10565. **(Chapter 3)**

2. **S. S. Hossain** and A. Samanta, How Do the Hydrocarbon Chain Length and Hydroxyl Group Position Influence the Solute Dynamics in Alcohol-Based Deep Eutectic Solvents? ***Phys. Chem. Chem. Phys.,*** **2018**, 20, 24613-24622. **(Chapter 4)**

3. **S. S. Hossain**, S. Paul and A. Samanta, Liquid Structure and Dynamics of Tetraalkylammonium Bromide-Based Deep Eutectic Solvents: Effect of Cation Chain Length. ***J. Phys. Chem. B,*** **2019**, 123, 6842-6850. **(Chapter 5)**

4. **S. S. Hossain**, S. Paul and A. Samanta, Complete Solvation Dynamics of Coumarin 153 in Tetraalkylammonium Bromide-Based Deep Eutectic Solvents. ***J. Phys. Chem. B,*** **2020**, 124, 12, 2473-2481. **(Chapter 6)**

5. **S. S. Hossain**, S. Paul and A. Samanta, Structural Stability and Conformational Dynamics of Cytochrome c in Deep Eutectic Solvents. ***(To be communicated)*** **(Chapter 7)**

Other Publications:

6. M. C. Sekhar, A. De, **S. S. Hossain** and A. Samanta, Roles of the Methyl and Methylene Groups of Mercapto Acids in the Photoluminescence Efficiency and Carrier Trapping Dynamics of CdTe QDs. ***Phys. Chem. Chem. Phys.,*** 2017, 19, 1536-1542.

7. S. Paul, **S. S. Hossain**, B. M. Divya and A. Samanta, Interactions between a Bioflavonoid and c-MYC Promoter G-Quadruplex DNA: Ensemble and Single-Molecule Investigations. ***J. Phys. Chem. B,*** 2019, 123, 2022-2031.

8. T. S. Mahapatra, A. Dey, H. Singh, **S. S. Hossain**, A. K. Mandal and A. Das, Two-Dimensional Lanthanide Coordination Polymer Nanosheets for Detection of FOX-7. ***Chem. Sci.*****,** 2020, 11, 1032-1042.

9. S. Paul, **S. S. Hossain** and A. Samanta, Insights into the Folding Pathway of a c-MYC Promoter Based i-Motif DNA in Crowded Environments at the Single-Molecule Level. ***J. Phys. Chem. B,*** 2020, 124, 5, 763-770.

10. A. Uddin, B. Roy, G. P. Jose, **S. S. Hossain** and P. Hazra, Sensing and Modulation of Amyloid Fibrils by Photo-Switchable Organic Dots. ***Nanoscale***, 2020, 12, 16805-16818.

11. S. Bhattacharya, G. Reddy, S. Paul, **S. S. Hossain**, S. S. K. Raavi, L. Giribabu, A. Samanta and V. R. Soma, Comparative Photophysical and Femtosecond Third-Order Nonlinear Optical Properties of Novel Imidazole Substituted Metal Phthalocyanines. ***Dyes Pigm***, 2021, 184, 108791-15.

12. A. Verma, **S. S. Hossain**, S. Sunkari, J. Reibenspies and S. Saha, Ligand Influence versus Electronic Configuration of d-Metal Ion in Determining the Fate of NIR Emission from LnIII Ions: A Case Study with CuII, NiII and ZnII Complexes. ***New J Chem. (Just accepted)***

List of Conference Presentations

Oral Presentations:

1. "Exploring the Liquid Structure and Dynamics of Alcohol-Based Deep Eutectic Solvents Using Ensemble and Single-Molecule Studies", ***National Conference on Emerging trends in Chemical Sciences (ETCS-2019),*** Aligarh Muslim University, Aligarh, India, February 23-24, 2019.

2. "Microscopic Structure and Dynamics of Ionic Deep Eutectic Solvents as Revealed by Single-Molecule and Ultrafast Fluorescence Techniques", ***17th Annual In-House Symposium of the School of Chemistry (Chemfest-2020),*** University of Hyderabad, Hyderabad, India, February 27-28, 2020.

Poster Presentations:

1. "Conventional and Single-Molecule Fluorescence Studies of Neutral and Charged Solutes in Choline Chloride Based Deep Eutectic Solvents", ***Newton Bhabha Researcher Links Workshop (NMSB-2017),*** IISER-Kolkata, India, December14-16, 2017.

2. "Solute Rotation and Translation Dynamics in an Ionic Deep Eutectic Solvent Based on Choline Chloride", ***14th Trombay Symposium on Radiation and Photochemistry (TSRP-2018),*** BARC-Mumbai, India, January 03-07, 2018.

3. "Effect of Hydrocarbon Chain Length and Hydroxyl Group Positioning at Hydrogen Bond Donor on the Rotational and Translational Dynamics of

Solutes in Alcohol-Based Deep Eutectic Solvents", ***15th Annual In-House Symposium of the School of Chemistry (Chemfest-2018),*** University of Hyderabad, Hyderabad, India, March 09-10, 2018.

4. "Effect of Deep Eutectic Solvents on the Structural Stability and Conformational Dynamics of a Protein", ***National Workshop on Fluorescence and Raman Spectroscopy (FCS-2019),*** TIFR-Hyderabad, Hyderabad, India, December 16-21, 2019.

List of Abbreviations

2DIR	two-Dimensional infrared
4-AP	4-aminophthalimide
9-PA	9-phenylanthracene
A488	alexa488
ANF	2-amino-7-nitrofluorene
ANS	1-anilinonaphthalene-8-sulfonic acid
ANT	anthracene
BBO	β-barium borate
C153	coumarin 153
CCD	charge-couple device
CD	circular dichroism
CFD	constant fraction discriminator
CFM	confocal fluorescence microscope
ChCl	choline chloride
Cytc	cytochrome c
DMASBT	trans-2-[4-(dimethylamino) styryl]-benzothiazole
DNA	deoxyribonucleic acid
DNSC	dansyl chloride
DESs	deep eutectic solvents
EG	ethylene glycol
EMIC	ethyl-3-methylimidazolium chloride
FCS	fluorescence correlation spectroscopy
FITC	fluorescein isothiocyanate
FL	fluorescein
FTIR	Fourier transforms infrared
FWHM	full-width at half-maximum
GdHCl	guanidine hydrochloride
HBA	hydrogen bond acceptor

HBD	hydrogen bond donor
ICT	intramolecular charge transfer
ILs	ionic liquids
IRF	instrument response function
MCA	multi-channel analyzer
NLO	non-linear optical
NMR	nuclear magnetic resonance
PB	phosphate buffer
PD	photo diode
PET	photoinduced electron transfer
Phe	phenylalanine
PMT	photomultiplier tube
R123	rhodamine 123
SED	Stokes-Einstein-Debye
SPAD	single photon avalanche photodiode
TAC	time to amplitude convertor
TCSPC	time-correlated single-photon counting
TDFSS	time-dependent fluorescence Stokes shift
TBAB	tetrabutylammonium bromide
TEAB	tetraethylammonium bromide
TPAB	tetrapropylammonium bromide
TRES	time-resolved emission spectra
TNS	2-(p-toluidinyl) naphthalene-6-sulfonic acid
TRFA	time-resolved fluorescence anisotropy
Trp	tryptophan
TTTR	time-tagged time-resolved
Tyr	tyrosine
UPC	upconversion
UV-vis	ultraviolet-visible
VFT	Vogel-Fulcher-Tamman

Chapter-Wise Organization of the Thesis

The thesis has been divided into eight chapters.

Chapter 1 presents an introduction of DESs. Following this, a brief description of various photophysical studies performed in this work have been presented. Introduction is further extended to present a brief discussion on structures and dynamics of protein molecules and how these are studied using fluorescence spectroscopy. Finally the chapter is concluded with discussion of the motivation behind the present thesis work.

Chapter 2 provides the details of the materials, experimental procedure, instrumentation and various methodologies adopted in the present study.

Chapter 3 describes rotation and translation dynamics of differently charged solute molecules in a choline chloride-based ionic DES.

Chapter 4 discusses how the hydrocarbon chain length and hydroxyl group position on the hydrogen bond donor in alcohol-based DESs influence the solute dynamics.

Chapter 5 explores the effect of cation chain length on the liquid structure and dynamics of tetraalkylammonium bromide-based DESs.

Chapter 6 presents complete dynamics of solvation of coumarin 153 in a set of three tetraalkylammonium bromide-based DESs.

Chapter 7 explores the effect of two alcohol-based DESs on the structural stability and conformational dynamics of cytochrome c.

Chapter 8 summarizes the findings of the present investigations by pointing out the future scope of the further studies.

Chapter 1

Introduction

Overview

This chapter begins with an introduction on DESs, highlighting their types, physicochemical properties and applications in different fields. Following this, a brief description of various photophysical studies, such as solvation dynamics, rotational diffusion dynamics and translational diffusion dynamics exploiting the fluorescence behavior of suitable molecular systems, carried out for the work presented in this thesis, are provided. In the later part of the chapter, introductory remarks on the structures and dynamics of protein molecules are presented. This is followed by a description of how their structural stability and conformational dynamics are studied using fluorescence spectroscopy. The chapter is concluded by describing the motivation behind the work presented in this thesis.

1.1. Deep Eutectic Solvents

1.1.1. A Brief Introduction

Solvents play a very crucial role in almost all areas of chemistry.[1] Due to their increasing demand in academic laboratories and industries, huge amount of chemical substances is used as solvents in both physical and chemical processes. Most of these conventional solvents are volatile organic compounds. These common solvents cause undesirable negative impacts on both humans and the environment due to their high level of toxicity along with high volatility, especially when used in bulk scale for industrial purposes.[2-4] Therefore, a significant effort has been directed towards the design and development of less hazardous, environmentally benign alternatives to the conventional solvents, over the last few decades.[3-5] This has led to the realization of the importance of a number of alternatives, such as supercritical fluids and ILs, as the reaction media.

Among these, ILs have gained special attention due to their unique properties and number of advantages over conventional solvents, such as low vapor pressure, wide liquidous range, tunable properties, moderate to high polarity, high thermal and chemical stability, and non-flammable nature.[6-10] Another key advantage of ILs is that they can be designed for specific applications by different combinations of cations and anions, due to which ILs are considered as a class of "Designer Solvent".[11] Several ILs have been designed and synthesized for various applications in diverse fields. However, the potential of ILs in large-scale applications has not been realized as, in addition to the high cost of the raw materials, later developments have indicated considerable toxicity and poor biodegradability of many of these solvents.[12-14] To overcome these limitations, developments of greener, cheaper and sustainable solvent systems started. In this context, the concept of DESs was introduced at the beginning of this century by Abbott and coworkers.[15-17]

In recent years, DESs are widely considered as an emerging class of environment-friendly green alternative not only to common organic solvents, but also to the ILs in a variety of applications.[17-25] This is because most of the DESs offer many additional advantages over the conventional ILs, such as relatively inexpensive raw materials, ease of preparation with 100% atom-economy, often made of natural and biodegradable constituents along with important properties similar to the ILs.

DESs are generally composed of a mixture of Lewis or Bronsted-Lowry acids and bases which are capable of associating with each other.[19, 22] Mixing of two or more such components in a certain mole ratio forms a eutectic system which is a stable liquid with melting point lower than either of the individual pure constituents. DESs are most often liquid at temperatures below 373 K.[22] Figure 1.1 schematically illustrates a representative phase diagram of a two-component system with eutectic behavior. Extensive interspecies hydrogen-bonding interactions between Lewis base (anion or HBA) and a HBD moiety is mainly responsible for depression of freezing points of the mixtures. It is important to mention here that the DESs are different from ILs primarily due to two reasons;[22] first, unlike ILs, they are not formed from systems composed entirely of ionic species and second, they can also be obtained from only non-ionic species.

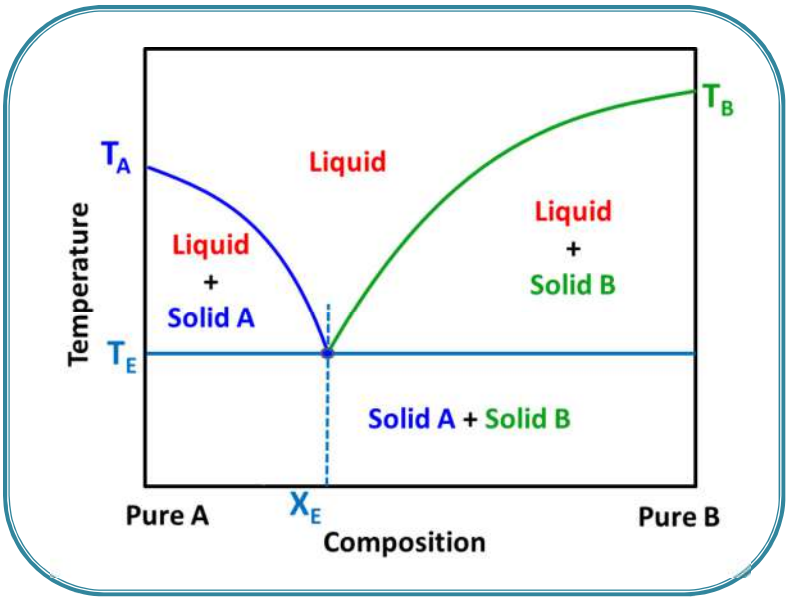

Figure 1.1. Schematic representation of phase diagram of a eutectic system of two components (A and B) with different melting points. T_A = melting point of pure A, T_B = melting point of pure B, T_E = melting point of mixture at eutectic composition (X_E).

A large number of DESs with desirable properties can be obtained by choosing appropriate starting components as well as by varying the stoichiometric molar ratio of the constituents.[19, 22] This flexibility allows convenient solvent engineering yielding a large number of DESs. This is why DESs are also termed as “Designer solvent”.

1.1.2. Classification

Since the report of the first DES (a mixture of metal chloride and quaternary ammonium salt) in 2001 by Abbott et al.[15] large numbers of DESs have been reported in the subsequent years.

DESs can generally be expressed by the following formula: Cat^+X^-zY.[22]

where, Cat^+ is the cation of any quaternary ammonium or phosphonium or sulfonium salt.

X^- is the Lewis base, generally a halide anion.

Y is the Bronsted-Lowry or Lewis acid and z represents the number of Y molecules.

Based on the nature of the complexing agents used for the formation of various DESs, they are classified into four types.[22, 26] A summary of the classification and their corresponding general formulae is presented in table 1.1.

Table 1.1. Classification of DESs in different categories along with their general formula.

Type	General formula	Terms
Type I	$Cat^+X^-zMCl_x$	M = Zn, In, Fe, Sn, Ga, Al, Ag
Type II	$Cat^+X^-zMCl_x \cdot yH_2O$	M = Cr, Ni, Co, Cu, Fe
Type III	Cat^+X^-zRP	P = COOH, $CONH_2$, OH
Type IV	$MCl_x + zRP$	M = Zn, Al and P = $CONH_2$, OH

Type I DESs are considered to be analogous to systems that contain imidazolium salts with metal halides. Examples of some type I DESs are chloroaluminate/imidazolium salt melt and mixtures of imidazolium salts like EMIC with various metal halides including AgCl, LiCl, $SnCl_2$, $ZnCl_2$, $FeCl_2$, $LaCl_3$ etc.

Type II DESs are slightly different from type I because they are associated with the hydrated metal halides instead of anhydrous metal halides. They are more popular than

type I because of larger availability and lower cost of hydrated metal halides as compared to nonhydrated ones used in the former.

Type III DESs are generally formed by mixing quaternary ammonium salts with various HBDs, such as amide, alcohol, amine, carboxylic acid, etc. This type of DESs is the most common due to the availability of a large number of HBDs. Their properties can easily be tuned for specific uses. They have been of major focus due to their ability to dissolve a wide range of transition metal species. The preparations of these DESs are quite simple and they are relatively unreactive with water.

Type IV DESs are those formed from metal halides and HBDs. Generally, inorganic cations do not form low melting eutectic solvents due to their high charge density. It has, however, been shown that the formation of type IV DESs is possible between metal halides and different HBDs with successful incorporation of transition metal salts ($ZnCl_2$) into DES by reacting with acetamide, urea, ethylene glycol, and hexanediol.[26]

In addition to those described above, some DESs are reported recently which do not belong to any of the above mentioned categories. For example, eutectic-based solvents which are composed of purely molecular constituents, such as mixture of acetamide and urea,[27] polyethylene glycol and acetamide,[28] *N*-methylacetamide/lauric acid mixture,[29] mixtures of acetamide and urea derivatives,[30] lauric acid/menthol mixture,[31] glycerol/lactic acid, and menthol/decanoic acid mixtures,[32] etc. Considering these, DESs can then be classified into two categories: ionic and non-ionic DESs. Ionic DESs can be formed by selecting one of the constituents as ionic, whereas in non-ionic DESs, both the constituents are non-ionic in nature.

However, among the aforementioned four classes of DESs, type III eutectic solvents, whose starting materials are readily available and are very easy to prepare and handle, has received considerable attention in the recent years for large-scale applications.[22] For the entire research presented in this thesis, we have worked specifically with only type III DESs. The structure of some halide salts and HBDs used for the preparation of various type III eutectic solvents are presented in Chart 1.1. Though, in principle, a large variety of DESs are possible to prepare simply by varying the combination of the constituents, most extensively studied ones are those consisting of a particular quaternary ammonium salt, (2-hydroxyethyl)trimethylammonium chloride, commonly known as choline chloride in combination with various HBDs like amine, amide, alcohol, carboxylic acid, etc.[19, 22]

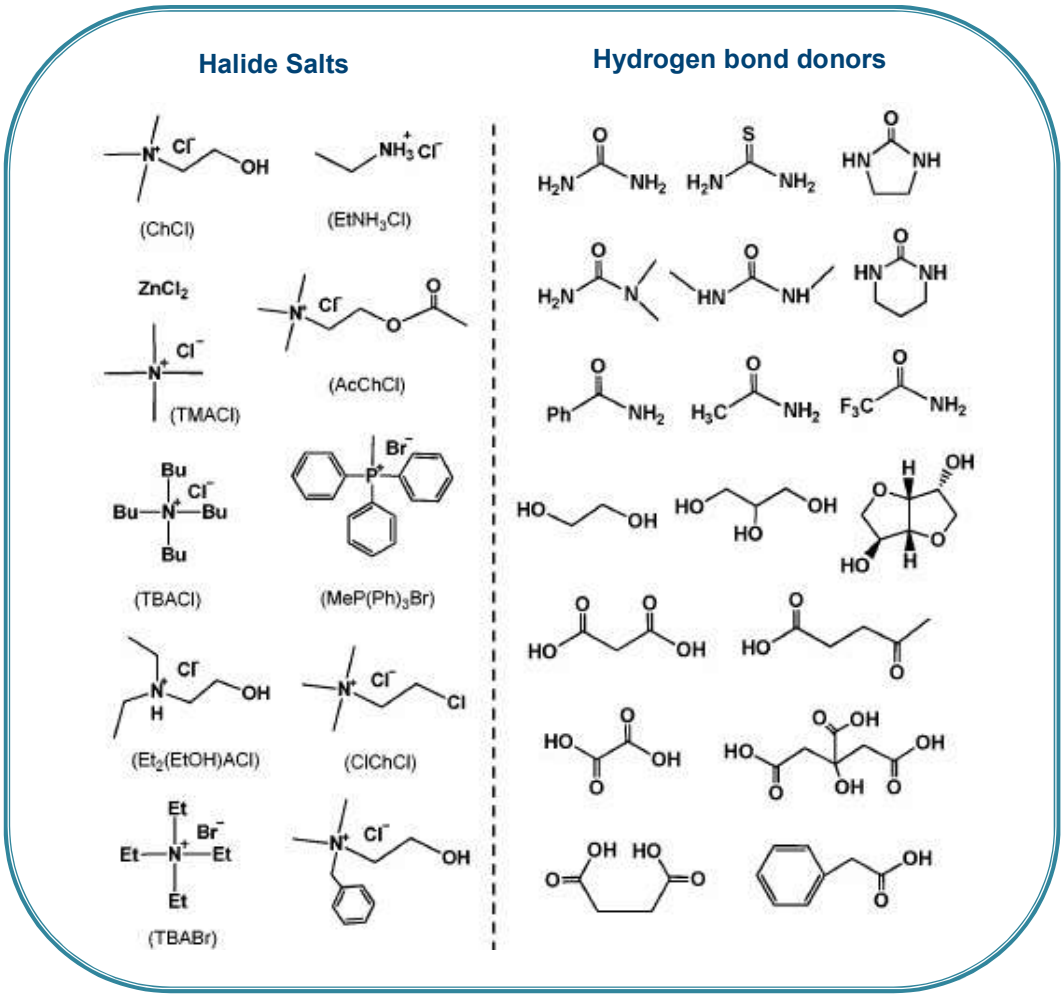

Chart 1.1. Structure of some common salts and HBDs used in the formation of type III DESs. (Adapted from reference 19)

1.1.3. Properties

DESs have gained considerable attention as unique novel media due to their various promising and attractive properties, such as negligible vapor pressure, often non-toxic, high thermal and chemical stability, wide liquidous range, moderate to high polarity, ability to dissolve both polar and nonpolar molecules, and many more.[19] As mentioned earlier, task-specific DESs with desirable physicochemical properties, such as freezing point, density, viscosity, conductivity and polarity, can easily be tailored by appropriate selection of the constituents as well as by varying their composition,[22] because the

properties of DESs are strongly dependent on the individual constituents. The key physicochemical properties of commonly available DESs are discussed below.

Freezing Point: Although most of the DESs reported till date have freezing point below 373 K, the number of DESs with freezing point below room temperature (298 K) is still very limited.[19, 22, 33] However, there are several examples for which the exact freezing point is very difficult to measure as they undergo glass formation, and hence show glass transition temperature.[33-37] Among those DESs whose freezing point is reported, it has been observed that the freezing point of different DESs varies widely with change of either of the constituents, though a clear correlation has not been observed. For instance, DESs composed of 1:2 molar mixtures of different ammonium salts and urea show very different freezing points ranging from 235 K to 386 K. Further, the molar ratio of a particular salt/HBD combination also significantly affects the freezing point of DESs. It has also been observed that even a small change in the structure of the DESs constituents (whether it is the anion/halide of the salt or the number of a particular functional group in HBD) has considerable impact on the freezing point of different DESs. For example, the freezing point of a set of choline salt-based DESs follows the order, $F^- > NO_3^- > Cl^- > BF_4^-$.[19] In another case, lowest freezing point is reported for 2,2,2-trifluoroacetamide, when compared a set of DESs based on ChCl with urea, thiourea, 1-methyl urea, 1,1-dimethyl urea, acetamide and 2,2,2-trifluoroacetamide.[19] This is presumably due to the difference in hydrogen bond forming ability of the DESs constituents.

Density: The density of DESs is found to be much higher than that of the conventional solvents.[19] Most of the commonly reported DESs have densities in the range of 1.0−1.35 g cm^{-3} at room temperature.[19, 38] However, the density values for those containing metallic salts, such as $ZnCl_2$–acetamide (1:4) and $ZnCl_2$–urea (1:3.5) are relatively higher, and lies in the range of 1.3−1.6 g cm^{-3}. It has been found, as seen in the case of freezing point, that the type of constituents of DESs and the salt to HBD molar ratio at which the solvent is formed, have a significant effect on the density of DESs.[19, 33] For instance, among DESs formed by ammonium and phosphonium-based salt with a particular HBD (say ethylene glycol), the former solvent shows lower density compared to the later. In another report, it is shown that the density of ChCl-glycerol DES increases with increasing percentage of glycerol.[39] The density of DESs consisting of HBD with only difference in the number of hydroxyl groups (glycerol and ethylene glycol) shows an increase of the value with the number of hydroxyl groups.[33] In case of ChCl and dicarboxylic acid-based DESs, density

decreases with gradual increase of the chain length of the diacids and follows the order: oxalic > malonic > glutaric.[33] Similarly, increasing the cation alkyl chain length in case of tetraalkylammonium bromide-based DESs decreases the density.[33] The observed trend of the density is attributed to a difference in molecular organization or packing of the constituents of DESs and thus, explained in terms of free volume available in the DESs. The temperature dependence of the density is also studied for ChCl-glycerol/ethylene glycol/urea DESs. In all cases, the density decrease with increase of the temperature due to thermal expansion.[40-42]

Viscosity: The use of many eutectic-based solvents has been limited due to their high viscosity as compared to the common organic solvents.[19, 33] In general, most of the common DESs have viscosities greater than 100 cP at room temperature. However, some DESs where ethylene glycol, phenol are used as HBD exhibit significantly low viscosity values (3-4 folds lower than 100 cP). The presence of extensive hydrogen-bonding network between the constituents of the DESs resulting in a lower mobility of the constituents is mainly responsible for their high viscosity. In this context, it is important to note that the reported viscosities for a particular DES from different sources show large difference.[33] This is probably due to the presence of any impurities, particularly water. As many DESs are highly hygroscopic in nature, their viscosity is expected to be extremely sensitive to the air moisture. Therefore, proper characterization of the water content is very crucial for reporting a reliable and reproducible viscosity data for any DES. Like the other physical properties discussed above, viscosities of DESs are closely dependent on the molecular structure of the DES components, salt/HBD molar ratio, etc. The viscosity of all DESs decreases significantly with increase of the temperature. Therefore, highly viscous DESs, which are not suitable for applications at room temperature, can easily be employed for applications at higher temperatures. The temperature dependence of the viscosity for DESs is described by using both Arrhenius and VFT model (equation 1.1). However, this dependence is best described by the VFT equation.[33, 38, 40, 43]

$$\eta = \eta_0 exp\left(\frac{B}{T - T_0}\right) \ldots\ldots\ldots\ldots (1.1)$$

where, η is the viscosity at absolute temperature T, η_0 is the viscosity at infinite temperature, B is the fragility parameter, and T_0 is a characteristic temperature for which η diverges.

Although, Abbott and co-workers analyzed the viscosity of DESs using the hole theory,[22] which was applied earlier for molten salts and ILs, later developments suggested that the hole theory solely cannot explain the viscosity of DESs as strong intermolecular interactions in these solvents and the size of the involved constituents have to be considered as well.[19, 33]

Conductivity: Considering the use of DESs as an electrolyte in electrochemical applications, the knowledge of their transport property like conductivity is very crucial. As conductivity is strongly correlated with viscosity, one can expect low conductivities for most of the DESs owing to their high viscosity. As anticipated, most of the studied DESs show conductivities lower than 1 mS cm^{-1} at room temperature.[19] However, ethylene glycol and imidazole-based DESs exhibit significantly large electrical conductivities due to their relatively low viscosities.[33, 44] In general, conductivity of DESs increases with increasing temperature due to decrease of viscosity. In line with the viscosity, the temperature dependence of the conductivity is also satisfactorily described by both the Arrhenius and the VFT model.[33] The conductivity of DESs also increases gradually with increasing concentration of the ionic constituents. However, this behavior is not generic for all DESs as it also depends on both the nature of the salt and the HBD, and various interactions between them.

Polarity: The polarity of a solvent is one of the most important physical properties that plays key role in controlling the ability to dissolve various substances. Despite this fact, the number of studies on the polarity measurements of DESs is relatively less. The microscopic polarity of DESs is characterized by using different polarity parameters, such as $E_T(30)$ or E_T^N and various solvatochromic probe molecules (both absorption and fluorescence based probes) shown in Chart 1.2.[45] The polarities of most of the commonly studied DESs are found to be significantly high.[46-48] These values are comparable or slightly higher than those of the primary alcohols like methanol, ethanol, but less than water.[47] In this context, one may note that the polarities of DESs are significantly higher than those of the many common and popular ILs.[47] However, like other physical parameters, polarity of the DESs depends on the nature of the constituents and their composition.[46] For example, among the DESs consisting of ChCl combined with different HBDs, such as urea, ethylene glycol, glycerol, and malonic acid, the largest $E_T(30)$ values are observed for glycerol-based DESs, which is followed by ethylene glycol and urea. On

the other hand, the $E_T(30)$ values for glycerol-based DESs studied at various molar ratios increase with increasing ChCl percentage in a linear fashion.[48]

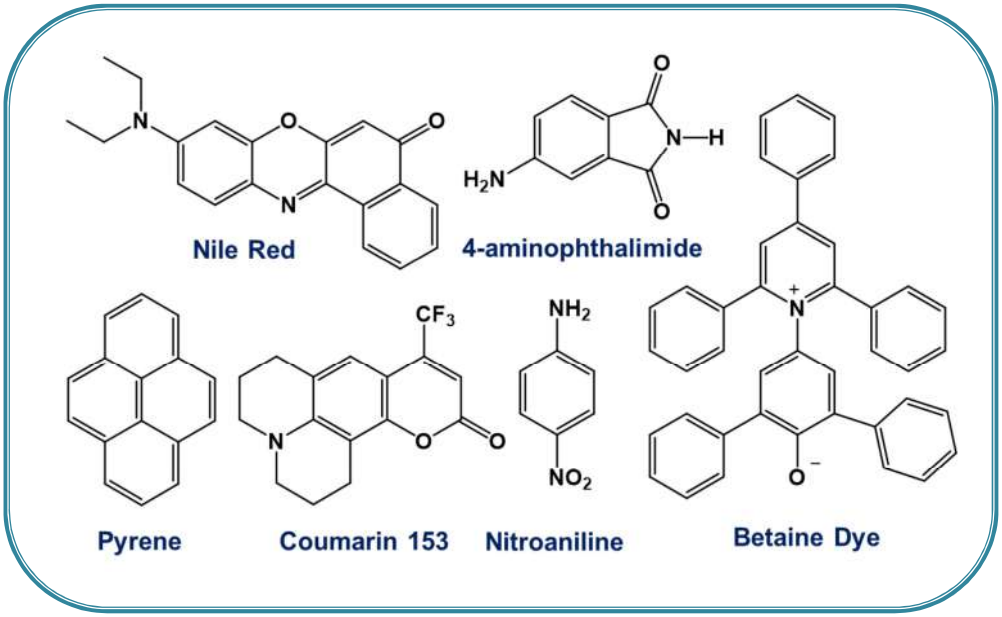

Chart 1.2. Structure of some solvatochromic probe molecules commonly used for estimation of polarity.

Refractive Index: The refractive index of DESs can be used sometimes for their characterization. The refractive indices for most of the reported DESs are close to or greater than 1.50 (ranges between 1.47 and 1.67). For example, the refractive indices of DESs composed of ChCl and urea, ethylene glycol and glycerol are found to be 1.5044, 1.4620 and 1.4868, respectively.[33] The refractive indices of another set of DESs containing benzyltriethylammonium salt and different HBDs, such as p-toluene sulfonic acid, citric acid and oxalic acid are found to be 1.5484, 1.5307 and 1.5172, respectively.[41] Like density, the refractive index of DES decreases monotonically with increasing temperature. This is due to the fact that the decrease in density with temperature provides more freedom for the light to pass through the solvents.[33, 41]

Thermal Stability: The thermal stability of DESs is determined in terms of decomposition temperature by using thermogravimetric analysis. The decomposition temperature (at 10% weight loss) of a series of DESs based on benzyltrialkylammonium salt with various

glycols is found to be in the range of 373 to 443 K, and follows the order: glycerol > triethylene glycol > diethylene glycol > ethylene glycol.[49] The thermal stability of some choline-based DESs, however, is found to be relatively higher with the decomposition temperatures between 543 and 553 K, which are comparable to many ILs.[50] Clearly, the thermal stability depends significantly on various factors, such as type of the salt and HBD, and chain length of the HBD. However, these values are well separated from their freezing point values, which imply quite a large liquidous range of the DESs.[50]

Volatility: DESs are generally expected to have negligible vapor pressure due to non-volatile nature of one of their constituents. Although studies dealing with the vapor pressure of DESs are very scarce, this parameter is reported for few DESs based on ammonium and phosphonium salt in combination with urea and glycerol. As expected, these DESs exhibit extremely low but detectable vapor pressure. The vapor pressures of these DESs are found to be in the range of 0.14 to 2.16 Pa at 343 K.[51] The lower vapor pressure for urea-based DESs as compared to glycerol-based DESs is in accordance with the very low vapor pressure of urea itself.[51]

Structural and Dynamical Features: The microscopic structural and dynamical features of a solvent are important for understanding various interactions operating in it as well as for controlling any chemical reactions in that solvent. These features are investigated both theoretically and experimentally only for some selected DESs and hence, are still not understood completely.[28, 29, 31, 52-62] However, these studies have revealed that the liquid state structure of these solvents is quite complex due to the presence of extensive interspecies hydrogen-bonding network and most of the DESs are spatially (structurally) and/or dynamically (temporally) heterogeneous in nature. The structural heterogeneity of DESs is determined by monitoring the steady-state excitation-wavelength dependent emission behavior of dipolar fluorescent molecules using fluorescence spectroscopy.[52-54] The heterogeneous structure of DESs containing polar and non-polar domains are proposed, and verified by FTIR and 2DIR spectroscopic studies.[29, 55, 56] Simulation studies have also shown the formation of heterogeneous domain-like structures in DESs owing to molecular-scale segregation of the solvent constituents.[57-60] The dynamical heterogeneity of DESs is confirmed through solute and solvation dynamics studies using time-resolved fluorescence spectroscopies.[28, 31, 52, 54] Furthermore, these studies have revealed that both these microscopic features are sensitive to the structural identity of HBAs as well as HBDs of the DESs.

1.1.4. Applications

Due to their attractive properties, DESs have found potential applications in a variety of fields. The initial usage of most of the DESs was limited to two major areas, metal processing and synthesis.[22] As DESs can dissolve various metal salts that include metal oxides and hydroxides, these have found application in electrochemical processes, such as metal extraction, metal recovery and metal finishing (electropolishing and electrodeposition) for metals that are normally difficult to process.[63-66] DESs have also been applied as environmentally benign alternatives for synthesis. They are successfully employed as reaction media in various organic syntheses.[18, 21, 67-69] They are also used in synthesis of many inorganic materials including metal organic frameworks, zeolite-type materials and carbon materials through the ionothermal synthesis strategy.[70, 71] Very recently, DESs have been used as an efficient media for synthesis of various functional materials and shape controlled synthesis of nanoparticles.[25, 72] DESs are also used in electrochemistry as promising electrolytes for dye-sensitized solar cell.[73, 74] Further, DESs are also used for the dissolution of some poorly soluble drugs, such as griseofulvin, itraconazole, danazol and so on.[75] Another interesting and emerging application of DESs is purification of biodiesel by extraction of glycerol from biodiesel.[76-78]

In recent years, with their developments, DESs have been successfully used as environmentally sustainable media in numerous fields, such as catalysis,[79, 80] biotechnology,[81, 82] polymerizations,[83, 84] carbon dioxide adsorption,[85, 86] and many more. However, a careful survey of the literature reveals that only a narrow range of commonly available DESs have been utilized so far for aforementioned applications, and there still lies huge scope of development of novel DESs for more widespread applications.

1.2. Photophysical Studies

Study of photophysical processes, such as rotational diffusion, translational diffusion, solvent relaxation, electron transfer, proton transfer, etc. in any unknown solvent is one of the useful approaches for understanding the nature of the solvent of interest.[87, 88] These dynamical processes offer an insight into the microscopic structure, dynamics and different types of interactions operating in the solvent, which play a key role in controlling

the rates of chemical reactions taking place in it, and help us to better understand the solvent.

Among the aforementioned dynamical processes, we exploit primarily the rotational diffusion, translational diffusion and solvation dynamics of various molecular systems by employing various fluorescence spectroscopic techniques to obtain an in-depth understanding of the microscopic physicochemical properties of the DESs studied in this work.

1.2.1. Solvation Dynamics

Solvation is a process in which a dissolved solute molecule in a solvent is stabilized by reorganization of the surrounding solvent molecules through various interactions between the solute and solvent molecules.[89] Solvation dynamics refers to the reorganization of the solvent molecules with time around the solute molecule until the system reaches an equilibrium and the time associated with this solvent reorganization is called solvent relaxation time (often popularly called solvation time).[89] The dynamics of solvation of a solvent system can be studied by many experimental techniques, such as dielectric relaxation,[90, 91] three-pulse photon echo peak shift,[92, 93] infrared spectroscopy[56, 94] and time-resolved fluorescence spectroscopy.[95-97] Among them, time-resolved fluorescence spectroscopy is the most commonly used one for this purpose due to its high temporal (~ tens of fs) resolution.[95, 98]

As solvation leads to a significant shift of the emission spectrum of a dipolar fluorescent molecule in polar solvent, the dynamics of solvation is studied by monitoring the TDFSS of the molecule in the time-resolved fluorescence experiment.[97, 99] In this study, the equilibrium charge distribution of a dipolar fluorescent molecule is suddenly perturbed by a short optical pulse excitation. This leads to a redistribution of charges in the solute molecule and creates a large change in the dipole moment. In response to this change, the solvent molecules start to rearrange and reorient themselves with time to attain the equilibrium again by stabilizing the newly created charge distribution of the system. During the stabilization, the fluorescence spectrum of the solute molecule shifts gradually towards longer wavelengths until a relaxed equilibrium state is reached. This time dependent shift of the fluorescence spectrum of the dipolar molecule is called as dynamic Stokes shift (or TDFSS).[87] This phenomenon is illustrated in Scheme 1.1.

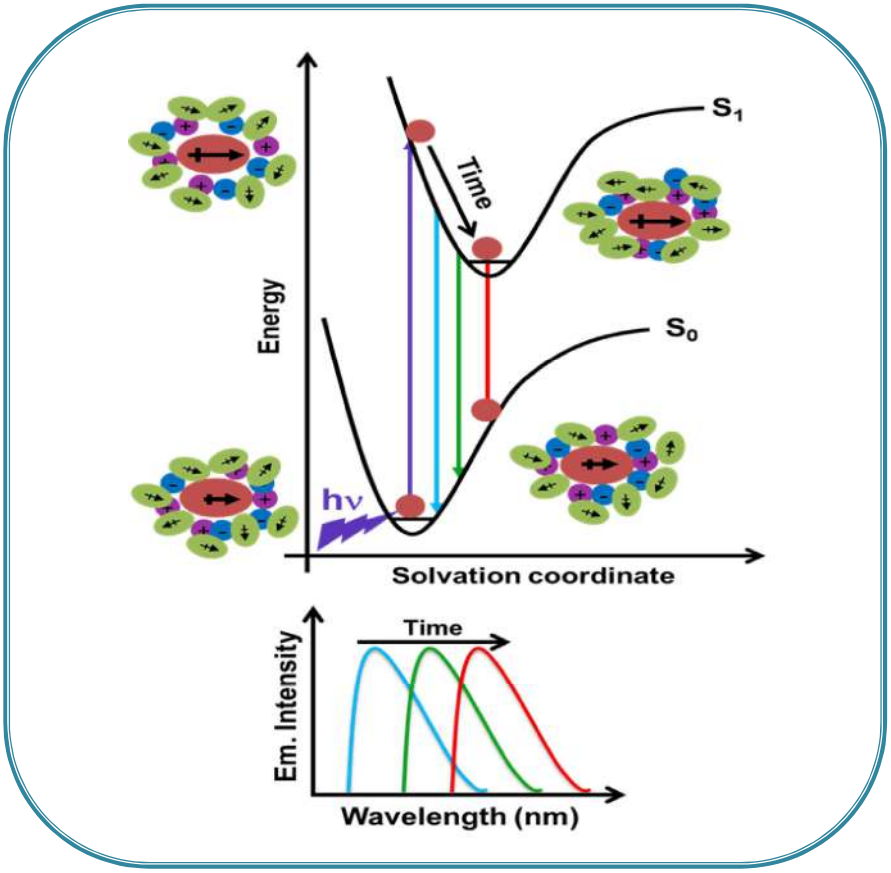

Scheme 1.1. Schematic illustration of solvent relaxation around a dipolar fluorescent molecule along with the dynamic Stokes shift.

The procedure for estimation of the TDFSS of a dipolar fluorescent molecule usually involves the following steps. First, one needs to measure the fluorescence decay profiles of the solute molecule at various wavelengths across the entire steady-state fluorescence spectrum. Then, TRES is constructed from these decay profiles and the steady-state fluorescence intensities. A detailed analysis of the TRES gives the TDFSS, which is used to calculate a dimensionless spectral shift correlation function (also called as solvation response function), S(t), given by equation 1.2.[87]

$$S(t) = \frac{\nu(t) - \nu(\infty)}{\nu(0) - \nu(\infty)} \ldots\ldots\ldots\ldots (1.2)$$

where, ν(0), ν(t), and ν(∞) are the peak frequencies (in cm^{-1}) immediately after laser excitation (t = 0), at any given time (t), and at a sufficiently long time for relaxation of the excited solute molecule to be complete (t = ∞).

The time-dependence of the spectral shift correlation function provides quantitative information on the nature and timescales of the solvation dynamics.[87, 97] It is pertinent to mention here that a dipolar molecule must fulfill the following criteria to be a good probe for the study of solvation dynamics;[87] a large change in dipole moment on excitation and sufficiently long fluorescence lifetime so that solvent relaxation is complete during this time. The molecular structures of some dipolar molecules, commonly used for the study of solvation dynamics using this method, are given in Chart 1.3.

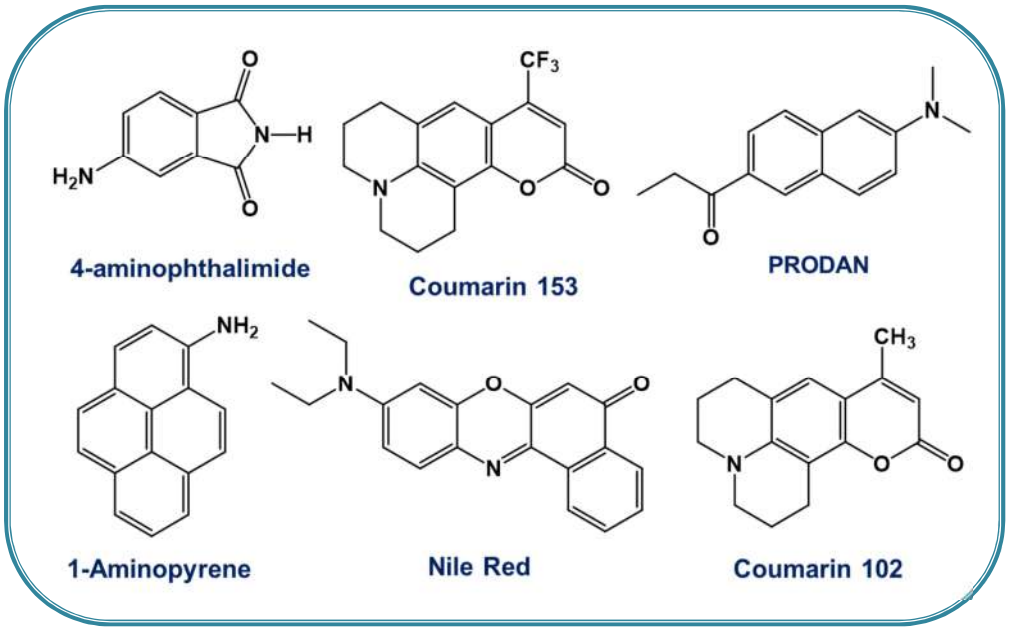

Chart 1.3. Structure of some dipolar probe molecules commonly used in the study of solvation dynamics.

1.2.2. Rotational Dynamics

The diffusive motion of a solute molecule in a solvent can generally be described by the change in its orientation (rotation diffusion) and position (translation diffusion).[100] The dynamics of these diffusion processes refer to the rate at which the solute molecule

diffuses in the solvent through the respective diffusive motion. The rate of these diffusive motions are mainly dependent on the shape and size of the solute molecule, interactions between the solute and solvent molecules, and the viscosity and temperature of the solvent, and thus provides valuable information about the solvent of interest.[87]

The rotational diffusion dynamics of a solute in a solvent can be studied by measuring the average angular displacement of the solute molecule by monitoring its time-dependence of the fluorescence anisotropy.[87] The fluorescence anisotropy is a measure of the extent of depolarization of the fluorescence of a solute molecule when excited with a polarized light. As rotational diffusion of solute molecule occurring between the times of absorption and subsequent emission causes depolarization of the fluorescence, one can study the rotational dynamics by looking into the time-dependence of the fluorescence anisotropy of the solute. The measurement of fluorescence anisotropy relies on the principle of photoselective excitation of the probe molecule using a polarized light. Generally, solute molecules are randomly oriented in a solution. Upon selective excitation, only those solute molecules preferentially absorb the excitation light whose absorption dipole moments are aligned towards the polarization of the excitation light. Immediately after the excitation, the fluorescence from the excited molecules is also polarized parallel to the polarization of the excitation light. As rotational diffusion of the excited solute molecules occur during its excited state lifetime, the direction of the emission dipole moment of the molecules changes with progress of time. This leads to depolarization of the fluorescence with time. Thus, fluorescence anisotropy measurements, which determine the average angular displacement of the solute molecules during its excited state lifetime, essentially determine the rate and extent of rotational diffusion of the molecules. The principle and method of measurement of the fluorescence anisotropy of a probe molecule is illustrated in Scheme 1.2.

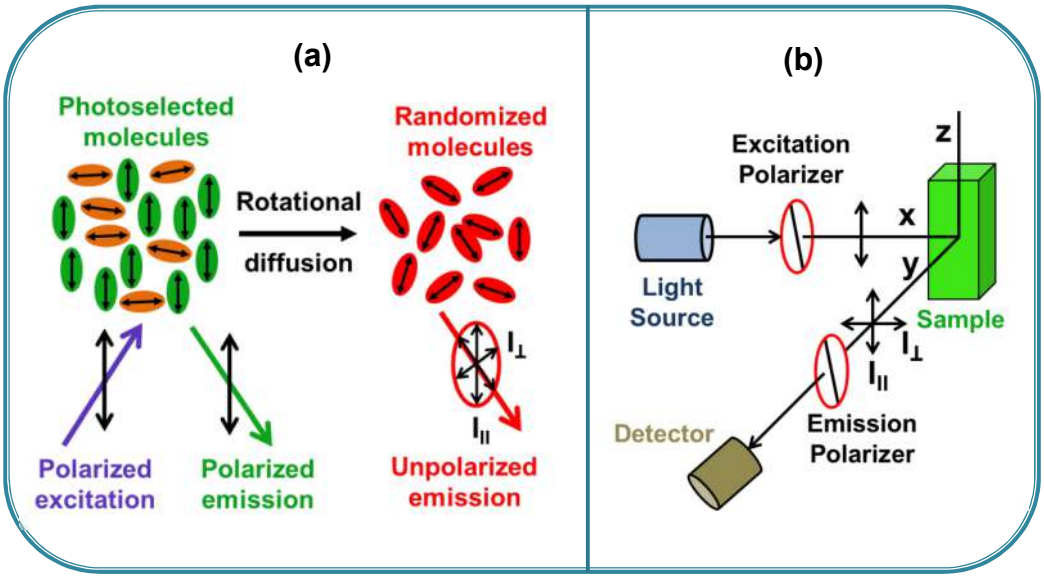

Scheme 1.2. Schematic diagram illustrating (a) principle and (b) method of fluorescence anisotropy measurement.

The measurement of fluorescence anisotropy of a solute molecule starts with excitation of the sample usually by a vertically polarized light followed by collection of the fluorescence intensity at two different polarizations, parallel (I_{II}) and perpendicular ($I_{\perp}$), with respect to the excitation polarizer. These intensity values can be used to calculate the fluorescence anisotropy using equation 1.3.[87]

$$r = \frac{I_{II} - I_{\perp}}{I_{II} + 2I_{\perp}} \quad \ldots\ldots\ldots\ldots\ldots\ldots (1.3)$$

In time-dependent anisotropy measurement, fluorescence intensity decays is used instead of steady-state fluorescence intensity. Molecules with sufficiently long fluorescence lifetime can be good probes for the study of rotational diffusion dynamics. The molecular structure of some commonly used molecules for rotational diffusion dynamics studies are given in Chart 1.4.

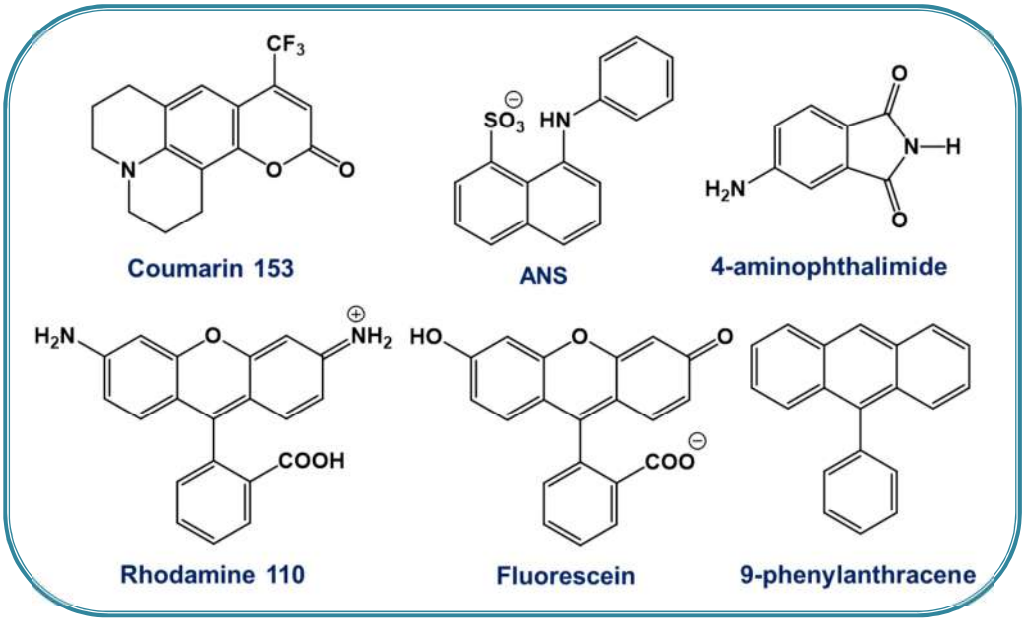

Chart 1.4. Structure of some molecules commonly used for rotational and translational dynamics studies.

1.2.3. Translational Dynamics

Along with the solvation and rotational dynamics, study of translational diffusion dynamics of various molecular systems in a solvent is also helpful for understanding the solvent of interest.[87] In order to monitor the translation diffusion process, one essentially needs to observe the extent and rate of mean-square displacement of a solute molecule with time. The dynamics of translation diffusion of a solute molecule in a solvent can be studied by looking into the mean-square displacement of the molecule employing FCS technique.[87] A detailed discussion on the FCS measurements is provided in Chapter 2.

FCS is an advanced and powerful single-molecule based technique,[87, 101, 102] in which the measurement is performed using freely diffusing molecules in a solution and the time-dependent fluorescence intensity fluctuations of extremely dilute solution of solute molecules (typically ~ nM) from a tiny observation/detection volume (~ fL) is analyzed. When a solute molecule randomly diffuses into and out of the observation volume, effective numbers of the molecules in the volume fluctuate with time. This leads to fluctuations of the fluorescence intensity. The fluctuations in the effective numbers of molecules and hence, the fluorescence intensity, will be slow when the molecules diffuse

slowly through the observation volume and will be fast when fast diffusion of the molecules occur. These fluctuating fluorescence signals can then be correlated to generate a correlation function. By analyzing the time-dependence of the correlation function one can obtain valuable information on the rate and nature of translation diffusion of the diffusing molecule. It is pertinent to mention here that one has to be very careful while choosing a probe molecule for measurement of the translation diffusion dynamics using FCS, because in addition to the translation diffusion, the intensity fluctuations can also occur from many other dynamic processes which are faster than the diffusion. A molecular system, which shows intensity fluctuation only due to the translation diffusion, can be a suitable probe for this specific purpose. Chart 1.4 shows the structure of some commonly used molecules for the translational diffusion dynamics studies.

1.3. Proteins

1.3.1. Structure of Proteins

Cells contain many highly complex molecules, commonly termed as macromolecules.[103] There are three major types of macromolecules present in a cell: carbohydrates, proteins and nucleic acids. These are responsible for most of the basic phenomena of life. Among these, proteins are one of the most important and interesting biomolecules in life sciences.

Proteins form the very basis of all life. They are the most abundant biomolecules in cells, which fill up about 50 % of the total dry weight of cells.[103, 104] They play a variety of crucial roles in cells and tissues, and involved in almost all life processes occurring in living systems. Proteins are polymers of amino acids.[103, 105] In other words, they can also be described as a long polypeptide chain consisting of many amino acids. Amino acids are carboxylic acids that contain a carboxyl group, an amino group, a hydrogen atom and a side chain (only variable component in all amino acids) in the alpha position (Scheme 1.3a) except proline. Large number of such amino acids linked covalently through the peptide bonds formed by the condensation reaction of two amino acid molecules with elimination of water (Scheme 1.3b) generates a long polypeptide chain.[105] A polypeptide chain contains two key structural components: the repeating part that forms backbone of the chain and the variable part that consists of different side chains of amino acids (Scheme 1.3c). Two ends of the polypeptide chain are termed as N-terminus (free amino

group present) and C-terminus (free carboxyl group present). Some proteins also contain other covalently bound components, coordinated metal ions and prosthetic groups.[105] It is important to mention here that proteins, which catalyze several biochemical reactions in all life-forms, are called enzymes.

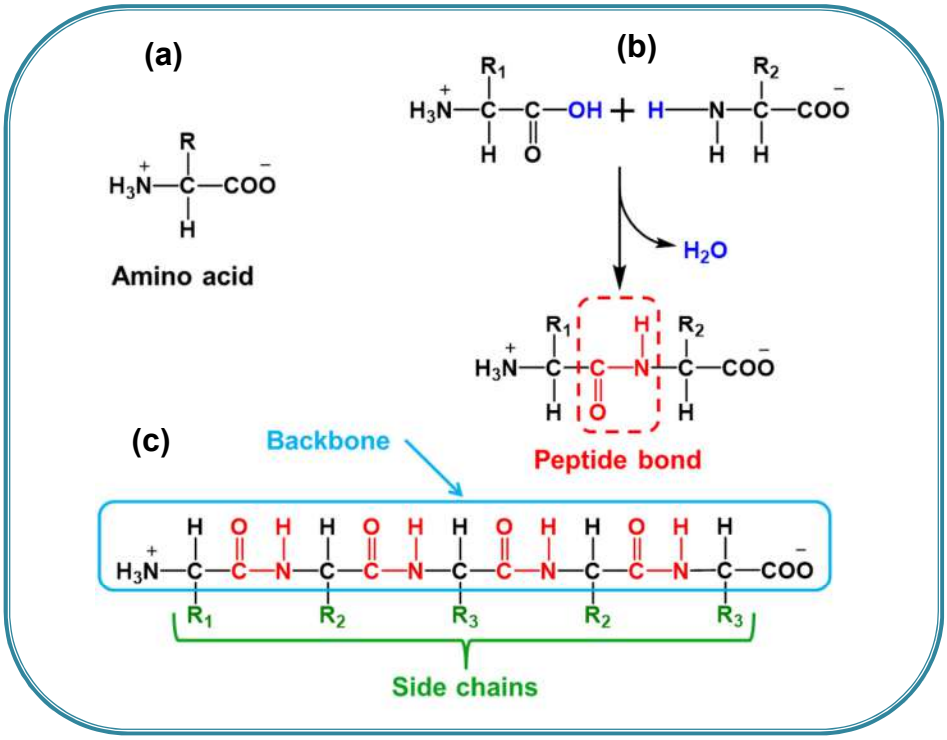

Scheme 1.3. (a) General structure of an amino acid, (b) formation of a peptide bond through covalent linking of two amino acids, and (c) various components of a polypeptide chain.

There are four different orders of protein structure: primary, secondary, tertiary and quaternary (Figure 1.2).[105, 106]

Primary Structure: The linear structure formed by a sequence of amino acids in the polypeptide chain of a protein is called its primary structure. The primary structure of a protein always starts with the N-terminal and ends with the C-terminal. Each protein is composed of a unique sequence of amino acids, and it is the unique amino acid sequence which determines the overall structure and function of that particular protein. Elimination

of any single amino acid or alternation its position can cause notable impact on both the structure and function of the protein.

Secondary Structure: Secondary structure of a protein comprises of stable and repetitive local patterns of adjacent amino acid residues in the polypeptide chain. It is stabilized through the formation of hydrogen bonding between the keto groups (partial negative charge) and the amino groups (partial positive charge) of different peptide bonds, either within the same polypeptide backbone or different. Depending on the pattern of the hydrogen bonds different types of the secondary structures can be formed. The most commonly found secondary structures of proteins are α-helices, β-sheets and turns. An α-helix is the right handed coil of polypeptide backbone around an imaginary axis that resembles a curled ribbon. Though the stability of the helical structure is mainly governed by the hydrogen bonding, it also depends on the interactions between the side chains of amino acids. Bulky side chains of amino acids destabilize the helical structure. In the β-sheet, two or many polypeptide chains are lined up next to each other and aligned in a zigzag fashion to form a blanket-like structure. Depending on whether the polypeptide chains are arranged in a parallel (all C-terminal ends are at the same side) or antiparallel fashion (different C-terminal ends are at the opposite side), the β-sheets are classified as parallel and antiparallel. The main difference between the helix and sheet structure is that in the former case hydrogen bonds are formed between the keto and the amino groups of the same polypeptide chain, whereas in the other case they occur between the amino groups of one chain and the keto groups of the adjacent chain. Turns are the type of structures in protein where the polypeptide chain reverses its overall direction. This is the element that makes the bridges between the successive runs of α-helix and β-sheet.

Tertiary Structure: Tertiary structure of a protein describes its global conformation that depends on the way various secondary elements are organized in space. The secondary structures of a polypeptide chain are folded in a specific fashion, where the hydrophilic amino acids lie exposed on the outside surface of its three dimensional conformation and the hydrophobic amino acids are cluster towards the interior of the protein structure. Protein tertiary structure is usually stabilized by various interactions between the side chain groups of the amino acids in polypeptide chains, such as hydrophobic and hydrophilic interactions, dipole-dipole interactions and hydrogen bonding. In addition to these interactions, disulfide bond (that is stronger than the other interactions), which is a

covalent bond formed between the sulfur containing side chains of amino acid (cysteine), contribute significantly to the stability of the tertiary structure.[105]

Quaternary Structure: Quaternary structure of protein describes how association of multiple polypeptide chains (also known as subunits) forms a single complex functional protein. In many proteins, only aforementioned three orders of structure are observed. However, some proteins composed of multiple polypeptide chains (either same or different) giving the protein its quaternary structure. One example of such protein is hemoglobin which contains four subunits. The interactions, which stabilize the quaternary structure, are the same that contribute to the tertiary structure.

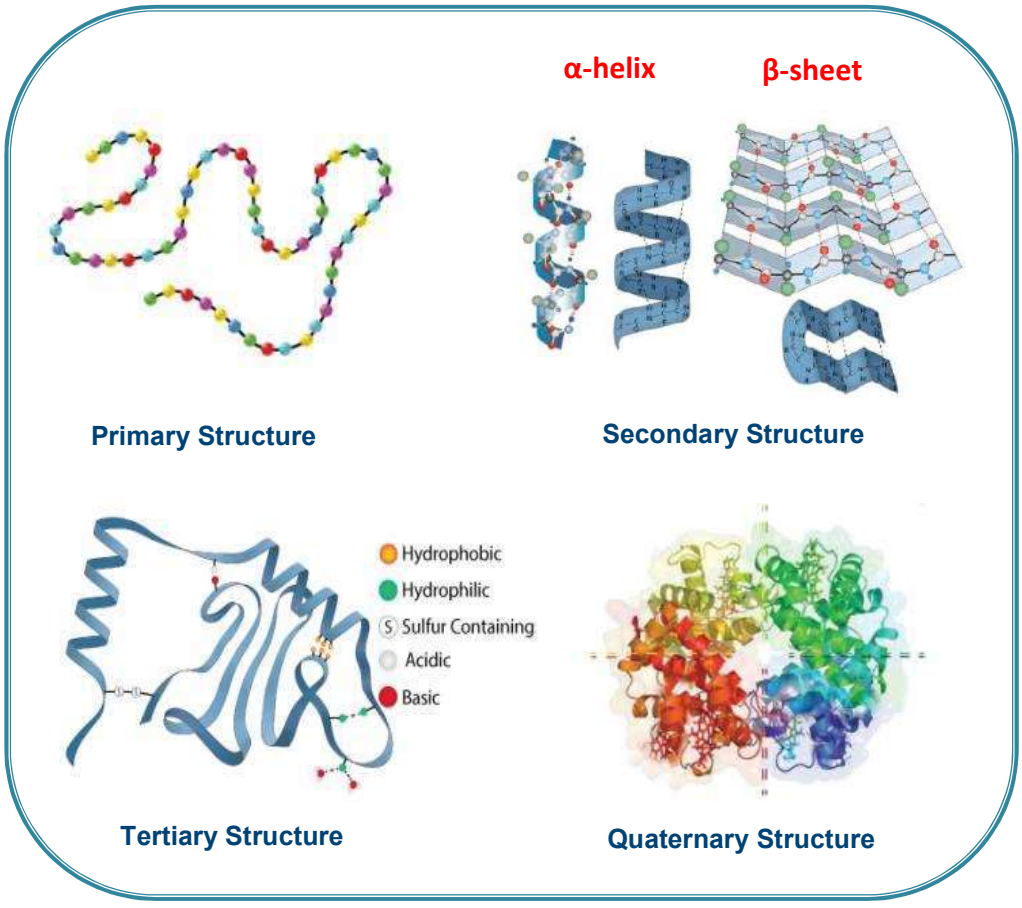

Figure 1.2. The primary, secondary, tertiary and quaternary structure of a protein. (Adapted from reference 106)

1.3.2. Stability, Dynamics and Function of Proteins

Soon after synthesis in ribosome, a polypeptide chain quickly forms a stable compact three-dimensional structure (or conformation). This particular conformation, which is essential for biological function of proteins, is called a native or folded state. As mentioned earlier, various stabilizing factors lead to such functional form. However, under certain conditions, this specific conformation of proteins is completely disrupted leading to a highly unstable conformation (which is nonfunctional in nature), called an unfolded or denatured state. In addition to these two conformations, various other structural changes often take place in proteins, which are commonly termed as intermediate states.[107, 108] This indicates that proteins are highly dynamic/flexible in nature.

Dynamics of proteins is usually characterized by various motions of large number of atoms and groups present in the polypeptide chain, within a wide range of time (10^{-15} to 10^{4} sec) and energy (0.1 to 100 kcal mol^{-1}).[108, 109] The inherent dynamics of proteins play very important role in determining their function.[109-111] This can be understood from the fact that the activity of a protein reduces with slowdown of the dynamics through temperature reduction. Thus, both native structure and dynamics of a protein are essential for its proper functioning.

1.3.3. Probing Structural Changes and Dynamics of Protein using Fluorescence Spectroscopy:

Fluorescence spectroscopy is a popular and sensitive technique that has been used extensively to study the structural changes and dynamics of various protein molecules.[87] Both intrinsic and extrinsic fluorescence of different protein molecules is used for this purpose.

Intrinsic Fluorescence: Unlike most of the macromolecules, proteins exhibit significant amount of fluorescence by itself, called intrinsic fluorescence.[112] This fluorescence of proteins arises due to some specific amino acids, such as Trp, Tyr and Phe (Chart 1.5). Among these amino acids, fluorescence property of Trp is most commonly used in probing the structure of protein molecules for the following reason.[87] It has sufficient fluorescence quantum yield. Selective excitation of only Trp is possible by exciting the protein at 295 nm as other two amino acids does not absorb at that wavelength. Its fluorescence (both maxima and intensity) is highly sensitive to the local environments. In general, Trp

displays an emission maximum around 350 nm in polar environment (water) at room temperature, but it appears ~ 10-20 nm blue shifted in relatively less polar environments. As a result, changes of the local environment around Trp residues during conformational change, protein-ligand binding, unfolding, subunit association and aggregation significantly affect their fluorescence property. Additionally, changes of the fluorescence anisotropies of both Trp and Tyr are sometimes used to probe dynamics of protein, because various motions such as the overall rotational diffusion and the segmental motion of protein alter this parameter (anisotropy). Thus, by carefully monitoring the changes in the intrinsic fluorescence properties of protein, valuable information regarding their structural changes and dynamics under various conditions can be obtained.[113]

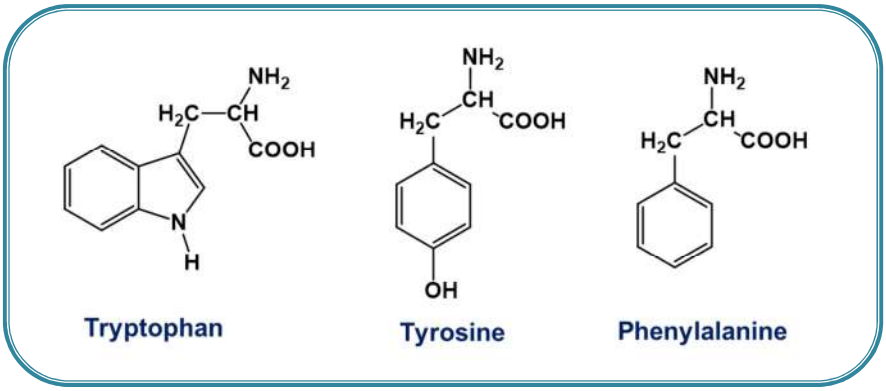

Chart 1.5. Structure of amino acids responsible for intrinsic fluorescence of proteins.

Extrinsic Fluorescence: The use of intrinsic fluorescence of protein is not possible or difficult in many cases due to the following reasons.[87] The intrinsic fluorescence of protein molecule is limited to only Trp and Tyr amino acids, and is extremely weak when present in less numbers (one or two). These amino acids absorb in the UV region where several solvents including ILs and DESs can cause large background during experiments owing to their own absorption. Additionally, the use of UV excitation is not advisable to study in cellular environment as it may cause serious damage to the cell organelles and tissues. Presence of many Trp residues in different environment of proteins also sometimes causes complicacy in interpretation of the data. Thus, an alternative way to overcome these shortcomings in probing structure and dynamics of protein is to use fluorescence of

externally added fluorophore (called extrinsic fluorescence) of choice. The main advantages of this method are as follows: one can choose the fluorophore which has absorption and emission in the longer wavelength so that their signal does not interfere with the solvent background signal. These fluorophores have high fluorescence quantum yield and their fluorescence properties are highly sensitive to any structural and dynamical changes of protein molecules.

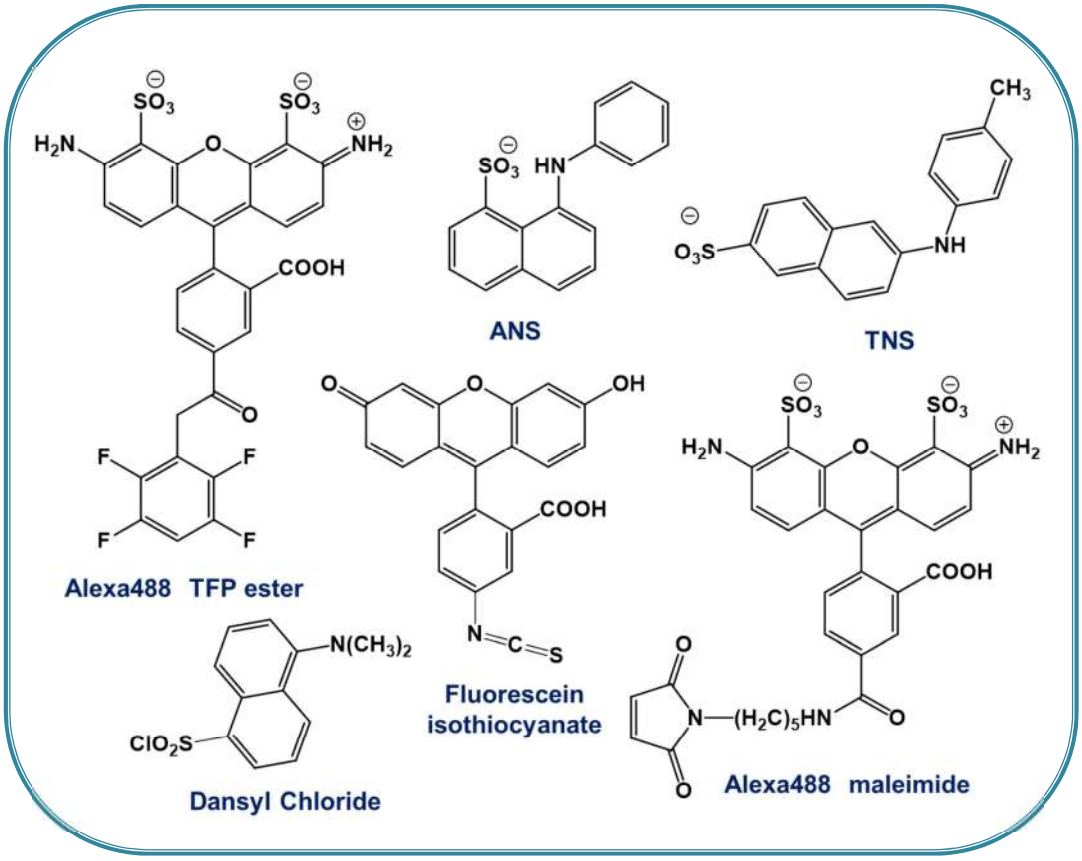

Chart 1.6. Structure of some fluorophores commonly used for extrinsic fluorescence of proteins.

The labeling of various protein molecules using external fluorophores can be done through either non-covalent or covalent binding (Chart 1.6). Some common examples of fluorophores that bind non-covalently to protein due to their stronger binding affinity are TNS and ANS.[87] The examples of other category fluorophores that bind covalently to several proteins through reaction with an amino or thiol group are FITC (amine reactive),

DNSC (amine reactive), A488 TFP ester (amine reactive) and A488 maleimide (thiol reactive). As any change of the protein structure leads to considerable change in the fluorescence properties of these fluorophore, it is possible to probe the protein structure and dynamics by carefully monitoring the variation of their fluorescence using different fluorescence-based spectroscopic and microscopic techniques.[87, 114]

1.4. Motivation behind the Thesis Work

The work presented in this thesis has been undertaken primarily to obtain a comprehensive understanding of the microscopic solution structure and dynamics of some alcohol-based DESs by studying photophysical processes, such as solvation dynamics, rotational diffusion dynamics and translational diffusion dynamics of different fluorescent molecular systems in these media. Additionally, the structural stability and conformational dynamics of a protein have also been studied in such DESs to obtain insight on the biophysical mechanism of protein-DESs interactions, which essentially govern the fate of the protein in such nonconventional media. It is important to mention here that even though a significant numbers of DESs have been explored, most of the studies have been focused on systems obtained by mixing of quaternary ammonium salts with amides and acids as HBDs, whose applications are often limited due to their high viscosity.[19, 22] The alcohol-based DESs can serve as useful media in such applications due to their much lower viscosity compared to the other DESs.[19, 22, 38, 115-117] This motivated us to work specifically with alcohol-based DESs.

Even though the alcohol-based DESs serve as useful media useful in a variety of applications,[17, 19, 22, 118] the microscopic solution structure and dynamics of these liquids are not well understood and issues like whether spatial and dynamic heterogeneity is a generic feature of all the ionic DESs is still unclear. Further, despite the fact that understanding of the solute-solvent interactions involving different solute molecules is very important for realization of the potential of these media as solvents; this aspect remains almost unexplored for DESs. Keeping these points in mind, herein we have attempted to address some of these issues for a less viscous ionic DES consisting of a 1:2 molar mixture of ChCl and ethylene glycol (Chart 1.7) by studying the rotational and translational diffusion dynamics of a neutral (C153) and two charged (R123 and FL) probe molecules (Chart 1.8)

with the help of fluorescence anisotropy measurements in ensemble condition and FCS measurements in single-molecule condition, respectively.

As mentioned previously, various physical properties of the DESs alter considerably with changes of salt and HBD structure. Recently, it has been observed that a change of the hydrocarbon chain length and hydroxyl group position of the diols (HBD) significantly influences the physical properties of the alcohol-based DESs.[119] In order to understand how such structural changes in HBD influence the microscopic structure, dynamics and interactions operating in these media, we have studied the rotational and translational diffusion dynamics of some carefully chosen molecules (both dipolar (C153 and 4-AP) and nonpolar, ANT) (Chart 1.8) using fluorescence anisotropy and FCS measurements in a series of ChCl/alcohol based DESs (Chart 1.7) differing in hydrocarbon chain length and positioning of the hydroxyl group at the HBD. Both dipolar and nonpolar molecules are employed in this work to understand whether these molecules experience similar environment and interactions in these media irrespective of their nature.

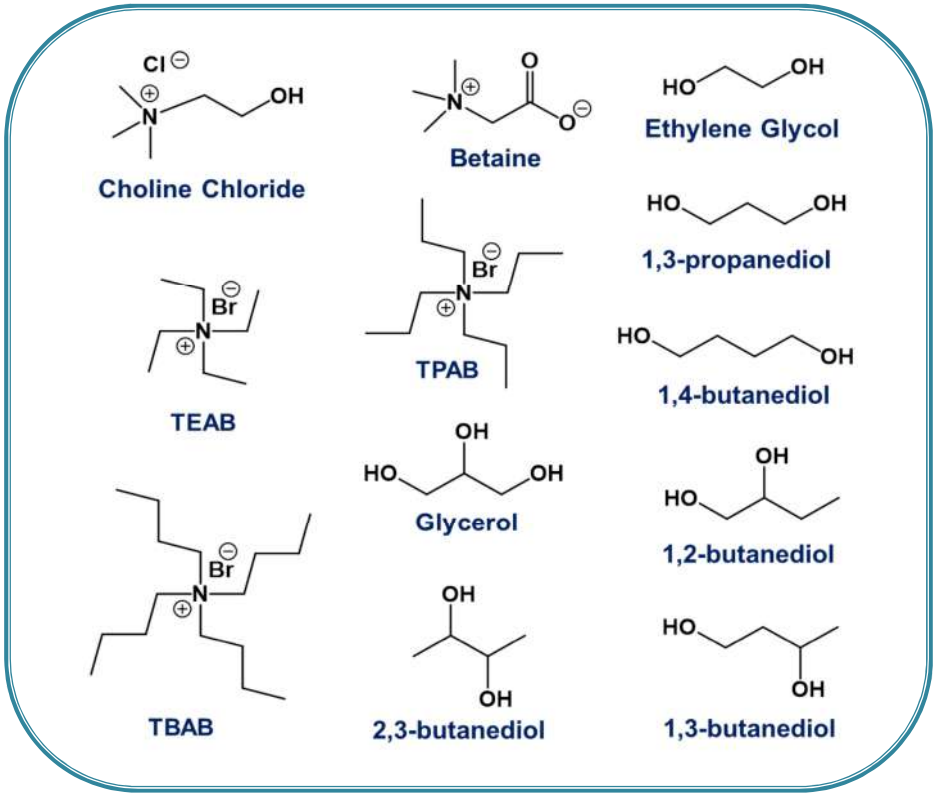

Chart 1.7. Structure of salts and HBDs of the DESs studied in this work.

A survey of the literature shows that large numbers of the works on DESs are application-oriented and most of which have been carried out in ChCl-based DESs.[19, 22, 118] Several new and promising DESs based on various other salts are gaining attention recently.[33, 49, 59, 120-130] However, the knowledge about the microscopic structural and dynamical features of these less-explored DESs is still lacking. Further, recognizing the fact that a change of the hydrocarbon chain length at HBD significantly modifies these fundamental features of the alcohol-based DESs, similar studies probing how the alkyl chain length attached to the cation of the salt influences these aspects need to be performed. Keeping these in mind, in this work, we aimed to obtain an in-depth insight into these aspects of a set of promising but less-explored eutectic solvents comprising tetraalkylammonium bromide salts and ethylene glycol (Chart 1.7) through characterization of the microscopic structure, dynamics, and solute-solvent interactions by monitoring the fluorescence response of two dipolar (C153 and 4-AP) and a nonpolar (9-PA) solutes (Chart 1.8) in these media.

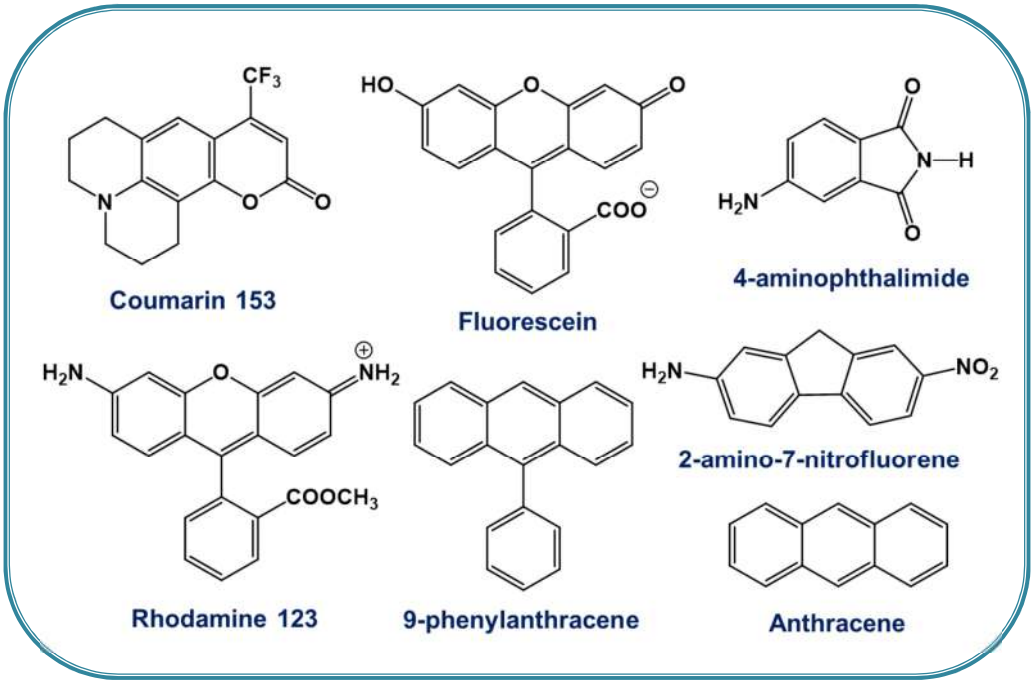

Chart 1.8. Structure of the probe molecules used for various photophysical studies in the DESs.

As the dynamics of solvation often determines the fate of many chemical processes and can uncover unique characteristics of a solvent,[97, 131] solvation dynamics has also been studied in some DESs in recent years.[28, 52-56, 132] Although the overall nature of solvation dynamics in DESs is understood qualitatively, very little of the early part of the solvation dynamics has been explored till date due to limited time-resolution of the TCSPC technique (the one employed in most of the cases). In view of the above, we have attempted to obtain insight into the complete solvation dynamics of C153 in some less-explored DESs comprising ethylene glycol and tetraalkylammonium bromide salts (Chart 1.7) with variable alkyl chain length. In order to capture the entire dynamics occurring in these solvents in a timescale of few femtoseconds to several nanoseconds, we have employed a combination of TCSPC and fluorescence UPC techniques for monitoring the TDFSS of C153 (Chart 1.8).

Very recently, DESs have received great attention in various bio-related fields like biocatalysis, and extraction and preservation of several biomolecules, such as protein, DNA, etc.[80, 133-137] Though few studies have been performed to explore the structure, stability and activity of some selected protein molecules in DESs,[138-140] these reports are qualitative and do not shed complete light on the molecular level interactions. Moreover, all these studies are conducted in ensemble conditions without any report at the single-molecule level, which gives better information about the structure and dynamics of the biomolecules. As protein molecules are highly dynamic in nature, it is very crucial to study the dynamics of the processes associated with them to completely understand their role in any biological function. Surprisingly, there are no studies so far on the conformational dynamics of any protein in these novel solvents. This motivated us to look into both the structural stability as well as conformational dynamics of protein molecule in DESs. In the present work, we have examined the influence of two DESs comprising betaine and ethylene glycol or glycerol (Chart 1.7) on the structural stability and conformational dynamics of a well-known protein, cytochrome c, both in single-molecule and ensemble conditions employing FCS and other biophysical methods, respectively.

References

1. E. Buncel and R. A. Stairs, *Solvent Effects in Chemistry, 2nd ed.*, 2015, Wiley: New York, USA.
2. D. Joshi and N. Adhikari, *J. Pharm. Res. Int.*, 2019, **28**, 1-18.
3. M. Tobiszewski, S. Tsakovski, V. Simeonov, J. Namieśnik and F. Pena-Pereira, *Green Chem.*, 2015, **17**, 4773-4785.
4. R. Gani, C. Jiménez-González and D. J. Constable, *Comput. Chem. Eng.*, 2005, **29**, 1661-1676.
5. P. Anastas and N. Eghbali, *Chem. Soc. Rev.*, 2010, ***39***, 301-312.
6. M. Petkovic, K. R. Seddon, L. P. N. Rebelo and C. S. Pereira, *Chem. Soc. Rev.*, 2011, **40**, 1383-1403.
7. R. D. Rogers and K. R. Seddon, *Science*, 2003, **302**, 792−793.
8. K. R. Seddon, *Nat. Mater.*, 2003, **2**, 363–365.
9. T. Welton, *Chem. Rev.*, 1999, **99**, 2071–2083.
10. N. V. Plechkova and K. R. Seddon, *Chem. Soc. Rev*, 2008, **37**, 123−150.
11. N. V. Plechkova and K. R. Seddon, *Methods and Reagents for Green Chemistry: An Introduction, Chapter 5*, 2007, 103-130.
12. M. A. Kareem, F. S. Mjalli, M. A. Hashim and I. M. Al Nashef, *J. Chem. Eng. Data*, 2010, **55**, 4632−4637.
13. A. Romero, A. Santos, J. Tojo and A. Rodríguez, *J. Hazard Mater*, 2008, **151**, 268-273.
14. A. S. Wells and V. T. Coombe, *Org. Process Res. Dev.*, 2006, **10**, 794-798.
15. A. P. Abbott, G. Capper, D. L. Davies, H. L. Munro, R. K. Rasheed and V. Tambyrajah, *Chem. Commun.*, 2001, 2010-2011.
16. A. P. Abbott, G. Capper, D. L. Davies, R. K. Rasheed and V. Tambyrajah, *Chem. Commun.*, 2003, **1**, 70−71.
17. A. P. Abbott, D. Boothby, G. Capper, D. L. Davies and R. K. Rasheed, *J. Am. Chem. Soc.*, 2004, **126**, 9142−9147.
18. C. Ruβ and B. Konig, *Green Chem.*, 2012, **14**, 2969−2982.
19. Q. Zhang, K. D. O. Vigier, S. Royer and F. Jé rôme, *Chem. Soc. Rev.*, 2012, **41**, 7108−7146.
20. M. Francisco, A. van den Bruinhorst and M. C. Kroon, *Angew. Chem., Int. Ed.*, 2013, **52**, 3074−3085.
21. D. A. Alonso, A. Baeza, R. Chinchilla, G. Guillena, I. M. Pastor and D. J. Ramón, *Eur. J. Org. Chem.*, 2016, **2016**, 612–632.
22. E. L. Smith, A. P. Abbott and K. S. Ryder, *Chem. Rev.*, 2014, **114**, 11060−11082.
23. A. Paiva, R. Craveiro, I. Aroso, M. Martins, R. L. Reis and A. R. C. Duarte, *ACS Sustain. Chem. Eng.*, 2014, **2**, 1063−1071.
24. Y. Dai, J. van Spronsen, G. J. Witkamp, R. Verpoorte and Y. H. Choi, *Anal. Chim. Acta*, 2013, **766**, 61−68.
25. D. V. Wagle, H. Zhao and G. A. Baker, *Acc. Chem. Res.*, 2014, **47**, 2299−2308.
26. A. P. Abbott, J. C. Barron, K. S. Ryder and D. Wilson, *Chem. Eur. J.*, 2007, **13**, 6495-6501.

27. A. Das, S. Das and R. Biswas, *J. Chem. Phys.* , 2015, **142**, 034505.
28. K. Mukherjee, E. Tarif, A. Barman and R. Biswas, *Fluid Phase Equilib.*, 2017, **448**, 22-29.
29. Y. Cui and D. G. Kuroda, *J. Phys. Chem. A* 2018, **122**, 1185−1193.
30. S. Suriyanarayanan, G. D. Olsson, S. Kathiravan, N. Ndizeye and I. A. Nicholls, *Int. J. Mol. Sci.*, 2019, **20**, 2857.
31. N. Subba, N. Das and P. Sen, *J. phys. Chem. B*, 2020, **124**, 6875-6884.
32. L. Percevault, A. Jani, T. Sohier, L. Noirez, L. Paquin, F. Gauffre and D. Morineau, *J. Phys. Chem. B*, 2020, **124**, 9126-9135.
33. G. García, S. Aparicio, R. Ullah and M. Atilhan, *Energy Fuels*, 2015, **29**, 2616−2644.
34. R. Craveiro, I. Aroso, V. Flammia, T. Carvalho, M. T. Viciosa, M. Dionísio, S. Barreiros, R. L. Reis, A. R. C. Duarte and A. Paiva, *J. Mol. Liq.*, 2016, **215**, 634-540.
35. F. Chemat, H. Anjum, A. M. Shariff, P. Kumar and T. Murugesan, *J. Mol. Liq.*, 2016, **218**, 301-308.
36. J. Wang and N. Baker Sheila, *Green Proc. Synth.*, 2018, **7**, 353-359.
37. A. Alhadid, L. Mokrushina and M. Minceva, *J. Mol. Liq.*, 2020, **314**, 11366.
38. F. S. Mjalli and J. Naser, *Asia-Pac. J. Chem. Eng.*, 2015, **10**, 273-281.
39. K. Shahbaz, S. Baroutian, F. S. Mjalli, M. A. Hashim and I. M. AlNashef, *Thermochim. Acta*, 2012, **527**, 59-66.
40. A. Yadav and S. Pandey, *J. Chem. Eng. Data*, 2014, **59**, 2221-2229.
41. M. B. Taysun, E. Sert and F. S. Atalay, *J. Chem. Eng. Data*, 2017, **62**, 1173−1181.
42. A. R. Harifi-Mood and R. Buchner, *J. Mol. Liq.*, 2017, **225**, 689-695.
43. H. Ghaedi, M. Ayoub, S. Sufian, A. M. Shariff and B. Lal, *J. Mol. Liq.*, 2017, **241**, 500-510.
44. L. Bahadori, N. S. A. Manan, M. H. Chakrabarti, M. A. Hashim, F. S. Mjalli, I. M. AlNashef, M. A. Hussain and C. T. J. Low, *Phys. Chem. Chem. Phys.*, 2013, **15**, 1707-1714.
45. C. Reichardt, *Chem. Rev.*, 1994, **94**, 2319-2358.
46. C. Florindo, A. J. S. McIntosh, T. Welton, L. C. Branco and I. M. Marrucho, *Phys. Chem. Chem. Phys.*, 2018, **20**, 206-213.
47. A. Pandey, R. Rai, M. Pal and S. Pandey, *Phys. Chem. Chem. Phys.*, 2014, **16**, 1559-1568.
48. A. P. Abbott, R. C. Harris, K. S. Ryder, C. D'Agostino, L. F. Gladdenb and M. D. Mantle, *Green Chem.*, 2011, **13**, 82-90.
49. A. Basaiahgari, S. Panda and R. L. Gardas, *J. Chem. Eng. Data*, 2018, **63**, 2613-2627.
50. D. Rengstl, V. Fischer and W. Kunz, *Phys. Chem. Chem. Phys.*, 2014, **16**, 22815-22822.
51. K. Shahbaz, F. S. Mjalli, G. Vakili-Nezhaad, I. M. AlNashef, A. Asadov and M. M. Farid, *J. Mol. Liq.*, 2016, **222**, 61-66.
52. A. Das and R. Biswas, *J. Phys. Chem. B*, 2015, **119**, 10102−10113.

53. B. Guchhait, S. Das, S. Daschakraborty and R. Biswas, *J. Chem. Phys.*, 2014, **140**, 104514.
54. A. H. Turner and D. Kim, *J. Chem. Phys.*, 2018, **149**, 174503.
55. S. Chatterjee, D. Ghosh, T. Haldar, P. Deb, S. S. Sakpal, S. H. Deshmukh, S. M. Kashid and S. Bagchi, *J. Phys. Chem. B*, 2019, **123**, 9355-9363.
56. Y. Cui, K. D. Fulfer, J. Ma, T. K. Weldeghiorghis and D. G. Kuroda, *Phys. Chem. Chem. Phys.*, 2016, **18**, 31471-31479.
57. V. Alizadeh, D. Geller, F. Malberg, P. B. Sánchez, A. Padua and B. Kirchner, *ChemPhysChem*, 2019, **20**, 1786-1792.
58. M. Brunner, S. Imberti, G. G. Warr and R. Atkin, *J. Phys. Chem. B*, 2020, **124**, 8651-8664.
59. S. McDonald, T. Murphy, S. Imberti, G. G. Warr and R. Atkin, *J. Phys. Chem. Lett.* , 2018, **9**, 3922-3927.
60. S. Kaur, A. Gupta and H. K. Kashyap, *J. Phys. Chem. B*, 2016, **120**, 6712-6720.
61. A. Faraone, D. V. Wagle, G. A. Baker, E. C. Novak, M. Ohl, D. Reuter, P. Lunkenheimer, A. Loidl and E. Mamontov, *J. Phys. Chem. B*, 2018, **122**, 1261-1267.
62. R. Stefanovic, M. Ludwig, G. B. Webber, R. Atkin and A. J. Page, *Phys. Chem. Chem. Phys.*, 2017, **19**, 3297-3306.
63. A. P. Abbott, G. Capper, K. J. McKenzie and K. S. Ryder, *J. Electroanal. Chem.*, 2007, **599**, 288-294.
64. A. P. Abbott, G. Capper, A. Glidle and K. S. Ryder, *Phys. Chem. Chem. Phys.*, 2006, **8**, 4214−4221.
65. A. P. Abbott, K. E. Ttaib, G. Frisch, K. J. McKenzie and K. S. Ryder, *Phys. Chem. Chem. Phys.*, 2009, **11**, 4269-4277.
66. A. P. Abbott, G. Capper, K. J. McKenzie and K. S. Ryder, *Electrochim. Acta*, 2006, **51**, 4420-4425.
67. P. M. Pawar, K. J. Jarag and G. S. Shankarling, *Green Chem.*, 2011, **13**, 2130-2134.
68. S. B. Phadtare and G. S. Shankarling, *Green Chem.*, 2010, **12**, 458-462.
69. N. Azizi, E. Batebi, S. Bagherpoura and H. Ghafuri, *RSC Adv.*, 2012, **2**, 2289-2293.
70. E. R. Cooper, C. D. Andrews, P. S. Wheatley, P. B. Webb, P. Wormald and R. E. Morris, *Nature*, 2004, **430**, 1012-1016.
71. E. R. Parnham and R. E. Morris, *J. Am. Chem. Soc.*, 2006, **128**, 2204-2205.
72. H.-G. Liao, Y.-X. Jiang, Z.-Y. Zhou, S.-P. Chen and S.-G. Sun, *Angew. Chem.*, 2008, **120**, 9240−9243.
73. H.-R. Jhong, D. S.-H. Wong, C.-C. Wan, Y. Wang, -Y. and T.-C. Wei, *Electrochem. Commun.*, 2009, **11**, 209-211.
74. C. A. Nkuku and R. J. LeSuer, *J. Phys. Chem. B*, 2007, **111**, 13271–13277.
75. H. G. Morrison, C. C. Sun and S. Neervannan, *Int. J. Pharm.*, 2009, **378**, 136-139.
76. D. Z. Troter, Z. B. Todorović, D. R. Đokić-Stojanović, O. S. Stamenković and V. B. Veljković, *Renew. Sust. Energ. Rev.*, 2016, **61**, 473-500.

77. K. Shahbaz, F. S. Mjalli, M. A. Hashim and I. M. ALNashef, *J. Applied Sci.*, 2010, **10**, 3349-3354.
78. K. Shahbaz, F. S. Mjalli, M. A. Hashim and I. M. AlNashef, *Energy Fuels*, 2011, **25**, 2671−2678.
79. Y. Gu and F. Jérôme, *Chem. Soc. Rev.*, 2013, **42**, 9550-9570.
80. P. Xu, G.-W. Zheng, M.-H. Zong, N. Li and W.-Y. Lou, *Bioresour. Bioprocess.*, 2017, ***4***, 34.
81. S. Mao, K. Li, Y. Hou, Y. Liu, S. Ji, H. Qin and F. Lu, *J. Chem. Technol. Biotechnol.*, 2018, **93**, 2729-2736.
82. Y. P. Mbous, M. Hayyan, A. Hayyan, W. F. Wong, M. A. Hashima and C. Y. Looi, *Biotechnol. Adv.*, 2017, **35**, 105-134.
83. D. Carriazo, M. C. Serrano, M. C. Gutiérrez, M. L. Ferrer and F. d. Monte, *Chem. Soc. Rev.*, 2012, **41**, 4996–5014.
84. J.-H. Liao, P.-C. Wu and Y.-H. Bai, *Inorg. Chem. Commun.*, 2005, **8**, 390−392.
85. R. B. Leron and M.-H. Li, *Thermochim. Acta*, 2013, **551**, 14−19.
86. R. B. Leron and M.-H. Li, *J. Chem. Thermodyn.*, 2013, **57**, 131−136.
87. J. R. Lakowicz, *Principles of Fluorescence Spectroscopy, 3rd ed.*, 2006, Springer: New York, USA.
88. G. R. Fleming, *Chemical Applications of Ultrafast Spectroscopy*, 1986, Oxford University Press: New York, USA.
89. C. Q. Sun, *Solvation Dynamics: A Notion of Charge Injection, 1st ed.*, 2019, Springer: Singapore.
90. S. Park and T. Joo, *J. Chem. Phys.*, 2009, **131**, 164508.
91. X.-X. Zhang, M. Liang, J. Hunger, R. Buchner and M. Maroncelli, *J. Phys. Chem. B*, 2013, **117**, 15356-15368.
92. T. Joo, Y. Jia, J.-Y. Yu, M. J. Lang and G. R. Fleming, *J. Chem. Phys.*, 1996, **104**, 6089.
93. M. Cho and G. R. Fleming, *J. Chem. Phys.*, 1993, **98**, 2848.
94. Z. Ren, A. S. Ivanova, D. Couchot-Vore and S. Garrett-Roe, *J. Phys. Chem. Lett.*, 2014, **5**, 1541-1546.
95. R. Jimenez, G. R. Fleming, P. V. Kumar and M. Maroncelli, *Nature*, 1994, **369**, 471-473.
96. A. Samanta, *J. Phys. Chem. B*, 2006, **110**, 13704-13716.
97. B. Bagchi and B. Jana, *Chem. Soc. Rev.*, 2010, **39**, 1936-1954.
98. S. K. Pal, J. Peon, B. Bagchi and A. H. Zewail, *J. Phys. Chem. B*, 2002, **106**, 12376-12395.
99. M. Maroncelli, J. McInnis and G. R. Fleming, *Science*, 1989, **243**, 1674-1681.
100. K. Makuch, R. Hołyst, T. Kalwarczyk, P. Garstecki and J. F. Brady, *Soft Matter*, 2020, **16**, 114-124.
101. D. Magde, E. L. Elson and W. W. Webb, *Phys. Rev. Lett.*, 1972, **29**, 705-708.
102. R. Rigler and E. S. Elson, *Fluorescence Correlation Spectroscopy: Theory and Applications*, 2001, Springer: New York, USA.
103. D. L. Nelson and M. M. Cox, *W. H. Freeman and Company: New York, USA.*, 2004.

104. K. A. Dill, K. Ghosh and J. D. Schmit, *Proc. Natl. Acad. Sci. USA*, 2011, **108**, 17876-17882.
105. E. Buxbaum, *Fundamentals of Protein Structure and Function, 2nd ed.*, 2015, Springer: New York, USA.
106. *https://content.byui.edu/file/a236934c-3c60-4fe9-90aa-d343b3e3a640/1/module3/readings/proteins.html*.
107. J. Evenas, S. Forsen, A. Malmendal and M. Akke, *J. Mol. Biol.*, 1999, **289**, 603-617.
108. K. Henzler-Wildman and D. Kern, *Nature*, 2007, **450**, 964-972.
109. H. Frauenfelder, S. G. Sligar and P. G. Wolynes, *Science*, 1991, ***254***, 1598-1603.
110. K. Teilum, J. G. Olsen and B. B. Kragelund, *Cell. Mol. Life Sci.*, 2009, **66**, 2231-2247.
111. P. K. Agarwal, *Microb. Cell Fact.*, 2006, **5**, 2.
112. J. W. Longworth, *Excited States of Proteins and Nucleic Acids, Chapter 6*, 1971, Plenum Press: New York, USA.
113. M. J. Kronman and L. G. Holmes, *Photochem. Photobiol*, 1971, **14**, 113-134.
114. K. Chattopadhyay, E. L. Elson and C. Frieden, *Proc. Natl. Acad. Sci. USA*, 2005, **102**, 2385-2389.
115. W. Bi, M. Tian and K. H. Row, *J. Chromatogr. A*, 2013, **1285**, 22-30.
116. H. Cruz, N. Jordão and L. C. Branco, *Green Chem.*, 2017, **19**, 1653-1658.
117. Z. S. Othman, N. H. Hassan and S. I. Zubairi, *AIP Conference Proceedings*, 2015, **1678**, 050004.
118. Baokun Tang and K. H. Row, *Monatsh Chem*, 2013, **144**, 1427-1454.
119. R. M. Harris, *PhD Thesis*, 2008, University of Leicester.
120. M. K. AlOmar, M. Hayyan, M. A. Alsaadi, S. Akib, A. Hayyan and M. A. Hashim, *J. Mol. Liq.*, 2016, **215**, 98-103.
121. J. Dou, Y. Zhao, F. Yin, H. Li and J. Yu, *Environ. Sci. Technol.*, 2019, **53**, 1031-1038.
122. B. Jibril, F. Mjalli, J. Naser and Z. Gano, *J. Mol. Liq.*, 2014, **199**, 462-469.
123. C. Li, D. Li, S. Zou, Z. Li, J. Yin, A. Wang, Y. Cui, Z. Yaoa and Q. Zhao, *Green Chem.*, 2013, **15**, 2793-2799.
124. J.-j. Li, H. Xiao, X.-d. Tang and M. Zhou, *Energy Fuels*, 2016, **30**, 5411-5418.
125. F. S. Mjalli, J. Naser, B. Jibril, V. Alizadeh and Z. Gano, *J. Chem. Eng. Data*, 2014, **59**, 2242-2251.
126. M. Mohan, P. K. Naik, T. Banerjee, V. V. Goud and S. Paul, *Fluid Phase Equilib.*, 2017, **448**, 168-177.
127. N. Nkosi, K. Tumba and S. Ramsuroop, *J. Chem. Eng. Data*, 2018, **63**, 4502-4512.
128. S. K. Shukla and J.-P. Mikkola, *Phys. Chem. Chem. Phys.*, 2018, **20**, 24591-24601.
129. A. R. R. Teles, E. V. Capela, R. S. Carmo, J. A. P. Coutinho, A. J. D. Silvestre and M. G. Freire, *Fluid Phase Equilib.*, 2017, **448**, 15-21.
130. R. Yusof, E. Abdulmalek, K. Sirat and M. B. A. Rahman, *Molecules*, 2014, **19**, 8011-8026.

131. A. Nitzan, *Chemical Dynamics in Condensed Phases*, 2006, Oxford University Press: New York, USA.
132. N. Subba, K. Polok, P. Piatkowski, B. Ratajska-Gadomska, R. Biswas, W. Gadomski and P. Sen, *J. Phys. Chem. B*, 2019, **123**, 9212-9221.
133. J. T. Gorke, F. Srienc and R. J. Kazlauskas, *Chem. Commun.*, 2008, 1235-1237.
134. A. Grudniewska, E. M. d. Melo, A. Chan, R. Gniłka, F. Boratyński and A. S. Matharu, *ACS Sustainable Chem. Eng.*, 2018, ***6***, 15791-15800.
135. D. Mondal, M. Sharma, C. Mukesh, V. Gupta and K. Prasad, *Chem. Commun.*, 2013, ***49***, 9606-9608.
136. M. Ruesgas-Ramón, M. L. Suárez-Quiroz, O. González-Ríos, B. Baréa, G. Cazals, M. C. Figueroa-Espinoza and E. Durand, *J. Sci. Food Agric.*, 2020, ***100***, 81-91.
137. Q. Zeng, Y. Wang, Y. Huang, X. Ding, J. Chen and K. Xu, *Analyst*, 2014, ***139***, 2565-2573.
138. R. Esquembre, J. M. Sanz, J. G. Wall, F. d. Monte, C. R. Mateo and M. L. Ferrer, *Phys. Chem. Chem. Phys.*, 2013, ***15***, 11248-11256.
139. H. Monhemi, M. R. Housaindokht, A. A. Moosavi-Movahedi and M. R. Bozorgmehr, *Phys. Chem. Chem. Phys.*, 2014, ***16***, 14882-14893.
140. A. Sanchez-Fernandez, K. J. Edler, T. Arnold, D. A. Venerod and A. J. Jackson, *Phys. Chem. Chem. Phys.*, 2017, ***19***, 8667-8670

Chapter 2

Materials, Methods and Instrumentation

Overview

This chapter provides information on the sources of chemicals, and preparation, characterization and purification of different substances used in this study. The procedures of sample preparation for different spectroscopic and microscopic experiments are also described. The working principle, instrumental setup and methods for acquisition and analysis of picosecond TCSPC, femtosecond fluorescence UPC and single-molecule FCS data are discussed in details. In addition, a brief account of other instruments used in this study, such as UV-vis spectrophotometer, spectrofluorometer, spectropolarimeter, ^{1}H-NMR, FTIR and viscometer are also provided.

2.1. Materials

Choline chloride (≥ 98%), betaine (≥ 99%), glycerol (≥ 99.5%), ethylene glycol/1,2-ethanediol (≥ 99%), 1,3-propanediol (98%), 1,4-butanediol (99%), 1,2-butanediol (≥ 98%), 1,3-butanediol (98%), and 2,3-butanediol (98%) were purchased from Sigma-Aldrich. Tetraethylammonium bromide (> 98%), tetrapropylammonium bromide (> 98%), and tetrabutylammonium bromide (> 99%) were procured from TCI Chemicals. These chemicals were dried under high vacuum for 30-40 hours prior to use. 4-aminophthalimide and laser grade coumarin 153 dye were obtained from TCI Chemicals and Eastman Kodak, respectively. Rhodamine 123, rhodamine 6G, fluorescein, anthracene, and 9-phenylanthracene were obtained from Sigma-Aldrich. Alexa Fluor 488 C_5 maleimide dye was purchased from Molecular Probes, Invitrogen. All these dyes were used as received. Methanol, ethanol, hexane, acetone, ethyl acetate were procured from Merck. Deuterated solvent, methanol-d_4 (CD_3OD, ≥ 99.8 atom %D) was purchased from Sigma-Aldrich and used as received. Guanidine hydrochloride (≥ 99%), disodium hydrogen phosphate (Na_2HPO_4, ≥ 98%) and sodium dihydrogen phosphate (NaH_2PO_4, ≥ 99%) were obtained from Merck and used as received. Various drying agents, such as phosphorous pentoxide (P_2O_5), iodine (I_2) and magnesium turnings as well as molecular sieves were obtained from local suppliers. Iso-1-cytochrome c from the yeast *Saccharomyces cerevisiae* and sephadex G-25 gel filtration medium were procured from Sigma-Aldrich. The purity of the reagents was checked using NMR, UV-vis absorption and emission spectroscopy. Milli-Q water was used for preparations of buffers and other aqueous medium based experiments.

2.2. Purification of Conventional Solvents

Various conventional solvents used at different stages of the experiments were purified by following the standard procedures available in the literature.[1] After drying, the purified solvents were stored in air tight glass bottles for further use with added molecular sieves to protect from the moisture.

Methanol and ethanol: Initially, refluxed for 3-4 hours with Mg turnings and iodine in a RB flask, and then distilled and stored under moisture free atmospheric conditions.

Hexane: The solvents were refluxed in presence of metallic sodium for 3-4 hours and then benzophenone was added after cooling. The dark solution was refluxed for another hour and then distilled and stored under moisture free atmospheric conditions.

Acetone and acetonitrile: The solvents were first refluxed for 3-4 hours with anhydrous P_2O_5 and then distilled and stored under moisture free conditions.

Ethyl acetate: After stirring with P_2O_5 for 3-4 hours, the solvent was distilled and stored under moisture free conditions.

Water: Milli-Q grade water was obtained from Millipore, Synergy Pack water purification system.

2.3 Sample Preparation

2.3.1. Preparation and Characterization of DESs

All the DESs were prepared following previously reported procedures.[2-5] Each salt/HBA and HBD combination was mixed in a particular molar ratio (details are provided in the subsequent chapters) in a conical flask and heated at 333-353 K in an oil bath with constant stirring until a transparent homogeneous liquid was obtained. The liquids were then slowly cooled down to the room temperature (298 K) and stored in an inert atmosphere prior to experiments. The purity of the prepared DESs (and their constituents) was checked through ^{1}H NMR spectroscopy (spectral data are provided in the Appendices). The structural identity of the DESs was confirmed by the FTIR spectra (see Appendices). Comparison of the NMR and FTIR spectra of the prepared DESs with the literature data of the DESs indicate that no side reactions occurred during the preparation of the DESs and the prepared liquids were pure.[6-9] The viscosities of the prepared DESs were measured at 298 K (see subsequent chapters), and were found to be in agreement with previously reported values.[3, 4, 10] The water content in the DESs was determined after drying under high vacuum for several hours, and the measured values (see subsequent chapters) were in good agreement with the literature data.[8, 11]

2.3.2. Preparation of Dye Solutions in DESs

Solutions of individual solutes were prepared in methanol/ethanol (except for ANT and 9-PA, which were prepared in hexane). A few microliters of freshly prepared solution of the solutes was transferred into a reagent bottle and the solvent was then evaporated by flowing ultra-high purity N_2 gas. Then, a measured amount of DES was added into the reagent bottle, tightly sealed with rubber septum and parafilm, and the solution was slightly heated and mixed thoroughly to ensure complete dissolution of the solutes. The

solution was then allowed to cool down slowly to the room temperature and was stored under inert atmosphere prior to experiments and used as stock solution. For all steady-state and time-resolved measurements (fluorescence intensity and anisotropy decay), the samples were prepared maintaining the concentration of the solutions such that the absorbance was less than 0.2 at the excitation wavelength (for 1 cm optical path) to avoid unnecessary problems due to inner filter effects. However, for fluorescence UPC measurements, a solution with absorbance value of around 1.5 at the excitation wavelength (for 1 cm optical length) was used. As the studied DESs are hygroscopic, the sample containing cells in all experiments were tightly sealed with rubber septum and parafilm to avoid absorption of moisture. A micromolar (μM) solution of the DESs was used for steady-state and time-resolved fluorescence measurements while nanomolar (nM) solution was used for the FCS measurements.

2.3.3. Protein Labeling and Sample Preparation

The covalent labeling of Cytc to its single free cysteine at position 102 with A488 dye was carried out following a reported method.[12] A488 was dissolved in 100 mM sodium phosphate buffer (pH 7.0). A five-fold molar excess of A488 was added to Cytc dissolved in the same buffer. The mixture was then kept in the dark for two hours at room temperature for completion of the reaction. The labeled protein was separated from excess free dye using a sephadex G-25 column (30 cm x 1.3 cm) pre-equilibrated with the buffered solution. Dye labeling was confirmed using absorption and fluorescence spectroscopy (Figure A4.3 of Appendices). The dye/protein ratio in the labeled protein was calculated using absorbance and molar extinction coefficient values (106 mM^{-1} cm^{-1} for Cytc at 410 nm[13] and 72 mM^{-1} cm^{-1} for A488 at 493 nm[14]) and was found to be ~ 0.98. Comparison of the absorption, fluorescence (Figure A4.3) and CD spectra (Figure A4.4) revealed that the labeling of A488 dye at position 102 of Cytc did not induce any detectable structural perturbation.[12]

The samples for all experiments were prepared in 100 mM phosphate buffered solution. Protein samples in various concentrations of DESs/GdHCl were prepared and kept overnight prior to experiments. The steady-state/time-resolved fluorescence and FCS measurements were performed with A488-labeled Cytc (Cytc-A488), whereas unlabeled Cytc was used for the CD and absorption measurements. The protein concentration in the samples used for steady-state (absorption or fluorescence)/time-resolved fluorescence and

CD measurements was about 4 and 40 μM, respectively. For FCS measurements the samples were prepared keeping A488 concentration of ~ 2 nM.

2.4. Methods and Instrumentation

2.4.1. Picosecond TCSPC Setup

TCSPC is a time-resolved fluorescence technique widely used for many applications, such as measurements of fluorescence lifetime, rotational diffusion dynamics, and solvation dynamics etc.[15, 16] It is a digital counting technique that relies on statistical method of counting. It acts like a stopwatch, where a sample is generally excited by a pulsed laser with high repetition rate (> kHz) to start the event which then subsequently stops after detection of a single photon from the sample. The time duration from the excitation of the sample to arrival of a single photon in the detector is stored as a histogram which represents the probability distribution of detection of single photon at different time. TCSPC can function both in forward and reverse modes. In the former case, a photon from the excitation laser source triggers the start signal, whereas the same job is done by a fluorescence photon from the sample in the latter case. Generally TCSPC instrument is used in the reverse mode, because in the forward mode, a major problem occurs due to a difference in rate between start and stop signal as the TCSPC electronics starts its signal by a high repetition rate laser with respect to the stop signal/emission photons from sample that has much slower detection rates (limited by the dead time of detectors).[16]

Various important components of a typical TCSPC setup operating in the reverse mode are shown in Scheme 2.1. The sequence of events for registering one detected photon of fluorescence is as follows. The experiment starts by the excitation laser pulse that simultaneously excites the samples and sends an excitation signal to a CFD (CFD1). The emitted photons from the sample are detected by a PMT after passing through a polarizer and monochromator. This signal is then received by a second CFD (CFD2), which accurately measures the arrival time of the emitted photon and sends the signal towards the TAC that triggers the charging of a capacitor in the TAC (start pulse) to start the voltage ramp. The other part of the excitation laser pulse (reference pulse) received by the CFD1 is now directed to the TAC (stop pulse) that discharges the capacitor and stops the voltage ramp. An electronic delay is incorporated to the reference pulse to ensure that the pulse arrives at the TAC after the start pulse. The resultant voltage developed in the voltage ramp of TAC is proportional to the time difference between the start and stop pulse (Δt).

This voltage is then amplified by a programmable gain amplifier (PGA) and later converted to a digital number by an analog-to-digital converter (ADC). This numerical

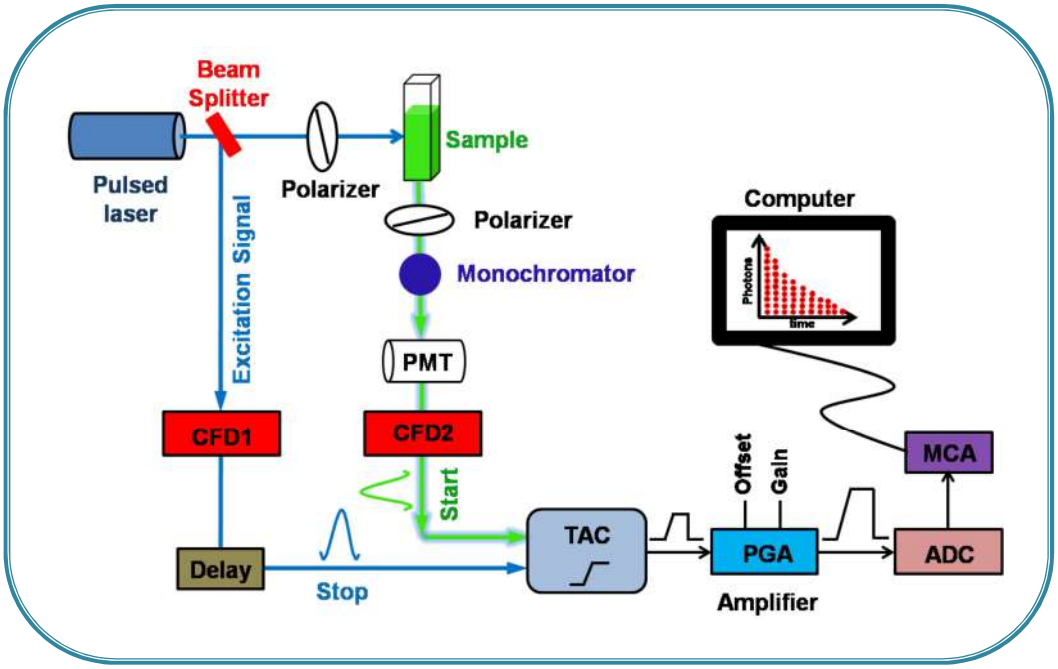

Scheme 2.1. Schematic diagram of a typical TCSPC setup operating in reverse mode.

value with the measured time delay is stored as a single photon event in the MCA. Repeating this whole single-photon counting cycle for a large number of times, a histogram of the fluorescence intensity with time can be constructed.

A picosecond TCSPC setup was used for carrying out various experiments, such as measurements of fluorescence intensity decay and fluorescence anisotropy decay.

2.4.1.1. Fluorescence Intensity Decay Measurements

For the entire thesis work, picoseconds/nanoseconds fluorescence intensity decay measurements were performed using a TCSPC spectrometer (Horiba JobinYvon IBH) in the reverse mode. The fluorescence intensity was collected at magic angle (54.7º) with respect to the vertical polarization of the excitation laser beam to avoid any contributions from fluorescence anisotropy.[15] PicoBrite diode lasers of 375, 405 and 481 nm (1 MHz repetition rate) were used as the excitation sources, and a micro-channel plate

photomultiplier tube (Hamamatsu R3809U-50) was used as the detector. The IRF of the setup, which is governed mainly by the FWHM of the excitation laser pulse (pulse width), was measured by placing a scatterer (dilute aqueous solution of Ludox) in place of the sample cell and was found to be in the range of 60 to 80 ps. The temperature dependent studies were performed using an external Julabo water circulator (model F32) bath. All the measured decay curves were analyzed by nonlinear least squares iteration method using IBH DAS6 (version 2.2) decay analysis software after deconvoluting the IRF from the decay curves. All the decay curves were fitted with an exponential function of the form given by equation 2.1 and the quality of the fit was assessed by the χ^2 values and distribution of the residuals plot.

$$I(t) = \sum_{i=1}^{n} a_i e^{-t/\tau_i} \quad \ldots\ldots\ldots\ldots\ldots\ldots (2.1)$$

where, τ_i and a_i are the time constant and associated amplitude, respectively.

2.4.1.2. Fluorescence Anisotropy Decay Measurements

The fluorescence anisotropy decay measurements were performed using the same TSCPC setup by placing a polarizer in the excitation beam path and another one in front of the detector. The fluorescence intensity in parallel (I_{II}) and perpendicular ($I_{\perp}$) polarization (with respect to the vertically polarized excitation laser beam) was collected alternatively for equal interval of time until the count difference between the two polarizations (at t = 0) was ~5000. The anisotropy measurements were performed at the respective fluorescence maxima of the probe molecules using a monochromator with a band pass of 2 nm. Time-resolved fluorescence anisotropy, r(t), was calculated using the following equation[15]

$$r(t) = \frac{I_{II} - GI_{\perp}}{I_{II} + 2GI_{\perp}} \quad \ldots\ldots\ldots\ldots\ldots\ldots (2.2)$$

where, G is the correction factor for the detector sensitivity to the polarization direction of the emission and was calculated following the same procedure as described above, but with only 5 cycles and horizontal polarization of the exciting laser beam. The rotational reorientation times for different systems were estimated by fitting the fluorescence anisotropy decay profiles following the same analysis procedure described for the fluorescence intensity decay measurements.

2.4.2. Femtosecond Fluorescence UPC Setup

Time-resolved fluorescence UPC is a technique that works on the principle of frequency mixing by NLO process of sum-frequency generation.[17] This technique has an advantage over TCSPC and other fluorescence-based techniques, such as streak camera, in terms of its temporal resolution, which is mainly limited by the width of the gate pulse (vide later section). A temporal resolution of about 100 fs or lesser can be achieved by exciting the sample using an ultra-short pulse of light. Additionally, the ability of exciting different samples over a wide range of wavelengths using ultra-short pulses of the tunable lasers and also using the NLO phenomena, such as second and third harmonic generation, make this technique superior than others. In UPC measurements, a sample is excited using an ultra-short optical pulse and the observed fluorescence is upconverted by mixing with another ultra-short pulse called as gate/probe pulse in a NLO crystal. The upconverted signal is observed through sum-frequency generation, a process that occurs at a particular orientation of the NLO crystal when the phase-matching conditions (equation 2.3) for both gate beam and fluorescence beam are satisfied (Scheme 2.2).[18]

$$n_{uc}\omega_{uc} = n_g\omega_g + n_f\omega_f \qquad \ldots\ldots\ldots\ldots\ldots\ldots (2.3)$$

where, ω_{uc}, ω_g and ω_f are the frequencies of the upconverted/sum-frequency, gate/probe and fluorescence beams, respectively, whereas n_{uc}, n_g and n_f are the refractive indices corresponding to the three beams.

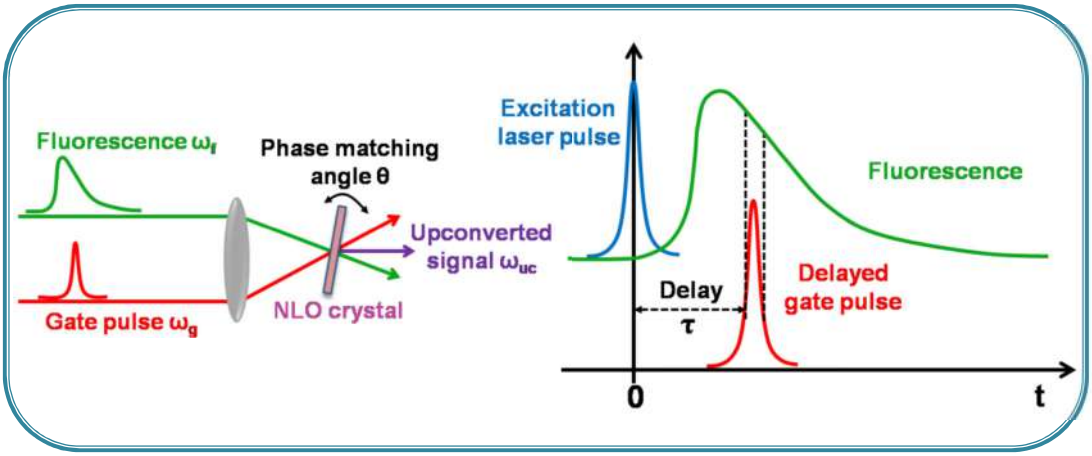

Scheme 2.2. Working principle of fluorescence upconversion technique.

The time-evolution of fluorescence intensity is obtained by recording the upconverted signal at different delay time of the gate pulse with respect to the pump/excitation pulse. The time interval between the pump pulse and the gate pulse is achieved by changing the path length of the gate pulse using a mechanical delay stage. The decay of the upconverted signal essentially represents the decay of fluorescence signal as the intensity of the gate pulse remains same for all the delay times. The intensity of the upconverted signal (I_{uc}) at any given delay time (τ) is proportional to the convolution function (equation 2.4) of the intensity of fluorescence (I_f) and gate beam (I_g).

$$I_{uc}(\tau) = \int_{-\infty}^{\infty} I_f(t) I_g(t-\tau) dt \quad \ldots\ldots\ldots\ldots\ldots\ldots (2.4)$$

The schematic diagram shown below (Scheme2.3) illustrates how time-evolution of the fluorescence intensity from the excited sample is measured.

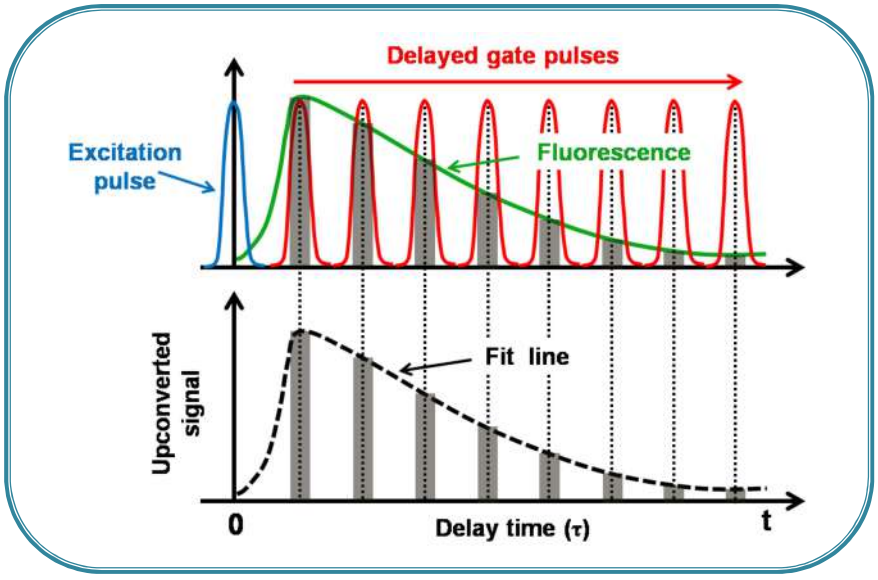

Scheme 2.3. Measurement of time-evolution of the fluorescence intensity at different delay time of the gate pulse using fluorescence upconversion technique.

The sub-picosecond fluorescence intensity decay profiles were measured using a UPC setup (FOG 100, CDP systems, Russia). The schematic diagram of the experimental setup of a typical femtosecond fluorescence UPC spectrometer is shown in Scheme 2.4. In our

UPC measurements, the samples were excited using second harmonic generated optical pulses from a mode-locked Ti:sapphire laser (MaiTai, Spectra Physics, USA). The center wavelength of the MaiTai, set at 800 nm (80 MHz, ~100 fs), was directed to a BBO nonlinear crystal (NLC1) to generate the second harmonic signal (400 nm). The output was then directed to a dichroic beam splitter, which reflected the 400 nm light (used as excitation beam) and transmitted the residual 800 nm light (used as gate beam). The excitation beam was then passed through a filter F_1 (to cut off the residual amount of the

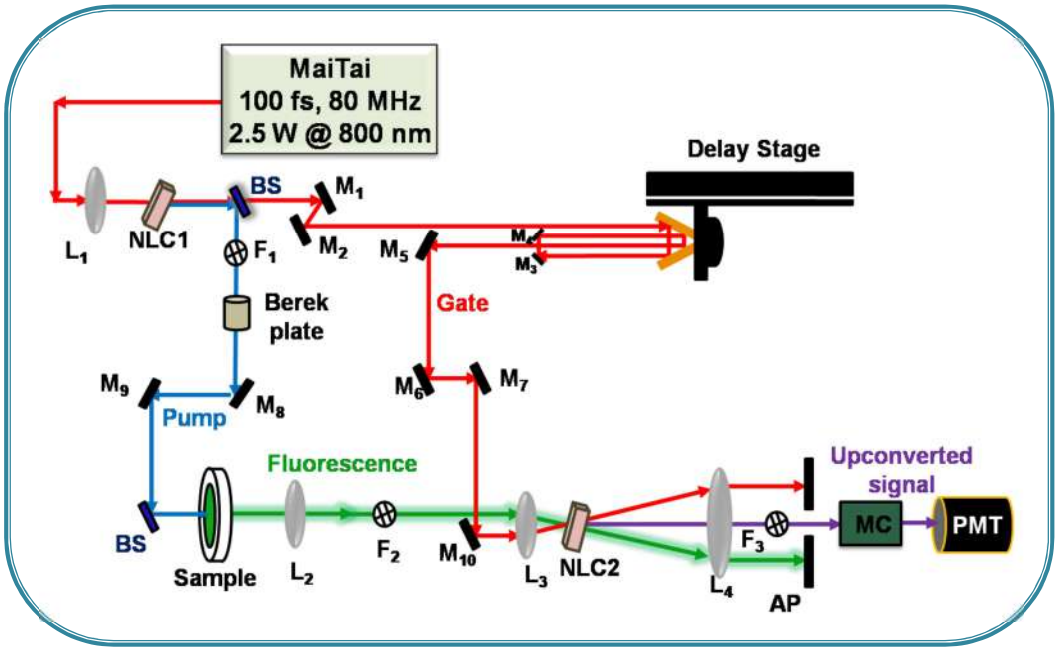

Scheme 2.4. Schematic diagram of the fluorescence upconversion setup. M_i= Mirror, L_i = Lens, F_i = Filter, BS = Beam splitter, AP = Iris aperture.

gate beam) followed by a Berek wave plate and was focused onto the sample. Berek wave plate is placed there in order to change the polarization of the excitation beam to magic angle (54.7°) with respect to the gate beam. The fluorescence signal from the sample was collected and collimated using a lens and was subsequently directed to a sum-frequency mixing BBO crystal (NLC2, 0.5 mm thick) after passing through a filter F_2 (to remove the residual amount of excitation beam). The gate beam, after passing through a motorized optical delay stage (~4 ns), was also directed to the NLC2. The fluorescence and the gate beam were mixed at NLC2 to produce the upconverted signal, which was then passed through a monochromator and directed to the PMT for detection. The monochromator

wavelength was adjusted to the same value as that of the upconverted signal. The IRF of the setup was estimated using the Raman scattering signal from water and was found to be ~ 200 fs. The samples were kept in a rotating cell (1.0 mm path length) to avoid photo-bleaching by exposure of the laser at a single spot. The data acquisition was performed with the Lumex software. All the intensity decay curves were fitted with an exponential function (equation 2.1) by nonlinear least squares iteration method using Igor pro (Version 6.37, Wavemetrics) software. The goodness of the fit was assessed by the χ^2 values and distribution of the residuals plot.

2.4.3. Time-Resolved CFM Setup

As its name suggests, the main aspect of a CFM is achieving a confocal geometry by using a high-power objective lens and placing a pinhole in the image plane of the optical pathway between the sample and detector.[19] The conjugation of the excitation focus and the pinhole creates a spatial filter that eliminates all the fluorescence signals not coming from the defined confocal plane (out-of-focus signals), and allow the signals only from the confocal plane to enter into the detector.[19] Optical layout of a typical CFM setup is presented in Scheme 2.5. The excitation laser beam is directed into a high-power

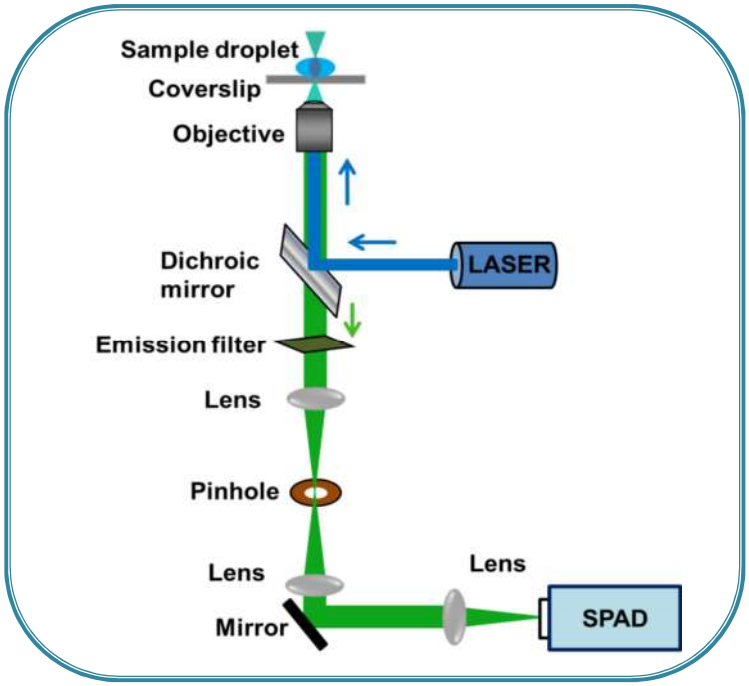

Scheme 2.5. Optical layout of a typical confocal fluorescence microscope setup.

microscope objective through a dichroic mirror, which focuses the laser beam onto the sample. The fluorescence signal from the sample is collected by the same objective and focused onto a pinhole placed in the image plane. Afterwards, the fluorescence signal is collected directly by a photon counting detector, preferably an avalanche photodiode or a photomultiplier with single photon sensitivity.

A time-resolved CFM setup was used to perform all the FCS measurements described in this thesis.

FCS Measurements

In FCS measurements, one analyzes the time-dependent fluorescence intensity fluctuations (by correlating the fluctuating signal) of a diffusing solute from a tiny observation/detection volume (Scheme 2.6a) to obtain valuable information on the dynamical processes occurring in a solution that results into the intensity fluctuations.[15, 20, 21] These processes are mainly translation diffusion, and some other processes like intersystem crossing, molecular interactions, conformational dynamics, excited-state reaction, etc. It is pertinent to mentioned here that, in order to observe an effective intensity fluctuation, these processes must occur within the diffusion time of the probe molecule (average time the molecule take to diffuse through the observation volume).[15, 21] The phenomenon of translation diffusion of a solute molecule through the observation volume and typical fluorescence intensity fluctuations is illustrated in Scheme 2.6b. An autocorrelation function can be generated by correlating this fluctuating fluorescence signal using the mathematical equation of the form:[15, 21]

$$G(\tau) = \frac{\langle \delta F(t) \delta F(t+\tau) \rangle}{\langle F(t) \rangle^2} \dots\dots\dots\dots\dots\dots (2.5)$$

where, $\langle F(t) \rangle$, $\delta F(t)$ and $\delta F(t+\tau)$ are the average fluorescence intensity, the fluctuations in intensity from the average value at time t and $(t+\tau)$ respectively, and are expressed as:

$$\delta F(t) = F(t) - \langle F(t) \rangle \dots\dots\dots (2.6a)$$

$$\delta F(t+\tau) = F(t+\tau) - \langle F(t) \rangle \dots\dots\dots (2.6b)$$

Analysis of the decay of autocorrelation function with time provides important information about the various dynamic processes occurring in the solution.

It is important to note here that, presence of a single molecule or very few molecules in the observation volume is very crucial to observe an effective fluorescence fluctuation, because a large number of molecules will not show any effective fluorescence fluctuation due to the presence of nearly same average number of molecules.[15, 20] To achieve this condition, a highly dilute solution of the samples (~ nM) and a very small observation volume (~ fL) is required. That is why a CFM is suitable for FCS measurement, where a small observation volume is created by the combination of a focused laser beam, an objectives lens with high numerical aperture (ideally > 0.9) and a pinhole.

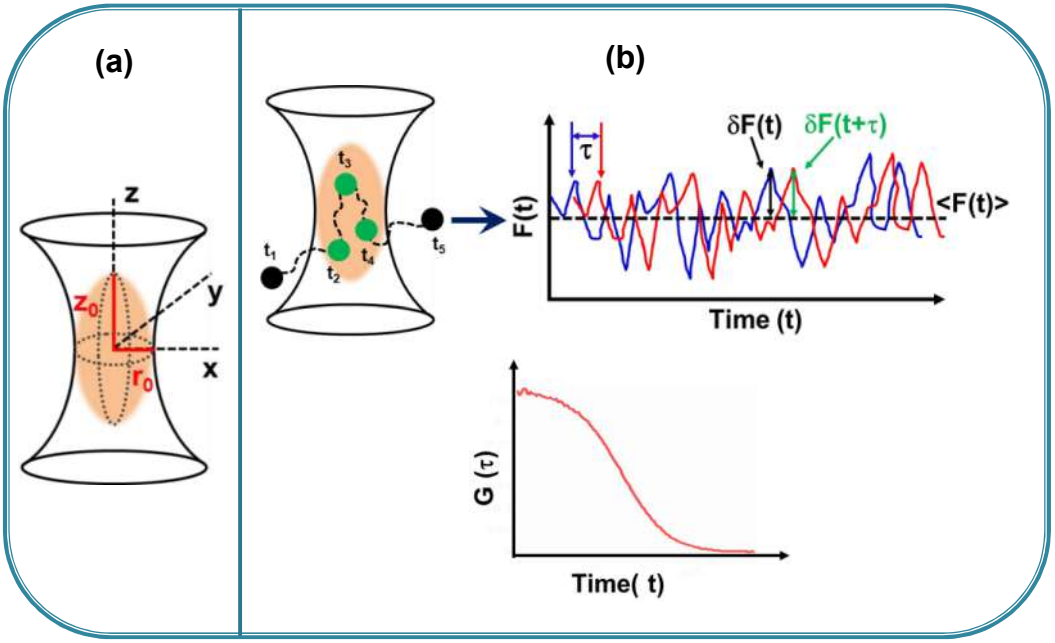

Scheme 2.6. (a) Ellipsoidal observation volume in a CFM setup. (b) Working principle of FCS measurements.

The schematic diagram of the CFM setup (MicroTime 200, PicoQuant) used in our studies is shown in Scheme 2.7. The microscope body of the setup was equipped with an inverted microscope (Olympus IX71) containing a water immersion objective (UPlansApo, NA 1.2, 60X). In our FCS measurements, the samples were excited using picosecond pulsed diode lasers (405 and 485 nm with fwhm 176 and 144 ps, respectively) with a repetition rate of 20 MHz. The output of the laser was coupled with the main optical unit (MOU) through a polarization maintaining single-mode optical fiber. In the main optical unit, the

excitation beam was collimated and directed into the back aperture (entrance port) of the microscope through reflection of the beam using a dichroic mirror (two different dichroic mirrors were used for 405 and 485 nm laser). The beam was subsequently focused onto the sample (~ 50 µL) placed on a cover slip using the objective. A beam splitter was placed in the excitation path (before the dichroic mirror) in order to direct a part of the laser light to a PD which was used for controlling the excitation laser power and the other part to a CCD that was used for focusing and judging the excitation beam quality. The fluorescence signal from the samples was collected by the same objective, and passed through the dichroic mirror followed by an appropriate long-pass filter (430 and 510 nm long-pass filters for 405 and 485 nm laser sources, respectively) to remove any excitation light. The signal was then spatially filtered by focusing onto a 50 µm diameter pinhole to cut off the out-of-focus signals, recollimated, and directed onto a (50:50) beam splitter prior to entering into two SPADs for detection. The fluorescence correlation traces were generated by cross-correlating the signals from the two SPAD detectors, which improve the signal quality and remove artifacts introduced by the individual detectors that generally originates during the generation of autocorrelation function. The data acquisition was

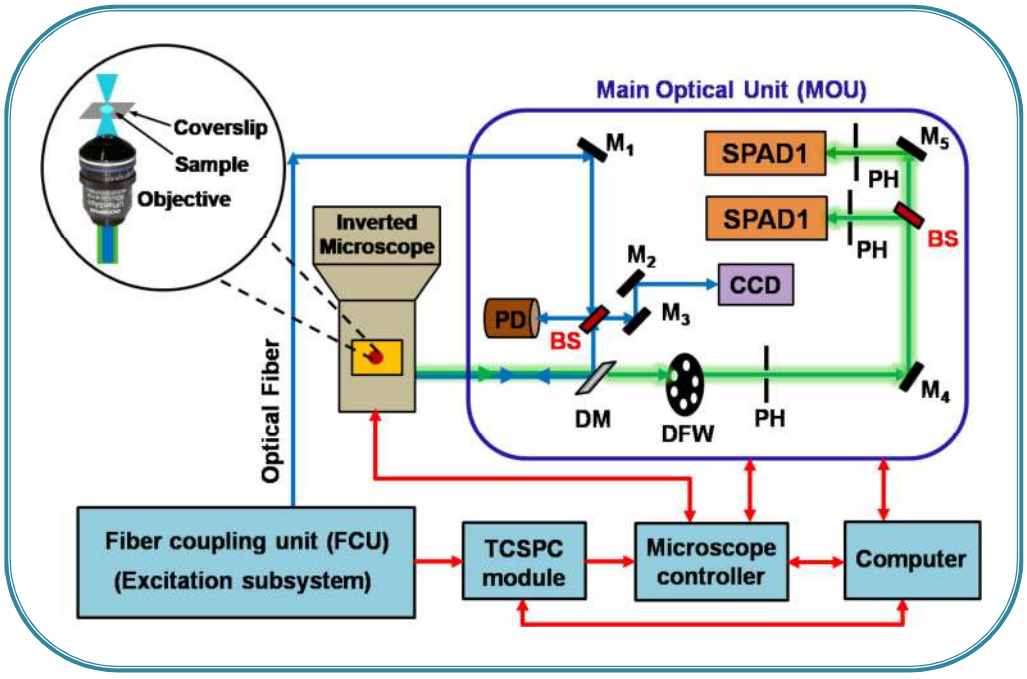

Scheme 2.7. Schematic diagram of the time-resolved CFM setup (adapted from PicoQuant MicroTime 200 user manual). M_i = Mirror, BS = Beam splitter, DM = Dichroic mirror, DFW = Detection filter wheel and PH = Pinhole.

performed in TTTR mode using a SymPhoTime software controlled PicoHarp300 TCSPC module (PicoQuant). During all FCS measurements, the excitation power was kept between ~3 to 15 μW. Low excitation power was used in order to avoid any contribution of background noise from solvents.

The decay of individual correlation data with respect to time was analyzed by fitting with different appropriate model equations presented below, depending on the nature of the dynamic processes, using the SymPhoTime (PicoQuant) and Igor Pro (version 6.37, Wavemetrics) softwares. The goodness of the fit was assessed by the χ^2 values and distribution of the residuals plot. The functional forms of different model equations are as follows:[15, 22]

1) **Single-component three dimensional (3D) diffusion only model:**

$$G(\tau) = \frac{1}{N}\left(1 + \frac{\tau}{\tau_D}\right)^{-1}\left[1 + \left(\frac{\tau}{k^2\tau_D}\right)\right]^{-1/2} \quad \ldots\ldots\ldots\ldots\ldots\ldots\ldots\ldots (2.7)$$

2) **Two-component 3D diffusion only model:**

$$G(\tau) = \frac{1}{N}\left\{\rho_1\left(1 + \frac{\tau}{\tau_{D1}}\right)^{-1}\left[1 + \left(\frac{\tau}{k^2\tau_{D1}}\right)\right]^{-1/2} + \rho_2\left(1 + \frac{\tau}{\tau_{D2}}\right)^{-1}\left[1 + \left(\frac{\tau}{k^2\tau_{D2}}\right)\right]^{-1/2}\right\} \ldots\ldots\ldots\ldots (2.8)$$

where, $\rho_1 + \rho_2 = 1$

3) **Anomalous diffusion model:**

$$G(\tau) = \frac{1}{N}\left[1 + \left(\frac{\tau}{\tau_D}\right)^{\beta}\right]^{-1}\left[1 + \frac{1}{k^2}\left(\frac{\tau}{\tau_D}\right)^{\beta}\right]^{-1/2} \quad \ldots\ldots\ldots\ldots\ldots\ldots\ldots\ldots (2.9)$$

4) **Single-component 3D diffusion model with an exponential term:**

$$G(\tau) = \left[1 + A\,exp\left(-\frac{\tau}{\tau_R}\right)\right]\frac{1}{N}\left(1 + \frac{\tau}{\tau_D}\right)^{-1}\left[1 + \left(\frac{\tau}{k^2\tau_D}\right)\right]^{-1/2} \quad \ldots\ldots\ldots (2.10$$

5) **Single-component 3D diffusion model with a stretched exponential term:**

$$G(\tau) = \left[1 + A\, exp\left(-\frac{\tau}{\tau_R}\right)^{\alpha}\right]\frac{1}{N}\left(1 + \frac{\tau}{\tau_D}\right)^{-1}\left[1 + \left(\frac{\tau}{k^2\tau_D}\right)\right]^{-1/2} \quad \ldots\ldots\ldots (2.11)$$

In the above equations, N is the average number of fluorescent molecules in the observation volume, τ_D is the average time taken for the molecule to diffuse through this volume i.e. diffusion time and τ is the delay or lag time. β ($0 < \beta < 1$) is the stretching exponent representing the distribution of τ_D. τ_R is the relaxation time for the exponential component and α ($0 < \alpha < 1$) is the stretching exponent representing the distribution of τ_R. k indicates the structure parameter of the observation volume and defined as $k = z_0/r$, where r_0 and z_0 are the axial and lateral radii of the observation volume, respectively. As the dimensions (r_0 and z_0) of the observation volume can be affected by the excitation wavelength and diameter of the pinhole, it is very crucial to calibrate these parameters during FCS experiments in order to determine accurate diffusion coefficients. Thus, the instrument was calibrated using dilute aqueous solutions of Rh6G with a known diffusion coefficient value of 426 $\mu m^2 s^{-1}$ and the estimated observation volume was found to be 0.45 fL and 0.8 fL for 405 nm and 485 nm excitation, respectively.[23]

The translation diffusion coefficients (Dt) of the probe molecules in the solutions were calculated using the diffusion times (τ_D) obtained from the above fits employing equation 2.12.

$$D_t = \frac{r_0^2}{4\tau_D} \quad \ldots\ldots\ldots\ldots\ldots\ldots (2.12)$$

2.4.4. Steady-State Spectral Measurements

2.4.4.1. Absorption and Fluorescence Measurements

Steady-state absorption and emission/excitation spectra of the samples were measured on a UV-Vis spectrophotometer (Cary 100, Varian) and spectrofluorometer (Fluorolog-3, HORIBA JobinYvon), respectively. The spectrophotometer consists of tungsten and deuterium lamps sources for the visible and UV regions, respectively and a PMT is used for detection. In the spectrofluorometer, Xenon lamp and PMT were used as the excitation source and detector, respectively. A quartz sample cell of 1 cm path length was used to record the absorption and emission/excitation spectra in the entire wavelength region. The fluorescence spectra were corrected for the instrumental response.

2.4.4.2. CD Measurements

The CD spectra of protein samples were recorded using a spectropolarimeter (Jasco J-810, Japan), in which Xenon lamp and PMT are used as the excitation source and detector, respectively. Quartz sample cell of 1 cm path length was used to record the CD spectra in the wavelength region of 200 – 450 nm. The spectra were recorded at 1 nm intervals with a scan speed of 50 nm min^{-1}. Each experiment was repeated in triplicate and an average of three scans was used for the final spectra. All the spectra were corrected for respective blank spectrum.

2.4.5. Other experimental techniques used in this work

The ^{1}H NMR and FTIR spectra were recorded using an NMR spectrometer (Bruker AVANCE, 500 MHz) and an FTIR spectrometer (Bruker Tensor II), respectively. The water contents of the DESs were measured using a Karl Fisher coulometer (METTLER TOLEDO DL39). The viscosity of the DESs and other viscous solvents were measured by a LVDV-III Ultra Brookfield Cone and Plate viscometer (1% accuracy and 0.2% repeatability). The temperature-dependent viscosity measurements were performed by using an external Julabo water circulator (model F32) bath.

2.5 Standard Error Limits

Standard error limits involved in the experimentally measured parameters are as follows:

λ_{max} (absorption/emission) = ± 2 nm

Quantum yield = ± 2-3%

Rotational relaxation time = ± 5%

Fluorescence lifetime = ± 5%

Viscosity = ± 2%

The error limits associated with the data for a) solvation dynamics studies, b) rotational dynamics studies and b) FCS studies are provided in the subsequent chapters.

References

1. D. D. Perrin, W. L. F. Armarego and D. R. Perrin, *Purification of Laboratory Chemicals*, 1980, Pergamon Press: New York, USA.
2. A. P. Abbott, G. Capper, D. L. Davies, R. K. Rasheed and V. Tambyrajah, *Chem. Commun.*, 2003, 1, 70−71.
3. R. Yusof, E. Abdulmalek, K. Sirat and M. B. A. Rahman, *Molecules*, 2014, 19, 8011-8026.
4. R. M. Harris, *PhD Thesis*, 2008, University of Leicester.
5. K. Z. Kučan, M. Perković, K. Cmrk, D. Načinović and M. Rogošić, *ChemistrySelect*, 2018, *3*, 12582-12590.
6. M. K. AlOmar, M. Hayyan, M. A. Alsaadi, S. Akib, A. Hayyan and M. A. Hashim, *J. Mol. Liq.*, 2016, 215, 98-103.
7. A. Basaiahgari, S. Panda and R. L. Gardas, *J. Chem. Eng. Data*, 2018, 63, 2613-2627.
8. C. Florindo, F. S. Oliveira, L. P. N. Rebelo, A. M. Fernandes and I. M. Marrucho, *ACS Sustain. Chem. Eng.*, 2014, 2, 2416−2425.
9. M. A. R. Martins, E. A. Crespo, P. V. A. Pontes, L. P. Silva, M. Bülow, G. J. Maximo, E. A. C. Batista, C. Held, S. P. Pinho and J. A. P. Coutinho, *ACS Sustain. Chem. Eng.*, 2018, 6, 8836-8846.
10. B. Jibril, F. Mjalli, J. Naser and Z. Gano, *J. Mol. Liq.*, 2014, 199, 462-469.
11. Wujie Guo, Yucui Hou, Shuhang Ren, Shidong Tian and W. Wu, *J. Chem. Eng. Data*, 2013, 58, 866−872.
12. J. Choi, S. Kim, T. Tachikawa, M. Fujitsuka and T. Majima, *Phys. Chem. Chem. Phys.*, 2011, *13*, 5651-5658.
13. D. R. Hickey, G. McLendon and F. Sherrnan, *J. Biol. Chem.*, 1988, *263*, 18298-18305.
14. C. Rischel, L. E. Jørgensen and Z. Földes-Papp, *J. Phys.: Condens. Matter*, 2003, *15*, S1725-S1735.
15. J. R. Lackowicz, *Principles of Fluorescence Spectroscopy*, 2006, Springer: New York, USA.
16. D. V. O'Connor and D. Phillips, *Time-Correlated Single Photon Counting*, 1984, Academic Press: New York, USA.
17. Y. R. Shen, *The Principles of Non-Linear Optics*, 1984, Willy: New York, USA.
18. J. Shah, *IEEE Journal of Quantum Electronics*, 1988, 24, 276-288.
19. W. E. Moerner and D. P. Fromm, *Rev. Sci. Instrum.*, 2003, 74, 3597-3619.
20. D. Magde, E. L. Elson and W. W. Webb, *Phys. Rev. Lett.*, 1972, 29, 705-708.
21. R. Rigler and E. S. Elson, *Fluorescence Correlation Spectroscopy: Theory and Applications*, 2001, Springer: New York, USA.
22. H. Sanabria, Y. Kubota and M. N. Waxham, *Biophys. J.*, 2007, 92, 313-322.
23. Z. Petrasek and P. Schwille, *Biophys J.*, 2008, 94, 1437−1448.

Chapter 3

Solute Rotation and Translation Dynamics in an Ionic Deep Eutectic Solvent Based on Choline Chloride

J. Phys. Chem. B, 2017, 121, 10556-10565

Overview

DESs are an emerging class of environment-friendly media useful in a variety of applications. However, the microscopic structure of these liquids is quite unclear and issues like whether spatial and dynamic heterogeneity is a generic feature of the ionic DESs and whether the solute molecules experience similar environment and interactions with the medium irrespective of their charge are still open. In this work, we have attempted to address some of these issues for ethaline, a less viscous and ionic DES consisting of a mixture of 1:2 mole ratio of choline chloride and ethylene glycol by monitoring the fluorescence response of a number of carefully chosen neutral and charged probe molecules in ensemble and single molecule conditions. Specifically, we have examined the liquid state structure of ethaline by studying the rotational and translational diffusion dynamics of the solutes measured by monitoring the time-dependence of fluorescence anisotropy in ensemble condition and fluorescence correlation signal of extremely dilute samples diffusing through confocal volume. These studies clearly reveal dynamic heterogeneity of the medium, though no spatial heterogeneity is observable through excitation wavelength dependent fluorescence measurements. The insights obtained from this study will be helpful in understanding the nature of solute-solvent interactions in this type of complex media.

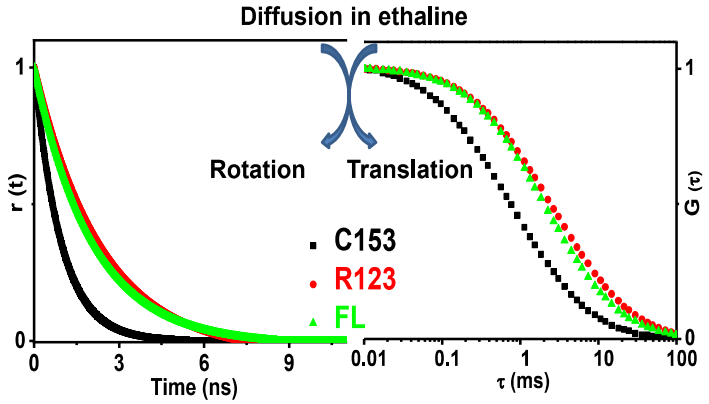

3.1. Introduction

The past two decades witnessed intense research activities on ILs in quest of environmentally benign alternatives to the conventional volatile organic compounds, which are used as common solvents.[1-8] However, the potential of ILs in large scale applications has not been realized as in addition to the high cost of the raw materials, later developments have indicated considerable toxicity and poor biodegradability of these solvents.[9-11]

DESs are now widely considered as novel environmentally benign alternative to the ILs because they not only exhibit many properties similar to the ILs, but also present significant advantages over the conventional ILs, such as low toxicity, biodegradability, cheaper raw materials and ease of preparation.[10-20] In addition, one can tune the properties of DESs over a wide range by adjusting the nature of the components as well as molar fraction of the constituents. These features of the DESs have garnered much recent attention as potential and useful media in numerous fields such as organic synthesis,[21-23] polymerizations,[20, 24] biodiesel purification,[25] electrochemistry,[26, 27] carbon dioxide adsorption,[28, 29] nanotechnology[30, 31] and metal processing.[32-35] The DESs are systems composed of mixture of a salt/HBA and a hydrogen-bond donor HBD forming a eutectic system with a much lower melting point than either of the individual components.[12, 19] Hydrogen-bonding interactions between salt/HBA and HBD are the main cause of large depression of freezing points of the mixtures.[15]

Based on the choice of constituents, one can obtain a large number of ionic and non-ionic DESs. Ionic DESs can be formed by selecting one of the constituents as ionic,[15] whereas in non-ionic DESs, both the constituents are non-ionic in nature.[36] Though, in principle, a large number of DESs are possible by varying the combination of the components,[12] most extensively studied ones are those consisting of the quaternary ammonium salt, (2-hydroxyethyl)trimethylammonium chloride, commonly known as ChCl and HBDs like amine, amide, alcohol and carboxylic acid etc. Since the first report on DES (1:2 molar mixture of ChCl and urea, commonly known as reline) by Abbott et al.,[18] several other combinations of HBDs and salts/HBAs have been explored and many theoretical and experimental studies have been carried out on these novel media.[12, 37-43] Edler and coworkers have studied the liquid structure of DES employing neutron diffraction experiment.[44] Very recently, Stefanovic et al.[45] and Kashyap and coworkers[46] have also investigated the nanostructure of some ChCl-based DESs theoretically, which reveal the

nature of interactions between the constituents of DESs. Abbott and coworkers[47-50] investigated extensively diffusion and dynamics in these solvents to understand the nature of intermolecular interactions in these media using ^{1}H pulsed field gradient NMR spectroscopy. Apart from these works, several fluorescence spectroscopic studies on different DESs have also been carried out.[36, 51-59] Biswas and coworkers[36, 51-56] have extensively studied (both theoretically and experimentally) a number of ionic and non-ionic DESs to investigate the structural details of these liquids. These studies have revealed that most of the DESs are heterogeneous[51, 54-56]. For example, mixtures of ChCl/urea and acetamide/electrolytes (ionic DESs) show both spatial and dynamic heterogeneity; in contrast, acetamide/urea (non-ionic DES) does not show any heterogeneity. Thus, whether heterogeneity it is a generic nature of all ionic DESs is unknown. Moreover, most of the fluorescence studies mentioned above have focused on probing the rotational diffusion in these media and only neutral probe molecules have been used for this purpose. What is still lacking is the information on translational diffusion of solute molecules in these media. Fluorescence studies involving ionic solutes in DESs, which can help understanding whether different solute molecules experience similar solute-solvent interactions irrespective of their charge, are also missing.

As, understanding the solute-solvent interactions involving different solute molecules is key to the realization of the potential of these media as solvents, we undertake this work on a less viscous ChCl-based ionic DES, ethaline (mixture of 1:2 mole ratio of ChCl and ethylene glycol, Chart 1.7), wherein we have used several neutral and charged fluorescent probe molecules (Chart 1.8). Specifically, to understand the solvent environments in this medium, we have studied the excitation wavelength dependence of the steady state fluorescence maximum of C153 and ANF, and the dynamics of rotational and translational diffusion of three carefully chosen fluorescent molecules of comparable sizes but differently charged, R123 (cationic), FL (anionic) and C153 (neutral), in ethaline with the help of time-resolved fluorescence anisotropy and FCS measurements.

3.2. Results and Discussion

3.2.1. Steady-State Measurements

The steady state absorption and emission spectra of C153, R123 and FL in ethaline at room temperature (298 K) are shown in Figure 3.1. The absorption maxima of C153, R123

and FL appear at 428, 513 and 497 nm, respectively and the corresponding emission maxima (λ_{emm}^{max}) appear at 540, 535 and 524 nm. Large Stokes shift of C153 is consistent with its environment sensitive fluorescence properties.[60] One can obtain an idea about the polarity of the microenvironment around C153 by comparing the measured λ_{emm}^{max} values in ethaline and in other conventional solvents of known polarities. This comparison indicates that C153 experiences methanol-like environment in ethaline.

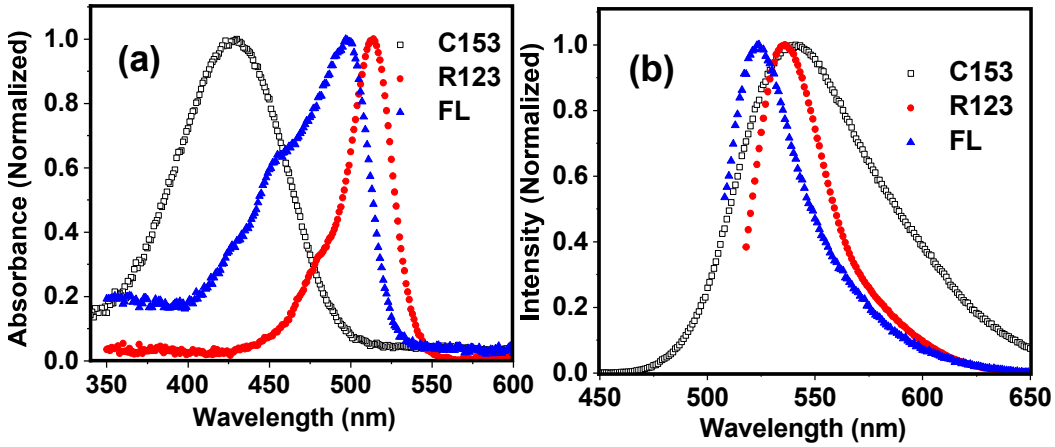

Figure 3.1. Normalized absorption (a) and emission (b) spectra of the solutes in ethaline at 298K. The emission spectra are recorded by exciting the samples at their respective absorption peak.

As the DESs are viscous media like the ILs, the dynamics of solvation in these media is much slower than that in conventional solvents like acetonitrile, water or ethanol. Consequently, in these media, it is possible to observe emission, which does not originate from the fully solvent-equilibrated state of the solute molecule. If the microenvironments around the fluorescent molecules are not identical, then under this condition one observes an excitation wavelength dependent shift of the fluorescence maximum of dipolar molecules reflecting the microheterogeneity of the medium.[61-65] As C153 has been used earlier for probing the heterogeneity in other DESs,[53, 54] we have examined its dependence of λ_{emm}^{max} on the excitation wavelength, λ_{exc}. However, unlike in other cases,[53, 54] this dependence is found to be insignificant (Figure 3.2a). As fluorescence lifetime (τ_f) of a molecule is an important factor in determining whether it will emit from an unrelaxed or fully-equilibrated state and that molecules with shorter τ_f are more likely to exhibit

excitation wavelength dependent fluorescence behavior,[64] we have also examined the λ_{exc} excitation wavelength dependence of λ_{emm}^{max} of ANF, whose τ_f (τ_f < 50 ps in 2-propanol[66]) is much shorter than that of C153 (τ_f = 4.7 ns in ethanol). However, ANF also presents a very similar picture (Figure 3.2b) and does not indicate any spatial heterogeneity of the medium. This observation is interesting as Biswas and coworkers observed significant excitation wavelength dependence of C153 and DMASBT in other ionic DESs such as (CH_3CONH_2 + $LiNO_3$/Br/ClO_4) mixtures[53] and reline (ChCl + urea)[54] indicating their spatial heterogeneity. It is thus evident that spatial heterogeneity is not a generic feature of all ionic DESs; rather, it depends significantly on the constituents of the DESs and various interactions between them.

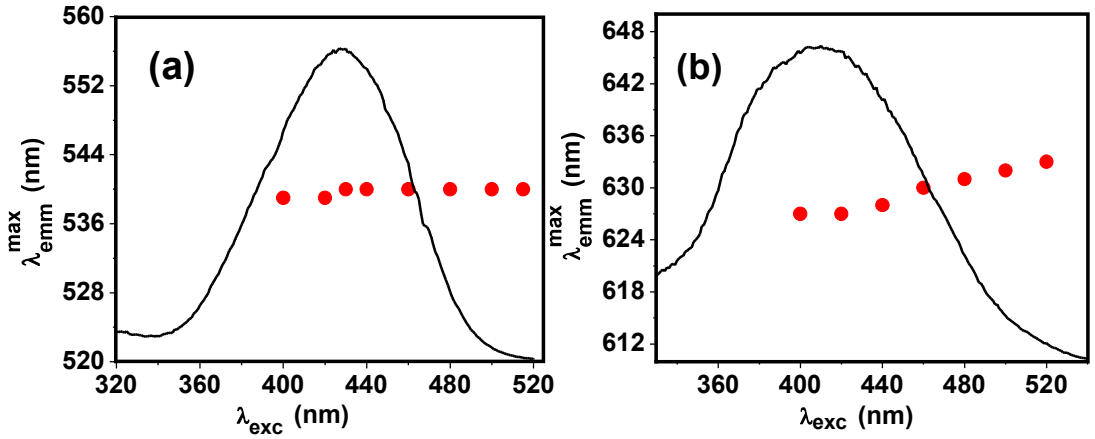

Figure 3.2. Dependence of the emission maximum (λ_{emm}^{max}) on the excitation wavelength (λ_{exc}) for C153 (a) and ANF (b) at 298K in ethaline. The excitation spectra of the individual solutes are also shown.

3.2.2. TRFA Measurements

The rotational dynamics of a molecular system is determined by the friction experienced by it in a medium and hence, it can provide valuable information on the microenvironments around the probe including solute-solvent interactions. To investigate the rotational motion, we studied time-resolved fluorescence anisotropy of C153, R123 and FL over a temperature range of 298–343 K. Representative anisotropy decay profiles of three solutes in ethaline at different temperatures are displayed in Figure 3.3. It is

evident that at any given temperature (for example 323K, Figure 3.3a), anisotropy decay of the neutral solute, C153, is significantly faster compared to the ionic solutes R123 and FL (both show similar decay profiles). As the sizes of the solute molecules are comparable (vide later), the observation indicates that the ionic solutes experience more friction in ethaline compared to the neutral one.

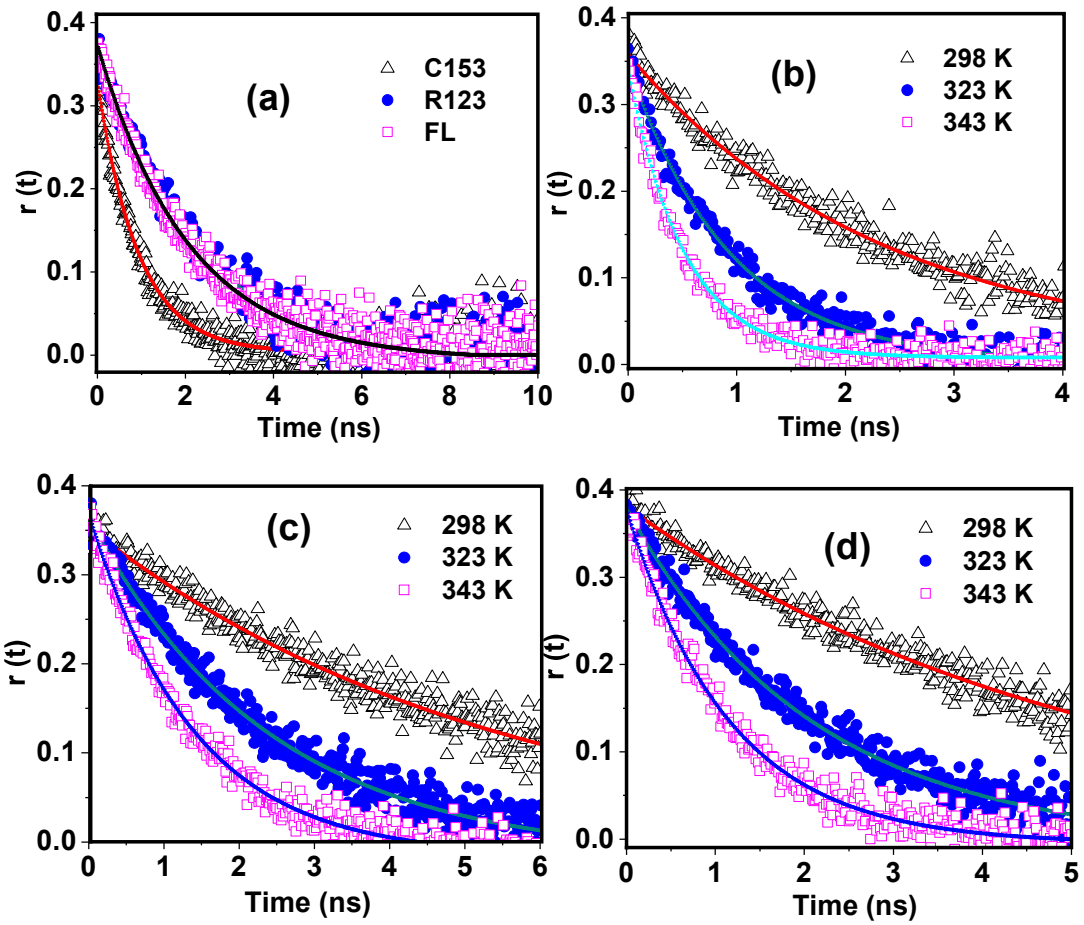

Figure 3.3. (a) Anisotropy decay profiles of the three solutes in ethaline at 323 K. The panels (b), (c) and (d) show the effect of temperature on the anisotropy decay profiles of C153, R123 and FL, respectively. The solid lines represent single exponential fit to the experimental anisotropy data. The excitation and monitoring wavelengths for C153 are 405 and 540 nm, respectively, while for R123 and FL, the excitation wavelength is 481 nm and monitoring wavelengths are 535 and 524 nm, respectively.

It is also seen that the anisotropy decay becomes faster for all three solutes at higher temperatures due to lowering of viscosity of the medium. The rotational reorientation

times (τ_r) of the solutes, estimated from single exponential fit to the experimental data are shown in Table 3.1 along with the measured viscosities of ethaline at different temperatures. The viscosity of the medium is found to follow the VFT equation[67] Figure 3.4 shows the temperature dependence of the viscosity.

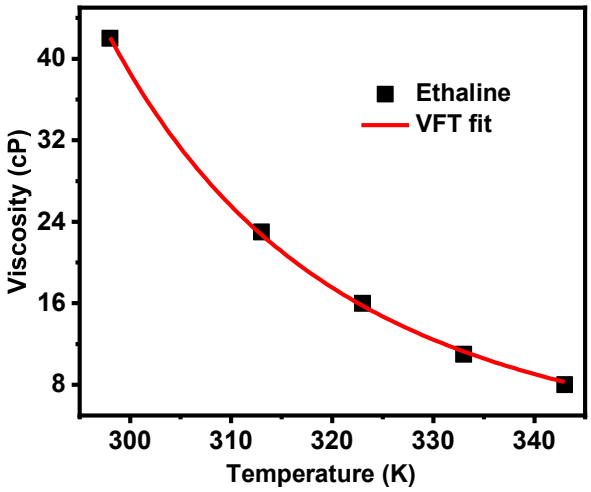

Figure 3.4. Viscosity (points) of ethaline at different temperatures together with the fit (solid line) according to the VFT equation.

Table 3.1. Estimated rotational reorientation times (ns) of the solutes in ethaline at different temperatures.

Temp. (K)	Viscosity (cP)	Rotational reorientation time (ns)		
		C153	R123	FL
298	42	2.25	5.62	5.10
313	23	1.28	3.40	2.78
323	16	0.93	2.38	2.08
333	12	0.70	1.79	1.49
343	08	0.51	1.39	1.15

Careful inspection of the data collected in Table 3.1 reveals that at any given temperature, the τ_r values of R123 and FL are higher than that of C153 by a factor of > 2. As the sizes

of three solutes are similar, the higher τ_r values for R123 and FL indicate their association with the solvent through electrostatic or hydrogen-bonding interaction.

We have analyzed the experimental results using SED hydrodynamic theory,[68, 69] which considers the solvent as a structureless continuum and according to which the rotational reorientation time (τ_r) of a solute in a solvent is given by

$$\tau_r = \frac{\eta V f C}{k_B T} \ldots\ldots\ldots\ldots\ldots (3.1)$$

where, *V*, *f* and *C* are the van der Waals volume, shape factor and boundary condition parameter of the solutes, respectively. η, k_B and *T* are the solvent viscosity, Boltzmann constant and absolute temperature of the system, respectively. The shape factor (*f*), which describes nonspherical nature of the solute, is a function of axial ratio of the semi axes. *C* indicates the degree of solute-solvent coupling, which in two limiting cases are stick (C_{stick} = 1) and slip ($0 < C_{slip} < 1$). The axial radii, van der Waals volumes, boundary conditions and shape factors for the probe molecules, C153, FL and R123 are collected in Table 3.2.

Table 3.2. Solute dimension, van der Waals volume, shape factor and boundary condition parameters calculated from the SED hydrodynamic theory.

Solute	Axial radii ($Å^3$)	van der Waals volume, V ($Å^3$)	Shape factors (f)	C_{slip}
C153[a]	6.1 x 4.8 x 2.2	246	1.71	0.240
R123	7.0 x 5.5 x 1.8	289[b]	2.10[b]	0.155[b]
FL[c]	6.4 x 5.5 x 1.8	267	1.93	0.139

[a,c] taken from ref. 66 and 68, respectively. [b] calculated using ref. 65, 69 and 70.

While these parameters for C153 and FL were obtained from literature,[70, 71] for R123, the V value was calculated using Edward's volume increment method[72] and the shape factor and boundary conditions were calculated following reported procedure.[69, 73] Briefly, the friction coefficients (ξ) for the stick and slip boundary conditions were obtained along three principal axes of rotation treating each solute as an asymmetric ellipsoid.[74] The

diffusion coefficients (D_i) were then computed along three axes using the Einstein relation,[75]

$$D_i = \frac{k_B T}{\xi_i} \ldots\ldots\ldots\ldots\ldots (3.2)$$

The rotational reorientation times (τ_r) of the solutes were calculated from the D_i values along a, b and c axis (assuming the transition dipole along the long axis of the solute) using following equation[76]

$$\tau_r = \frac{1}{12}\left(\frac{4D_a + D_b + D_c}{D_aD_b + D_bD_c + D_cD_a}\right) \ldots\ldots\ldots\ldots (3.3)$$

The parameters, f and C_{slip} were then estimated from the calculated τ_r value for stick and slip boundary conditions using equation 3.1.

The τ_r values are plotted against η/T for all three solutes, indicating the slip and stick lines in Figure 3.5. Table A1.1 summarizes the predicted slip and stick rotation times. The Figure 3.5 shows that the rotational times of neutral solute C153 lie between the slip and stick lines, whereas for positively charged R123 and negatively charged FL, the rotational behaviour is very similar and the dynamics follows stick predictions of the SED theory indicating strong association of these solutes with the solvent.[73] As these solutes are charged, this association is likely to be due to electrostatic interaction between the positively charged solutes R123 and the chloride anion of the ethaline, and between negatively charged FL and choline cation of ethaline. However, as hydrogen-bonding interaction of R110 (which is very similar to R123) and FL is known to be the major reason for their stick behavior in ILs,[77] it is most likely that the stick behavior in ethaline is primarily due to the hydrogen-bonding interaction between R123 (or FL) and constituents of ethaline as both ChCl and ethylene glycol possess hydrogen-bond forming functionalities.

A fit of the experimental data to $\tau_r = A(\eta/T)^P$ (dashed lines in Figure 3.5) shows significant nonlinearity, which is evident from the departure of the 'p' value from unity, highlighting the deviation of τ_r from the SED hydrodynamic theory.

$\tau_r = (13.38 \pm 0.66)(\eta/T)^{0.88\pm0.02}$ (N = 5, R = 0.9) for C153

$\tau_r = (27.70 \pm 1.59)(\eta/T)^{0.81\pm0.02}$ (N = 5, R = 0.99) for R123

$\tau_r = (28.45 \pm 1.8\ )(\eta/T)^{0.87\pm0.03}$ (N = 5, R = 0.996) for FL

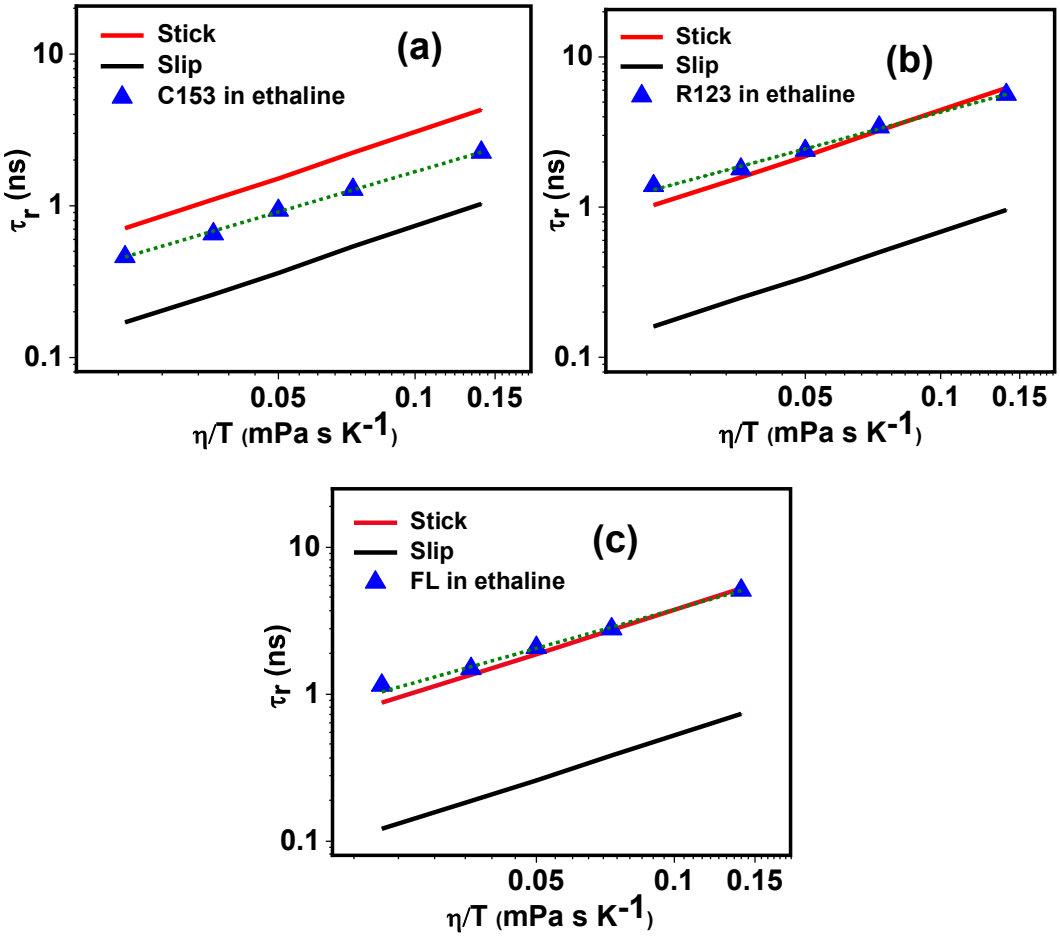

Figure 3.5. Plots of τ_r Vs η/T for C153 (a), R123 (b) and FL(c) in ethaline. The solid triangles indicate the experimentally measured rotational times and the dashed lines represent fit to the data according to $\tau_r = A(\eta/T)^p$. The 'p' values obtained from the fits are shown in the figure. The stick (red) and slip (black) lines, computed using SED theory are also shown.

The 'p' values obtained from the fits lie between 0.81 and 0.88, indicating viscosity-diffusion decoupling in ethaline. As this 'p' value is very close to 1 for common organic solvents, which are homogeneous in nature, this fractional viscosity dependence of

rotational diffusion time (i.e. a breakdown of hydrodynamic behavior) is due to the dynamic heterogeneity of the medium, as found in recent studies.[53, 54] This dynamic heterogeneity is shown to be the result of hydrogen-bond fluctuation and consequent motion of particles, which is very different from hydrodynamic diffusion,[47] such as orientational jumps and it can cause viscosity-diffusion decoupling.[78, 79] We thus conclude that fluctuation of hydrogen-bond network in ethaline due to such orientational jumps contribute to this kind of observation. That dynamic heterogeneity of a medium does not require the presence of spatially distributed microenvironments (spatial heterogeneity), is well documented for other systems.[80]

3.2.3. FCS Measurements

To further understand the nature of the medium, we have studied the translational diffusion of the molecules in single molecule condition using FCS technique. To the best of our knowledge, no measurement based on FCS technique has been made so far to study the translational motion of a solute molecule in these media. Figure 3.6 shows the time-dependence of fluorescence correlation of the three systems in ethaline. The data was analyzed using both single-component diffusion (equation 2.7) and anomalous diffusion model (equation 2.9). However, the anomalous diffusion model, which considers stretching exponent, β (a parameter that quantifies the degree of deviation from normal diffusion) to describe the decay of fluorescence correlation, fits the data much better compared to the single-component diffusion model (as decided by the residuals and $\chi 2$ values) for all three systems. This point is illustrated through single-component fits to the data (Figure 3.6) and fit residuals using both models in Figure A1.3. In addition to these two models, one could have also fitted the data to two-component (bimodal) diffusion model (equation 2.8), which considers diffusion of solutes in different subpopulations (spatially distributed microenvironments). However, as we could not observe such microenvironments through excitation wavelength dependence measurements, we did not fit the data to two-component diffusion model.

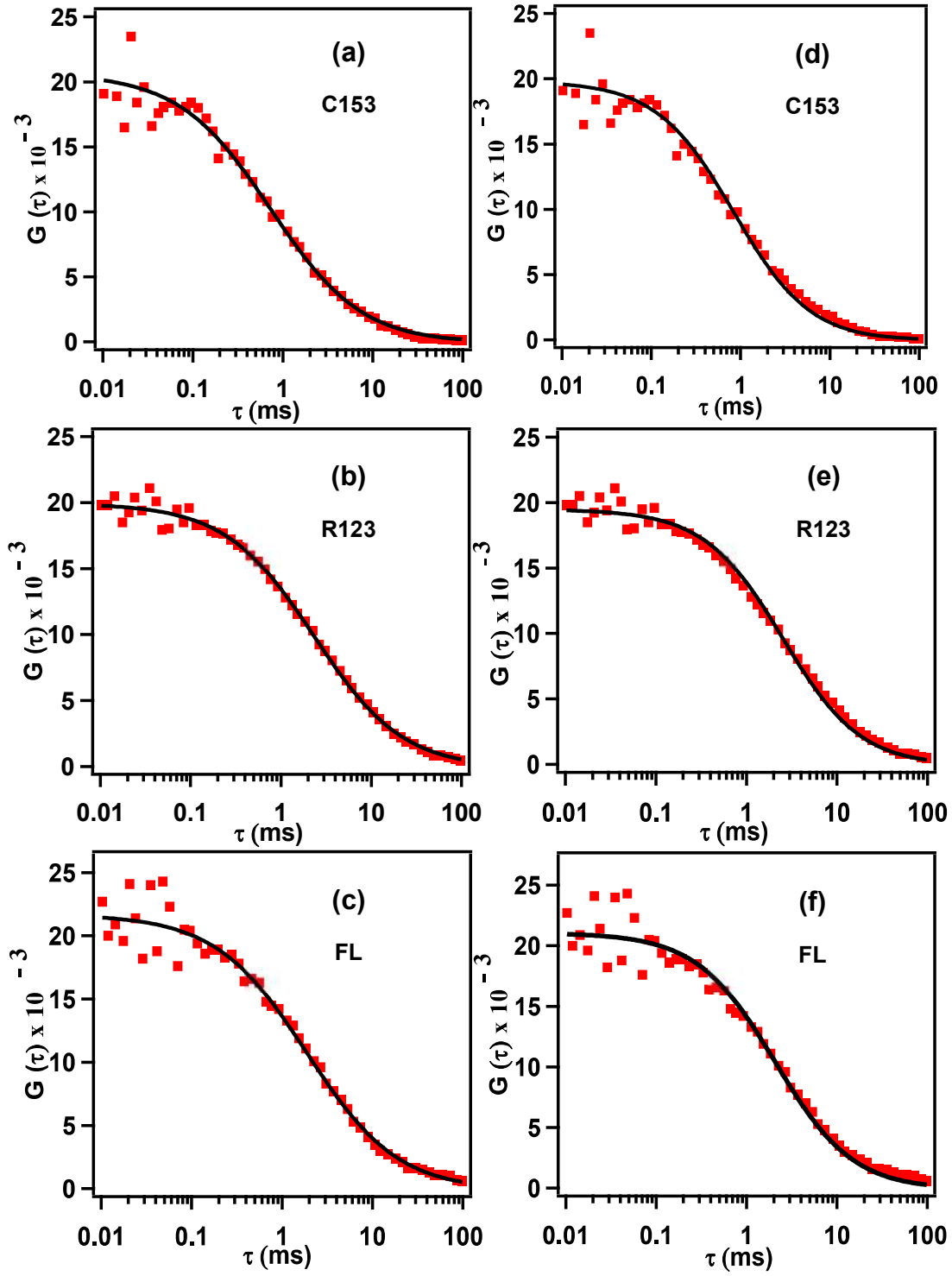

Figure 3.6. Fluorescence correlation curves for the diffusion of the solutes in ethaline. The points are the experimental data and the solid lines represent best fit to the data using an anomalous diffusion model (Left panel: a, b, c) and a single-component diffusion model (Right panel: d, e, f). The excitation wavelengths are 405 nm for C153 and 485 nm for R123 and FL.

The diffusion coefficients of three solutes estimated from these fits are collected in Table 3.3 along with the β values. The latter, which lies between 0.84 and 0.86, indicates a distribution of translational diffusion time (τ_D), and suggests that the dynamics of translational diffusion of chosen molecules are diverse in nature. As these solute molecules exhibit single component translational diffusion ($\beta = 1$) in conventional homogeneous solvents, the anomalous diffusion of solutes in ethaline can be attributed to the dynamic heterogeneity, which describes that the mean square displacement of solute molecules follows a sub-diffusive behavior, $\langle r(\tau)^2 \rangle \propto \tau^{\beta}$, ($\beta < 1$) instead of the normal Brownian diffusion ($\beta = 1$). In this context, we note the recent observation of anomalous diffusion of Nile Red in ILs and its interpretation in terms of dynamic heterogeneity in ILs. [81]

Table 3.3. FCS fittings parameters using the anomalous diffusion model.

Solute	D_t ($\mu m^2 s^{-1}$)	β
C153	17.8	0.84
R123	8.9	0.86
FL	10.9	0.86

Further, Table 3.3 shows that the observed diffusion coefficients (D_t) of the ionic solutes are significantly smaller than that of the neutral solute. It is evident that the translational diffusion of C153 is faster by a factor of almost 2 as compared to R123. These observations can be explained considering stronger association of the ionic solutes with ethaline due to electrostatic and hydrogen-bonding interactions between the ionic solutes and the constituents of ethaline. These findings are in good agreement with the results obtained in ensemble condition using time-resolved fluorescence anisotropy measurements. Thus, both translational and rotational motions of charged solutes in ethaline are significantly different than those of neutral one, and the formers are experiencing stronger solute-solvent interactions in this ionic medium.

3.3. Summary

The translational and rotational diffusion dynamics of the molecular systems reveal dynamic heterogeneity in ethaline though no static heterogeneity of the medium could be detected. Specifically, the dynamic heterogeneity in the medium is established from the departure of the reorientation times of the solutes from their hydrodynamic behavior and anomalous translational diffusion observed for solutes in FCS measurements. Furthermore, both translational and rotational diffusion dynamics show the charged solutes to experience stronger solute-solvent interactions in ethaline as a consequence of mutual effect of the electrostatic and hydrogen-bonding interactions between solutes and constituents of ethaline. The present findings are likely to be helpful towards the development and applications of this class of novel solvents.

References

1. R. D. Rogers and K. R. Seddon, *Science*, 2003, **302**, 792−793.
2. K. R. Seddon, *Nat. Mater.*, 2003, **2**, 363–365.
3. T. Welton, *Chem. Rev.*, 1999, **99**, 2071–2083.
4. J. Dupont, *Acc. Chem. Res*, 2011, **44**, 1223−1231.
5. *The Physical Chemistry of Ionic Liquids (Special issue on ionic liquids), J. Phys. Chem. B*, 2007, **111**, 4639−5029.
6. *The Physical Chemistry of Ionic Liquids (Special issue on ionic liquids), Phys. Chem. Chem. Phys*, 2010, **12**, 1629−2032.
7. J. G. Huddleston and R. D. Rogers, *Chem. Commun*, 1998, 1765–1766.
8. N. V. Plechkova and K. R. Seddon, *Chem. Soc. Rev*, 2008, **37**, 123−150.
9. M. A. Kareem, F. S. Mjalli, M. A. Hashim and I. M. Al Nashef, *J. Chem. Eng. Data*, 2010, **55**, 4632−4637.
10. A. Romero, A. Santos, J. Tojo and A. Rodríguez, *J. Hazard Mater*, 2008, **151**, 268-273.
11. A. S. Wells and V. T. Coombe, *Org. Process Res. Dev.*, 2006, **10**, 794-798.
12. Q. Zhang, K. D. O. Vigier, S. Royer and F. Jé rôme, *Chem. Soc. Rev.*, 2012, **41**, 7108−7146.
13. A. P. Abbott, D. Boothby, G. Capper, D. L. Davies and R. K. Rasheed, *J. Am. Chem. Soc.*, 2004, **126**, 9142−9147.
14. A. P. Abbott, D. L. Davies, G. Capper, R. K. Rasheed and V. Tambyrajah, *U.S. Patent 7*, 2007, **183**, 433.
15. M. Francisco, A. van den Bruinhorst and M. C. Kroon, *Angew. Chem., Int. Ed.*, 2013, **52**, 3074−3085.
16. Y. Dai, J. van Spronsen, G. J. Witkamp, R. Verpoorte and Y. H. Choi, *Anal. Chim. Acta*, 2013, **766**, 61−68.

17. A. Paiva, R. Craveiro, I. Aroso, M. Martins, R. L. Reis and A. R. C. Duarte, *ACS Sustain. Chem. Eng.*, 2014, **2**, 1063−1071.
18. A. P. Abbott, G. Capper, D. L. Davies, R. K. Rasheed and V. Tambyrajah, *Chem. Commun.*, 2003, **1**, 70−71.
19. E. L. Smith, A. P. Abbott and K. S. Ryder, *Chem. Rev.*, 2014, **114**, 11060−11082.
20. J.-H. Liao, P.-C. Wu and Y.-H. Bai, *Inorg. Chem. Commun.*, 2005, **8**, 390−392.
21. C. Ruβ and B. Konig, *Green Chem.*, 2012, **14**, 2969−2982.
22. S. K. Ghosh and R. Nagarajan, *RSC Adv.*, 2016, **6**, 27378.
23. D. A. Alonso, A. Baeza, R. Chinchilla, G. Guillena, I. M. Pastor and D. J. Ramón, *Eur. J. Org. Chem.*, 2016, 612–632.
24. D. Carriazo, M. C. Serrano, M. C. Gutie´rrez, M. L. Ferrer and F. d. Monte, *Chem. Soc. Rev.*, 2012, **41**, 4996–5014.
25. K. Shahbaz, F. S. Mjalli, M. A. Hashim and I. M. AlNashef, *Energy Fuels*, 2011, **25**, 2671−2678.
26. C. A. Nkuku and R. J. LeSuer, *J. Phys. Chem. B*, 2007, **111**, 13271–13277.
27. H.-R. Jhong, D. S.-H. Wong, C.-C. Wan, Y. Wang, -Y. and T.-C. Wei, *Electrochem. Commun.*, 2009, **11**, 209-211.
28. R. B. Leron and M.-H. Li, *Thermochim. Acta*, 2013, **551**, 14−19.
29. R. B. Leron and M.-H. Li, *J. Chem. Thermodyn.*, 2013, **57**, 131−136.
30. D. V. Wagle, H. Zhao and G. A. Baker, *Acc. Chem. Res.*, 2014, **47**, 2299−2308.
31. H.-G. Liao, Y.-X. Jiang, Z.-Y. Zhou, S.-P. Chen and S.-G. Sun, *Angew. Chem.*, 2008, **120**, 9240−9243.
32. A. P. Abbott and K. J. McKenzie, *ChemPhysChem*, 2006, **8**, 4265−4279.
33. A. P. Abbott, G. Capper, K. J. McKenzie and K. S. Ryder, *Electrochim. Acta*, 2006, **51**, 4420−4425.
34. A. P. Abbott, G. Capper, D. L. Davies, R. K. Rasheed and P. Shikotra, *Inorg. Chem.*, 2005, **44**, 6497−6499.
35. A. P. Abbott, G. Capper, A. Glidle and K. S. Ryder, *Phys. Chem. Chem. Phys.*, 2006, **8**, 4214−4221.
36. A. Das, S. Das and R. Biswas, *J. Chem. Phys.* , 2015, **142**, 034505.
37. G. García, S. Aparicio, R. Ullah and M. Atilhan, *Energy Fuels*, 2015, **29**, 2616−2644.
38. R. Yusof, E. Abdulmalek, K. Sirat and M. B. A. Rahman, *Molecules*, 2014, **19**, 8011-8026.
39. C. Florindo, F. S. Oliveira, L. P. N. Rebelo, A. M. Fernandes and I. M. Marrucho, *ACS Sustain. Chem. Eng.*, 2014, **2**, 2416−2425.
40. S. L. Perkins, P. Painter and C. M. Colina, *J. Chem. Eng. Data*, 2014, **59**, 3652−3662.
41. D. V. Wagle, G. A. Baker and E. Mamontov, *J. Phys. Chem. Lett.*, 2015, **6**, 2924−2928.
42. A. Yadav and S. Pandey, *J. Chem. Eng. Data*, 2014, **59**, 2221−2229.
43. A. Yadav, J. R. Kar, M. Verma, S. Naqvi and S. Pandey, *Thermochim. Acta.*, 2015, **600**, 95-101.

44. O. S. Hammond, D. T. Bowron and K. J. Edler, *Green Chem.*, 2016, **18**, 2736-2744.
45. R. Stefanovic, M. Ludwig, G. B. Webber, R. Atkin and A. J. Page, *Phys. Chem. Chem. Phys.*, 2017, **19**, 3297-3306.
46. S. Kaur, A. Gupta and H. K. Kashyap, *J. Phys. Chem. B*, 2016, **120**, 6712-6720.
47. C. D. Agostino, R. C. Harris, A. P. Abbott, L. F. Gladden and M. D. Mantle, *Phys. Chem. Chem. Phys.*, 2011, **13**, 21383–21391.
48. A. P. Abbott, R. C. Harris, K. S. Ryder, C. D'Agostino, L. F. Gladden and M. D. Mantle, *Green Chem.*, 2011, **13**, 82–90.
49. C. D'Agostino, L. F. Gladden, M. D. Mantle, A. P. Abbott, I. A. Essa, A. Y. M. Al-Murshedi and R. C. Harris, *Phys. Chem. Chem. Phys.*, 2015, **17**, 15297-15304.
50. A. P. Abbott, C. D'Agostino, S. J. Davis, L. F. Gladden and M. D. Mantle, *Phys. Chem. Chem. Phys.*, 2016, **18**, 25528-25537.
51. B. Guchhait, H. A. R. Gazi, H. K. Kashyap and R. Biswas, *J. Phys. Chem. B*, 2010, **114**, 5066-5081.
52. B. Guchhait, S. Daschakraborty and R. Biswas., *J. Chem. Phys.*, 2012, **136**, 174503.
53. B. Guchhait, S. Das, S. Daschakraborty and R. Biswas, *J. Chem. Phys.*, 2014, **140**, 104514.
54. A. Das and R. Biswas, *J. Phys. Chem. B*, 2015, **119**, 10102−10113.
55. K. Mukherjee, A. Das, S. Choudhury, A. Barman and R. Biswas, *J. Phys. Chem. B*, 2015, **119**, 8063−8071.
56. T. Pal and R. Biswas, *Chem. Phys. Letters*, 2011, **517**, 180-185.
57. A. Pandey, R. Rai, M. Pal and S. Pandey, *Phys. Chem. Chem. Phys.*, 2014, **16**, 1559-1568.
58. A. Pandey and S. Pandey, *J. Phys. Chem. B*, 2014, **118**, 14652-14661.
59. A. Pandey, A. Yadav, Bhawna. and S. Pandey, *J. Lumin.*, 2017, **183**, 494-506.
60. R. Baumann, C. Ferrante, E. Kneuper, F.-W. Deeg and C. Brauchle, *J. Phys. Chem. A*, 2003, **107**, 2422-2430.
61. A. N. Rubinov and V. I. Tomin, *Opt. Spektr.*, 1970, **29**, 1082–1086.
62. W. C. Galley and R. M. Purkey, *Proc. Natl. Acad. Sci. U.S.A.*, 1970, **67**, 1116.
63. G. Weber and M. Shinitzky, *Proc. Natl. Acad. Sci. U.S.A.*, 1970, **65**, 823-830.
64. P. K. Mandal, M. Sarkar and A. Samanta, *J. Phys. Chem. A*, 2004, **108**, 9048-9053.
65. A. P. Demchenko, *Luminescence.*, 2002, **17**, 19−42.
66. L. A. Hallidy and M. R. Topp, *Chem. Phys. Letters*, 1977, **48**, 40-45.
67. F. S. Mjalli and J. Naser, *Asia-Pac. J. Chem. Eng.*, 2015, **10**, 273–281.
68. G. R. Fleming, *Chemical Applications of Ultrafast Spectroscopy*, 1986, Oxford University Press: New York, USA.
69. J. A. Ingram, R. S. Moog, N. Ito, R. Biswas and M. Maroncelli, *J. Phys. Chem. B*, 2003, **107**, 5926-5932.
70. H. Jin, G. A. Baker, S. Arzhantsev, J. Dong and M. Maroncelli, *J. Phys. Chem. B*, 2007, **111**, 7291–7302.
71. L. Karve and G. B. Dutt, *J. Phys. Chem. B*, 2012, **116**, 9107−9113.

72. J. T. Edward, *J. Chem. Educ.*, 1970, **47**, 261−270.
73. D. C. Khara and A. Samanta, *Phys. Chem. Chem. Phys.*, 2010, **12**, 7671–7677.
74. R. J. Sension and R. M. Hochstrasser, *J. Chem. Phys.*, 1993, **98**, 2490.
75. A. Einstein, *Investigations on the Theory of Brownian Movement*, 1956, Dover: New York, USA.
76. R. S. Hartman, D. S. Alavi and D. H. Waldeck, *J. Phys. Chem.* , 1991, **95**, 7872-7880
77. V. Gangamallaiah and G. B. Dutt, *J. Phys. Chem. B*, 2012, **116**, 12819−12825.
78. S. Das, R. Biswas and B. Mukherjee, *J. Phys. Chem. B*, 2015, **119**, 11157-11168.
79. S. Das, R. Biswas and B. Mukherjee, *J. Phys. Chem. B*, 2015, **119**, 274-283.
80. R. Richert, *J. Phys.: Condens. Matter*, 2002, **14**, R703-R738.
81. E. C. Wu, H. J. Kim and L. A. Peteanu, *J. Phys. Chem. B*, 2017, **121**, 1100−1107.

Chapter 4

How Do the Hydrocarbon Chain Length and Hydroxyl Group Position Influence the Solute Dynamics in Alcohol-Based Deep Eutectic Solvents?

Phys. Chem. Chem. Phys., 2018, 20, 24613-24622

Overview

Some of the interesting properties of DESs have stimulated investigations on the microscopic solution structure, solute-solvent interactions and solute/solvation dynamics in these media. Even though the alcohol-based DESs, due to their low viscosity, serve as useful media in various applications, little is known about the structure and dynamics of these solvents. In order to obtain insight into the microscopic structure and interactions operating in these media, we have studied the rotational and translational diffusion dynamics of some carefully chosen molecular systems (both dipolar and nonpolar) using TRFA and FCS techniques in a series of choline chloride/alcohol based DESs differing in hydrocarbon chain length and positioning of the hydroxyl group at the HBD. The results reveal an increase of both spatial and dynamic heterogeneity upon increase in chain length of one of the components of these solvents. No significant variation of heterogeneity, however, could be observed with change in the hydroxyl group position. The analysis of the experimental results indicate that solute-solvent hydrogen-bonding interaction plays a dominant role in determining both rotational and translational diffusion dynamics of 4-AP in these DESs.

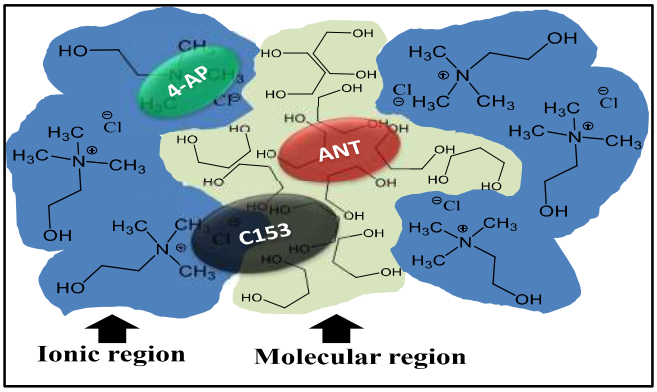

4.1. Introduction

DESs have garnered considerable attention in recent years as new environmentally benign solvents with potential applications in diverse fields such as organic synthesis,[1, 2] catalysis,[3] metal processing,[4-6] polymerizations,[7, 8] biodiesel purification,[9] electrochemistry,[10, 11] nanotechnology,[12, 13] biotechnology[14] and carbon dioxide adsorption.[15, 16] Due to several important features such as low toxicity, biodegradability, biocompatibility, ease of preparation from cheaper raw materials and wide tunability of properties, most of these novel media have emerged as better alternatives not only to common molecular solvents,[2, 17, 18] but also to the ILs.[19-23]

DESs generally consist of a salt or HBA and a HBD. Mixing of two or more such components in a certain mole ratio forms a eutectic system, which shows large depression of melting temperature (much lower than either of the individual pure constituents) owing to extensive interspecies hydrogen-bonding interactions.[19, 24] A large numbers of DESs can be obtained by appropriate selection of individual components as well as by varying molar ratio of the constituents.[23] This flexibility makes convenient solvent engineering yielding a large number of ionic and non-ionic DESs with desirable properties. The most common and popular DESs are composed of quaternary ammonium salts like ChCl as HBA and readily available materials like amides, alcohols, acids, sugars etc. as HBD.[23]

Several theoretical and experimental studies have been performed in recent years to explore the structure, dynamics, and molecular level interactions of these media.[17, 25-42] Abbott and co-workers have studied diffusion and dynamics in these media using ^{1}H pulsed field gradient NMR spectroscopy.[17, 25, 26] Biswas and co-workers have investigated structural as well as dynamical aspects of several DESs both theoretically and experimentally.[29-34, 43] Even though a large number of DESs has been explored, most of the studies have focused on systems obtained by mixing of quaternary ammonium salts with amides and acids as HBDs. Not much is known, however, about the structure and dynamics of the alcohol-based eutectic systems, which are quite useful as media in various applications[19, 24 44-46] due to their significantly lower viscosity compared to the other DESs. As understanding of the physicochemical properties of a solvent system is key to its exploitation of its potential in applications, we recently studied the microscopic solution structure and solute-solvent interactions in one of the alcohol-based DESs, namely, ethaline.[47]

Recognizing the fact that a change of the hydrocarbon chain length and hydroxyl group position of the diols (one of the components of DESs) significantly influences the physical properties of the alcohol-based DESs,[48] we investigate how these factors influence the microscopic solution structure, diffusion dynamics of solute molecules and nature of solute-solvent interactions in this class of DESs. For this purpose, we have chosen three fluorescent systems, whose rotational diffusion dynamics is studied by monitoring time-dependence of the fluorescence anisotropy and translational diffusion by fluorescence correlation spectroscopy measurements in a series of DESs comprising ChCl (as HBA) and six different diols (as HBD). The six diols chosen in this study (Chart 1.7) differ in their chain length or hydroxyl group position. The compositions of the DESs along with their abbreviations are presented in Table 4.1. The first three DESs contain diols of different chain length, whereas in last four, the diols vary in their hydroxyl group position maintaining the same chain length. Dipolar solutes, C153 and 4-AP and nonpolar solute, ANT (Chart 1.8) are chosen as the fluorescent probe molecules. Of the two dipolar solutes, 4-AP is chosen for high sensitivity of its fluorescence properties to hydrogen-bonding interactions.[49, 50] ANT is chosen for its tendency to reside in relatively nonpolar region of an organized assembly comprising regions with different polarities.[49, 51]

Table 4.1. Description of the DESs used in this study.

Sl. No.	Salt	HBDs	Mole ratio (Salt: HBD)	Abbreviation	Water content (wt %)
1	ChCl	1,2-ethanediol	1:3	CC12ED	0.160
2	ChCl	1,3-propanediol	1:3	CC13PD	0.122
3	ChCl	1,4-butanediol	1:3	CC14BD	0.133
4	ChCl	1,2-butanediol	1:4	CC12BD	0.205
5	ChCl	1,3-butanediol	1:4	CC13BD	0.218
6	ChCl	2,3-butanediol	1:4	CC23BD	0.164

4.2. Results and Discussion

4.2.1. Steady-State Measurements

The steady-state excitation (λ_{exc}^{max}) and emission maxima (λ_{emm}^{max}) of C153, 4-AP and ANT in six DESs at room temperature (298 K) are collected in Table 4.2 and the corresponding spectra are displayed in Figure 4.1. It is evident that the λ_{exc}^{max} values of the solutes do not vary with change of solvents. As far as the λ_{emm}^{max} values are concerned, though ANT shows very similar emission behavior in all solvents, the λ_{emm}^{max} values of C153 and 4-AP show significant solvent dependence. Nearly 9-10 nm blue shift of λ_{emm}^{max} is observed for these two systems with increasing hydrocarbon chain length. No effect of the hydroxyl group position is observed on the λ_{emm}^{max} value of C153 except in CC14BD. The latter is presumably due to different salt:HBD mole ratio (see Table 4.1) in this DES. For 4-AP, a small variation of λ_{emm}^{max} is observed with change in hydroxyl group position, but no clear trend could be identified. This small variation of λ_{emm}^{max} is a reflection of the sensitivity of the fluorescence properties of 4-AP on hydrogen-bonding interactions.[52] The blue shift of the λ_{emm}^{max} values of C153 and 4-AP with increasing hydrocarbon chain length of HBDs suggests these probes to experience a less polar environment in DESs comprising longer alkyl chain length diols.

Table 4.2. Steady-state excitation and emission maxima (nm) of C153, 4-AP and ANT in six DESs at room temperature (298 K).

DESs	C153		4-AP		ANT	
	λ_{exc}^{max}	λ_{emm}^{max}	λ_{exc}^{max}	λ_{emm}^{max}	λ_{exc}^{max}	λ_{emm}^{max}
CC12ED	426	540	371	514	360	404
CC13PD	426	536	371	508	360	404
CC14BD	426	533	371	505	360	403
CC12BD	426	530	371	510	360	403
CC13BD	426	530	370	505	359	403
CC23BD	426	530	371	509	359	403

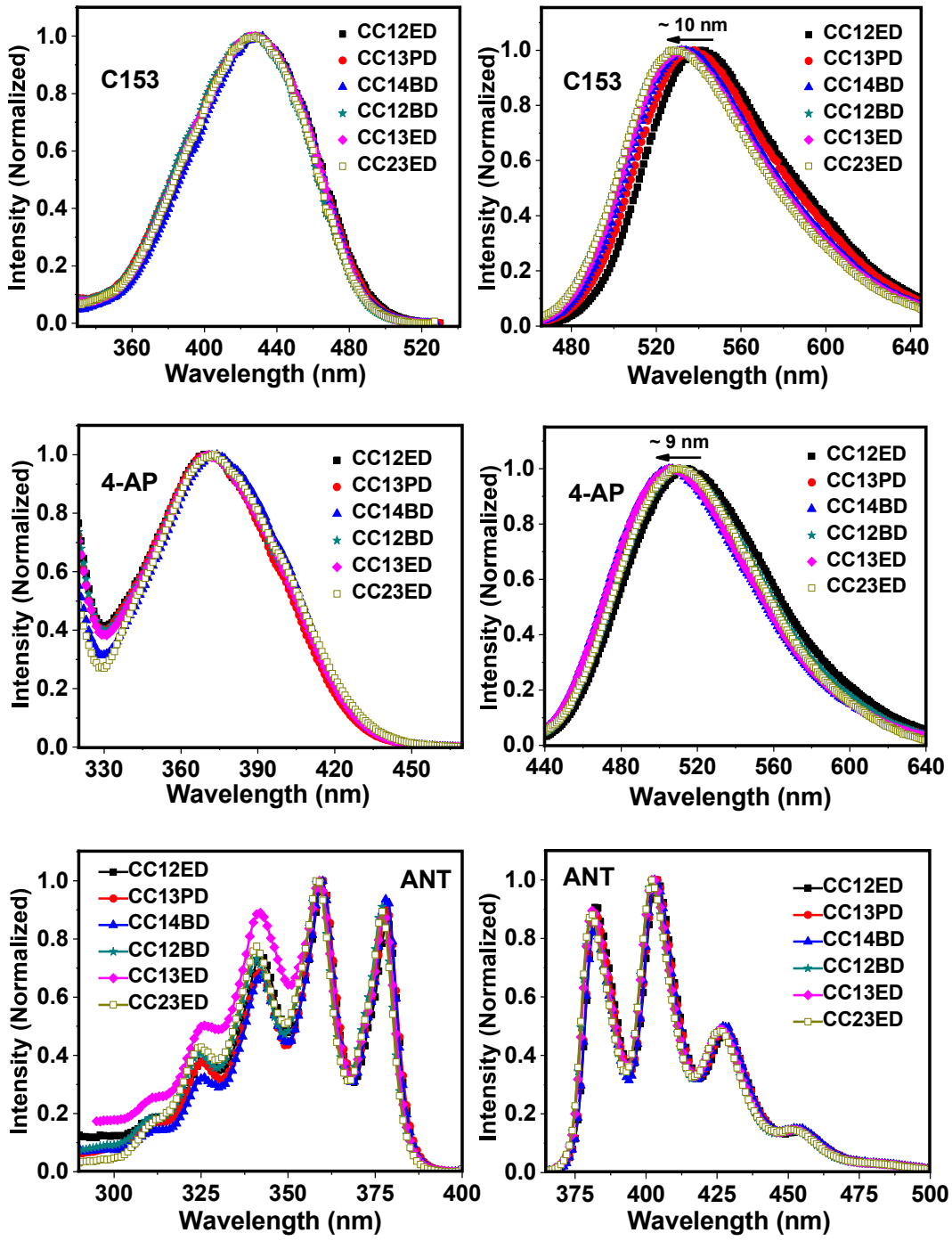

Figure 4.1. Normalized excitation (left panel) and emission (right panel) spectra of the solutes in six DESs at 298K. The emission/excitation spectra are recorded by exciting the samples at their respective maxima of excitation/emission spectra.

We also examined the excitation wavelength (λ_{exc}^{max}) dependence of λ_{emm}^{max} of the dipolar molecules, C153 and 4-AP to find out whether any signature of the microheterogeneity of these media could be observed.[29, 47, 53] Biswas and co-workers indeed observed significant λ_{exc}^{max} dependence of C153 in other DESs.[29, 31] Figure 4.2a-b shows, however, that none of the two dipolar probes exhibits any λ_{exc}^{max} dependent emission behavior in any DESs. However, as it is well known that molecules with shorter τ_f are more likely to exhibit excitation wavelength dependent fluorescence behavior in viscous media,[53] we have also examined λ_{exc}^{max} dependence of λ_{emm}^{max} of ANF, whose τ_f (τ_f < 50 ps in 2-propanol[54]) is much shorter than that of C153 (τ_f = 4.1 ns in methanol) or 4-AP (τ_f = 6.8 ns in methanol). Interestingly, as can be seen from Figure 4.2c, ANF shows appreciable dependence of

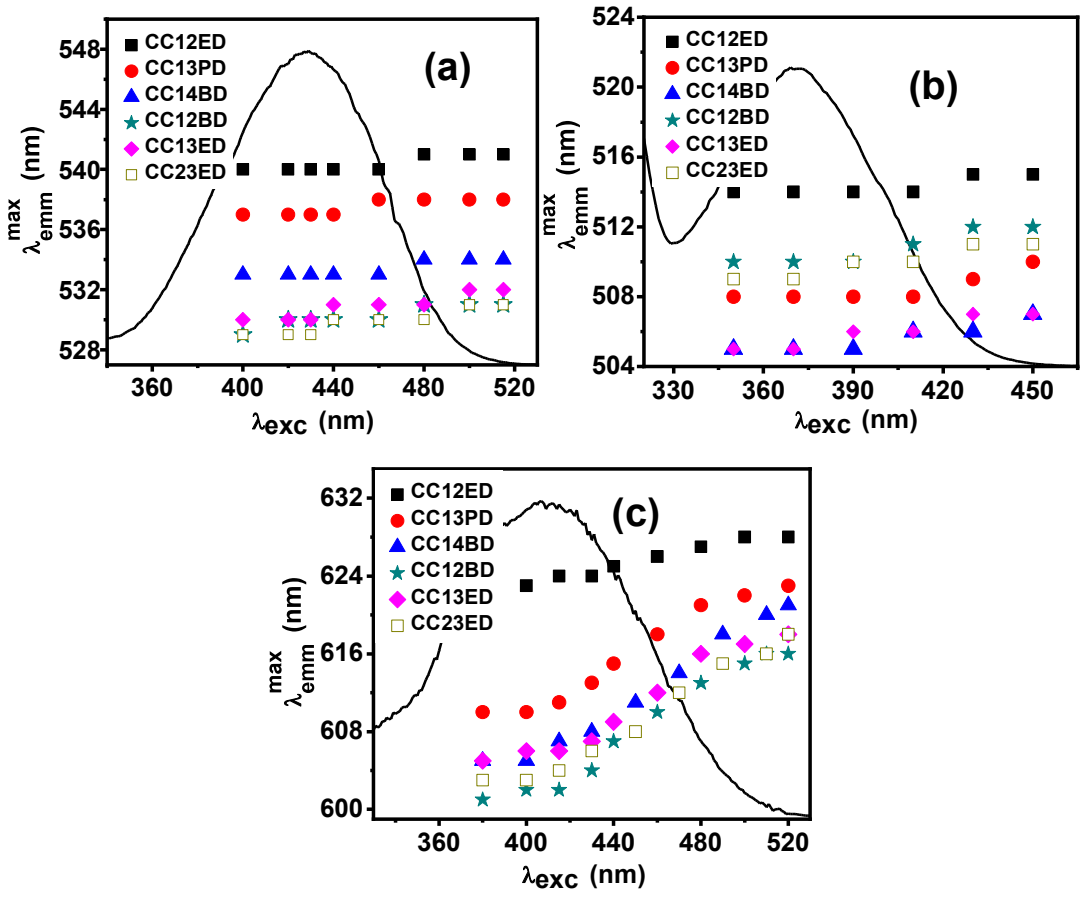

Figure 4.2. Dependence of the emission maximum (λ_{emm}^{max}) on the excitation wavelength (λ_{exc}^{max}) for C153 (a), 4-AP (b) and ANF (c) at 298K in DESs. Representative excitation spectra of the solutes are also shown by solid lines.

λ_{emm}^{max} on the excitation wavelength. This increasing excitation wavelength dependent fluorescence behavior in DESs with longer chain length diols indicates spatial heterogeneity of the solvents arising from the formation of nanoscale heterogeneous structure through segregation of ionic and molecular domain/region. A similar line of reasoning has been used for other eutectic systems.[31, 37, 38, 55] However, DESs formed between ChCl and different isomers of butanediol (which differs in position of hydroxyl groups) show identical dependence indicating very similar heterogeneous structure perhaps due to their same chain length.

4.2.2. TRFA Measurements

As stated earlier, in order to understand the microenvironments around the solute molecules and nature of solute-solvent interactions, we have studied the rotational diffusion of C153, 4-AP and ANT in these media by monitoring the time-dependence of fluorescence anisotropy of the systems over a temperature range of 298–343 K. Representative fluorescence anisotropy decay profiles of the solutes in six DESs at 298 K are shown in Figure 4.3. The rotational reorientation times (τ_r) of the solutes in these DESs are obtained by fitting the anisotropy data to single-exponential function of the form: $r(t) = r_0 \exp(-t/\tau_r)$. The measured τ_r values of the solutes at 298 K are collected in Table 4.3, while those at all the temperatures are provided in Table A2.1. Table 4.3 shows that at 298 K, the τ_r values are very similar for 4-AP and C153 in CC12ED. However, these values differ significantly with increasing chain length and hydroxyl group position of the diols. As the size of 4-AP is almost half than that of C153 (vide later), much higher τ_r value of 4-AP compared to C153 in these solvents suggests hindrance of its rotational diffusion due to strong solute-solvent association/interactions. On the other hand, though the size of ANT is comparable with 4-AP, its τ_r value is lowest in any given solvent indicating that it does not experience strong interaction (like that faced by 4-AP) with the solvents. The above results clearly indicate that these solute molecules experience very different interactions in any given DESs.

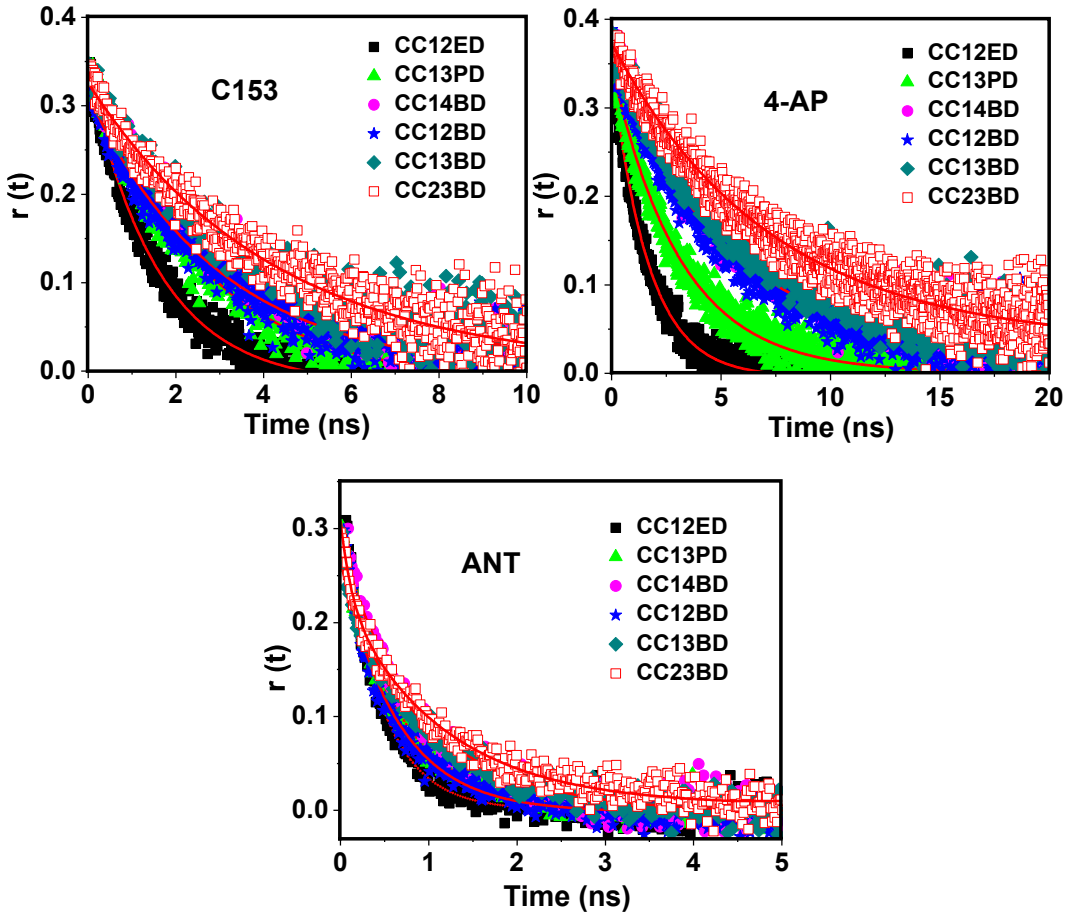

Figure 4.3. Anisotropy decay profiles of the solutes in six DESs at isothermal (298 K) condition. The solid lines represent single-exponential fit to the decay profiles. The excitation wavelength for C153/4-AP and ANT are 405 and 375 nm, respectively. All the decay profiles are recorded by monitoring at respective emission maxima of solutes in six DESs.

We have also examined the fluorescence anisotropy decay profiles of the solutes in iso-viscous condition (30 cP) by adjusting the temperatures of the solvents, and are shown in Figure 4.4. The τ_r values of C153 and ANT measured under this condition (Table 4.4) show small variation with increasing hydrocarbon chain length and remain almost constant with change in hydroxyl group position; however, these values for 4-AP differ more significantly in both situations. These are very interesting observations, and a more detailed and quantitative discussion on rotational dynamics of the solutes in these media, therefore, is presented below using the SED hydrodynamic theory.[56]

Table 4.3. Estimated rotational reorientation times (ns) of the solutes in various DESs at isothermal condition (298 K).

DESs	Viscosity (cP)	Rotational reorientation time (ns)		
		C153	4-AP	ANT
CC12ED	30	1.58	1.65	0.44
CC13PD	53	2.64	3.14	0.66
CC14BD	84.5	3.53	5.08	0.84
CC12BD	72	2.99	5.30	0.64
CC13BD	97	3.83	5.96	0.97
CC23BD	112	4.17	7.20	0.99

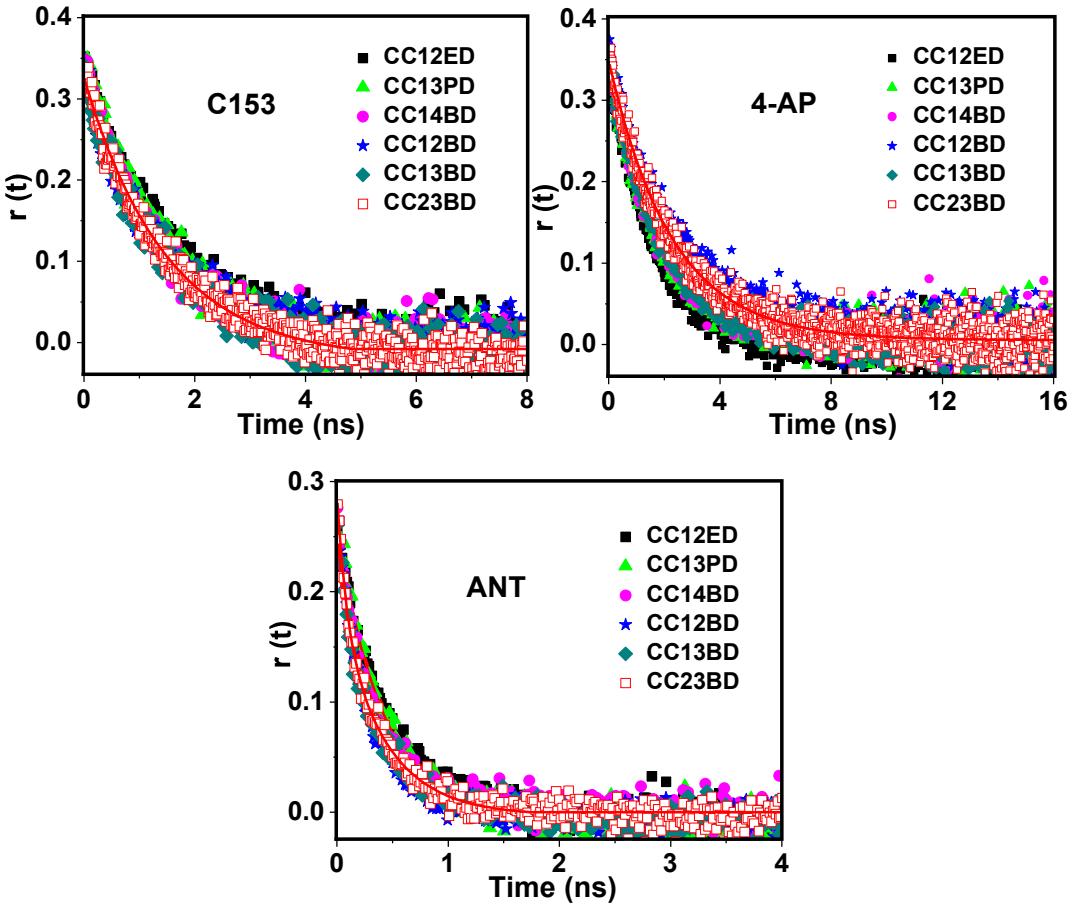

Figure 4.4. Anisotropy decay profiles of the solutes in six DESs at isoviscous (30 cP) condition. The solid lines represent single-exponential fit to the decays. The excitation wavelength for C153/4-AP and ANT are 405 and 375 nm, respectively. All the decay profiles are recorded by monitoring at respective emission maxima of solutes.

Table 4.4. Estimated rotational reorientation times (ns) of the solutes in various DESs at isoviscous condition (30 cP).

DESs	Viscosity (cP)	Rotational reorientation time (ns)		
		C153	4-AP	ANT
CC12ED	30	1.58	1.65	0.44
CC13PD		1.59	1.89	0.41
CC14BD		1.46	1.93	0.35
CC12BD		1.45	2.36	0.33
CC13BD		1.45	2.07	0.33
CC23BD		1.44	2.26	0.34

According to this theory, the τ_r value of a solute in a solvent continuum of viscosity η at temperature T is given by equation 3.1, where, V, f and C are respectively the van der Waals volume, shape factor and boundary condition parameter of the solutes and k_B is Boltzmann constant. The shape factor (f), which is a function of axial ratio of the semi axes, describes nonspherical nature of the solutes, which are treated as asymmetric ellipsoids. C indicates the extent of coupling between the solute and the solvent; hydrodynamic slip ($0 < C_{slip} < 1$) and stick ($C_{stick} = 1$) are the two limiting cases. The V, f and C values for the three solutes are taken from literatures[49, 57] and collected in Table 4.5.

Table 4.5. Solute dimensions, van der Waals volumes, shape factors and boundary condition parameters calculated from the SED hydrodynamic theory.

Solute	Axial radii ($Å^3$)	van der Waals volume, V ($Å^3$)	Shape factors (f)	C_{slip}
C153[a]	6.1 x 4.8 x 2.2	246	1.71	0.24
4-AP[b]	5.0 x 3.5 x 1.8	134	1.60	0.11
ANT[b]	5.9 x 3.9 x 1.8	175	1.30	0.29

[a] values are taken from ref. 57. [b] values are taken from ref. 49.

Typical plots of the measured τ_r values of the solutes versus η/T in CC12ED are shown in Figure 4.5 along with the slip and stick lines. The plots in other DESs are displayed in Figure A2.1, A2.2, and A2.3. Figure 4.5 shows that C153 reorientation times lie between

the slip and stick lines, 4-AP exhibits superstick behavior and ANT shows slip behavior. The superstick behavior of 4-AP is an indication of its strong association with the constituents of the solvent. This must be due to specific hydrogen-bonding interaction of 4-AP with the hydroxyl groups of the eutectic solvent as this is well documented in both conventional solvents[52] and ionic liquids.[49, 58] The slip behavior of ANT is because of its lack of interaction with the solvent due to its nonpolar nature and location in the hydrocarbon dominated molecular domain/region.

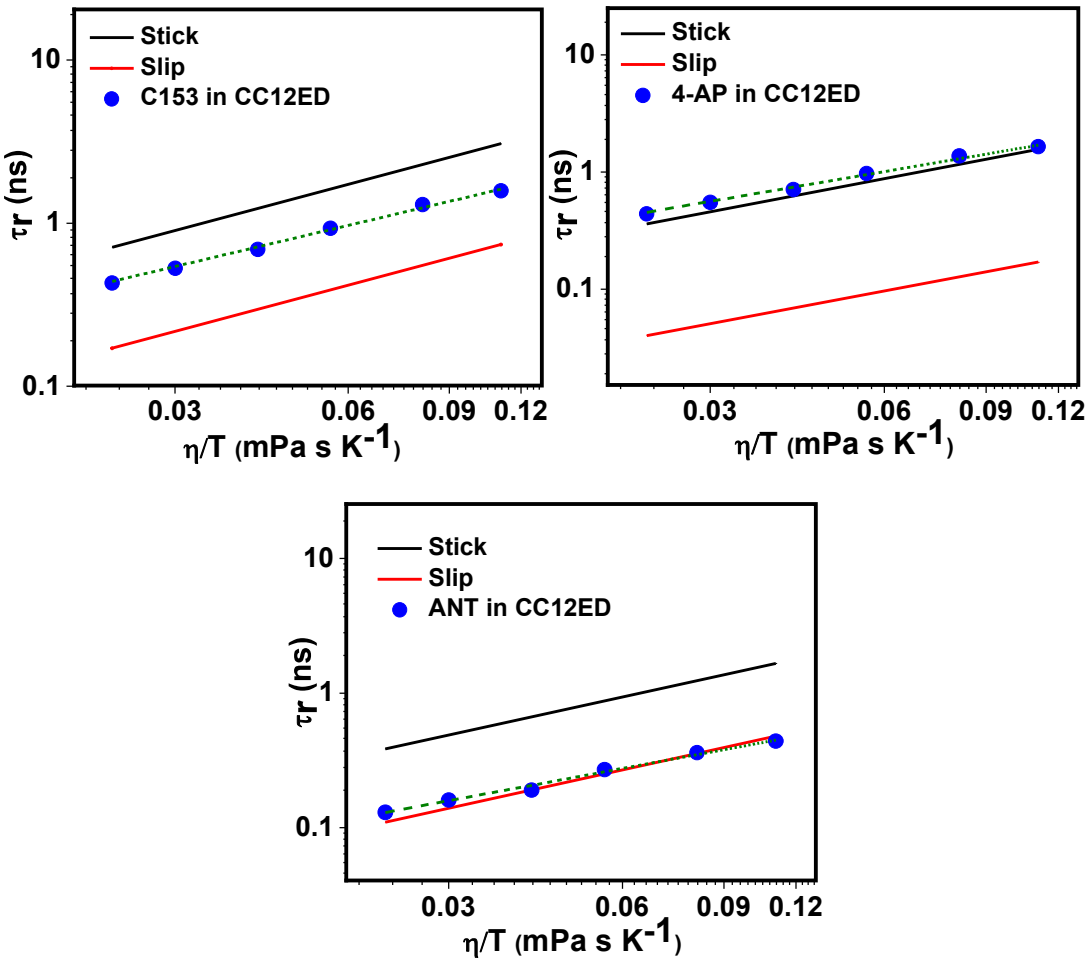

Figure 4.5. Plots of τ_r vs η/T for three solutes in CC12ED system. The solid circles indicate the experimental rotational times and the dashed lines represent fit to the data according to $\tau_r = A(\eta/T)^p$. Computed stick (black) and slip (red) lines using SED theory are also shown.

A similar analysis in other DESs reveals that the superstick behavior of 4-AP is more pronounced (Figure A2.1) with increasing chain length indicating stronger hydrogen-bonding interaction with the latter members of the series (leading to a slower rotation). On the other hand, the τ_r values of ANT changes from slip to subslip behavior (Figure A2.2) with increasing chain length due to lower friction experienced in larger solvents comprising a higher non polar fraction arising from increasing hydrocarbon chain length of the diols. In this context, it is noteworthy that the subslip behavior of rotational dynamics is sometimes (like in ionic liquids[50]) considered to be due to void spaces created from increasing chain length, which reduce the rotational friction. However, unlike the two other probes, τ_r values of C153 changes marginally towards the slip line with increasing chain length, that too only at low temperature. At higher temperature, it shows very similar behavior in all solvents (Figure A2.3).

The experimental τ_r values of the solutes are fitted to $\tau_r = A(\eta/T)^p$ in each DES (shown as dashed line in the τ_r vs η/T plots). The A and p values obtained from these fits are presented in Table 4.6. The p values show significant departure from unity, indicating deviation of the rotational dynamics from the SED hydrodynamic behavior. This fractional viscosity dependence (or departure from the SED theory) is a reflection of the dynamic heterogeneity of the media,[29, 31, 47] which arises from fluctuations of the hydrogen-bonding network in these media and consequent motion of its constituents.

Table 4.6. Parameters A [$ns\ K\ (mPa\ s^{-1})$] and p for the solutes obtained from least-squares fits of τ_r vs η/T plots in DESs.

DESs	C153		4-AP		ANT	
	A	*p*	*A*	*p*	*A*	*p*
CC12ED	10.8 ± 0.2	0.84 ± 0.02	10.9 ± 0.2	0.85 ± 0.02	2.6 ± 0.2	0.82 ± 0.03
CC13PD	11.0 ± 0.3	0.81 ± 0.01	13.4 ± 0.2	0.84 ± 0.02	2.5 ± 0.1	0.80 ± 0.02
CC14BD	9.3 ± 0.3	0.77 ± 0.02	14.8 ± 0.3	0.85 ± 0.01	2.2 ± 0.1	0.76 ± 0.01
CC12BD	9.0 ± 0.2	0.77 ± 0.01	17.9 ± 0.3	0.85 ± 0.01	2.0 ± 0.1	0.77 ± 0.02
CC13BD	9.1 ± 0.3	0.76 ± 0.02	15.3 ± 0.3	0.83 ± 0.01	2.2 ± 0.1	0.77 ± 0.01
CC23BD	8.9 ± 0.3	0.76 ± 0.02	16.6 ± 0.2	0.84 ± 0.02	2.1 ± 0.1	0.75 ± 0.01

As can be seen, the departure of the *p* values from unity for C153 and ANT increases with increasing hydrocarbon chain length. The *p* values, however, remain nearly constant upon change of hydroxyl group position. This suggests that dynamic heterogeneity is more pronounced in media comprising diols with longer chain length, but it does not vary with change in hydroxyl group position. Nearly constant (and high) *p* values for 4-AP in all six DESs indicate that 4-AP molecules experience relatively less and very similar dynamic heterogeneity in these media, perhaps due to its strong association with constituents of the solvents, which does not allow much fluctuations of the hydrogen-bonding network. Further, Table 4.6 shows that the *A* (= VfC/k_B) values decrease marginally for C153 and ANT with increase in hydrocarbon chain length but remain almost constant upon change of the hydroxyl group position. Considering that f/k_B is constant for a given solute and the volume of the solvents (*V*) increases with increasing chain length of HBDs, the decrease of the *A* values suggest a decrease of solute-solvent coupling with increasing chain length. Unlike C153 and ANT, the *A* values for 4-AP increase significantly with increasing chain length suggesting stronger coupling in the latter media. Some variation of the *A* value with change in the hydroxyl group position indicates change in coupling with the hydroxyl group position too.

To corroborate these conclusions, we have calculated the solute-solvent coupling constant (C_{obs}) from the experimental τ_r values using $C_{obs} = \tau_r/\tau_{stick}$ (where, τ_{stick} is the rotational time calculated using SED hydrodynamic theory) and presented in Table 4.7. A careful inspection of the data reveals that the C_{obs} values decrease marginally for C153 and ANT with increasing chain length but shows no significant variation with hydroxyl group position. This trend is the same as seen for the *A* values in the previous section, indicating faster rotation of the solutes with increasing chain length. Interestingly, the C_{obs} values for 4-AP increase significantly with increase of chain length, suggesting slower rotational diffusion due to an enhanced hydrogen-bonding interaction between the solute and constituents of the solvents. These observations can be rationalized considering formation of a nanoheterogeneous domain-like structure[31, 37, 38, 55] consisting of ionic and molecular regions in DESs containing longer chain length diols, where different solute molecules reside in different environments (Scheme 4.1). 4-AP molecule resides in the ionic polar region, ANT resides specifically in molecular region (relatively nonpolar region), and C153 being larger in size, locates itself at the boundary between ionic and molecular regions. This heterogeneous structure becomes pronounced with increasing hydrocarbon chain length of diols, but does not change with the position of the hydroxyl groups. A

similar picture also emerged from the steady-state measurements. With increase in the hydrocarbon chain length of HBDs, the fraction of molecular environment (nonpolar region) as well as overall size of the solvent increases offering a lower friction to C153 and ANT leading to a decrease of the C_{obs} values. In contrast, as 4-AP molecules reside in ionic polar region of these solvents, an increase in nonpolar fraction (or hydrocarbon chain length of HBDs) forces the 4-AP molecules to come closer towards the hydroxyl groups of the diols offering stronger hydrogen-bonding interaction with the solvents resulting in an increase in C_{obs} values.

Table 4.7. Calculated solute-solvent coupling constants (C_{obs}) of the solutes in six DESs.

DESs	C_{obs} [a]		
	C153	4-AP	ANT
CC12ED	0.55 ± 0.01	1.12 ± 0.02	0.30 ± 0.01
CC13PD	0.56 ± 0.005	1.29 ± 0.01	0.26 ± 0.01
CC14BD	0.51 ± 0.01	1.33 ± 0.01	0.23 ± 0.01
CC12BD	0.51 ± 0.01	1.64 ± 0.02	0.21 ± 0.02
CC13BD	0.50 ± 0.015	1.41 ± 0.02	0.22 ± 0.005
CC23BD	0.49 ± 0.02	1.51 ± 0.01	0.22 ± 0.01

[a] average of C_{obs} values obtained at six temperatures from 298-343 K.

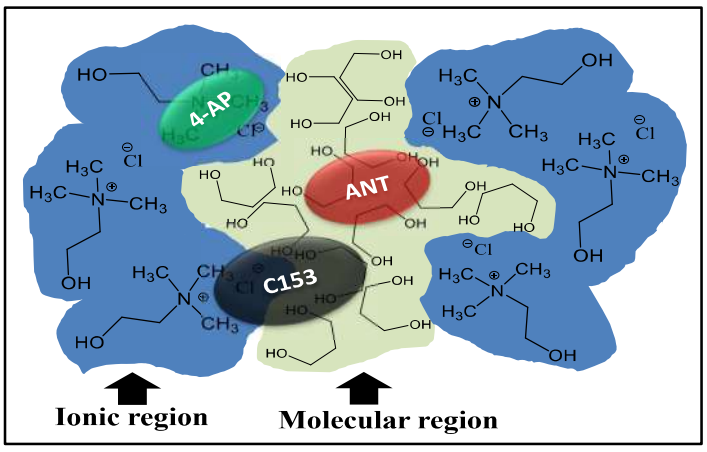

Scheme 4.1. A schematic representation showing different domain/region in DESs and possible location of various solutes in these regions.

Unlike the other two solutes, C_{obs} values for 4-AP molecules vary significantly with the hydroxyl group position. A careful inspection of the data presented in Table 4.7 reveals a higher C_{obs} value and stronger solute-solvent association in solvents (CC12BD and CC23BD), where the hydroxyl groups are adjacent to each other.

4.2.3. FCS Measurements

We have studied the translation diffusion dynamics of C153 and 4-AP in these solvents by single-molecule based FCS technique. ANT could not be studied for its blue fluorescence and lack of suitable excitation source. Representative fluorescence correlation curves of C153 and 4-AP in CC12ED at 298 K are shown in Figure 4.6. The correlation curves $G(\tau)$ of the solute molecules in all media were fitted to both single-component diffusion (equation 2.7) and anomalous diffusion ($\beta < 1$) model (equation 2.9), but, as judged by distribution of the residuals and χ^2 values of the fits, the anomalous diffusion model fits the data much better compared to the single-component diffusion model.

Figure 4.7 compares the fitted (to anomalous diffusion model) correlation curves of the solutes in the DESs. The diffusion coefficients (D_t) of the solutes in the DESs, calculated using the τ_D values obtained from fits, using equation 2.12 are collected in Table 4.8 along with the β values. It can be seen that the β values for both solutes deviate significantly from unity in these media. Considering the fact that these molecules show a single-component diffusion in conventional solvents, this deviation of the β values from unity can be attributed to the dynamic heterogeneity of the media, as described in earlier reports.[47, 59] The deviation of the stretching exponent β from unity suggests that the mean square displacement of the probe molecules follows a sub-diffusive behavior, $\langle r(\tau)^2 \rangle \propto \tau^{\beta}$ (with $\beta < 1$), instead of the normal Brownian diffusion ($\beta = 1$) due to dynamic heterogeneity in these complex media.[25, 47, 59] Further, the data presented in Table 4.8 shows that the deviation of the β value of C153 from unity increases with increase in chain length indicating greater dynamic heterogeneity in solvents containing HBDs with higher chain length. The near-constancy of the β value in solvents with different hydroxyl group position indicates negligible variation of dynamic heterogeneity. On the other hand, these values for 4-AP are very similar in both situations. These results are consistent with the trends observed for the rotational diffusion of the solutes.

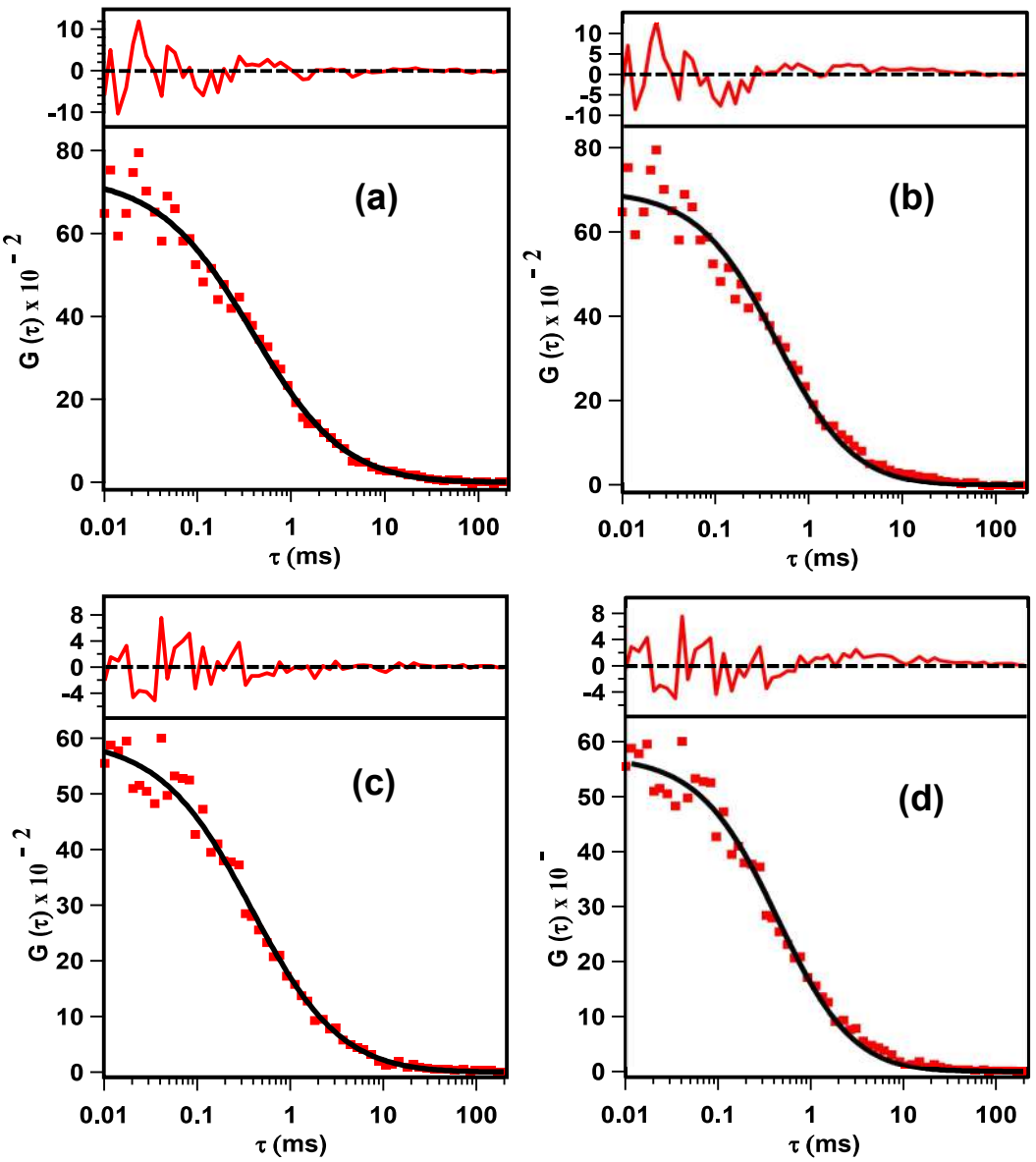

Figure 4.6. Fluorescence correlation curves of C153 (a,b) and 4-AP (c,d) in CC12ED DESs. The points are the experimental data, and the solid lines represent fit to the data using an anomalous diffusion model (left panel: a,c) and a single-component diffusion model (right panel: b,d). The residuals depicting quality of the fits are also shown at the top of each curve.

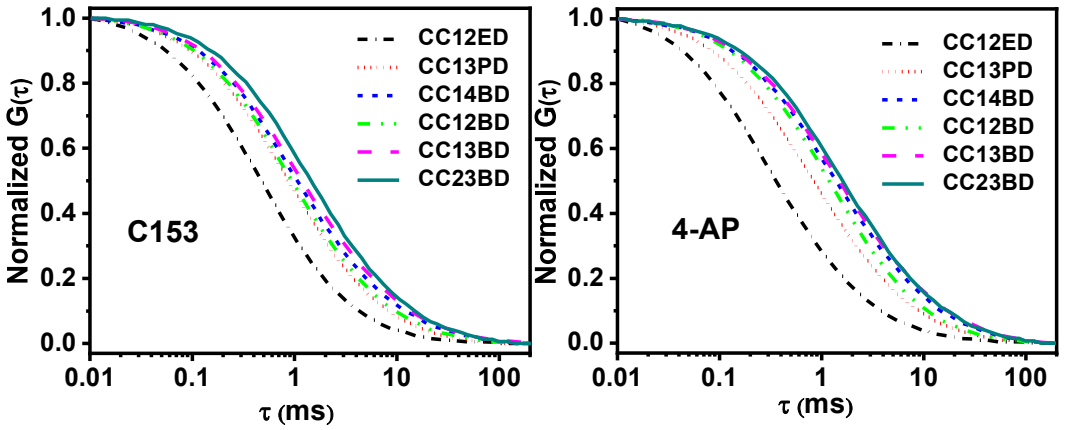

Figure 4.7. The fitted correlation curves (normalized) of the solutes in six DESs using the anomalous diffusion model.

In addition, we note that the D_t value of each solute correlates nicely with the viscosity of the media. However, there are two interesting points to note. First, even though 4-AP is much smaller than C153, the D_t value of 4-AP is comparable or lower than that of C153 in these solvents. Second, the D_t value of 4-AP decreases more sharply compared to C153. These trends, which are similar to those observed for the rotational dynamics of the solutes in these media, confirm strong association of 4-AP molecules with the constituents of the solvents due to strong solute-solvent hydrogen-bonding interaction.

Table 4.8. Estimated diffusion coefficients (D_t in $\mu m^2 s^{-1}$) and stretching exponents (β) obtained from the fits using anomalous diffusion model for the solutes in DESs.

DESs	C153		4-AP	
	D_t	β	D_t	β
CC12ED	32.9 ± 4.2	0.87 ± 0.02	35.4 ± 3.6	0.86 ± 0.02
CC13PD	18.2 ± 2.4	0.85 ± 0.01	16.9 ± 3.5	0.86 ± 0.03
CC14BD	15.6 ± 1.5	0.82 ± 0.02	10.5 ± 2.0	0.87 ± 0.02
CC12BD	16.1 ± 0.8	0.83 ± 0.02	12.9 ± 1.3	0.86 ± 0.03
CC13BD	12.0 ± 1.0	0.83 ± 0.03	9.8 ± 1.1	0.85 ± 0.03
CC23BD	10.1 ± 1.2	0.82 ± 0.03	7.7 ± 0.9	0.87 ± 0.01

4.3. Summary

In summary, we have studied the rotational and translational diffusion of some selected neutral fluorescent molecules in six ChCl-diol based DESs to find out the effect of hydrocarbon chain length and hydroxyl group positioning (at HBDs) of the eutectic systems on the respective diffusion dynamics. The results obtained from measurements in ensemble and single molecule conditions are in excellent agreement with each other and reveal several interesting outcomes. Specifically, the excitation wavelength dependent fluorescence studies reveal an evolution of spatial heterogeneity with increase in chain length of the HBDs in these solvents. The time-resolved fluorescence anisotropy and FCS studies show significant increase of dynamic heterogeneity with increasing chain length of the HBDs. The variation of spatial and dynamic heterogeneity with change in hydroxyl group position is found to be insignificant. Additionally, this study shows that the solute molecules reside in different environments of the nanoheterogeneous structure of these solvents and specific solute-solvent hydrogen-bonding interaction plays a crucial role in determining both rotational and translational diffusion dynamics of 4-AP in these DESs.

References

1. C. Ruβ and B. Konig, *Green Chem.*, 2012, **14**, 2969−2982.
2. D. A. Alonso, A. Baeza, R. Chinchilla, G. Guillena, I. M. Pastor and D. J. Ramón, *Eur. J. Org. Chem.*, 2016, **2016**, 612–632.
3. Y. Gu and F. Jérôme, *Chem. Soc. Rev.*, 2013, **42**, 9550-9570.
4. A. P. Abbott, G. Capper, K. J. McKenzie and K. S. Ryder, *Electrochim. Acta*, 2006, **51**, 4420−4425.
5. A. P. Abbott, G. Capper, D. L. Davies, R. K. Rasheed and P. Shikotra, *Inorg. Chem.*, 2005, **44**, 6497−6499.
6. A. P. Abbott, G. Capper, A. Glidle and K. S. Ryder, *Phys. Chem. Chem. Phys.*, 2006, **8**, 4214−4221.
7. D. Carriazo, M. C. Serrano, M. C. Gutiérrez, M. L. Ferrer and F. d. Monte, *Chem. Soc. Rev.*, 2012, **41**, 4996–5014.
8. J.-H. Liao, P.-C. Wu and Y.-H. Bai, *Inorg. Chem. Commun.*, 2005, **8**, 390−392.
9. D. Z. Troter, Z. B. Todorović, D. R. Đokić-Stojanović, O. S. Stamenković and V. B. Veljković, *Renew. Sust. Energ. Rev.*, 2016, **61**, 473-500.
10. C. A. Nkuku and R. J. LeSuer, *J. Phys. Chem. B*, 2007, **111**, 13271–13277.
11. H.-R. Jhong, D. S.-H. Wong, C.-C. Wan, Y. Wang, -Y. and T.-C. Wei, *Electrochem. Commun.*, 2009, **11**, 209-211.
12. D. V. Wagle, H. Zhao and G. A. Baker, *Acc. Chem. Res.*, 2014, **47**, 2299−2308.

13. H.-G. Liao, Y.-X. Jiang, Z.-Y. Zhou, S.-P. Chen and S.-G. Sun, *Angew. Chem.*, 2008, **120**, 9240−9243.
14. Y. P. Mbous, M. Hayyan, A. Hayyan, W. F. Wong, M. A. Hashima and C. Y. Looi, *Biotechnol. Adv.*, 2017, **35**, 105-134.
15. R. B. Leron and M.-H. Li, *Thermochim. Acta*, 2013, **551**, 14−19.
16. R. B. Leron and M.-H. Li, *J. Chem. Thermodyn.*, 2013, **57**, 131−136.
17. A. P. Abbott, R. C. Harris, K. S. Ryder, C. D'Agostino, L. F. Gladden and M. D. Mantle, *Green Chem.*, 2011, **13**, 82–90.
18. Baokun Tang and K. H. Row, *Monatsh Chem*, 2013, **144**, 1427-1454.
19. Q. Zhang, K. D. O. Vigier, S. Royer and F. Jé rôme, *Chem. Soc. Rev.*, 2012, **41**, 7108−7146.
20. A. P. Abbott, D. Boothby, G. Capper, D. L. Davies and R. K. Rasheed, *J. Am. Chem. Soc.*, 2004, **126**, 9142−9147.
21. A. P. Abbott, G. Capper, D. L. Davies, R. K. Rasheed and V. Tambyrajah, *Chem. Commun.*, 2003, **1**, 70−71.
22. A. Paiva, R. Craveiro, I. Aroso, M. Martins, R. L. Reis and A. R. C. Duarte, *ACS Sustain. Chem. Eng.*, 2014, **2**, 1063−1071.
23. M. Francisco, A. van den Bruinhorst and M. C. Kroon, *Angew. Chem., Int. Ed.*, 2013, **52**, 3074−3085.
24. E. L. Smith, A. P. Abbott and K. S. Ryder, *Chem. Rev.*, 2014, **114**, 11060−11082.
25. C. D'Agostino, R. C. Harris, A. P. Abbott, L. F. Gladden and M. D. Mantle, *Phys. Chem. Chem. Phys.*, 2011, **13**, 21383–21391.
26. C. D'Agostino, L. F. Gladden, M. D. Mantle, A. P. Abbott, I. A. Essa, A. Y. M. Al-Murshedi and R. C. Harris, *Phys. Chem. Chem. Phys.*, 2015, **17**, 15297-15304.
27. O. S. Hammond, D. T. Bowron and K. J. Edler, *Green Chem.*, 2016, **18**, 2736-2744.
28. R. Stefanovic, M. Ludwig, G. B. Webber, R. Atkin and A. J. Page, *Phys. Chem. Chem. Phys.*, 2017, **19**, 3297-3306.
29. A. Das and R. Biswas, *J. Phys. Chem. B*, 2015, **119**, 10102−10113.
30. A. Das, S. Das and R. Biswas, *J. Chem. Phys.* , 2015, **142**, 034505.
31. B. Guchhait, S. Das, S. Daschakraborty and R. Biswas, *J. Chem. Phys.*, 2014, **140**, 104514.
32. B. Guchhait, S. Daschakraborty and R. Biswas., *J. Chem. Phys.*, 2012, **136**, 174503.
33. K. Mukherjee, A. Das, S. Choudhury, A. Barman and R. Biswas, *J. Phys. Chem. B*, 2015, **119**, 8063−8071.
34. T. Pal and R. Biswas, *Chem. Phys. Letters*, 2011, **517**, 180-185.
35. S. Das, R. Biswas and B. Mukherjee, *J. Phys. Chem. B*, 2015, **119**, 11157-11168.
36. S. Das, R. Biswas and B. Mukherjee, *J. Phys. Chem. B*, 2015, **119**, 274-283.
37. S. Kaur, A. Gupta and H. K. Kashyap, *J. Phys. Chem. B*, 2016, **120**, 6712-6720.
38. A. Faraone, D. V. Wagle, G. A. Baker, E. C. Novak, M. Ohl, D. Reuter, P. Lunkenheimer, A. Loidl and E. Mamontov, *J. Phys. Chem. B*, 2018, **122**, 1261-1267.

39. E. O. Fetisov, D. B. Harwood, I. F. W. Kuo, S. E. E. Warrag, M. C. Kroon, C. J. Peters and J. I. Siepmann, *J. Phys. Chem. B*, 2018, **122**, 1245-1254.
40. A. Pandey, R. Rai, M. Pal and S. Pandey, *Phys. Chem. Chem. Phys.*, 2014, **16**, 1559-1568.
41. A. Pandey, A. Yadav, Bhawna. and S. Pandey, *J. Lumin.*, 2017, **183**, 494-506.
42. A. Pandey, Bhawna, D. Dhingra and S. Pandey., *J. Phys. Chem. B*, 2017, **121**, 4202-4212.
43. B. Guchhait, H. A. R. Gazi, H. K. Kashyap and R. Biswas, *J. Phys. Chem. B*, 2010, **114**, 5066-5081.
44. W. Bi, M. Tian and K. H. Row, *J. Chromatogr. A*, 2013, **1285**, 22-30.
45. Z. S. Othman, N. H. Hassan and S. I. Zubairi, *AIP Conference Proceedings*, 2015, **1678**, 050004.
46. H. Cruz, N. Jordão and L. C. Branco, *Green Chem.*, 2017, **19**, 1653-1658.
47. S. S. Hossain and A. Samanta, *J. Phys. Chem. B*, 2017, **121**, 10556-10565.
48. R. M. Harris, *PhD Thesis*, 2008, University of Leicester.
49. D. C. Khara, J. P. Kumar, N. Mondal and A. Samanta, *J. Phys. Chem. B*, 2013, **117**, 5156-5164.
50. S. K. Das and M. Sarkar, *J. Phys. Chem. B*, 2012, **116**, 194-202.
51. A. I. Zvaigzne, J. Wolfe and W. E. A. Jr., *J. Chem. Eng. Data*, 1994, **39**, 541-543.
52. G. Saroja, T. Soujanya, B. Ramachandram and A. Samanta, *J. Fluoresc.*, 1998, **8**, 405-410.
53. P. K. Mandal, M. Sarkar and A. Samanta, *J. Phys. Chem. A*, 2004, **108**, 9048-9053.
54. L. A. Hallidy and M. R. Topp, *Chem. Phys. Letters*, 1977, **48**, 40-45.
55. Y. Cui and D. G. Kuroda, *J. Phys. Chem. A* 2018, **122**, 1185−1193.
56. G. R. Fleming, *Chemical Applications of Ultrafast Spectroscopy*, 1986, Oxford University Press: New York, USA.
57. H. Jin, G. A. Baker, S. Arzhantsev, J. Dong and M. Maroncelli, *J. Phys. Chem. B*, 2007, **111**, 7291–7302.
58. J. A. Ingram, R. S. Moog, N. Ito, R. Biswas and M. Maroncelli, *J. Phys. Chem. B*, 2003, **107**, 5926-5932.
59. E. C. Wu, H. J. Kim and L. A. Peteanu, *J. Phys. Chem. B*, 2017, **121**, 1100−1107.

Chapter 5

Liquid Structure and Dynamics of Tetraalkylammonium Bromide-Based Deep Eutectic Solvents: Effect of Cation Chain Length

J. Phys. Chem. B, 2019, 123, 6842-6850

Overview

Large numbers of the works on DESs have been focused on a particular ammonium salt, ChCl. In recent times, several new DESs based on various other salts have emerged across several fields. However, knowledge about the microscopic structural and dynamical features of these less-explored DESs that is essential for exploiting their potential is still lacking. In this work, we make an attempt to obtain some insight into these aspects of a set of less-explored DESs comprising tetraalkylammonium bromide salts and ethylene glycol by monitoring the fluorescence response of some carefully chosen dipolar (C153 and 4-AP) and nonpolar (9-PA) solutes in these media. Specifically, we have studied the translational and rotational diffusion dynamics of these molecular systems using single-molecule based FCS technique and ensemble-based TRFA measurements. These results point to spatial and dynamic heterogeneity of these DESs, which becomes prominent in systems comprising cation with a longer alkyl chain length. This study reveals that diffusion dynamics of the probe molecules are determined not only by the solvent bulk viscosity, but also depends on their microenvironments and solute-solvent interactions experienced in these media.

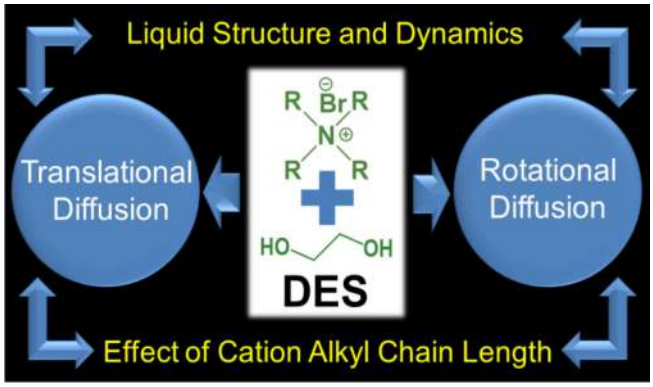

5.1. Introduction

DESs are an emerging class of environmentally sustainable solvents with potential to overcome many limitations of the conventional volatile organic solvents and ionic liquids ILs.[1-7] While similar in many ways to the ILs, these DESs are more favoured green alternative to the organic solvents in a variety of applications because of relatively inexpensive starting materials, often made of natural and biodegradable constituents, ease of preparation and low toxicity.[1-4, 6, 8-10] These solvents are generally obtained by mixing a salt/HBA and a HBD.[1] A large number of such mixtures with desirable properties can be prepared by judicious choice of the constituents and also by varying their stoichiometric molar ratio.[1, 11]

A survey of the literature shows that most of the works on DESs are application oriented and fundamental studies directed towards understanding their physicochemical properties in terms of microscopic structure, dynamics, solute-solvent interactions, etc. are rather limited.[1, 2, 5, 8-10, 12-21] These studies, most of which have been carried out in ChCl based DESs, have brought into light spatial and/or dynamic heterogeneity of these solvents, which contribute to some of the unique properties of these DESs. Several new but promising DESs based on various other salts are gaining attention recently.[22-34] However, little is known about the microscopic structural and dynamical features of these less-explored substances that are necessary for realization of the successful utility of these mixtures in different fields.

The objective of this study is to obtain an understanding of some of these promising, but less-explored eutectic solvents through characterization of the microscopic structure, dynamics, and solute-solvent interactions. Additionally, we probe how the alkyl chain length attached to the cation of the salt influences these fundamental aspects. For this purpose, we have chosen three DESs[22, 34] based on tetraalkylammonium bromide salts with different alkyl chain length and ethylene glycol (Table 5.1) and examined their liquid state structure and dynamics by probing the translation and rotation diffusion dynamics of dipolar molecules, C153 and 4-AP and nonpolar molecule, 9-PA in these media. An identical salt/HBD molar ratio (1:3) in these DESs is chosen to ensure that observed changes in fluorescence properties of the probe molecules in different DESs are not due to any variation of the concentration of the salt or ethylene glycol (HBD). The translation diffusion dynamics of the solutes is studied using FCS technique, whereas, the rotational

diffusion dynamics is investigated by monitoring time-dependent fluorescence anisotropy of the systems. Chart 1.7 and 1.8 depicts the molecular structures of the constituents of the DESs and the solute molecules used in this study, respectively. The idea behind employing multiple probe molecules with different functional groups is that the chosen systems are expected to place themselves in different locations of a structured medium and together they will present a complete picture of all possible microenvironments and interactions operative in the media,[35, 36] and provide comprehensive insights into the structural and dynamical aspects of these less-explored DESs.

Table 5.1. Description of the DESs used in this study

Sl. No.	Salt	HBD	Mole ratio (Salt: HBD)	Abbreviation	Water content (wt %)
1	TEAB	EG	1:3	TEAB-EG	0.09
2	TPAB	EG	1:3	TPAB-EG	0.07
3	TBAB	EG	1:3	TBAB-EG	0.08

5.2. Results and Discussion

5.2.1. Steady-State Measurements: Microscopic Polarity and Liquid Structure

The steady-state excitation and emission spectra of the probe molecules in DESs were measured at room temperature (298 K), and are presented in Figure 5.1. The spectral data, which is summarized in Table 5.2, shows that the excitation maxima (λ_{exc}^{max}) of all solute molecules are independent of the solvents, whereas the emission maxima (λ_{emm}^{max}) of the dipolar solutes (C153 and 4-AP) show noticeable solvent dependence (a blue shift of 6-9 nm with increase in the alkyl chain length of the constituent cation of the DESs). The observed solvent dependence of λ_{exc}^{max} and λ_{emm}^{max} of the probe molecules is consistent with literature.[37, 38] Only the λ_{emm}^{max} values of C153 and 4-AP are sensitive to the solvent as emission of these two dipolar systems originates from ICT state, whose position is dependent both on polarity of the media and hydrogen bonding interaction with the solvent. The λ_{emm}^{max} values of these two indicate that these molecules experience a less

polar environment with increase in alkyl chain length of the cation of the solvent.[39] A comparison of the measured λ_{emm}^{max} values of the two molecules with those in other conventional solvents and DESs reveals that the polarity of the microenvironment sensed by the two dipolar probes in the present DESs is similar to that of methanol and that experienced in ChCl-diol based eutectic solvents.[15, 40]

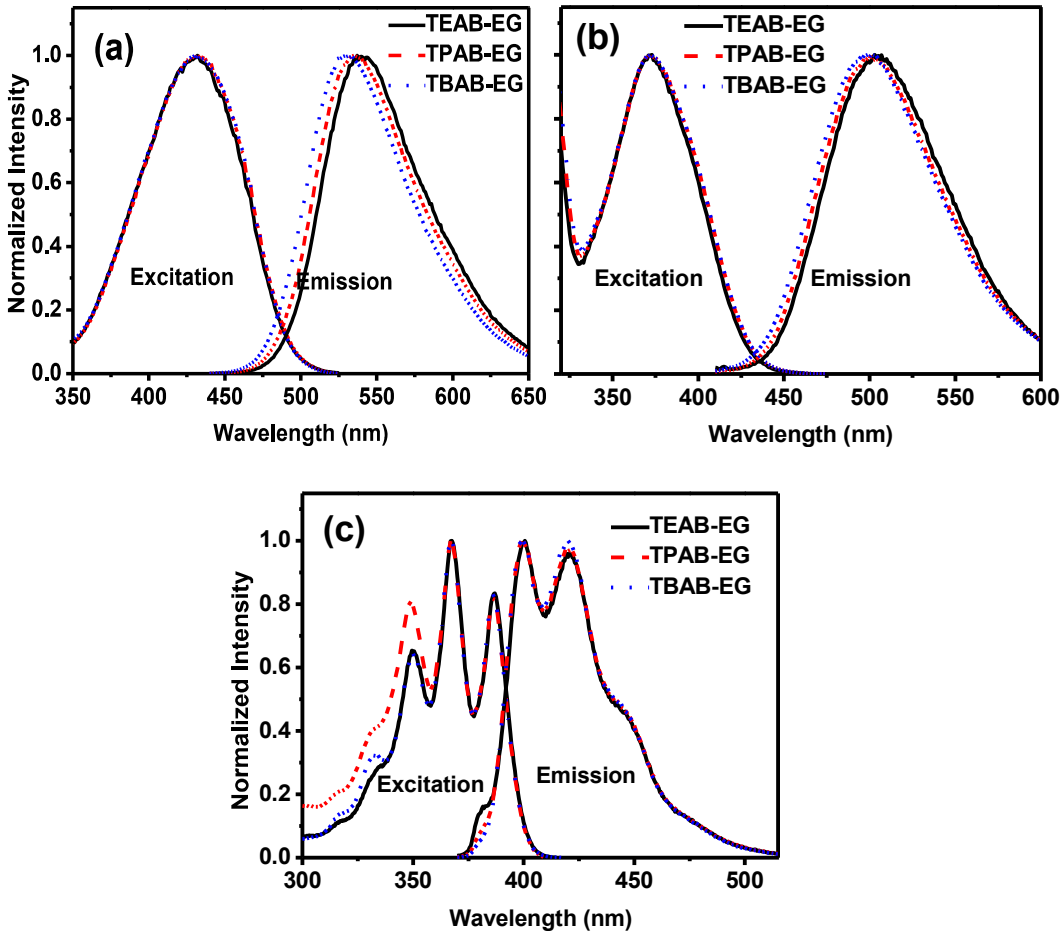

Figure 5.1. Normalized excitation and emission spectra of C153 (a), 4-AP (b) and 9-PA (c) in three DESs at 298K. The emission/excitation spectra are recorded by exciting the samples at their respective maxima of excitation/emission spectra.

Table 5.2. Steady-state excitation and emission maxima (nm) of the solutes in DESs at 298 K

DESs	C153		4-AP		9-PA	
	λ_{exc}^{max}	λ_{emm}^{max}	λ_{exc}^{max}	λ_{emm}^{max}	λ_{exc}^{max}	λ_{emm}^{max}
TEAB-EG	430	539	372	504	387	400
TPAB-EG	430	535	371	501	387	400
TBAB-EG	430	530	372	498	387	400

One of the approaches to examine whether a polar viscous medium like DES is spatially heterogeneous or not is by studying dependence of the λ_{emm}^{max} value on λ_{exc} of dipolar molecules, which fulfill certain criteria.[41-43] A dipolar molecule can exhibit excitation-wavelength-dependent shift of its λ_{emm}^{max} in viscous polar environment, when excited at its long-wavelength absorption edge. The phenomenon, known as "red-edge effect", is observed in polar viscous media for molecules which exhibit a large change in dipole moment on excitation and are characterized by short fluorescence lifetime.[41, 43] In order to explore the microscopic liquid structure of the present DESs in terms of the spatial heterogeneity, if any, we have examined λ_{exc} dependence of λ_{emm}^{max} of ANF, a molecule which exhibits a huge change in dipole moment ($\Delta\mu$= 25 D[41]) on excitation and characterized by a very short excited state lifetime (τ_f) (τ_f < 50 ps in 2-propanol[44]) compared to C153 (τ_f = 4.1 ns in methanol[40]) and 4-AP (τ_f = 6.8 ns in methanol[40]), which do not exhibit any excitation wavelength dependent fluorescence behavior (Figure A3.3). Figure 5.2 show that ANF exhibits significant excitation wavelength dependence of λ_{emm}^{max} in all three DES indicating heterogeneous nature of theses solvents. That, C153 and 4-AP do not show any λ_{exc} dependence, but only ANF does, is primarily because as τ_f of ANF is much shorter than the average solvent relaxation time (τ_s) of common DESs,[45, 46] and hence, the emission, instead of originating from a fully solvent-equilibrated state, occurs from a state determined by the λ_{exc} value. A more prominent excitation wavelength dependent emission behavior in longer alkyl chain length containing DESs indicates an enhanced spatial heterogeneity of these media. This enhanced spatial heterogeneity of the

long alkyl chain length containing DESs is very similar to that observed for various ILs.[39, 47-49] Hence, by drawing an analogy with the ILs one can infer that the spatial heterogeneity of these DESs arises from the formation of hydrophobic and hydrophilic domain-like structure due to segregation of the alkyl chains from the ionic moieties of the cation and hydroxyl moieties of the HBD.[13, 39, 47-50]

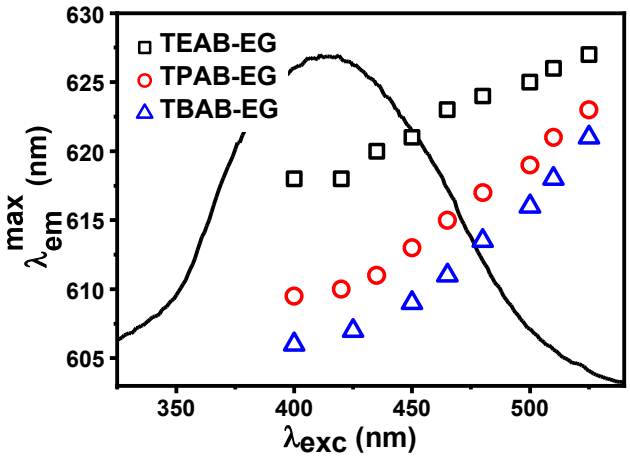

Figure 5.2. Dependence of the emission maximum (λ_{emm}^{max}) on the excitation wavelength (λ_{exc}) for ANF at 298 K in three DESs. Representative excitation spectrum of ANF is also shown.

5.2.2. FCS Measurements: Translational Diffusion Dynamics

As diffusion of a molecule depends on its surrounding environment and the interactions it experiences with the solvent, one can obtain an understanding of the nature of the medium by monitoring the diffusion dynamics of the probe molecules. Single-molecule based FCS technique is a powerful and sensitive tool for studying diffusion and hence, for characterization of microscopic structural and dynamical features of complex media like ILs and DESs.[40, 47, 51, 52] We have studied the translation diffusion of C153 and 4-AP in the chosen DESs using this technique. Figure 5.3 shows representative time-dependence of the fluorescence correlation data of the two probe molecules in TPAB-EG at 298 K (data in other DESs are in Figure A3.4 and A3.5). As the fits of the correlation data to a single-component diffusion model (equation 2.7) were found unsatisfactory, the data were fitted to anomalous diffusion model (equation 2.9), according to which the mean square

displacement of the solute molecules follows a sub-diffusive behavior, $\langle r(\tau)^2 \rangle \propto \tau^{\beta}$ (with $\beta < 1$), instead of normal Brownian diffusion ($\beta = 1$).[53]

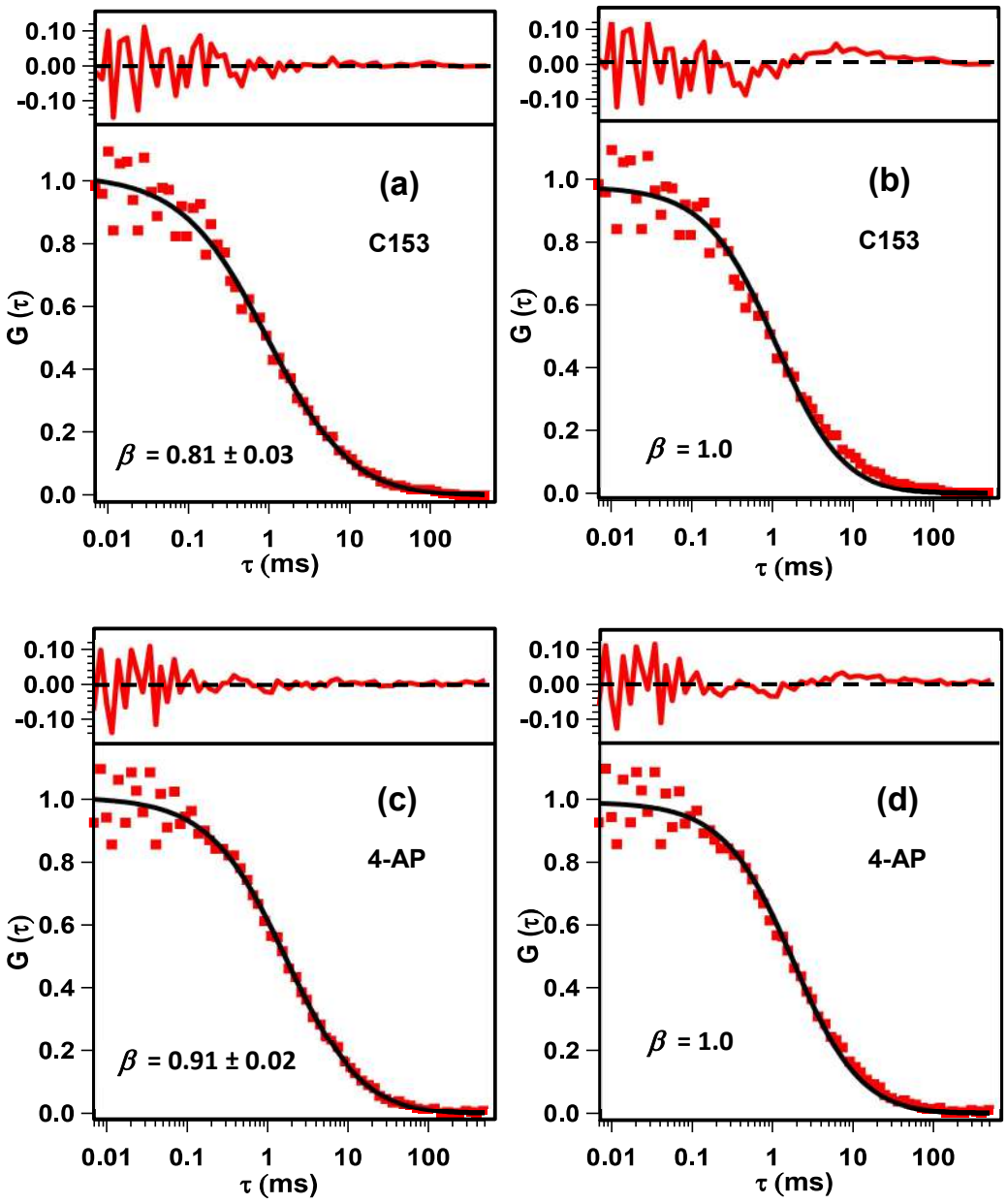

Figure 5.3. Normalized fluorescence correlation data of C153 and 4-AP in TPAB-EG. The solid lines represent fit to the data using anomalous diffusion model (left panel: a, c) and single-component diffusion model (right panel: b, d). The β values obtained from the fits are shown in the figure. The residuals showing the quality of the fits are also shown at the top of each panel.

Table 5.3. Estimated diffusion coefficients (D_t in $\mu m^2 s^{-1}$) and stretching exponents (β) for the solutes in DESs.

DESs	Viscosity (cP)	C153		4-AP	
		D_t	β	D_t	β
TEAB-EG	28.0	31.6 ± 4.7	0.87 ± 0.02	25.0 ± 3.9	0.90 ± 0.03
TPAB-EG	72.5	14.5 ± 1.9	0.81 ± 0.03	8.1 ± 2.5	0.91 ± 0.02
TBAB-EG	98.0	11.4 ± 1.6	0.72 ± 0.03	4.8 ± 1.1	0.88 ± 0.02

It is seen that the D_t value of both solutes decreases substantially from TEAB-EG to TBAB-EG mainly due to increasing viscosity of the solvents. Another point to note is that the D_t value of 4-AP is smaller than that of C153 in all the solvents, even though the size of 4-AP (134 $Å^3$) is almost half than that of C153 (246 $Å^3$).[40] This observation clearly suggests strong association of 4-AP with the constituents of DESs, which must be through strong solute-solvent hydrogen-bonding interaction, as 4-AP is well-known for such interaction both in molecular solvents[54] and ILs.[35, 48] Another point to note is that the D_t value of 4-AP decreases more sharply compared to C153 with increasing cation chain length of the DESs (Figure 5.4). This indicates that the change in the D_t values is not solely due to solvent viscosity.

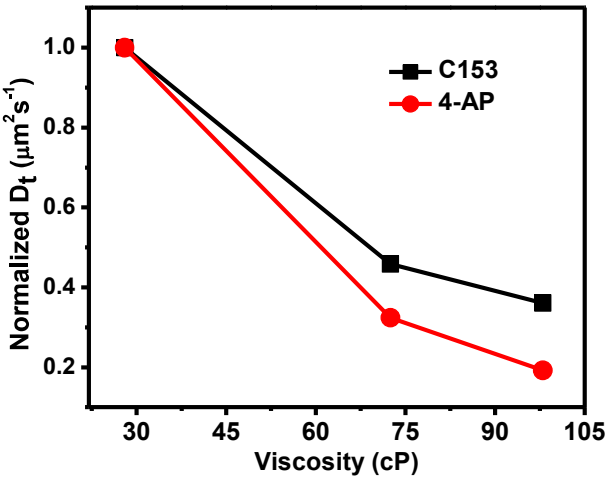

Figure 5.4. Viscosity dependence of the Dt values (normalized) of C153 and 4-AP in DESs.

An important point to note here is that the stretching exponent β deviates notably from unity for both solutes in these solvents. As these solute molecules show single-component translational diffusion in homogeneous media,[49] the observed deviation in the present case indicates dynamic heterogeneity in these solvents, which results from the fluctuations of the hydrogen-bond network and consequent motion of the constituents of these media.[45, 55] In this context, it is pertinent to note that FCS studies have been performed earlier to study the translation diffusion dynamics of several solute molecules in ILs and DESs.[40, 47, 49, 56] Wu et al. observed anomalous diffusion dynamics of Nile Red in ILs, which they explained in terms of dynamic heterogeneity of the solvent.[56] We have also recently attributed similar anomalous diffusion dynamics of dipolar molecules in a series of ChCl-diol based DESs containing different hydrocarbon chain length of the HBD (diol) due to dynamic heterogeneity of the media.[40]

Further, Table 5.3 shows that, while the deviation of the β value for C153 is more prominent in solvent containing cation with longer alkyl chain length, for 4-AP, the β value is almost constant (and high) in all three DESs. These indicate that unlike C153, which experiences increasing dynamic heterogeneity in solvents containing larger cation, 4-AP experiences relatively less and very similar dynamic heterogeneity in these solvents. The latter can be explained considering strong association of the 4-AP molecules with constituents of the solvents. Our previous study also revealed a similar increase of dynamic heterogeneity of the ChCl-diol based DESs with increase in hydrocarbon chain length of the HBD.[40]

5.2.3. TRFA Measurements: Rotational Diffusion Dynamics

To probe the microenvironments around the probe molecules in these solvents, we have also studied time-resolved fluorescence anisotropy of C153, 4-AP and 9-PA in all three DESs over a temperature range from 298-348 K. Representative anisotropy decay profiles (Figure 5.5) of the solutes highlight the influence of solvents. The decay profiles are found to be bi-exponential for C153, but single-exponential for the other two systems in all DESs at all temperatures.

The measured rotational reorientation times (τ_r) of the solutes at six different temperatures are plotted in Figure 5.6 and Table A3.1. At any given temperature (for example, 298K, Table 5.4) in a given DES, the τ_r values of C153 and 9-PA are much smaller than that of 4-AP even though two former solutes are twice as large compared to the latter. The

difference in τ_r values of 4-AP from other two solutes is more prominent in longer alkyl chain length containing solvents, where it is more associated with the solvent. As expected, the τ_r values of the solutes decrease with increasing temperature in all DESs due to decrease of solvent viscosity (Table A3.1). We have also measured and compared the τ_r values of the solutes in isoviscous condition by adjusting the temperatures of the media to find out the difference in interactions between the probe molecules and solvents (Table 5.4). Under isoviscous condition, the τ_r values of C153 and 9-PA are lower in higher alkyl chain length containing solvent, but for 4-AP the trend is quite opposite. This also indicates that the solute-solvent interactions experienced by the probes are quite different.

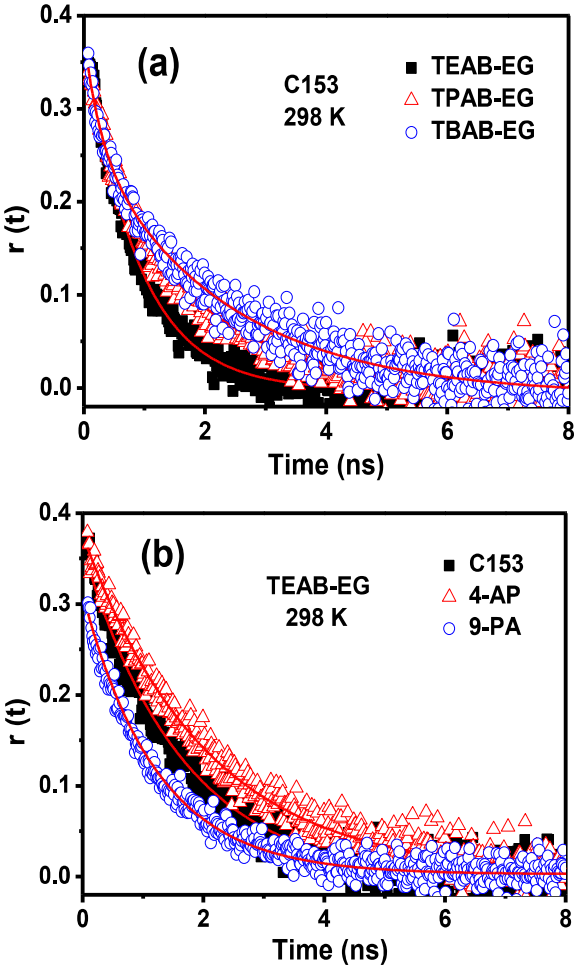

Figure 5.5. (a) Anisotropy decay profiles of C153 in DESs at 298 K. Panel (b) compares the anisotropy decay profiles of the three solutes in TEAB-EG. The solid lines represent fit to the experimental data. The excitation wavelengths for C153 and 4-AP is 405, while for 9-PA, the excitation wavelength is 375 nm. In all cases the monitoring wavelengths are steady-state emission peak maxima.

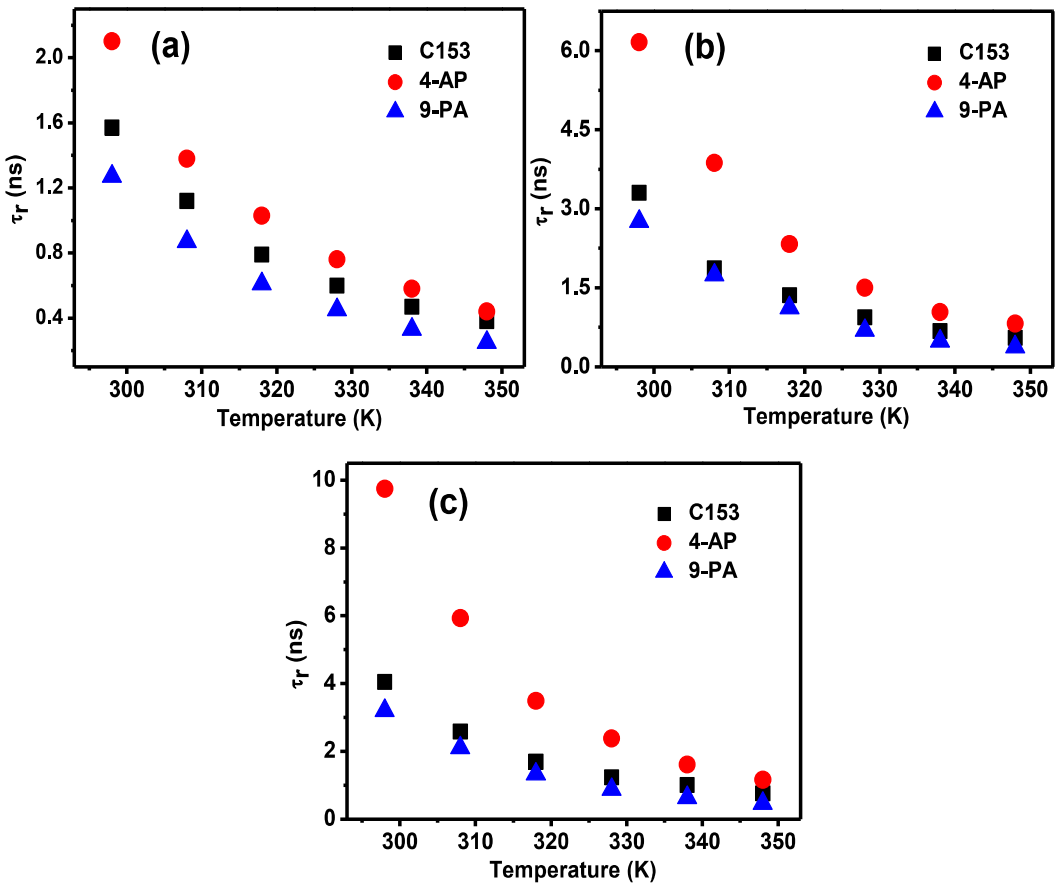

Figure 5.6. (a) Temperature dependence of the τr values of the solutes in TEAB-EG (a), TPAB-EG (b), and TBAB-EG (c).

Table 5.4. Estimated τ_r values (ns) of the solutes in DESs under different conditions.

DESs	Viscosity (cP)	Isothermal (298 K)			Isoviscous (28 cP)		
		C153[a]	4-AP	9-PA	C153[a]	4-AP	9-PA
TEAB-EG	28.0	1.57	2.10	1.27	1.57	2.10	1.27
TPAB-EG	72.5	3.30	6.16	2.76	1.46	2.51	1.18
TBAB-EG	98.0	4.05	9.75	3.20	1.39	2.90	1.11

[a]average τ_r values (ns).

We now analyze the measured rotational diffusion dynamics in terms of the SED hydrodynamic theory;[52, 57] according to which the reorientation time (τ_r) of a probe

molecule in a solvent of viscosity η at temperature T is given by equation 3.1, where, V and f are the van der Waals volume and shape factor of the molecule, respectively, and k_B is Boltzmann constant. The shape factor (f) describes non-spherical nature of the probe molecules, which are treated as asymmetric ellipsoids. C is the boundary condition parameter that represents two limiting cases for the degree of solute-solvent interactions, where $C_{stick} = 1$ for stick condition and $0 < C_{slip} < 1$ for slip condition. The V, f and C values for the probe molecules are taken from literatures[36, 40] and collected in Table 5.5.

Table 5.5. Solute size, shape parameters and boundary condition parameters (C_{slip}) of the solutes calculated from the SED hydrodynamic theory.

Solute	Axial radii (Å^3)	van der Waals volume, V (Å^3)	Shape factors (f)	C_{slip}
C153[a]	6.1 x 4.8 x 2.2	246	1.71	0.24
4-AP[a]	5.0 x 3.5 x 1.8	134	1.60	0.11
9-PA[b]	5.7 x 5.5 x 1.8	236	1.73	0.12

[a] taken from ref. 40. [b] taken from ref. 36.

Figure 5.7 depicts plots of the measured τ_r values of the solutes against η/T in TEAB-EG along with the hydrodynamic stick and slip lines. Similar plots in other two solvents, TPAB-EG and TBAB-EG, are provided in Figure A3.6. It is evident that the τ_r values of both C153 and 9-PA lie between the slip and stick lines in TEAB-EG. They, however, gradually shift toward the slip boundary condition at low temperature, with increasing cation alkyl chain length of the DESs. In contrast, 4-AP exhibits a super-stick behavior in TEAB-EG and the super-stick nature increases with increasing alkyl chain length. This super-stick behavior of 4-AP is reported previously both in conventional solvents and ILs and attributed to strong association of 4-AP with the solvents through hydrogen-bonding interactions.[35, 48, 52, 58] A similar stick/super-stick rotational dynamics of 4-AP is also observed in ChCl-diol based DESs due to the same reason.[40] The other two systems (C153 and 9-PA) are, however, not associated like 4-AP and exhibit faster rotation. We have also estimated the solute-solvent coupling constant (C_{obs}) from the experimental τ_r value and calculated rotational reorientation time (τ_{stick}) for stick boundary conditions using $C_{obs} = \tau_r/\tau_{stick}$. These values (Table 5.6) are lower for C153 and 9-PA in longer alkyl chain length containing solvents, but for 4-AP, the trend is very opposite. This observation is in agreement with the trend observed earlier.

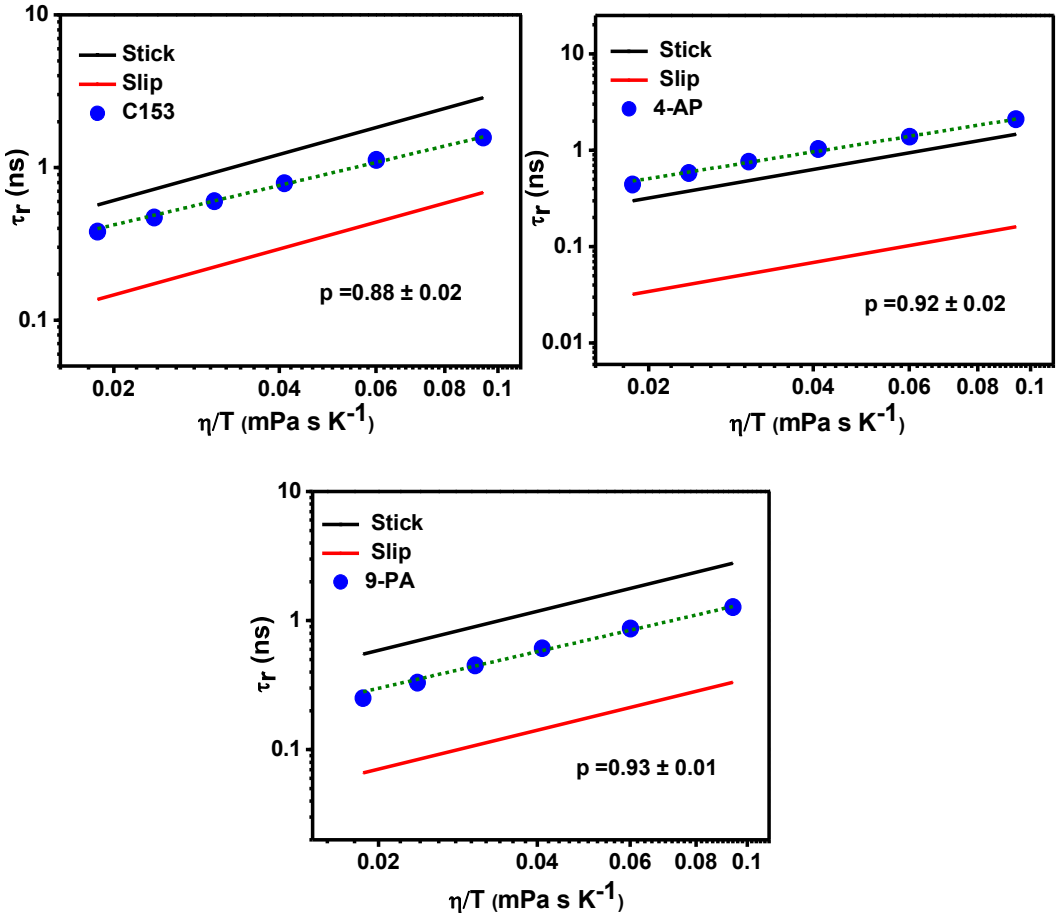

Figure 5.7. Plots of τ_r vs η/T for three solutes in TEAB-EG. The solid circles are the measured rotational times and the dashed lines represent fit to the data according to $\tau_r = A(\eta/T)^p$. The p values obtained from the fits are shown in the figure. The stick (black) and slip (red) lines, computed using SED theory, are also shown.

Table 5.6. Calculated C_{obs} values of the solutes in six DESs at 298 K.

DESs	C_{obs}		
	C153	4-AP	9-PA
TEAB-EG	0.55 ± 0.02	1.44 ± 0.02	0.46 ± 0.02
TPAB-EG	0.45 ± 0.01	1.63 ± 0.02	0.38 ± 0.015
TBAB-EG	0.41 ± 0.01	1.91 ± 0.03	0.33 ± 0.01

Next, we check the linearity of the measured τ_r values with η/T by fitting the data to equation $\tau_r = A(\eta/T)^p$, where any deviation of the value of parameter (p) from unity would indicate a departure from the SED hydrodynamic behavior and the degree of viscosity-diffusion coupling.[45, 51] The p values obtained from fits of the τ_r values using this equation (dashed lines in Figure 5.7 and Figure A3.6) are presented in Table 5.7. The deviation of the p values from unity (p <1) reflects viscosity-diffusion decoupling due to dynamic heterogeneity of the media.[45, 50] A larger deviation of the p values from unity for both C153 and 9-PA with increase in cation alkyl chain length indicates an enhanced dynamic heterogeneity of these media. For 4-AP, the p values are high in all three DESs and they hardly vary with cation alkyl chain length suggesting that it experiences relatively less and similar dynamic heterogeneity in these media due to strong interaction with the solvents. A similar increase of the heterogeneity in ChCl-diol based DESs with increasing hydrocarbon chain length of the HBD is also reported recently.[40]

Table 5.7. *p* values obtained from least-squares fits of τ_r vs η/T plots in DESs.

DESs	C153	4-AP	9-PA
	p	*p*	*p*
TEAB-EG	0.88 ± 0.02	0.92 ± 0.02	0.93 ± 0.01
TPAB-EG	0.83 ± 0.03	0.90 ± 0.03	0.87 ± 0.02
TBAB-EG	0.76 ± 0.02	0.91 ± 0.02	0.82 ± 0.02

This steady change of the coupling constants as well as the degree of nonlinearity of the τ_r values on η/T with increasing cation alkyl chain length can be explained considering the existence of spatial heterogeneities in these DESs (which is indeed observed from the steady-state measurements) due to the formation of organized domain-like structure consisting of polar and nonpolar regions. The association of the alkyl chains attached to the cations induces formation of nonpolar domains, whereas the Coulombic interactions between the ionic moieties and hydrogen-bonding interactions with hydroxyl moieties of the HBD give rise to the ionic polar domains.[13, 50] The formation of this type of domains owing to molecular scale segregation in other DESs has already been established by neutron diffraction studies and simulations.[23] The experimental data presented here suggests that 4-AP molecules reside in the polar region, 9-PA resides specifically in

nonpolar region, and C153 aligns itself at the interface of nonpolar and polar regions. As the cation alkyl chain length increases, the size of the nonpolar domain and excluded volume due to lower packing (void space) also increases, As a consequence, a reduced friction is experienced by C153 and 9-PA molecules and their rotation diffusion becomes faster. On the other hand, with increasing hydrophobic chain length, as overall nonpolar fraction of the solvents increases, more 4-AP molecules move closer towards the -OH groups in the polar region and the solute rotation diffusion becomes slower due to enhanced hydrogen-bonding interaction. Similar effect of domain formation on rotational diffusion of probe molecules has already been described in ILs.[48]

5.3. Summary

We have studied translational and rotational diffusion dynamics of some selected solute molecules in a series of less-explored DESs by monitoring their fluorescence response to obtain an understanding of the liquid state structure of these solvents. The results suggest both spatial and dynamic heterogeneity in these media, which becomes more pronounced in longer alkyl chain containing more viscous solvents. The spatial heterogeneity of these media, which arises from molecular scale domain formation due to segregation of the ionic moieties (along with the hydroxyl moieties of the HBD) and the hydrophobic alkyl chain of the salt, becomes more pronounced in longer chain length containing solvents. As the probe molecules reside in the different regions of the solvents, they experience different solute-solvent interactions and exhibit translational and rotational dynamics. The present findings and recent results[40] show that the spatial and dynamic heterogeneity of the ionic DESs can be modified significantly by tuning the hydrocarbon chain length of both HBA and HBD of the solvents.

References

1. E. L. Smith, A. P. Abbott and K. S. Ryder, *Chem. Rev.*, 2014, **114**, 11060−11082.
2. A. P. Abbott, G. Capper, D. L. Davies, R. K. Rasheed and V. Tambyrajah, *Chem. Commun.*, 2003, **1**, 70−71.
3. D. A. Alonso, A. Baeza, R. Chinchilla, G. Guillena, I. M. Pastor and D. J. Ramón, *Eur. J. Org. Chem.*, 2016, **2016**, 612–632.
4. A. Paiva, R. Craveiro, I. Aroso, M. Martins, R. L. Reis and A. R. C. Duarte, *ACS Sustain. Chem. Eng.*, 2014, **2**, 1063−1071.

5. Q. Zhang, K. D. O. Vigier, S. Royer and F. Jé rôme, *Chem. Soc. Rev.*, 2012, **41**, 7108−7146.
6. C. Ruβ and B. Konig, *Green Chem.*, 2012, **14**, 2969−2982.
7. A. P. Abbott, D. Boothby, G. Capper, D. L. Davies and R. K. Rasheed, *J. Am. Chem. Soc.*, 2004, **126**, 9142−9147.
8. A. P. Abbott, G. Capper, A. Glidle and K. S. Ryder, *Phys. Chem. Chem. Phys.*, 2006, **8**, 4214−4221.
9. A. P. Abbott, G. Capper, K. J. McKenzie and K. S. Ryder, *Electrochim. Acta*, 2006, **51**, 4420−4425.
10. H. Cruz, N. Jordão and L. C. Branco, *Green Chem.*, 2017, **19**, 1653-1658.
11. M. Francisco, A. van den Bruinhorst and M. C. Kroon, *Angew. Chem., Int. Ed.*, 2013, **52**, 3074−3085.
12. K. Shahbaz, F. S. Mjalli, M. A. Hashim and I. M. AlNashef, *Energy Fuels*, 2011, **25**, 2671−2678.
13. S. Kaur, A. Gupta and H. K. Kashyap, *J. Phys. Chem. B*, 2016, **120**, 6712-6720.
14. A. Pandey and S. Pandey, *J. Phys. Chem. B*, 2014, **118**, 14652-14661.
15. A. Pandey, R. Rai, M. Pal and S. Pandey, *Phys. Chem. Chem. Phys.*, 2014, **16**, 1559-1568.
16. R. Stefanovic, M. Ludwig, G. B. Webber, R. Atkin and A. J. Page, *Phys. Chem. Chem. Phys.*, 2017, **19**, 3297-3306.
17. D. V. Wagle, G. A. Baker and E. Mamontov, *J. Phys. Chem. Lett.*, 2015, **6**, 2924−2928.
18. A. Yadav and S. Pandey, *J. Chem. Eng. Data*, 2014, **59**, 2221−2229.
19. Y. Cui and D. G. Kuroda, *J. Phys. Chem. A* 2018, **122**, 1185−1193.
20. A. Faraone, D. V. Wagle, G. A. Baker, E. C. Novak, M. Ohl, D. Reuter, P. Lunkenheimer, A. Loidl and E. Mamontov, *J. Phys. Chem. B*, 2018, **122**, 1261-1267.
21. C. D'Agostino, R. C. Harris, A. P. Abbott, L. F. Gladden and M. D. Mantle, *Phys. Chem. Chem. Phys.*, 2011, **13**, 21383–21391.
22. R. Yusof, E. Abdulmalek, K. Sirat and M. B. A. Rahman, *Molecules*, 2014, **19**, 8011-8026.
23. S. McDonald, T. Murphy, S. Imberti, G. G. Warr and R. Atkin, *J. Phys. Chem. Lett.* , 2018, **9**, 3922-3927.
24. A. R. R. Teles, E. V. Capela, R. S. Carmo, J. A. P. Coutinho, A. J. D. Silvestre and M. G. Freire, *Fluid Phase Equilib.*, 2017, **448**, 15-21.
25. N. Nkosi, K. Tumba and S. Ramsuroop, *J. Chem. Eng. Data*, 2018, **63**, 4502-4512.
26. F. S. Mjalli, J. Naser, B. Jibril, V. Alizadeh and Z. Gano, *J. Chem. Eng. Data*, 2014, **59**, 2242-2251.
27. M. Mohan, P. K. Naik, T. Banerjee, V. V. Goud and S. Paul, *Fluid Phase Equilib.*, 2017, **448**, 168-177.
28. J. Dou, Y. Zhao, F. Yin, H. Li and J. Yu, *Environ. Sci. Technol.*, 2019, **53**, 1031-1038.
29. J.-j. Li, H. Xiao, X.-d. Tang and M. Zhou, *Energy Fuels*, 2016, **30**, 5411-5418.

30. C. Li, D. Li, S. Zou, Z. Li, J. Yin, A. Wang, Y. Cui, Z. Yaoa and Q. Zhao, *Green Chem.*, 2013, **15**, 2793-2799.
31. S. K. Shukla and J.-P. Mikkola, *Phys. Chem. Chem. Phys.*, 2018, **20**, 24591-24601.
32. M. K. AlOmar, M. Hayyan, M. A. Alsaadi, S. Akib, A. Hayyan and M. A. Hashim, *J. Mol. Liq.*, 2016, **215**, 98-103.
33. B. Jibril, F. Mjalli, J. Naser and Z. Gano, *J. Mol. Liq.*, 2014, **199**, 462-469.
34. G. García, S. Aparicio, R. Ullah and M. Atilhan, *Energy Fuels*, 2015, **29**, 2616−2644.
35. S. K. Das and M. Sarkar, *J. Phys. Chem. B*, 2012, **116**, 194-202.
36. K. S. Mali, G. B. Dutt and T. Mukherjee, *J. Chem. Phys.*, 2008, **128**, 054504.
37. T. Soujanya, R. W. Fessenden and A. Samanta, *J. Phys. Chem.*, 1996, **100**, 3507-3512.
38. A. Samanta and R. W. Fessenden, *J. Phys. Chem. A*, 2000, **104**, 8577-8582.
39. D. C. Khara and A. Samanta, *J. Phys. Chem. B*, 2012, **116**, 13430-13438.
40. S. S. Hossain and A. Samanta, *Phys. Chem. Chem. Phys.*, 2018, **20**, 24613-24622.
41. A. Samanta, *J. Phys. Chem. B*, 2006, **110**, 13704-13716.
42. P. K. Mandal, M. Sarkar and A. Samanta, *J. Phys. Chem. A*, 2004, **108**, 9048-9053.
43. A. P. Demchenko, *Luminescence*, 2002, **17**, 19-42.
44. L. A. Hallidy and M. R. Topp, *Chem. Phys. Letters*, 1977, **48**, 40-45.
45. A. Das and R. Biswas, *J. Phys. Chem. B*, 2015, **119**, 10102−10113.
46. Adam H. T and D. Kim, *J. Chem. Phys.*, 2018, **149**, 174503-174507.
47. S. Patra and A. Samanta, *J. Phys. Chem. B*, 2012, **116**, 12275-12283.
48. D. C. Khara, J. P. Kumar, N. Mondal and A. Samanta, *J. Phys. Chem. B*, 2013, **117**, 5156-5164.
49. D. K. Sasmal, A. K. Mandal, T. Mondal and K. Bhattacharyya, *J. Phys. Chem. B*, 2011, **115**, 7781-7787.
50. B. Guchhait, S. Das, S. Daschakraborty and R. Biswas, *J. Chem. Phys.*, 2014, **140**, 104514.
51. S. S. Hossain and A. Samanta, *J. Phys. Chem. B*, 2017, **121**, 10556-10565.
52. J. R. Lakowicz, *Principles of Fluorescence Spectroscopy, 3rd ed.*, 2006, Springer: New York, USA
53. H. Sanabria, Y. Kubota and M. N. Waxham, *Biophys. J.*, 2007, **92**, 313-322.
54. G. Saroja, T. Soujanya, B. Ramachandram and A. Samanta, *J. Fluoresc.*, 1998, **8**, 405-410.
55. S. Das, R. Biswas and B. Mukherjee, *J. Phys. Chem. B*, 2015, **119**, 274-283.
56. E. C. Wu, H. J. Kim and L. A. Peteanu, *J. Phys. Chem. B*, 2017, **121**, 1100−1107.
57. G. R. Fleming, *Chemical Applications of Ultrafast Spectroscopy*, 1986, Oxford University Press: New York, USA.
58. J. A. Ingram, R. S. Moog, N. Ito, R. Biswas and M. Maroncelli, *J. Phys. Chem. B*, 2003, **107**, 5926-5932.

Chapter 6

Complete Solvation Dynamics of Coumarin 153 in Tetraalkylammonium Bromide-Based Deep Eutectic Solvents

J. Phys. Chem. B, 2020, 124, 2473-2481

Overview

In order to obtain insight into the structure and dynamics of some less-explored DESs comprising ethylene glycol and tetraalkylammonium bromide salts with variable alkyl chain length, we have captured complete dynamics occurring in these solvents in a timescale of few femtoseconds to several nanoseconds by monitoring the TDFSS of C153 employing a combination of TCSPC and fluorescence UPC techniques. The solvent response function constructed from the measured data reveals a sub-picosecond component (~ 0.8 ps, 20-35%) in addition to a slow component (180-475 ps) with a distribution of relaxation time. The slow time component is found to be strongly dependent on the viscosity of the medium, indicating that it arises from the diffusive motions of the solvent constituents into and out of the solvation shell, whereas the ultrafast time component, which is nearly independent of the solvent viscosity, arises from fast local motions of the constituents in the immediate vicinity of the solute molecule.

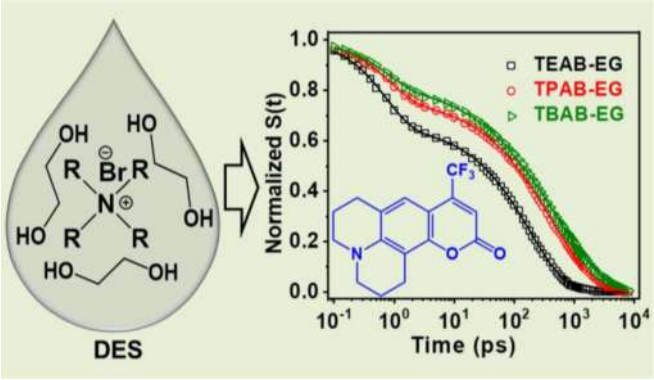

6.1. Introduction

Due to their attractive properties, the DESs have gained considerable attention in recent years as environment-friendly designer solvents in various fields.[1-6] These are composed of two or more components (usually a salt/HBA and a HBD), which self-associate through hydrogen-bonding interactions forming a stable liquid with melting point lower than that of the pure components.[4, 5] A large number of eutectic mixtures can be obtained by varying the constituents and their molar ratios.[4, 7] Due to the ease of preparation, relatively inexpensive starting materials, often natural and biodegradable constituents and the possibility of designing task-specific solvents, the DESs can be a potential green alternative to the conventional volatile organic solvents and the ILs.[1, 4-6, 8]

Notwithstanding their applications, [4, 9-24] the structure and dynamics of the DESs are not very well understood from the studies made so far on the diffusion dynamics of constituents of the DESs[6, 25-28] and translational and rotational diffusion dynamics of organic probe molecules in these media.[29-36] While Abbott and co-workers investigated molecular and ionic diffusion of the constituents in these solvents using pulsed field gradient NMR spectroscopy,[6, 25, 26] Biswas and co-workers studied rotational diffusion of several molecular systems in a number of DESs to understand the dynamics of these liquids.[33-36] We have recently investigated the translational and rotational diffusion dynamics of some probe molecules employing fluorescence correlation spectroscopy and time-resolved fluorescence anisotropy measurements.[29-31] These studies have revealed significant to moderate spatial and/or dynamic heterogeneity of these DESs, depending on the constituents.

As the dynamics of solvation often determines the fate of many chemical processes,[37, 38] and can uncover unique characteristics of a solvent such as its microheterogeneity, solvation dynamics has also been studied in some eutectic mixtures in recent years.[32-36, 39-41] Since solvation leads to a significant shift of the emission spectrum of a dipolar solute molecule in polar media, the dynamics of solvation is frequently studied by sudden perturbation of the charge distribution of a dipolar fluorescent molecule by a short optical pulse excitation and then monitoring the TDFSS of the system.[38, 42-44] In addition to the studies based on this methodology,[32-36] Cui et al. and Chatterjee et al. have independently studied solvation dynamics of an ionic probe molecule recently in ChCl-based DESs using FTIR and 2DIR spectroscopy.[39, 40] In another study, Subba et al. have examined solvation dynamics in an non-ionic DES employing transient absorption spectroscopy.[41] These

studies indicate that solvation in DESs is significantly slower than in common organic solvents and is quite similar to that in ILs. The timeresolved component of the dynamics is bimodal in nature and the average solvation time is dependent on the viscosity of the media. Though the slow nature of solvation dynamics in DESs is understood qualitatively, very little of the early part of the solvation dynamics has been explored till date. The TDFSS measurements carried out so far could not capture the fast solvation response due to limited time-resolution (typically 25-50 ps) of the technique.[42, 44] On the other hand, the FTIR and 2DIR studies could not reliably estimate the slower component (occurring in a timescale ranging from hundreds of picoseconds to nanoseconds) of the solvation dynamics due to short vibrational lifetime of the probe used.[40, 45] Another point to take note of in this context is that majority of the studies carried out so far were focused on ChCl-based DESs leaving many other salt-based DESs unexplored.

In view of above, herein we focus on a set of less-explored DESs and attempt to capture the complete solvation dynamics (occurring between few femtoseconds and several nanoseconds) of C153 by monitoring its TDFSS using a combination of femtosecond fluorescence UPC and TCSPC techniques. We have chosen for this study a homologous series of DESs[29] comprising 3:1 molar mixture of ethylene glycol and tetraalkylammonium bromide salts with variable alkyl chain length (Table 6.1). The choice of the molecular probe (C153) is guided by its rigid structure, large change of dipole moment upon electronic excitation ($\Delta\mu$ = ~ 7.0 D), large shift of emission maximum as a function of the solvent polarity, relatively long fluorescence lifetime (~ 4.5 ns), and its extensive use as a probe for the study of solvation dynamics in a variety of media including ILs and DESs.[43, 44, 46-48] Table 6.1 provides necessary details of the DESs along with their abbreviations. Chart 1.7 and 1.8, respectively, provides molecular structure of the DESs components and the probe molecule used in this study.

Table 6.1. Description of the DESs used in this study.

Sl. No.	Salt	HBD	Mole ratio (Salt: HBD)	Abbreviation
1	TEAB	EG	1:3	TEAB-EG
2	TPAB	EG	1:3	TPAB-EG
3	TBAB	EG	1:3	TBAB-EG

6.2. Results and Discussion

6.2.1. Steady-State Measurements

The steady-state absorption and emission spectra of C153 in the chosen DESs at room temperature (298 K) are shown in Figure 6.1 and the corresponding peak positions are collected in Table 6.2. The spectral shapes are found to be very similar in all three DESs and they closely resemble those in conventional polar solvents[49, 50] like water and methanol or in ILs[51, 52] and other DESs.[31, 50] As far as the absorption and emission peak positions are concerned, they appear at wavelengths similar to those observed in ChCl-based DESs, indicating that the microenvironment around C153 in these solvents is comparable to that in ChCl/alcohol-based DESs.[31, 50] Comparable absorption and emission maxima of C153 in these DESs and various commonly used ILs also suggests a similar environment is experienced by the probe molecule in these two types of solvents.[48, 53] While the absorption maximum appears at ~ 430 nm in all three DESs, the emission peak position shifts towards lower wavelength (from 540 to 530 nm) with increase in alkyl chain length of the cationic constituent of the solvents. The enhanced sensitivity of the emission peak position on the solvent is consistent with a higher excited state dipole moment of C153,[54] and the observed peak shift indicates a less polar nature of the solvent containing a longer alkyl chain length.[48, 52, 55]

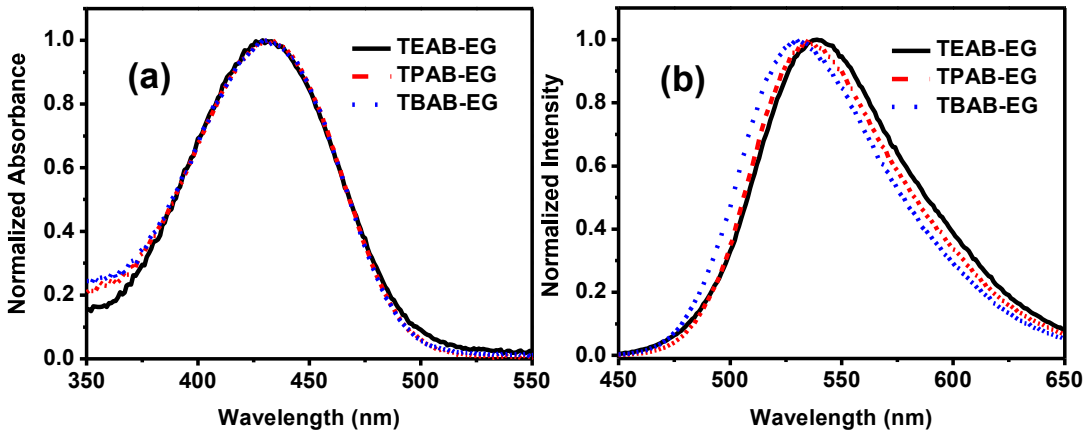

Figure 6.1. Steady-state absorption (a) and emission (b) spectra of C153 in chosen DESs at 298 K. The emission spectra are recorded by exciting the samples at 430 nm.

Before studying the dynamics of solvation, we have estimated the static solvation parameters, solvation free energy difference ($\Delta_{sol}G$) and solvent contribution to nuclear reorganization energy (λ_{sol}) associated with the $S_0 \leftrightarrow S_1$ transition of C153 in these solvents using[47, 48]

$$\Delta_{sol}G = \frac{1}{2}h\{\nu_{abs} - \nu(\infty)\} - \Delta G_0 \dots\dots\dots\dots (6.1)$$

$$\lambda_{sol} = \frac{1}{2}h\{\nu_{cal}(0) - \nu(\infty)\} \dots\dots\dots\dots (6.2)$$

where, ν_{abs} is the absorption peak frequency (in cm^{-1}), $\nu_{cal}(0)$ and $\nu(\infty)$ are the emission peak frequencies immediately after excitation (t = 0) and at a sufficiently long time (t = ∞), when solvent relaxation is expected to be complete. The $\nu_{cal}(0)$ values are estimated following a procedure recommended by Fee and Maroncelli,[56] whereas the $\nu(\infty)$ values are obtained from the time-resolved fluorescence measurements (details in a later section). ΔG_0 is the gas-phase free energy difference for C153 (296 kJ mol^{-1}).[48] The estimated $\Delta_{sol}G$ and λ_{sol} values for C153 in these DESs, which are presented in Table 6.2 along with the measured peak frequencies, are comparable to the respective values reported in various ILs.[47, 48, 53] This is understood considering very similar values of the steady-state absorption and emission maxima of C153 in these DESs and various ILs.[48, 53] A close inspection of the data reveals that both the parameters ($\Delta_{sol}G$ and λ_{sol}) change substantially with change in chain length of the cationic moiety, showing good correlation with the solvent polarity of these DESs and demonstrating its role in the solvation process in DESs.

Table 6.2. Peak positions, $\Delta_{sol}G$ and λ_{sol} values of C153 in the DES used in this study.

DESs	ν_{abs} (10^3 cm^{-1})	ν_{emn} (10^3 cm^{-1})	$\nu_{cal}(0)$[a] (10^3 cm^{-1})	$\nu(\infty)$[b] (10^3 cm^{-1})	$-\Delta_{sol}G$ ($kJmol^{-1}$)	λ_{sol} ($kJmol^{-1}$)
TEAB-EG	23.26	18.52	20.37	18.49	46.30	11.20
TPAB-EG	23.23	18.69	20.34	18.61	45.60	10.50
TBAB-EG	23.26	18.87	20.37	18.72	44.90	9.80

[a] estimated following ref. 56, [b] estimated from the time-resolved measurements.

6.2.2. TDFSS Measurements

As stated earlier, we have studied the dynamics of solvation of C153 by measuring its TDFSS in these DESs. As solvation takes long time to complete in viscous media like ILs and DESs and that solvation also has a fast component,[40, 41, 48, 57] which was not time-resolved previously through TDFSS measurements, we have employed both UPC and TCSPC techniques to capture the complete dynamics ranging from few femtoseconds time scale to several nanoseconds. Figure 6.2 and 6.3 show that the fluorescence decay profiles of C153 are dependent on the monitoring wavelengths. The observation that at shorter wavelengths, fluorescence intensity decays steadily with time, but at longer wavelengths, the decay is preceded by a rise component is indicative of solvation dynamics in these

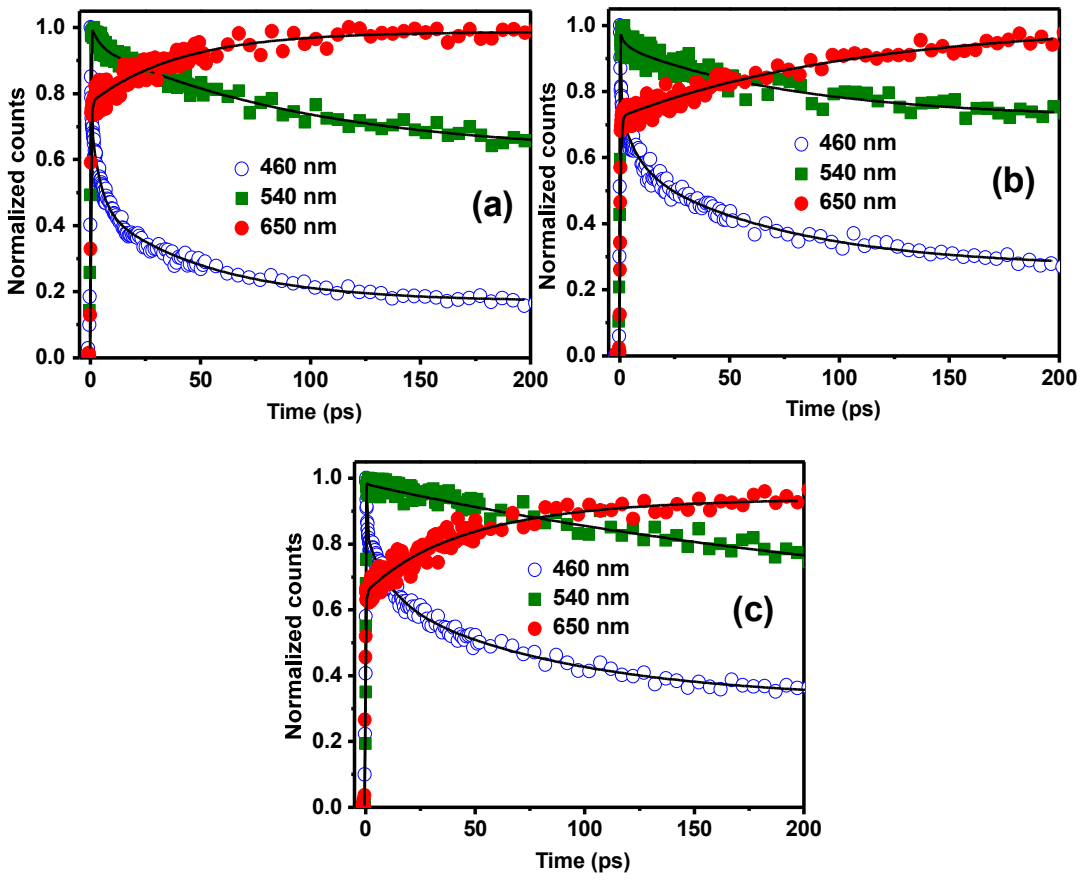

Figure 6.2. Representative wavelength-dependent fluorescence decay profiles of C153 (λ_{exc} = 400 nm) in the short time scale obtained from the UPC measurements in TEAB-EG (a), TPAB-EG (b), and TBAB-EG (c). The symbols denote the experimental data and the solid lines represent multi-exponential fit to the data using equation 2.1.

solvents. In each solvent, we have recorded the decay curves at several (18-20) wavelengths across the entire fluorescence spectrum of C153 (460 to 650 nm) using both UPC and TCSPC techniques. These decay curves are fitted independently to a multi-exponential function (equation 2.1)

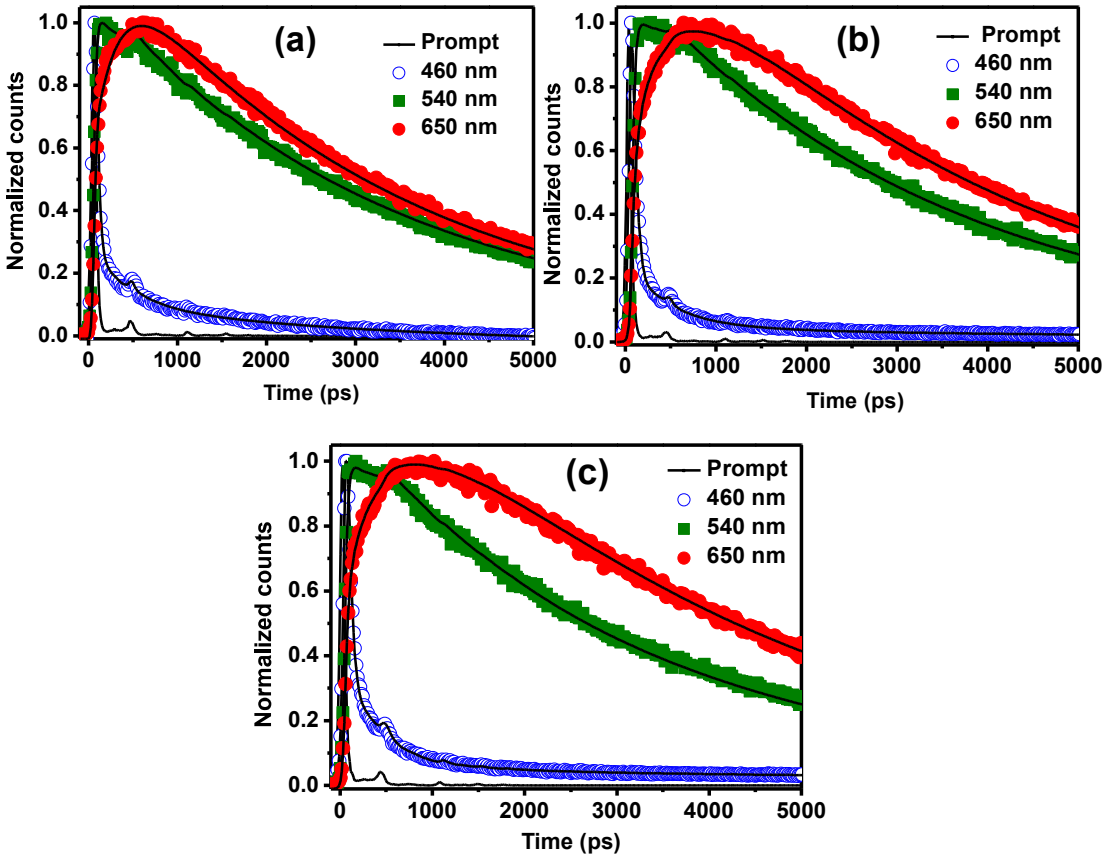

Figure 6.3. Representative wavelength-dependent fluorescence decay profiles of C153 (λ_{exc} = 405 nm) obtained from the TCSPC measurements in TEAB-EG (a), TPAB-EG (b), and TBAB-EG (c). The symbols denote the experimental data and the solid lines represent multi-exponential fit to the data using equation 2.1.

TRES at various times are then constructed using the obtained decay parameters and the steady-state emission data following a standard procedure.[42, 46] Figure 6.4, which displays representative TRES of C153 at few selected times in three DESs, shows a shift of the fluorescence spectra to lower energy with time indicating stabilization of the emitting state of C153 through solvent reorganization/relaxation. In Figure 6.4, the spectra up to 100 ps were reconstructed from the UPC data and those beyond from the TCSPC data. A slight

mismatch of the peak positions measured by two techniques over 100-400 ps time range, as observed here, is not uncommon.[48, 57] The spectra at the common time points (100-400 ps) obtained from the two techniques were matched by uniformly shifting the UPC data following reported procedures.[48, 57]

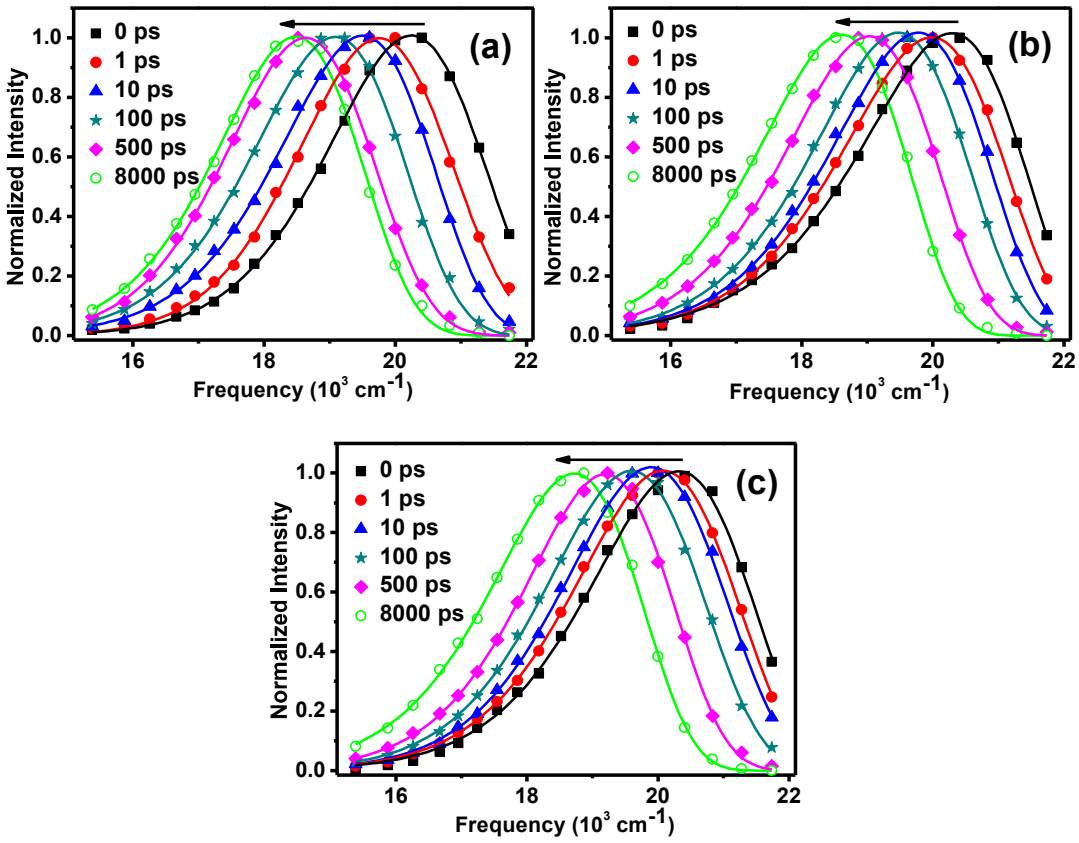

Figure 6.4. Representative time-resolved emission spectra of C153 at different times in TEAB-EG (a), TPAB-EG (b), and TBAB-EG (c). The spectra up to 100 ps are reconstructed from the UPC data and the longer-time spectra are reconstructed from the TCSPC data. The solid lines represent fit of the experimental data to log-normal function (equation 6.3).

In order to parameterize the time-evolution of the reconstructed emission spectra and to estimate the peak frequencies at different times, the TRES are fitted to log-normal line shape function (equation 6.3), a commonly used representation of the emission spectra:[57, 58]

$$I(\nu) = I_0 \exp\{-\ln(2)[\ln(1+\alpha)/\gamma]^2\} \quad \text{for } \alpha > -1$$

$$= 0 \qquad \text{for } \alpha \leq -1 \quad \ldots\ldots\ldots\ldots (6.3)$$

where, $\alpha = 2\gamma(\nu-\nu_p)/\Delta$, and the four parameters, ν_p, I_0, Δ and γ describe the peak frequency (in cm^{-1}), peak intensity, FWHM and asymmetry of the band-shape, respectively. Figure 6.4 shows that the shapes of the reconstructed emission spectra are well described by this function (solid lines).Important to note here is that total dynamic fluorescence Stokes shifts ($\Delta\nu = \nu(\infty) - \nu(0)$) observed for C153 in this study are 1766, 1687 and 1602 cm^{-1} in TEAB-EG, TPAB-EG, and TBAB-EG, respectively (Table 6.3). These values are significantly higher than the observed shift of C153 in other DESs.[32, 33, 35, 36] This is not surprising as these TDFFS studies were based on TCSPC technique, where a large portion of the early part of the total dynamics was missed due to lower time resolution (typically 50-100 ps).[32, 33, 35, 36] It is important to note that the reported magnitude of the total shifts of C153 in earlier studies of solvation dynamics in common ILs,[48] which captured the complete dynamics, are comparable to the present values. This indicates that we have been able to capture almost the entire solvation dynamics in the present case. This is also evident from the fact that the missing component ($\Delta\nu_{miss}$) of the dynamics, as estimated following the procedure recommended by Fee and Maroncelli,[56] is found to be only 3-6% (Table 6.3).

The normalized solvation response function, S(t), which is commonly used to describe the solvation dynamics in a medium, is constructed from the estimated peak frequencies of the TRES at different times using equation 1.2.[59, 60] Figure 6.5 shows time-dependence of the normalized S(t) of C153 in different DESs. To obtained quantitative information on the solvation dynamics, the data is fitted to equation 6.4, which contains sum of a single exponential function with relaxation time τ_1 and a stretched exponential function with relaxation time τ_2.[47, 57]

$$S(t) = f_1 \exp(-t/\tau_1) + f_2 \exp(-t/\tau_2)^{\alpha} \dots\dots\dots\dots\dots (6.4)$$

where, f_1 and f_2 are the amplitude associated with relaxation time τ_1 and τ_2, respectively, and α ($0 < \alpha < 1$) is the stretching exponent representing distribution of the relaxation time τ_2. It may be noted here that a simple biexponential fit (equation 6.4 with $\alpha = 1$) to the data, which described the time dependence of S(t) in ChCl-based DESs, [32, 33] is found unsatisfactory in the present case. This difference is not surprising since in previous studies a large portion of the early part of the total dynamics (as seen earlier) was missed.

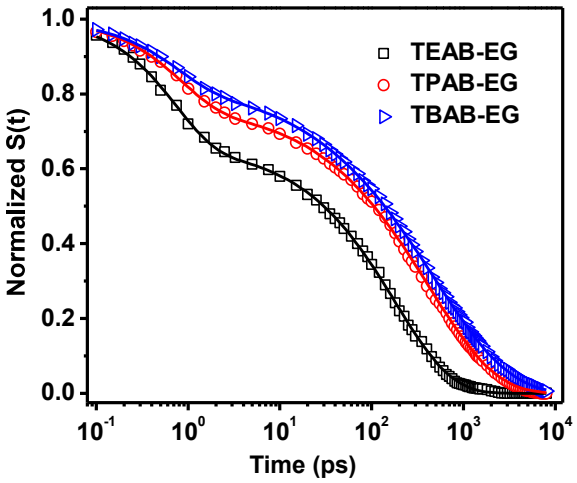

Figure 6.5. Time-dependence of S(t) in different DESs. The symbols denote the experimental data and the solid lines represent fit to the data using equation 6.4.

The time components of the dynamic solvation response, estimated from the fits (equation 6.4 with $\alpha < 1$), are collected in Table 6.3. As can be seen, the solvation is characterized by a distinct ultrafast component, τ_1 of ~ 0.8 ps and a slower component, τ_2 (180 – 475 ps depending on the DESs) with a distribution of relaxation time. This kind of two solvation components of comparable values were also reported in ILs with similar viscosity.[47, 48] The integral time corresponding to the slow stretched exponential component (τ_{st}) is calculated from the observed τ_2 values using equation 6.5 (where Γ is gamma function).

$$\tau_{st} = \frac{\tau_2}{\alpha}\Gamma(\alpha^{-1}) \dots\dots\dots\dots\dots (6.5)$$

Table 6.3. Parameters obtained by fitting of S(t) to equation 6.6 in different DESs along with observed Stokes shift and missing percentage.

DESs	τ_1 (ps)	f_1	τ_2 (ps)	f_2	α	τ_{st} (ps)[a]	$\Delta\nu$ (cm^{-1})[b]	$\Delta\nu^c_{miss}$ (%)
TEAB-EG	0.72	0.34	181	0.66	0.71	226	1766	6.10
TPAB-EG	0.80	0.23	424	0.77	0.60	638	1687	2.60
TBAB-EG	0.79	0.17	475	0.83	0.54	832	1602	2.60

[a] calculated using equation 6.5; [b]$\Delta\nu = \nu(\infty) - \nu(0)$, is total observed dynamic fluorescence Stokes shift; [c]calculated following ref. 56.

It is clear from the Table that this slow stretched component of the relaxation time (τ_{st}) is strongly dependent on the solvent, unlike the ultrafast component (τ_1). The plots in Figure 6.6a and b show that the slow component is strongly dependent on the viscosity of the medium, much like that observed in ILs suggesting that this component is associated with diffusional motions of the solvent constituents surrounding the probe molecule.[43, 44, 48] Further, Table 6.3 suggests that the slow component is not single-exponential rather have a distribution of time constant, which is represented by a stretched-exponential relaxation with values of α less than unity. This broadly distributed time component may arise from heterogeneous diffusional motions present in the solvents. Another possible origin of this distribution could be the involvement of multiple processes arising from independent movements of each solvent constituent.[63] However, as heterogeneity in these DESs is well

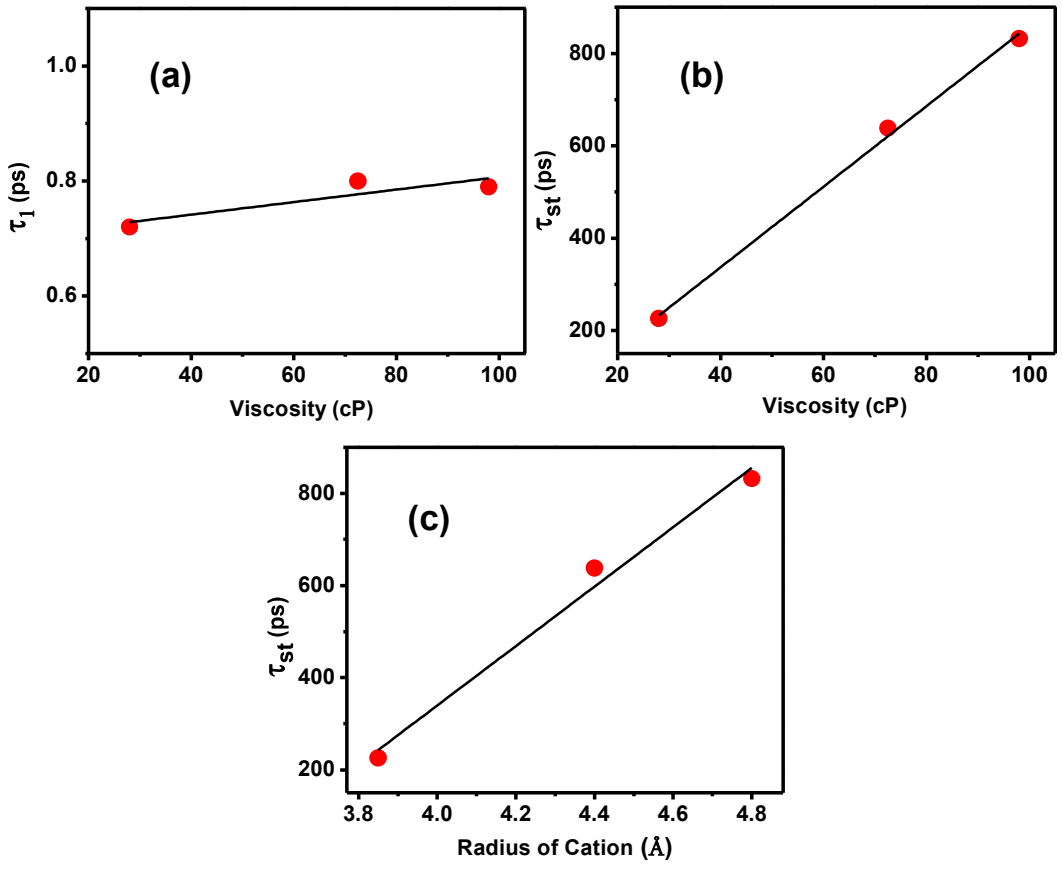

Figure 6.6. Dependence of the fast (a) and slow time components (b) of the solvation on viscosity of the DESs. The panel (c) shows the dependence of the slow time component on cationic radii of the DESs. The values of the cationic radii are taken from previous literature61, 62. The solid lines through the data represent the result of a linear fit.

documented,[29] we suggest that it is the heterogeneous diffusional motions, which contribute to the slow component. This can be due to nonhydrodynamic diffusive motions involving center of mass movements like rotation-translation coupling motions and/or jump moves of the solvent constituents into and out of the solvation shell leading to bulk structural reorganization.[33, 40, 64] Here, we note that such rotation-translation coupling motions, jump moves of the solvent constituents are already demonstrated in case of DESs.[27, 33, 34, 64] One more interesting observation from the Table 6.3 is that the α values associated with the slow component deviates further from unity (0.71 to 0.54) in solvents with longer alkyl chain length of the cation. The larger departure of the α values from unity, which indicates a wider distribution of the slow time component, suggests heterogeneous diffusional motions as the main origin of the slow component and corroborates our assignment. This finding is in accordance with that made in an earlier study based on fluorescence correlation spectroscopy and time-resolved fluorescence anisotropy measurements, which indicated a greater heterogeneity for DESs comprising cations with longer alkyl chain length.[29]

In contrast, the ultrafast sub-picosecond component, which is nearly independent of the solvent viscosity, can be attributed to fast relaxation of the local environment created by DESs constituents that arises due to only minor readjustments of the intermolecular hydrogen-bonding, positions and orientations of the constituents present in immediate vicinity of the probe molecule within the solvation shell.[33, 39, 40]

In order to understand the influence of alkyl chain length (or ionic radius) of the cation on the individual solvation component, we have examined the dependence of the slow solvation time (τ_{st}) with the cation radius (i.e., size) in Figure 6.6c. A linear relationship between the two suggests that this slow solvation component, which arises from the diffusive movements in DESs, strongly depends on the size of cationic constituent of these solvents. As far as the ultrafast solvation component is concerned, Table 6.3 shows that even though this time constant does not vary significantly, the weightage (amplitude) associated with this component (f_1) decreases significantly from 0.34 to 0.17 upon increasing cation alkyl chain length (i.e., size). The decrease in weightage of this component with increase in the chain length suggests reduction in contribution of the fast local motions of the constituents in DESs comprising longer alkyl chain cations; a similar observation is reported in ILs as well.[48] A recent MD simulation and ab-initio computational study in ChCl-based DESs also indicates that in-plane local motions in the

first solvation shell and translational motions into and out of the solvation shell of the cation influence the fast and slow components of the solvation, respectively.[40] Hence, we conclude that the fast and slow components of the solvation response in these DESs arise respectively from the local motions and heterogeneous diffusive motions of the constituents, and the cationic moiety plays a significant role in defining the solvation dynamics in these DESs.

6.3. Summary

In summary, we have been able to capture the complete solvation dynamics of C153 by monitoring its time-dependence of the fluorescence Stokes shift using a combination of UPC and TCSPC techniques in a series of relatively less-explored DESs comprising ethylene glycol and tetraalkylammonium bromide salts with variable alkyl chain length. The study reveals temporally diverse nature of the solvation in these DESs, characterized by a distinct fast sub-picosecond component and a slow component with a distribution of the relaxation time. The ultrafast subpicosecond component arises from rapid local structural relaxation in the immediate vicinity of the solute molecule within the solvation shell, whereas the broadly distributed slow component arises from heterogeneous dynamical processes due to nonhydrodynamic diffusive motions of the solvent constituents into and out of the solvation shell that cause bulk structural relaxation. It is also found that the length of the alkyl chain and hence, the size of the cationic component greatly influences the solvation dynamics in these solvents.

References

1. A. P. Abbott, D. Boothby, G. Capper, D. L. Davies and R. K. Rasheed, *J. Am. Chem. Soc.*, 2004, **126**, 9142−9147.
2. A. P. Abbott, G. Capper, D. L. Davies, R. K. Rasheed and V. Tambyrajah, *Chem. Commun.*, 2003, **1**, 70−71.
3. D. A. Alonso, A. Baeza, R. Chinchilla, G. Guillena, I. M. Pastor and D. J. Ramón, *Eur. J. Org. Chem.*, 2016, **2016**, 612–632.
4. E. L. Smith, A. P. Abbott and K. S. Ryder, *Chem. Rev.*, 2014, **114**, 11060−11082.
5. Q. Zhang, K. D. O. Vigier, S. Royer and F. Jé rôme, *Chem. Soc. Rev.*, 2012, **41**, 7108−7146.
6. A. P. Abbott, R. C. Harris, K. S. Ryder, C. D'Agostino, L. F. Gladden and M. D. Mantle, *Green Chem.*, 2011, **13**, 82–90.
7. M. Francisco, A. van den Bruinhorst and M. C. Kroon, *Angew. Chem., Int. Ed.*, 2013, **52**, 3074−3085.
8. C. Ruβ and B. Konig, *Green Chem.*, 2012, **14**, 2969−2982.

9. A. P. Abbott, G. Capper, A. Glidle and K. S. Ryder, *Phys. Chem. Chem. Phys.*, 2006, **8**, 4214−4221.
10. H. Cruz, N. Jordão and L. C. Branco, *Green Chem.*, 2017, **19**, 1653-1658.
11. K. Shahbaz, F. S. Mjalli, M. A. Hashim and I. M. AlNashef, *Energy Fuels*, 2011, **25**, 2671−2678.
12. G. García, S. Aparicio, R. Ullah and M. Atilhan, *Energy Fuels*, 2015, **29**, 2616−2644.
13. Y. Gu and F. Je´roˆme, *Chem. Soc. Rev.*, 2013, **42**, 9550-9570.
14. J. T. Gorke, F. Srienc and R. J. Kazlauskas, *Chem. Commun.*, 2008, 1235-1237.
15. R. B. Leron and M.-H. Li, *Thermochim. Acta*, 2013, **551**, 14−19.
16. C. Li, D. Li, S. Zou, Z. Li, J. Yin, A. Wang, Y. Cui, Z. Yaoa and Q. Zhao, *Green Chem.*, 2013, **15**, 2793-2799.
17. J.-j. Li, H. Xiao, X.-d. Tang and M. Zhou, *Energy Fuels*, 2016, **30**, 5411-5418.
18. H.-G. Liao, Y.-X. Jiang, Z.-Y. Zhou, S.-P. Chen and S.-G. Sun, *Angew. Chem.*, 2008, **120**, 9240−9243.
19. H.-R. Jhong, D. S.-H. Wong, C.-C. Wan, Y. Wang, -Y. and T.-C. Wei, *Electrochem. Commun.*, 2009, **11**, 209-211.
20. X. Li, M. Hou, B. Han, X. Wang and L. Zou, *J. Chem. Eng. Data*, 2008, **53**, 548–550.
21. D. Carriazo, M. C. Serrano, M. C. Gutiérrez, M. L. Ferrer and F. d. Monte, *Chem. Soc. Rev.*, 2012, **41**, 4996–5014.
22. C. L. Boldrini, N. Manfredi, F. M. Perna, V. Trifiletti, V. Capriati and A. Abbotto, *Energy Technol.*, 2017, **5**, 345-353.
23. D. Z. Troter, Z. B. Todorović, D. R. Đokić-Stojanović, O. S. Stamenković and V. B. Veljković, *Renew. Sust. Energ. Rev.*, 2016, **61**, 473-500.
24. B.-Y. Zhao, P. Xu, F.-X. Yang, H. Wu, M.-H. Zong and W.-Y. Lou, *ACS Sustain. Chem. Eng.*, 2015, **3**, 2746−2755.
25. C. D'Agostino, L. F. Gladden, M. D. Mantle, A. P. Abbott, I. A. Essa, A. Y. M. Al-Murshedi and R. C. Harris, *Phys. Chem. Chem. Phys.*, 2015, **17**, 15297-15304.
26. C. D'Agostino, R. C. Harris, A. P. Abbott, L. F. Gladden and M. D. Mantle, *Phys. Chem. Chem. Phys.*, 2011, **13**, 21383–21391.
27. S. Das, R. Biswas and B. Mukherjee, *J. Phys. Chem. B*, 2015, **119**, 11157-11168.
28. D. V. Wagle, G. A. Baker and E. Mamontov, *J. Phys. Chem. Lett.*, 2015, **6**, 2924−2928.
29. S. S. Hossain, S. Paul and A. Samanta, *J. Phys. Chem. B*, 2019, ***123***, 6842−6850.
30. S. S. Hossain and A. Samanta, *J. Phys. Chem. B*, 2017, **121**, 10556-10565.
31. S. S. Hossain and A. Samanta, *Phys. Chem. Chem. Phys.*, 2018, **20**, 24613-24622.
32. Adam H. T and D. Kim, *J. Chem. Phys.*, 2018, **149**, 174503-174507.
33. A. Das and R. Biswas, *J. Phys. Chem. B*, 2015, **119**, 10102−10113.
34. B. Guchhait, S. Das, S. Daschakraborty and R. Biswas, *J. Chem. Phys.*, 2014, **140**, 104514.
35. K. Mukherjee, E. Tarif, A. Barman and R. Biswas, *Fluid Phase Equilib.*, 2017, **448**, 22-29.
36. E. Tarif, J. Mondal and R. Biswas, *J. Phys. Chem. B*, 2019, **123**, 9378-9387.

37. A. Nitzan, *Chemical Dynamics in Condensed Phases*, 2006, Oxford University Press: New York, USA.
38. B. Bagchi and B. Jana, *Chem. Soc. Rev.*, 2010, **39**, 1936-1954.
39. S. Chatterjee, D. Ghosh, T. Haldar, P. Deb, S. S. Sakpal, S. H. Deshmukh, S. M. Kashid and S. Bagchi, *J. Phys. Chem. B*, 2019, **123**, 9355-9363.
40. Y. Cui, K. D. Fulfer, J. Ma, T. K. Weldeghiorghis and D. G. Kuroda, *Phys. Chem. Chem. Phys.*, 2016, **18**, 31471-31479.
41. N. Subba, K. Polok, P. Piatkowski, B. Ratajska-Gadomska, R. Biswas, W. Gadomski and P. Sen, *J. Phys. Chem. B*, 2019, **123**, 9212-9221.
42. J. R. Lakowicz, *Principles of Fluorescence Spectroscopy, 3rd ed.*, 2006, Springer: New York, USA.
43. A. Samanta, *J. Phys. Chem. B*, 2006, **110**, 13704-13716.
44. A. Samanta, *J. Phys. Chem. Lett.*, 2010, **1**, 1557-1562.
45. Z. Ren, A. S. Ivanova, D. Couchot-Vore and S. Garrett-Roe, *J. Phys. Chem. Lett.*, 2014, **5**, 1541-1546.
46. R. Karmakar and A. Samanta, *J. Phys. Chem. A*, 2002, **106**, 4447-4452.
47. S. Arzhantsev, H. Jin, G. A. Baker and M. Maroncelli, *J. Phys. Chem. B*, 2007, **111**, 4978-4989.
48. X.-X. Zhang, M. Liang, N. P. Ernsting and M. Maroncelli, *J. Phys. Chem. B*, 2013, **117**, 4291-4304.
49. I. Eom and T. Joo, *J. Chem. Phys.*, 2009, **131**, 244507-244507.
50. A. Pandey, R. Rai, M. Pal and S. Pandey, *Phys. Chem. Chem. Phys.*, 2014, **16**, 1559-1568.
51. P. K. Chowdhury, M. Halder, L. Sanders, T. Calhoun, J. L. Anderson, D. W. Armstrong, X. Song and J. W. Petrich, *J. Phys. Chem. B*, 2004, **108**, 10245-10255.
52. D. C. Khara and A. Samanta, *J. Phys. Chem. B*, 2012, **116**, 13430-13438.
53. H. Jin, G. A. Baker, S. Arzhantsev, J. Dong and M. Maroncelli, *J. Phys. Chem. B*, 2007, **111**, 7291–7302.
54. A. Samanta and R. W. Fessenden, *J. Phys. Chem. A*, 2000, **104**, 8577-8582.
55. S. K. Das, D. Majhi, P. K. Sahu and M. Sarkar, *RSC Adv.*, 2015, **5**, 41585-41594.
56. R. S. Fee and M. Maroncelli, *Chem. Phys.*, 1994, **183**, 235−247.
57. Y. Kimura, A. Kobayashi, M. Demizu and M. Terazima, *Chem. Phys. Lett.*, 2011, **513**, 53-58.
58. D. B. Siano and D. E. Metzler, *J. Chem. Phys.*, 1969, **51**, 1856-1861.
59. B. Bagchi, D. W. Oxtoby and G. R. Fleming, *Chem. Phys.*, 1984, **86**, 257-267.
60. G. V. D. Zwan and J. T. Hynes, *J. Phys. Chem.*, 1985, **89**, 4181-4188.
61. E. Bart, A. Meltsin and D. Huppert, *J. Phys. Chem.*, 1994, **98**, 3295-3299.
62. D. H. Aue, H. M. Webb and M. T. Bowers, *J. Am. Chem. Soc.*, 1976, **98**, 318-329.
63. S. D. Verma, S. A. Corcelli and M. A. Berg, *J. Phys. Chem. Lett.*, 2016, **7**, 504-508.
64. K. Mukherjee, A. Das, S. Choudhury, A. Barman and R. Biswas, *J. Phys. Chem. B*, 2015, **119**, 8063−8071.

Chapter 7

Structural Stability and Conformational Dynamics of Cytochrome c in Deep Eutectic Solvents

(To be communicated)

Overview

DESs are a new class of environment-friendly media that recently received great attention in various bio-related fields like biocatalysis, and extraction and preservation of biomolecules. In order to understand the structure and function of proteins in these media, we study how two structurally related less-explored DESs comprising betaine and ethylene glycol (Bet-EG) or glycerol (Bet-GL) influence the structural stability and conformational dynamics of Cytc with the help of single-molecule-based FCS technique and several ensemble-based biophysical methods. The FCS studies on Alexa 488 dye-labelled Cytc allow the estimation of size (20.5 ± 1.5 Å) of the protein and capture its conformational dynamics (54 ± 2 μs) in the native state. It is observed that both size and conformational dynamics of the protein are influenced by the DESs; the effect, however, is more pronounced in the case of Bet-EG. The ensemble-based measurements, such as steady-state and time-resolved fluorescence on labelled Cytc and CD and UV-vis absorption on wild-type Cytc, reveals that the protein structure unfolds completely by Bet-EG; whereas the tertiary structure is slightly altered by Bet-GL. The findings of the present study clearly reveals that these DESs interact differently with the protein owing to the difference in the number of hydroxyl groups and/or viscosity of the DESs, and suggest that HBD of the solvents play a crucial role in controlling the structural stability and conformational dynamics of Cytc in these DESs.

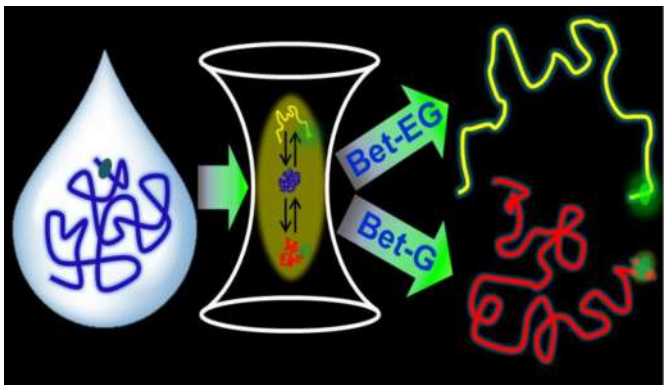

7.1. Introduction

Development of novel environment-friendly solvent systems is an important aspect in green chemistry.[1] A neoteric class of solvents, commonly known as DESs,[2] has gained considerable attention in recent years from both academic and industrial research communities due to their interesting properties.[3, 4] These solvents, which generally formed by interaction between HBAs and HBDs,[3, 4] have been found to be quite promising in a wide range of applications like biocatalysis, and extraction and preservation of various biomolecules, such as protein, DNA etc.[4-10]

As successful utilization of the DESs as media for biocatalytic reaction requires an understanding of the influence of the DESs on the structural stability of protein molecules in these media,[11] few theoretical and experimental studies have been performed in recent years to explore the structure, stability and activity of some selected protein molecules in DESs.[12-14] Esquembre et al. have studied the stability of hen egg white lysozyme in ChCl-based DESs with the help of fluorescence and CD spectroscopy.[12] Edler et al. have studied the effect of two ChCl-based DESs on lysozyme and bovine serum albumin by means of CD and small-angle neutron scattering experiments.[14] The effect of a DES, ChCl-Urea, on the structure of Candida Antarctica lipase B has also been studied using molecular dynamic simulations.[13] These studies suggest that the structure and stability of proteins in these solvents depends considerably on the constituents of the mixtures. We note, however, that all the aforementioned studies are conducted in ensemble conditions that too are primarily focused only on ChCl-based DESs. Similar studies in other salt-based DESs, which are essential for better understanding of the protein-DES interactions, are lacking. Moreover, there is very little information available on the conformational dynamics of the proteins in DESs, which is crucial for realization of the function of proteins in these novel solvents because dynamics builds the gap between structure and funcion.[15] Thus, to gain a deeper understanding of the biophysical mechanism of the protein-DES interactions, it is necessary to perform studies on both the structural stability as well as conformational dynamics employing different proteins and a wider variety of other DESs.

In view of the above, we have examined the effect of two structurally similar DESs comprising a less-explored salt, betaine and glycerol (Bet-GL) or ethylene glycol (Bet-EG) (Chart 1.7), which differs in number of the hydroxyl groups, on the structural stability and conformational dynamics of a well-known protein, yeast iso-1-cytochrome c (Cytc, 108 residues, ~13 kDa, Chart 7.1). Considering our recent work, where it has been observed

that single-molecule-based FCS is a sensitive tool for the investigation of structural change and conformational dynamics of Cytc in similar complex media like ILs,[16] here we have employed this technique along with various ensemble-based biophysical methods, such as steady-state absorption, fluorescence, CD, and time-resolved fluorescence spectroscopy, for this purpose. We have also studied the effect of a protein denaturing agent, GdHCl, on Cytc, and compared it with the effect of the DESs. The reasons for selection of the betaine-based DESs are as follows. Betaine is a naturally occurring derivative of amino acid (glycine), it is non-toxic in nature, it is present as an osmolyte in various organisms and helps proteins to counteract the effect of different extreme environmental conditions.[17, 18] Further, recognizing the promising results of ChCl/Glycerol DES towards protein structure and reactivity, we have chosen glycerol and ethylene glycol as HBDs in this study to understand the role of hydroxyl group of the alcohol-based DESs on the protein structural stability and conformational dynamics. The choice of the particular protein as a model is governed by the fact that it has a single free cysteine at position 102 which allows easy site specific labelling by covalent binding of maleimide-based dyes (A488 in the present case) for probing the structural change and conformational dynamics of the protein using FCS measurements.[19-21]

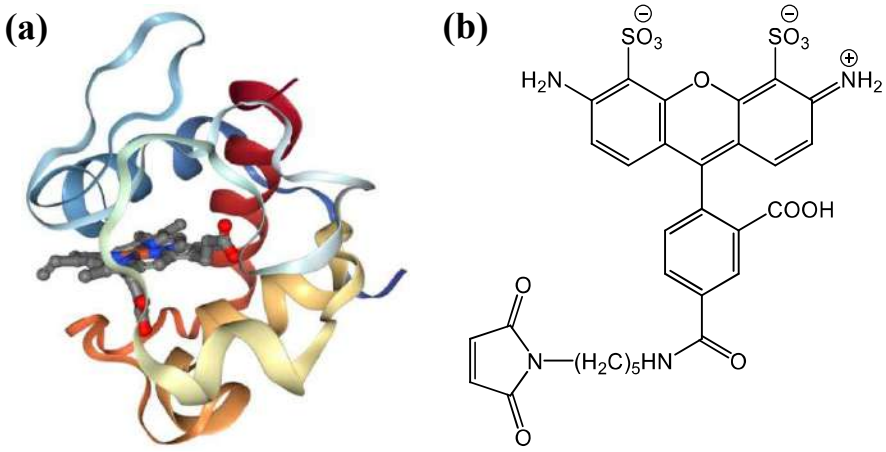

Chart 7.1. Structure of (a) yeast iso-1-cytochrome c (PDB ID: 1YCC) and (b) Alexa fluor 488 C_5 maleimide dye.

7.2. Results and Discussion

7.2.1. Steady-State and Time-Resolved Fluorescence Measurements

The steady-state fluorescence spectra of A488-labelled Cytc (Cytc-A488) in presence of different quantities (0 to 95%, v/v) of DESs in aqueous phosphate buffered solution (pH=7) at room temperature are shown in Figure 7.1a-b. With progressive increase in concentration of the DESs, the fluorescence of Cytc-A488 becomes more intense. In its native state of Cytc-A488, the fluorescence is largely quenched due to PET between the dye molecule and the amino acid residues (e.g., tryptophan, tyrosin etc.) of Cytc.[16, 20] However, in the unfolded state of Cytc-A488 as PET is suppressed, the fluorescence of the

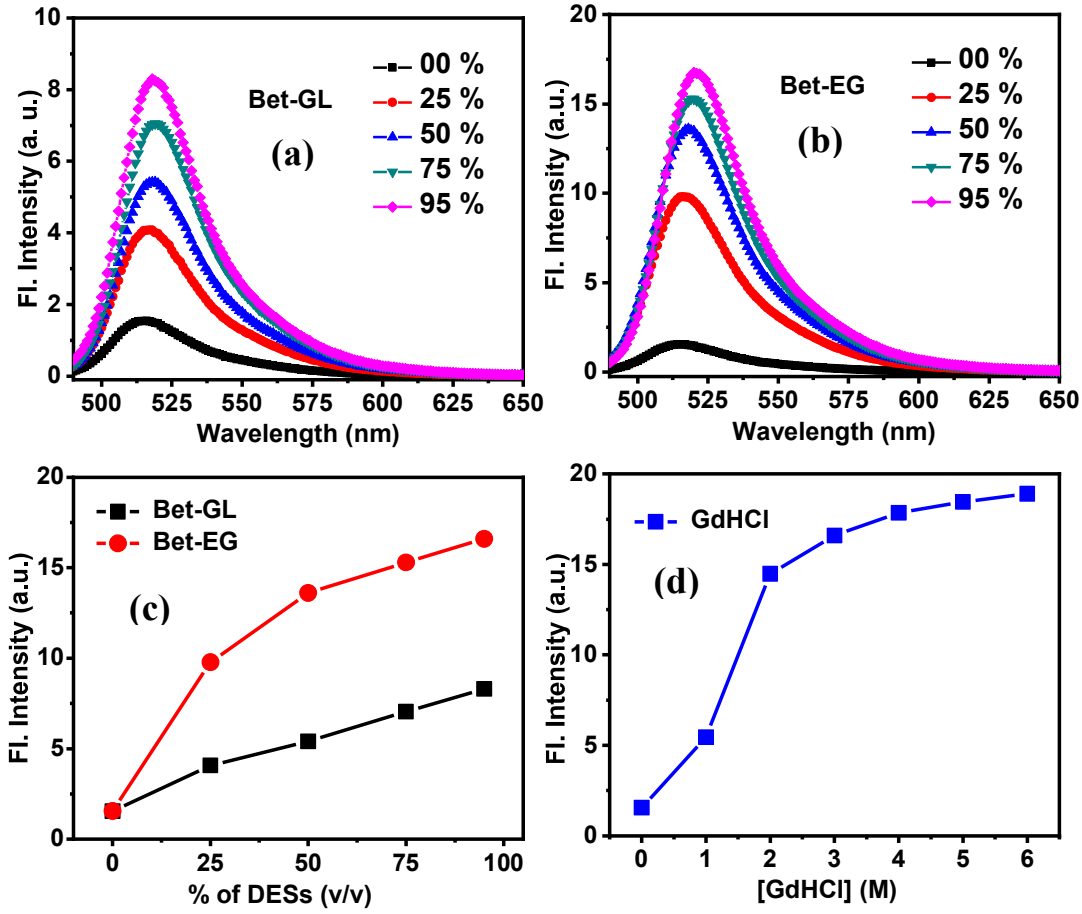

Figure 7.1. Fluorescence spectra of Cytc-A488 in aqueous phosphate buffered solution (pH = 7) containing different quantities of Bet-GL (a) and Bet-EG (b) (λ_{exc} = 480 nm). Panels (c) and (d) are plots of the peak fluorescence intensity of Cytc-A488 versus the amount of the DESs and GdHCl, respectively.

system goes up. This is why common denaturant like GdHCl, which unfolds the native structure of the protein, also enhances the fluorescence of Cytc-A488 (Figure A4.5). Hence, it is evident that the observed increase in fluorescence intensity upon addition of DESs is due to a structural transformation of Cytc from its native to the unfolded state.[16, 20] A comparison of the fluorescence data suggests a stronger influence of Bet-EG on the protein native structure compared to Bet-GL.[22, 23]

The fluorescence decay profiles of Cytc-A488 in the presence of different quantities of DESs and GdHCl at room temperature are shown in Figure 7.2 and Figure A4.6, respectively. The decay profiles, in all the cases, are found to be biexponential in nature; $I(t) = a_1\exp(-t/\tau_1)+a_2\exp(-t/\tau_2)$, where τ_1 and τ_2 are lifetime components and a_1 and a_2

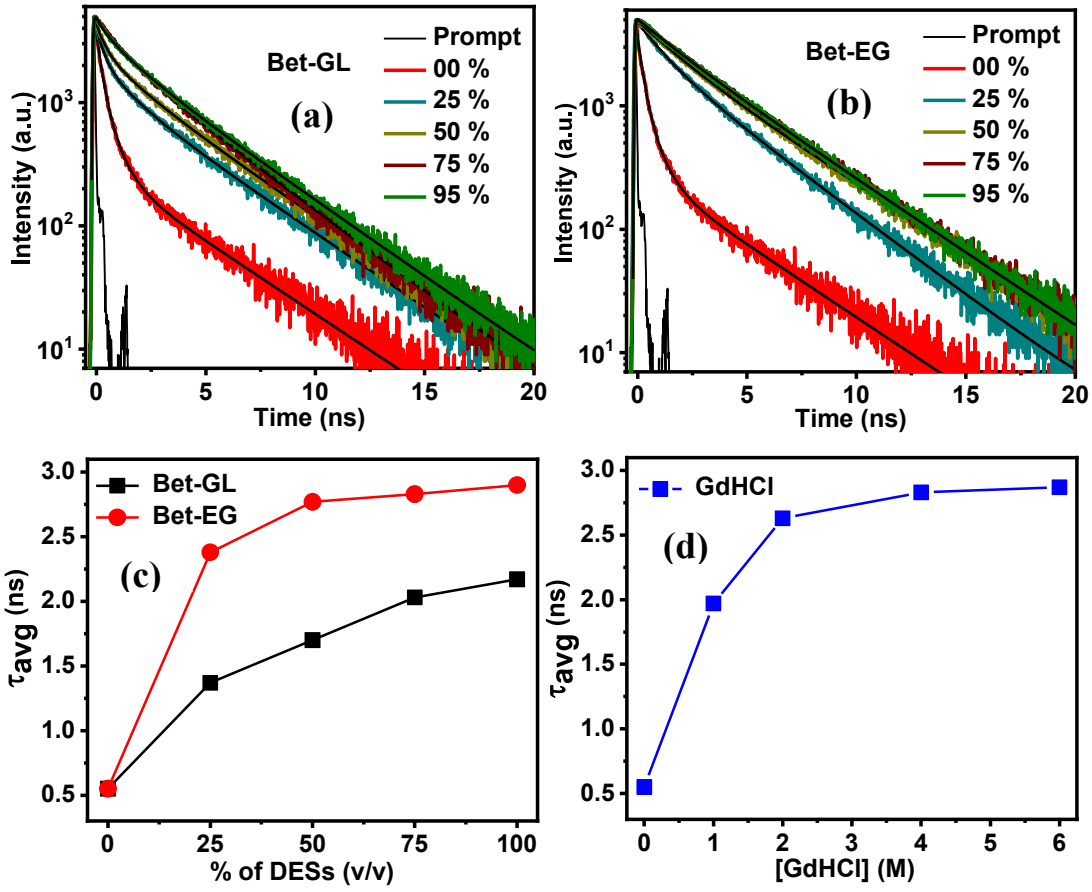

Figure 7.2. Fluorescence decay profiles of Cytc-A488 for different concentration of DESs (a, b) in aqueous phosphate buffered solution (pH = 7). Panels (c) and (d) are plots of the average fluorescence lifetimes of Cytc-A488 versus the amount of the DESs and GdHCl, respectively. (λ_{exc} =481 nm, λ_{em} = 515 nm)

are associated amplitudes. The estimated decay parameters are presented in Table 7.1. The shorter (τ_1) and longer (τ_2) lifetime components (0.35 and 3.24 ns) in buffered solution represent the native and unfolded states of the protein, respectively.[16, 20] With gradual addition of DESs, the shorter lifetime value changes to 1.19 ns and its amplitude decreases from 93 to 25% for Bet-EG, whereas these values changes to 0.90 ns and 48%, respectively, for Bet-GL. As far as the longer lifetime is concerned, though its value always lies between 3.3 to 3.4 ns in both the DESs, its contribution increases to 75 and 52%, respectively, in case of Bet-EG and Bet-GL. As a result, the average lifetime values, which is considerably shorter in buffered solution, increases gradually with increasing concentration of the DESs. A close resemblance of this increase in Bet-EG and GdHCl, which is in line with the steady-state measurements, clearly indicates that Bet-EG shifts the equilibrium toward the unfolded state in significantly greater extent than by Bet-GL.

Table 7.1. Fluorescence decay parameters of Cytc-A488 for different concentration of the additives.

Solvent	τ_1 [ns] (a_1)	τ_2 [ns] (a_2)	τ_{avg} [ns][a]
Only buffered solution	0.35 (0.93)	3.24 (0.07)	0.55
25 % Bet-G	0.43 (0.68)	3.37 (0.32)	1.37
50 % Bet-G	0.52 (0.59)	3.40 (0.41)	1.70
75 % Bet-G	0.75 (0.52)	3.42 (0.48)	2.03
95 % Bet-G	0.90 (0.48)	3.35 (0.52)	2.17
25 % Bet-EG	0.95 (0.42)	3.42 (0.58)	2.38
50 % Bet-EG	1.20 (0.31)	3.48 (0.69)	2.77
75 % Bet-EG	1.17 (0.27)	3.45 (0.73)	2.83
95 % Bet-EG	1.19 (0.25)	3.47 (0.75)	2.90
1.0 M GdHCl	0.68 (0.52)	3.37 (0.48)	1.97
2.0 M GdHCl	1.00 (0.31)	3.36 (0.69)	2.63
4.0 M GdHCl	1.15 (0.25)	3.39 (0.75)	2.83
6.0 M GdHCl	1.19 (0.23)	3.37 (0.77)	2.87

[a] $\tau_{avg} = (a_1\tau_1 + a_2\tau_2)/ a_1 + a_2$ (where, $a_1 + a_2 = 1$).

7.2.2. FCS Measurements

In order to obtain a more clear picture of the folding-unfolding of the protein in DESs, we have examined the fluorescence behaviour of Cytc-A488 using the single-molecule-based FCS technique, which is known to be a sensitive and powerful tool for studying the size and conformational dynamics of biomolecules.[22-32] Figure 7.3 shows the time-dependence of the fluorescence correlation of Cytc-A488 in aqueous phosphate buffered solution at room temperature containing different quantities of DESs and GdHCl. As the correlation data does not fit satisfactorily to the single-component diffusion model (equation 2.7), but quite well to equation 2.11, which involves single-component diffusion along with a stretched exponential term, the later model is used for analysis of the data of Cytc-A488. Since a single-component diffusion model perfectly describes the correlation data of free

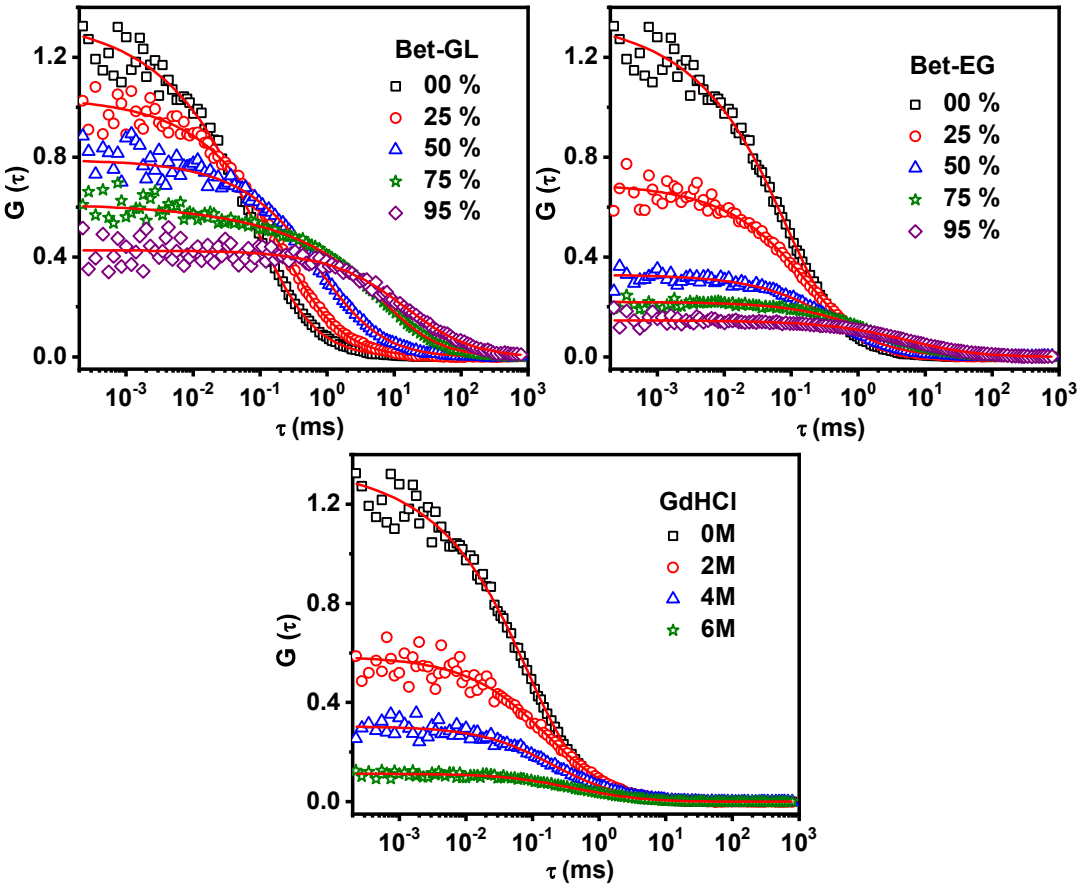

Figure 7.3. FCS data of Cytc-A488 along with fits to model containing single-component diffusion with a stretched exponential term (equation 2.11) for different concentration of DESs and GdHCl in aqueous phosphate buffered solution (pH=7).

A488 (Figure A4.7) even for excitation power (~ 45 μW) much higher than that used in our experiment (~ 15 μW),[20] it is evident that processes like intersystem crossing, which become dominant for higher laser power, are not responsible for the exponential term in our measurements on Cytc-A488. Hence, the additional exponential component arises from conformational fluctuations of the protein, which occurs during its passage through the observation volume.[22, 25]

Figure 7.3 shows that with increase in proportion of the DESs in the medium, the G(τ) values at τ = 0 (henceforth represented as G(0)) decreases and the correlation traces shift towards a longer time, the latter is more clearly visible from the normalized traces (Figure 7.4). The former suggests an increase in the effective number of molecules in the unfolded state within the observation volume that undergoing intensity fluctuation (G(0) is related to N as G(0) = 1/N(1+A), where A is ratio of the number of molecules present in the

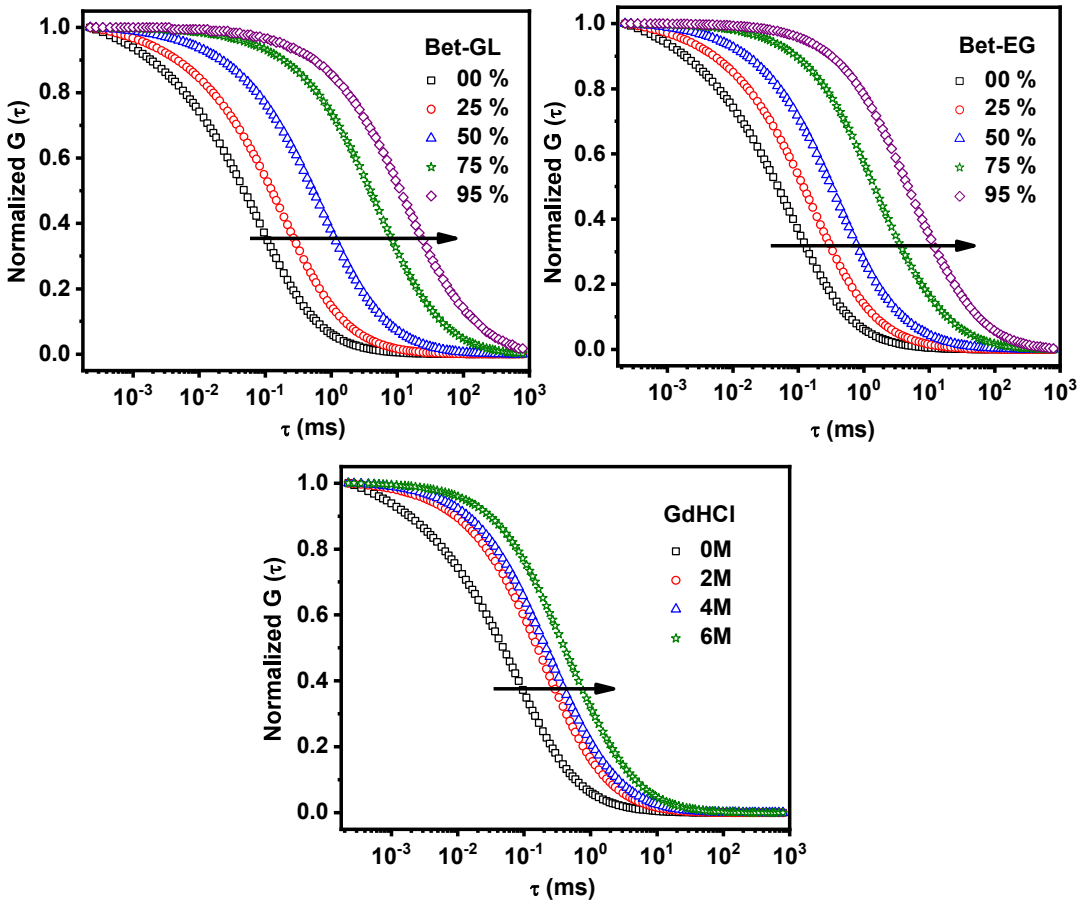

Figure 7.4. Normalized fitted (equation 2.11) correlation traces of Cytc-A488 for different concentrations of DESs and GdHCl in aqueous buffered solution (pH=7).

native state to the unfolded state). The latter represents a slowing down of the diffusion of Cytc-A488, which could be either due to an increase of the viscosity of the solution and/or increase in the size of the protein.

Generally, the hydrodynamic radius (r_H) of the protein is estimated from the measured diffusion coefficient ($D_t = r_0^2/4\tau_D$) value using the Stokes-Einstein equation (equation 7.1),[33]

$$r_H = \frac{k_B T}{6\pi\eta D} \quad \ldots\ldots\ldots\ldots\ldots (7.1)$$

As addition of the DESs and GdHCl in aqueous buffered solution changes the viscosity and refractive index of the medium (which can leads to inaccurate estimation of r_H),[22, 23, 29] we have estimated the r_H values after correcting for both viscosity and refractive index mismatches using equation 7.2.[24, 28]

$$\frac{r_H^{protein}}{r_H^{R6G}} = \frac{\tau_D^{protein}}{\tau_D^{R6G}} \quad \ldots\ldots\ldots\ldots\ldots (7.2)$$

The r_H value of the protein in the aqueous buffered solution is estimated to be 20.5 Å, which agrees well with the literature value of the horse-heart Cytc protein (104 residues).[16, 23, 34] The measured r_H value of the protein in its native state is also in agreement with that predicted value (18.5 Å) by the empirical formula, $r_H = 4.75N^{0.29}$ Å (where N is the number of amino acid residues in the protein).[35]

The change in the r_H values of Cytc with increasing concentrations of the DESs and GdHCl are shown in Figure 7.5, and the correspondence values are presented in Table 7.2. As can be seen, the r_H values increases with addition of both the DESs, and reaches a value of 30.8 and 25.1 Å for Bet-EG and Bet-GL, respectively. The former value is very close to that observed in 6M GdHCl (31.5 Å), where the protein structure unfolds completely and that predicted for the unfolded state of Cytc (31.9 Å) according to the empirical formula, $r_H = 2.11N^{0.57}$ Å.[35] The r_H value for the maximum concentration (95 % (v/v)) of Bet-GL is same with that observed for lowest concentration (25 % (v/v)) of Bet-EG. This clearly implies that the change in the protein structure is significantly greater in Bet-EG compared to that in Bet-GL. This is in agreement with the steady-state and time-resolved

fluorescence data confirming that while Bet-EG destabilizes the protein structure almost completely, the extent of this deleterious effect is considerably less in case of Bet-GL.

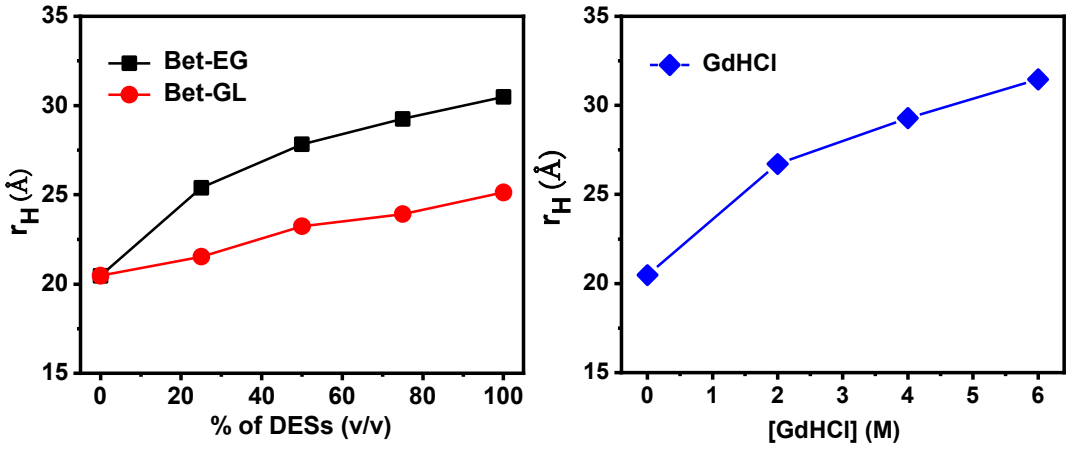

Figure 7.5. Variation of the measured r_H values of Cytc with increasing concentration of the DESs and GdHCl.

Table 7.2. Estimated parameters from the fitting of FCS data (to equation 2.11) of Cytc-A488 for different concentration of the DESs and GdHCl.

Solvent	τ_D(ms)	τ_R(μs)	α	r_H(Å)
Only buffered solution	0.25± 0.02	54.0± 1.8	0.44± 0.02	20.5 ± 1.5
25 % Bet-G	0.60± 0.03	56.7± 1.5	0.48± 0.04	21.5± 1.0
50 % Bet-G	2.10± 0.07	58.5± 1.5	0.55± 0.03	23.2± 1.2
75 % Bet-G	10.10±1.25	59.8±2.1	0.60± 0.05	23.9± 1.5
95 % Bet-G	48.00±3.50	60.7± 1.0	0.62± 0.02	25.1± 1.0
25% Bet-EG	0.55± 0.04	64.2±3.3	0.52± 0.03	25.4± 1.4
50% Bet-EG	1.45± 0.03	67.4± 1.4	0.60± 0.03	27.8± 2.0
75% Bet-EG	4.59±0.09	69.6±2.7	0.70± 0.03	29.3± 1.0
95% Bet-EG	11.28±1.50	72.3±3.5	0.76± 0.03	30.8± 1.7
2.0 M GdHCl	0.33± 0.02	65.8± 1.6	0.59± 0.03	26.7±2.2
4.0 M GdHCl	0.51± 0.03	68.6±3.0	0.70± 0.07	29.3± 1.9
6.0 M GdHCl	0.85± 0.06	73.3±2.5	0.79± 0.04	31.5± 1.5

The estimated time constant corresponding to the exponential term (τ_R) in buffered solution is 54 μs, which is very similar to the timescales observed for many proteins and attributed to the conformational dynamics of the proteins in their native state.[16, 20, 22, 23, 36, 37] It is to be mentioned here that the τ_R values also corrected for viscosity of the medium (as done for the $r_H$values) using the formula,

$$\tau_R = \tau_R^{uncorr} \times \frac{\tau_D^{buffer}}{\tau_D^{sample}} \quad \ldots\ldots\ldots\ldots\ldots\ldots (7.3)$$

where, τ_R^{uncorr} denotes the viscosity uncorrected relaxation time, and τ_D^{buffer} and τ_D^{sample} are diffusion times of R6G in buffer and different solutions, respectively.

As can be seen, an increase in the τ_R value (Figure 7.6 and Table 7.2) for higher concentrations of the DESs indicating slowing down of the conformational dynamics in these media. A comparison of these values with those observed for 6M GdHCl (73.3 μs) traces that the conformational dynamics is significantly slower in Bet-EG as compared to Bet-GL. This is understood considering the fact that in the case of Bet-EG, where the protein structure unfolded almost completely, the conformational fluctuation occur slowly because the side chain residues of quencher amino acids of the protein has to diffuse through a longer distance to quench the fluorescence of A488 dye.[23] This is consistent with the increase in size of the protein in the DESs.

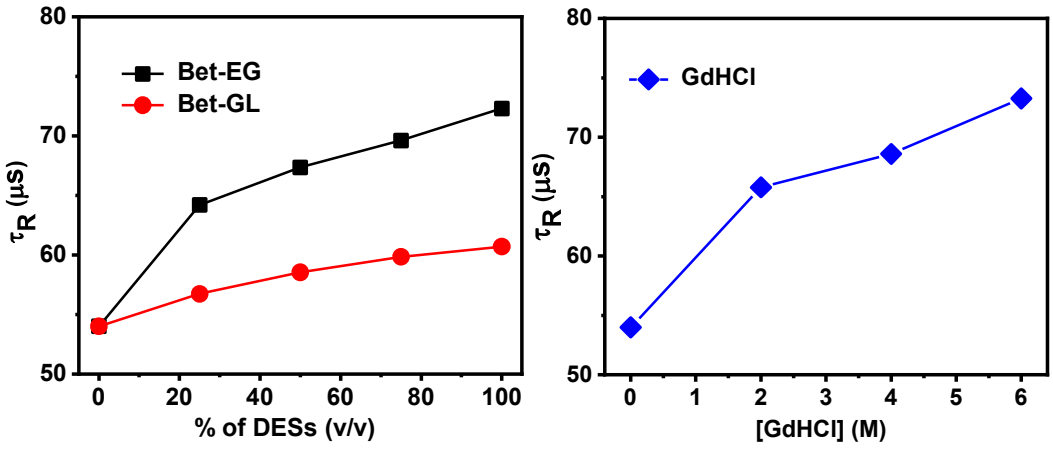

Figure 7.6. Variation of the measured τ_R values of Cytc with increasing concentration of the DESs and GdHCl.

Further, it can be seen that the observed conformational dynamics of the protein is best described by a distribution of the exponential term (τ_R value) given by the stretching parameter α (equation 2.11), whose value is found to be 0.44 in the native state of Cytc. This indicates heterogeneous nature of the conformational dynamics arising from different short and long range fluctuations of the protein structures. Such heterogeneity in the conformational dynamics of proteins is expected considering the complexity of the conformational fluctuations, and similar results are indeed observed earlier for many proteins.[38-41] A careful inspection of the α values estimated at different concentration of the DESs and GdHCl shows that, while this value increases from 0.44 (in buffered solution) to 0.62 in 95% (v/v) Bet-GL, it changes to 0.76 in 95% (v/v) Bet-EG, which is quite close to the value observed in 6M GdHCl (0.79). This is presumably due to the increase in the distance between the side chain residues of the quencher amino acids and the dye molecule upon unfolding, which leads to a decrease in the effective fluctuations (particularly the short range fluctuations) of the system and hence fluorescence intensity fluctuations.

7.2.3. CD Measurements

To understand the increase of size and slower conformational dynamics of Cytc on addition of the DESs, we have probed the structural changes of the protein for different concentrations of the solvents using CD spectroscopy. We have recorded CD spectra of Cytc in the near-UV and Soret-region. The far-UV measurements are not performed due to the presence of strong absorption of the studied DESs in this region. The change in the near-UV CD (250-350 nm) spectra, which provides information on the tertiary structure of the protein,[42-44] with increasing concentration of the DESs and GdHCl are shown in Figure 7.7. The spectra display two distinct minima at 282 and 289 nm in buffered solution, characteristics of the native state Cytc.[16, 42, 45] Upon addition of 95% (v/v) Bet-EG, both the characteristic minima disappeared completely, similar to that observed for GdHCl, whereas these minima still exist in 95% (v/v) Bet-GL. This indicates that the tertiary structure of the protein is disrupted completely in the former DES, whereas in the latter case the structure is preserved significantly. This corroborates the earlier results observed through the fluorescence spectroscopy.

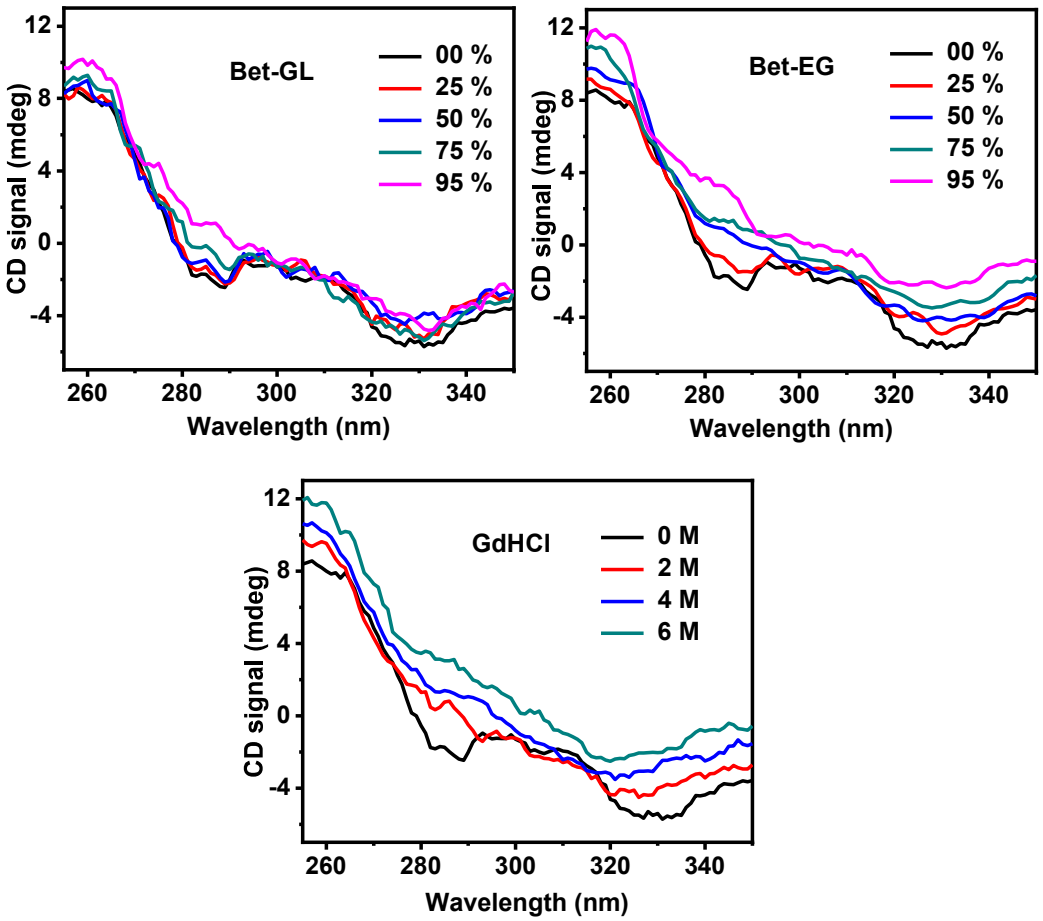

Figure 7.7. Near-UV CD spectra of Cytc for different concentration of DESs and GdHCl in aqueous buffered solution.

As the Soret-region CD spectrum of heme-proteins strongly depends on the immediate environment of the heme moiety,[42, 46] we have monitored the CD spectra of Cytc in this region (360-450 nm) to get further insight into the effect of these DESs on the native structure of the heme crevice (Figure 7.8). In absence of the additives, Cytc exhibits a strong negative band at about 418 nm and a strong positive band at around 408 nm, which are characteristics of the native state Cytc.[44, 46, 47] However, the negative band gradually disappears and converted completely to a single positive band in Bet-EG (similar to what is observed for GdHCl), whereas the negative band still exists with the positive one for the same concentration of Bet-GL. This indicates that the coupling between the heme iron and the nearby aromatic residues is disrupted completely in Bet-EG, but remain largely intact

in Bet-GL.[45-47] The near-UV and Soret-region CD data, thus, clearly reveals that Bet-GL induces a partial unfolding of the native structure of Cytc, whereas Bet-EG results in complete unfolding of not only the global tertiary structure but also disrupts the local environment of the protein heme moiety.

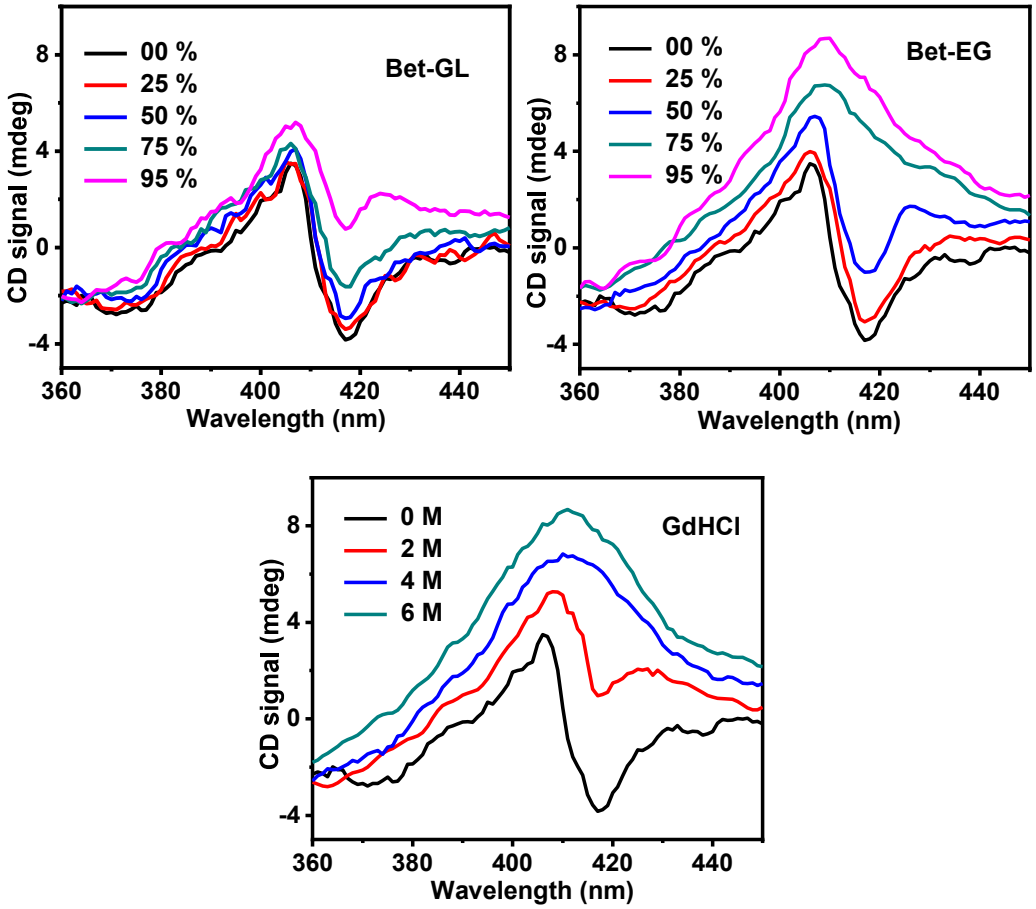

Figure 7.8. Soret-region CD spectra of Cytc for different concentration of DESs and GdHCl in aqueous buffered solution.

7.2.4. UV-vis absorption Measurements

Considering the fact that the Soret-region absorption spectrum of heme proteins gives important information about the possible structural changes of Cytc in the heme vicinity,[44, 48] we have recorded the absorption spectra of the protein in this region. The variation of the Soret band with increasing concentration of the DESs and GdHCl are shown in Figure

7.9. The band with a maximum around 409 nm in the buffered solution is characteristics of the native Cytc, which is an indicative of the presence of both axial ligands, His18 and Met80 to the heme iron.[47, 48] A blue shift of the Soret band along with increase in the absorbance value is observed with increasing addition of the both the DESs. The changes in the absorbance value and band maxima, however, are significantly less in Bet-GL as compared to Bet-EG, clearly indicates that the latter DES disrupts the heme iron ligation completely and hence, the tertiary structure of the protein. However, the extent of this structural perturbation is significantly less in the former case.

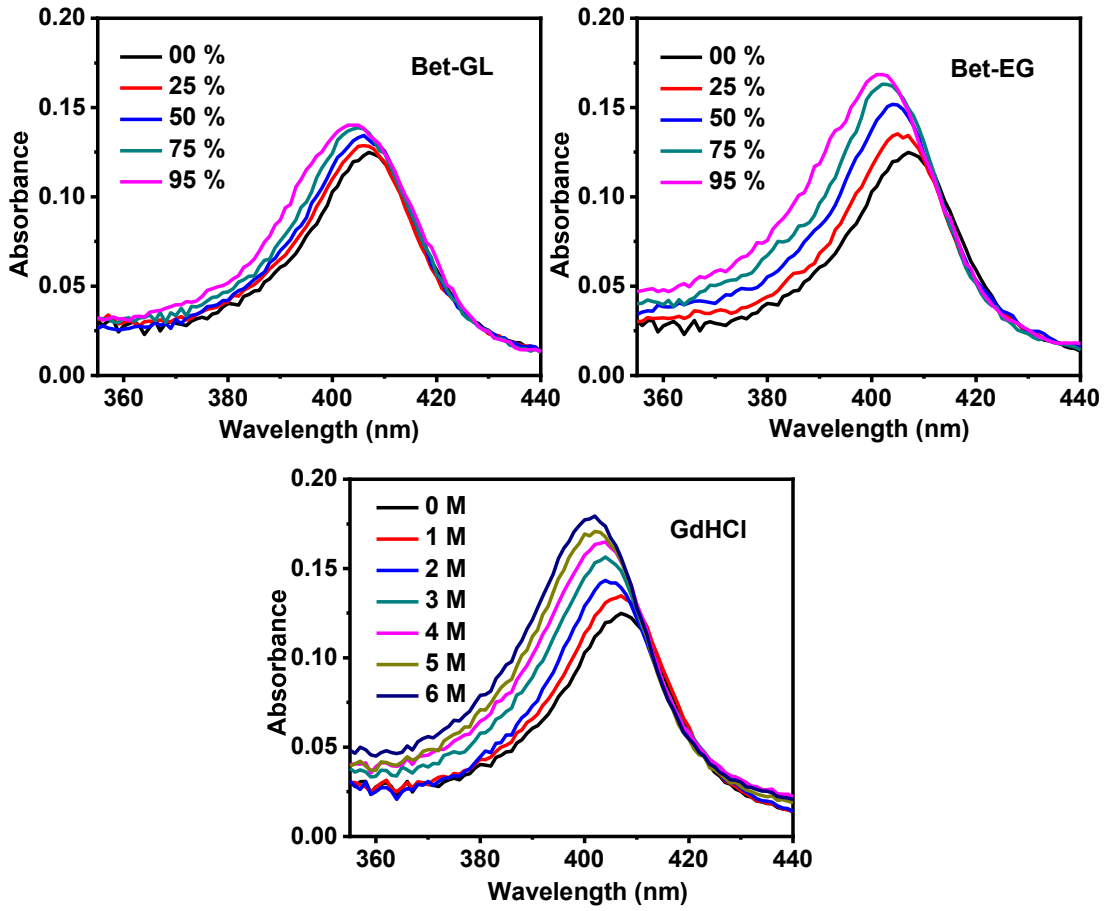

Figure 7.9. Soret-region absorption spectra of Cytc for different concentration of DESs and GdHCl in aqueous buffered solution.

Thus, taken as a whole, it can be concluded that Bet-EG alters the tertiary structure of Cytc completely to the unfolded state, whereas Bet-GL alters the structure slightly. These results, therefore, suggest that HBD of the DESs play a crucial role in controlling the

structural stability and conformational dynamics of Cytc in these DESs. This perhaps arises from the difference in the hydrogen-bonding interactions between the alcoholic constituents of the DESs (due to number of hydroxyl groups) and the protein amino acid residues and/or water molecules adjacent to the protein surface which, in turn, affect the hydration layer of the protein around its surface resulting in changes of the conformation.[49] Also, as ethylene glycol is smaller in size compared to glycerol, it can easily interact with the heme moiety and interfere with the heme ligation leading to substantial perturbation of the tertiary structure and hence, significant unfolding of the protein structure, whereas, being larger in size, glycerol molecules are preferentially excluded from such sites leading to minimal effect to the protein structure.[50] Another factor that can also contribute to the difference in DESs behaviour is huge difference in the DES viscosity (Bet-EG, 65 cP vs Bet-GL, 1300 cP); higher viscosity of the Bet-GL imposes more restriction on the flexible movements of the protein amino acid residues as well as chain dynamics,[12, 51] which results into a more compact and stable protein structure.

7.3. Summary

The influence of two betaine-alcohol based DESs on the structural stability and conformational dynamics of Cytc is studied. The results obtained by both single-molecule and ensemble measurements are in excellent agreement, and they reveal an interesting difference in influence on the structure of Cytc by the two DESs. It is quite interesting that even though the native structure of Cytc is disturbed by both the DESs; unlike Bet-EG (which unfolds the protein structure almost completely), Bet-GL holds the protein structure significantly and hence, the structural stability and conformational dynamics. This difference in the behaviour of the DESs is arising due to the difference in the mutual effect of the hydrogen-bonding interactions between the DESs and the protein amino acid residues and/or water molecules adjacent to the protein surface as well as DES viscosity. This study demonstrates how subtle change in structure of one of the constituents of the DESs can have a widely different outcome on the stability and conformational dynamics of the heme protein in the selected DESs. We believed that the knowledge acquired from this study will help designing better DESs for protein stabilization and its application in these media.

References

1. P. Anastas and N. Eghbali, *Chem. Soc. Rev.*, 2010, *39*, 301-312.
2. A. P. Abbott, D. Boothby, G. Capper, D. L. Davies and R. K. Rasheed, *J. Am. Chem. Soc.*, 2004, *126*, 9142-9147.
3. E. L. Smith, A. P. Abbott and K. S. Ryder, *Chem. Rev.*, 2014, *114*, 11060-11082.
4. Q. Zhang, K. D. O. Vigier, S. Royer and F. Jérôme, *Chem. Soc. Rev.*, 2012, *41*, 7108-7146.
5. J. T. Gorke, F. Srienc and R. J. Kazlauskas, *Chem. Commun.*, 2008, 1235-1237.
6. M. Ruesgas-Ramón, M. L. Suárez-Quiroz, O. González-Ríos, B. Baréa, G. Cazals, M. C. Figueroa-Espinoza and E. Durand, *J. Sci. Food Agric.*, 2020, *100*, 81-91.
7. P. Xu, G.-W. Zheng, M.-H. Zong, N. Li and W.-Y. Lou, *Bioresour. Bioprocess.*, 2017, *4*, 34.
8. A. Grudniewska, E. M. d. Melo, A. Chan, R. Gniłka, F. Boratyński and A. S. Matharu, *ACS Sustain. Chem. Eng.*, 2018, *6*, 15791-15800.
9. Q. Zeng, Y. Wang, Y. Huang, X. Ding, J. Chen and K. Xu, *Analyst*, 2014, *139*, 2565-2573.
10. D. Mondal, M. Sharma, C. Mukesh, V. Gupta and K. Prasad, *Chem. Commun.*, 2013, *49*, 9606-9608.
11. J. M. Berg, J. L. Tymoczko and L. Stryer, *Biochemistry, 6th ed.*, 2006, W. H. Freeman: New York, USA.
12. R. Esquembre, J. M. Sanz, J. G. Wall, F. d. Monte, C. R. Mateo and M. L. Ferrer, *Phys. Chem. Chem. Phys.*, 2013, *15*, 11248-11256.
13. H. Monhemi, M. R. Housaindokht, A. A. Moosavi-Movahedi and M. R. Bozorgmehr, *Phys. Chem. Chem. Phys.*, 2014, *16*, 14882-14893.
14. A. Sanchez-Fernandez, K. J. Edler, T. Arnold, D. A. Venerod and A. J. Jackson, *Phys. Chem. Chem. Phys.*, 2017, *19*, 8667-8670
15. H. Frauenfelder, S. G. Sligar and P. G. Wolynes, *Science*, 1991, *254*, 1598-1603.
16. A. Pabbathi and A. Samanta, *J. Phys. Chem. B*, 2020, 124, 8132-8140.
17. K. C. Hayes, A. Pronczuk, M. W. Cook and M. C. Robbins, *Food. Chem. Toxicol.*, 2003, *41*, 1685-1700.
18. P. H. Yancey, *J. Exp. Biol.*, 2005, *208*, 2819-2830.
19. A. Kumar, M. Bisht and P. Venkatesu, *Int. J. Biol. Macromol.*, 2017, *96*, 611-651.
20. J. Choi, S. Kim, T. Tachikawa, M. Fujitsuka and T. Majima, *Phys. Chem. Chem. Phys.*, 2011, *13*, 5651-5658.
21. H. Chen, S. S. Ahsan, M. E. B. Santiago-Berrios, H. D. Abruña and W. W. Webb, *J. Am. Chem. Soc*, 2010, *132*, 7244-7245.
22. A. Pabbathi, S. Ghosh and A. Samanta, *J. Phys. Chem. B*, 2013, *117*, 16587-16593.
23. S. S. Mojumdar, R. Chowdhury, S. Chattoraj and K. Bhattacharyya, *J. Phys. Chem. B*, 2012, *116*, 12189-12198.
24. K. Chattopadhyay, S. Saffarian, E. L. Elson and C. Frieden, *Biophys. J.*, 2005, *88*, 1413-1422.

25. H. Chen, E. Rhoades, J. S. Butler, S. N. Loh and W. W. Webb, *Proc. Natl. Acad. Sci. U.S.A.*, 2007, *104*, 10459-10464.
26. A. Pabbathi, S. Patra and A. Samanta, *ChemPhysChem*, 2013, *14*, 1441-2449.
27. A. Pabbathi and A. Samanta, *J. Phys. Chem. B*, 2015, *119*, 11099-11105.
28. E. Sherman, A. Itkin, Y. Y. Kuttner, E. Rhoades, D. Amir, E. Haas and G. Haran, *Biophys. J.*, 2008, *94*, 4819-4827.
29. R. Yadav, B. Sengupta and P. Sen, *J. Phys. Chem. B*, 2014, *118*, 5428-5438.
30. K. Gurunathan and MarciaLevitus, *Prog. Nucleic Acid Res. Mol. Biol.*, 2008, *82*, 33-69.
31. M. Schüttpelz, J. C. Schöning, S. Doose, H. Neuweiler, E. Peters, D. Staiger and M. Sauer, *J. Am. Chem. Soc.*, 2008, *130*, 9507-9513.
32. M. M. Islam, S. Barik, N. Preeyanka and M. Sarkar, *J. Phys. Chem. B*, 2020, 124, 961−973.
33. J. R. Lakowicz, *Principles of Fluorescence Spectroscopy, 3rd ed.*, 2006, Springer: New York, USA.
34. P. Bharmoria, T. J. Trivedi, A. Pabbathi, A. Samanta and A. Kumar, *Phys. Chem. Chem. Phys.*, 2015, *17*, 10189-10199.
35. D. K. Wilkins, S. B. Grimshaw, V. r. Receveur, C. M. Dobson, J. A. Jones and L. J. Smith, *Biochemistry*, 1999, *38*, 16424-16431.
36. M. C. R. Shastry and H. Roder, *Nature Struct. Biol.*, 1998, *5*, 385-392.
37. C. Rischel, L. E. Jørgensen and Z. Földes-Papp, *J. Phys.: Condens. Matter*, 2003, *15*, S1725-S1735.
38. H. Yang, G. Luo, P. Karnchanaphanurach, T.-M. Louie, I. Rech, S. Cova, L. Xun and X. S. Xie, *Science*, 2003, *302*, 262-266.
39. B. Pradhan, C. Engelhard, S. V. Mulken, X. Miao, G. W. Canters and M. Orrit, *Chem. Sci.*, 2020, *11*, 763-771.
40. X. Tan, P. Nalbant, A. Toutchkine, D. Hu, E. R. Vorpagel, K. M. Hahn and H. P. Lu, *J. Phys. Chem. B*, 2004, *108*, 737-744.
41. A. Gupta, T. J. Aartsma and G. W. Canters, *J. Am. Chem. Soc.*, 2014, *136*, 2707-2710.
42. H. A. Havel, *Spectroscopic Methods For Determining Protein Structure In Solution*, 1996, VCH: New York, USA.
43. S. M. Kelly and N. C. Price, *Curr. Protein Pept. Sci.*, 2000, *1*, 349-384.
44. M. Bisht, D. Mondal, M. M. Pereira, M. G. Freire, P. Venkatesu and J. A. P. Coutinho, *Green Chem.*, 2017, *19*, 4900-4911.
45. T. J. T. Pinheiro, G. A. Elöve, A. Watts and H. Roder, *Biochemistry*, 1997, *36*, 13122-13132.
46. R. Santucci and F. Ascoli, *J. Inorg. Biochem.*, 1997, *68*, 211-214.
47. D. K. Sahoo, S. Jena, K. D. Tulsiyan, J. Dutta, S. Chakrabarty and H. S. Biswal, *J. Phys. Chem. B*, 2019, *123*, 10100-10109.
48. R. F. Latypov, H. Cheng, N. A. Roder, J. Zhang and H. Roder, *J. Mol. Biol.*, 2006, *357*, 1009-1025.
49. P. Huang, A. Dong and W. S. Caughey, *J. Pharm. Sci*, 1995, 84, 387-392.

50. N. Chéron, M. Naepels, E. Pluhařová and D. Laage, *J. Phys. Chem. B*, 2020, 124, 1424-1437.
51. M. Jacob, T. Schindler, J. Balbach and F. X. Schmid, *Proc. Natl. Acad. Sci. USA*, 1997, 94, 5622–5627.

Chapter 8

Concluding Remarks

Overview

This chapter summarizes the results of the investigations carried out during the course of the present thesis work. The scope of future studies based on the current findings is also discussed.

8.1 Summary

The work reported in this thesis has been performed to obtain a comprehensive understanding of the microscopic solution structure and dynamics of some alcohol-based DESs by studying various photophysical processes of different selected fluorescent molecules in these DESs. Additionally, the structural stability and conformational dynamics of a protein has also been studied in such DESs to obtain insight into the mechanism of protein-DESs interactions, which essentially govern the fate of the protein in such nonconventional media. The findings of the work are summarized below.

As understanding the solute-solvent interactions involving different solute molecules is essential for realization of the potential of DESs as novel media, here we have attempted to investigate this aspect in a less-viscous ionic DES consisting of ChCl and ethylene glycol by studying the rotational and translational diffusion dynamics of C153, R123 and FL using time-resolved fluorescence anisotropy and FCS measurements, respectively. These studies reveal the presence of dynamic heterogeneity in this solvent though no static heterogeneity of the medium could be detected. The dynamic heterogeneity in the DES is established from the departure of the reorientation times of the probe molecules from their hydrodynamic behavior and anomalous translational diffusion of the molecules in FCS measurements. Furthermore, both translational and rotational diffusion dynamics show the charged solutes to experience stronger solute-solvent interactions in this solvent as a consequence of mutual effect of the electrostatic and hydrogen-bonding interactions between probe molecules and constituents of the DES.

Considering that a structural change of the HBD significantly influences the physical properties of the DESs, we have studied the rotational and translational diffusion dynamics of some dipolar (C153 and 4-AP) and nonpolar (ANT) solute molecules using time-resolved fluorescence anisotropy and FCS measurements, respectively, in a series of ChCl-diol based DESs differing in hydrocarbon chain length and positioning of the hydroxyl group at the HBD to find out the effect of such structural changes on the microscopic structure, dynamics and solute-solvent interactions in these media. The results obtained from these studies reveal several interesting outcomes. Specifically, the excitation wavelength dependent fluorescence studies reveal an evolution of spatial heterogeneity with increase in chain length of the HBDs in these solvents. The anisotropy and FCS studies show significant increase of dynamic heterogeneity with increasing chain length of the HBDs. The variation of spatial and dynamic heterogeneity with change in

hydroxyl group position is found to be insignificant. Additionally, this study shows that the probe molecules reside in different environments of the nanoheterogeneous structure of these solvents and specific solute-solvent hydrogen-bonding interaction plays a crucial role in determining both rotational and translational diffusion dynamics of the molecules in these DESs.

Further, having understood that a change of the hydrocarbon chain length of HBD significantly modifies microscopic structural and dynamical features of DESs, we have attempted here to probe how the alkyl chain length of the cation of the salt influences these aspects for a set of promising but less-explored eutectic solvents comprising tetraalkylammonium bromide salts and ethylene glycol. The results suggest presence of both spatial and dynamic heterogeneity in this set of DESs too, which becomes more pronounced in longer alkyl chain containing solvents. The spatial heterogeneity in these DESs is arising from molecular scale domain formation due to segregation of the ionic moieties (along with the hydroxyl moieties of the HBD) and the hydrophobic alkyl chain of the salt, and becomes more pronounced in longer chain length containing solvents. This study also reveals that the probe molecules reside in the different regions of the solvents; consequently, they experience very different solute-solvent interactions. Hence, present findings along with the previous work clearly suggest that the spatial and dynamic heterogeneity of the ionic DESs can be modified significantly by tuning the hydrocarbon chain length of either of the constituents of these solvents.

Considering the fact that study of solvation dynamics can uncover unique characteristics of a solvent, we have attempted to obtain an insight into the complete solvation dynamics of C153 in some less-explored DESs by monitoring its time-dependence of the fluorescence Stokes shift using a combination of UPC and TCSPC techniques. The study reveals temporally diverse nature of the solvation in these DESs, characterized by a distinct ultrafast subpicosecond component and a slow picosecond component with a distribution of the relaxation time. A detailed analysis of the results reveal that the ultrafast component arises from rapid local structural relaxation in the immediate vicinity of the probe molecule within the solvation shell, whereas the broadly distributed slow component arises from heterogeneous dynamical processes due to nonhydrodynamic diffusive motions of the solvent constituents into and out of the solvation shell that cause bulk structural relaxation. It is also found that the length of the alkyl chain and hence, the size of the cation of the salt greatly influences the solvation dynamics in these solvents.

In the last work of the thesis, the influence of two betaine-alcohol based DESs, Bet-EG and Bet-G, on the structural stability and conformational dynamics of cytochrome c is studied by using FCS and various biophysical methods. The results obtained by both single-molecule and ensemble measurements are in excellent agreement, and they reveal an interesting difference in influence on the structure of Cytc by the two DESs. The results show that even though the native structure of Cytc is disturbed by both the DESs; unlike Bet-EG (which unfolds the protein structure almost completely), Bet-GL holds the protein structure significantly and hence, the structural stability and conformational dynamics. This difference in the behaviour of the DESs is arising due to the difference in the mutual effect of the hydrogen-bonding interactions between the DESs and the protein amino acid residues and/or water molecules adjacent to the protein surface as well as DES viscosity. This study clearly demonstrates how subtle change in structure of one of the constituents of the DESs can have a widely different outcome on the stability and conformational dynamics of the heme protein in the selected DESs.

8.2 Future Scope

As we have discussed earlier, several DESs are highly viscous, which sometimes limit their applications. The alcohol-based DESs can serve as useful media in such applications due to their significantly lower viscosity. This is why we have worked specifically with the alcohol-based DESs here. Another practical approach that has been adopted for reducing the viscosity of many DESs is mixing with water or other molecular solvents. However, studies have indicated that addition of water or other molecular solvents considerably alter most of the other physicochemical properties of these novel media. Thus, these systems need to be understood fully before their application in various sectors. Hence, it will be interesting to study the effect of such dilution on the microscopic structure and dynamics of these systems.

A survey of the literature suggests that most of the works on DESs have been carried out in systems based on a particular salt (i.e. ChCl). Several new but promising DESs based on various other salts are gaining attention recently. However, the microscopic structural and dynamical features of such less-explored DESs that is necessary for realization of their successful utility in various fields, is poorly understood. Here we have explored a set of

such new DESs. Hence, performing fundamental studies on many others DESs will be an important area of research for development of new DESs with desirable properties.

Knowing the importance of the solvation dynamics studies towards understanding the nature of the DESs, we have captured almost complete dynamics of the solvation of C153 in a set of DESs. However, such studies are very few in numbers. Similar studies on different solute molecules capable of specific interactions with many other DESs employing various experimental and theoretical methods will be extremely useful for a comprehensive appreciation of this aspect.

Though few studies have been performed recently to explore the structure, stability and activity of some protein molecules in DESs, these reports are qualitative and do not shed complete light on the molecular level interactions. What we have understood from the findings of our study and the existing literature is that the structure and dynamics of proteins in DESs depend on the nature of both proteins and DESs, and the biophysical mechanism governing the protein-DESs interaction is yet to be understood clearly. This suggests that further studies on various protein molecules in a wide variety of DESs are necessary to improve our understanding on such systems. The findings of these studies will definitely contribute towards a better understanding of the nature of protein-DESs interactions which can be utilised for designing new DESs for various biotechnological applications.

Appendices

Appendix 1

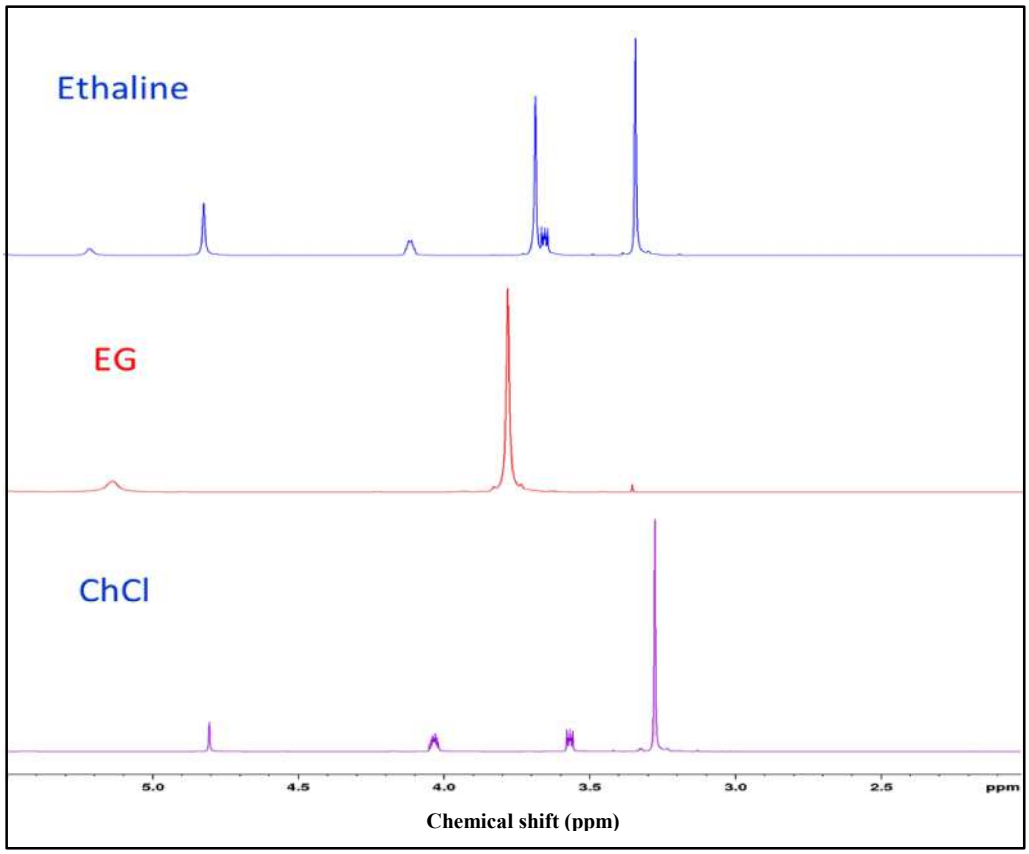

Figure A1.1. 1H-NMR spectra of choline chloride (ChCl), ethylene glycol (EG) and prepared ethaline (CD3OD as reference).

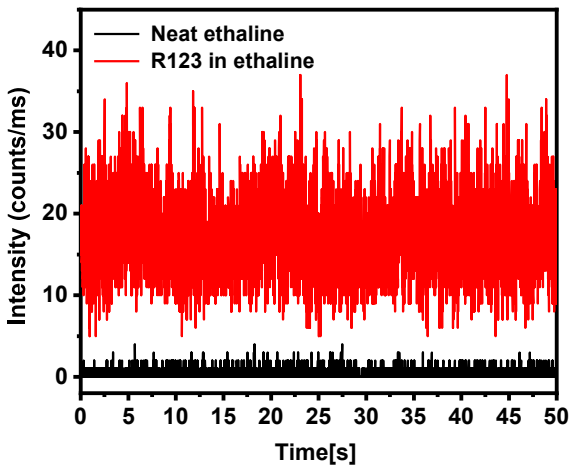

Figure A1.2. The fluorescence intensity time trace of ethaline only and R123 in ethaline (λ_{exc} = 485 nm).

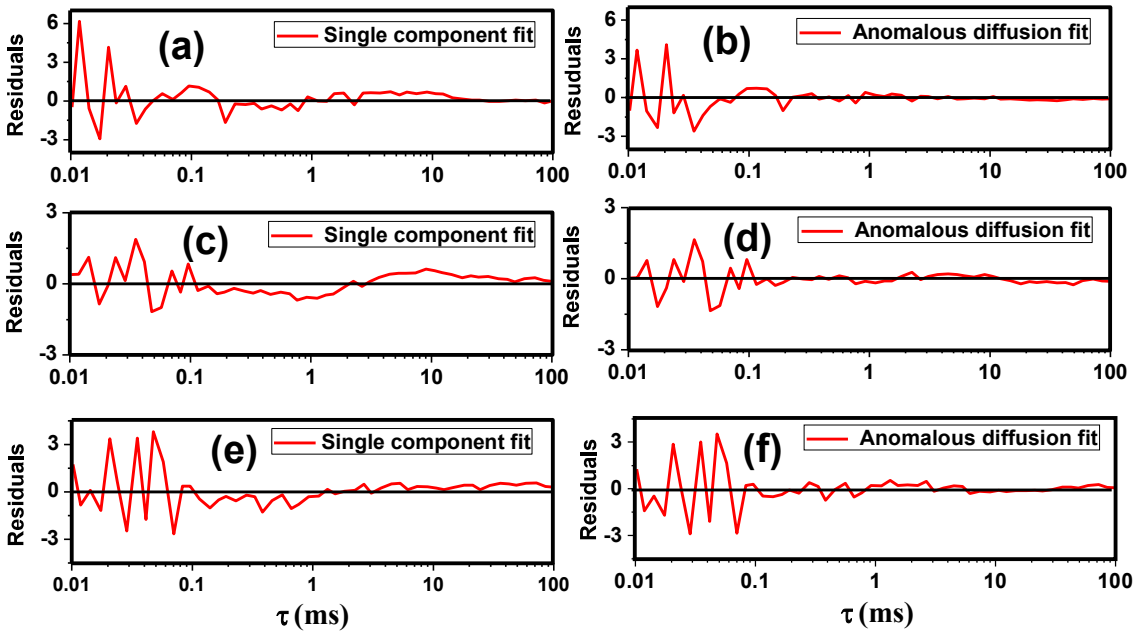

Figure A1.3. Residuals of the fits of fluorescence correlation curve for C153 (a, b), R123 (c, d), and FL (e, f) using both single component and anomalous diffusion model.

Table A1.1. Reorientation times (ns) of solutes for slip and stick lines at different temperatures calculated using Stokes-Einstein-Debye (SED) hydrodynamic theory.

Temp (K)	C153		R123		FL	
	Slip	Stick	Slip	Stick	Skip	Stick
298	1.03	4.29	0.96	6.20	0.74	5.26
313	0.54	2.24	0.50	3.23	0.38	2.74
323	0.36	1.51	0.34	2.18	0.26	1.87
333	0.26	1.10	0.25	1.58	0.19	1.36
343	0.17	0.71	0.16	1.03	0.12	0.88

Appendix 2

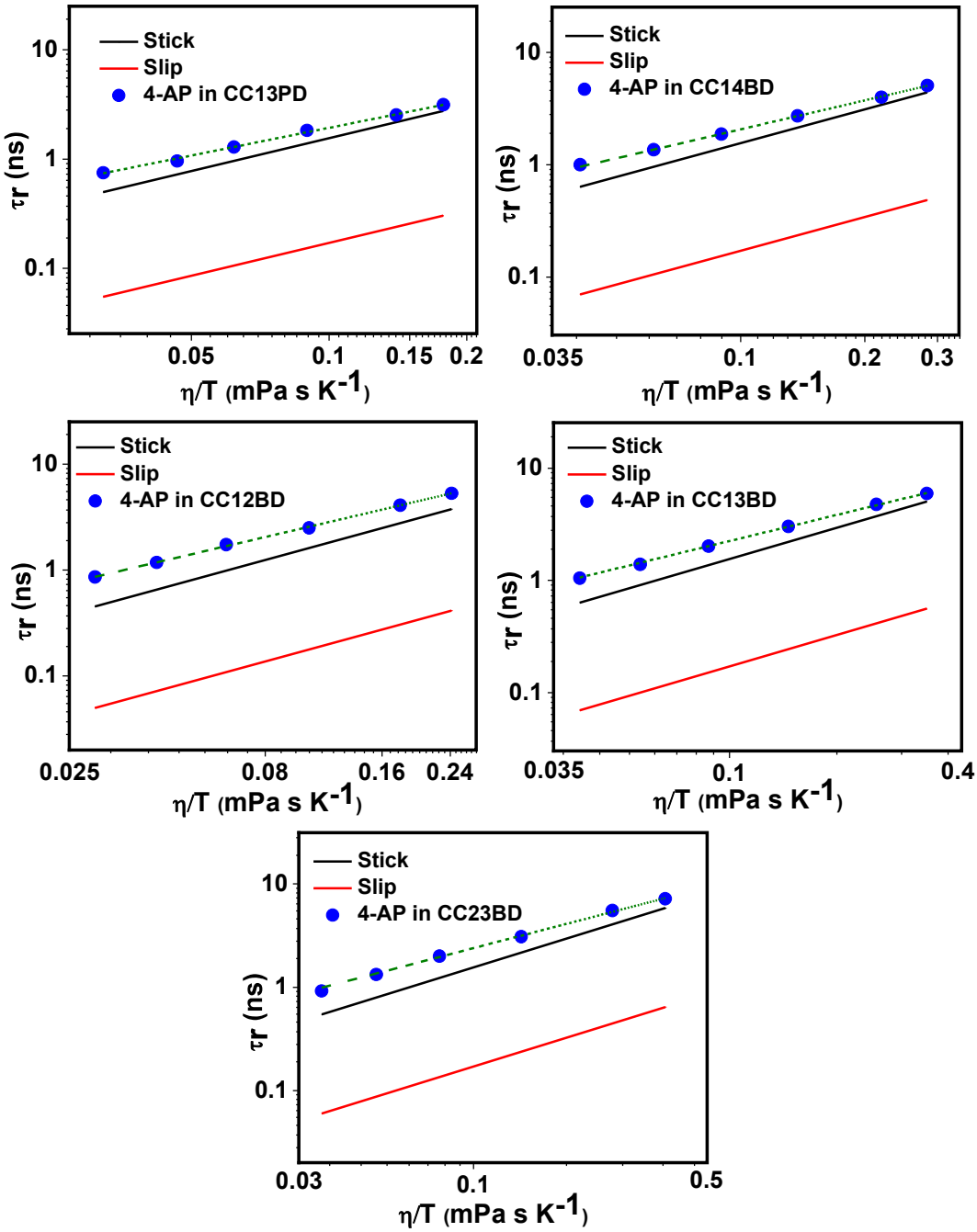

Figure A2.1. Plots of τ_r vs η/T for 4-AP in DESs. The solid circles indicate the experimental rotational times and the dashed lines represent fit to the data according to $\tau_r = A(\eta/T)^p$. Computed stick (black) and slip (red) lines using SED theory are also shown.

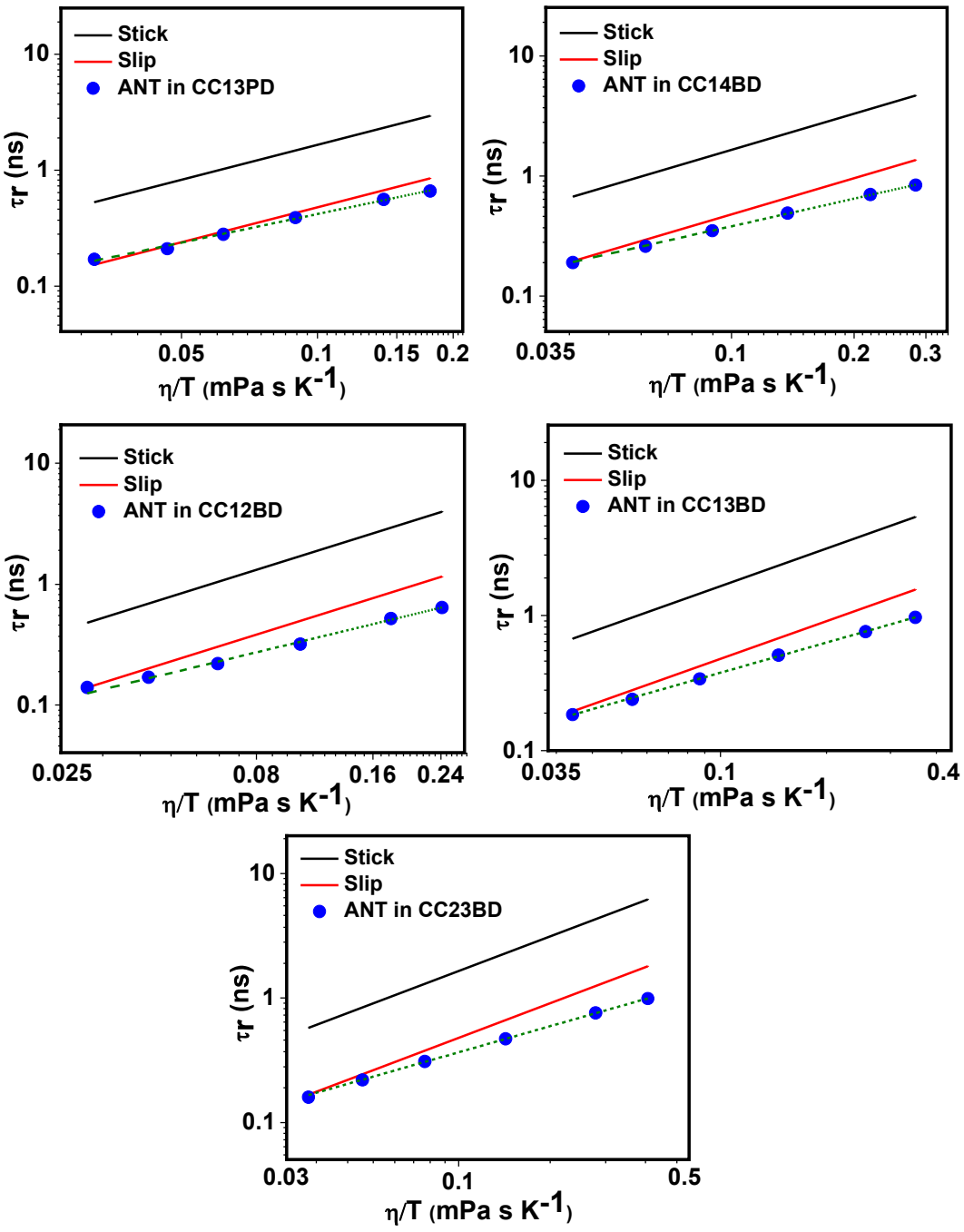

Figure A2.2. Plots of τ_r vs η/T for ANT in DESs. The solid circles indicate the experimental rotational times and the dashed lines represent fit to the data according to $\tau_r = A(\eta/T)^p$. Computed stick (black) and slip (red) lines using SED theory are also shown.

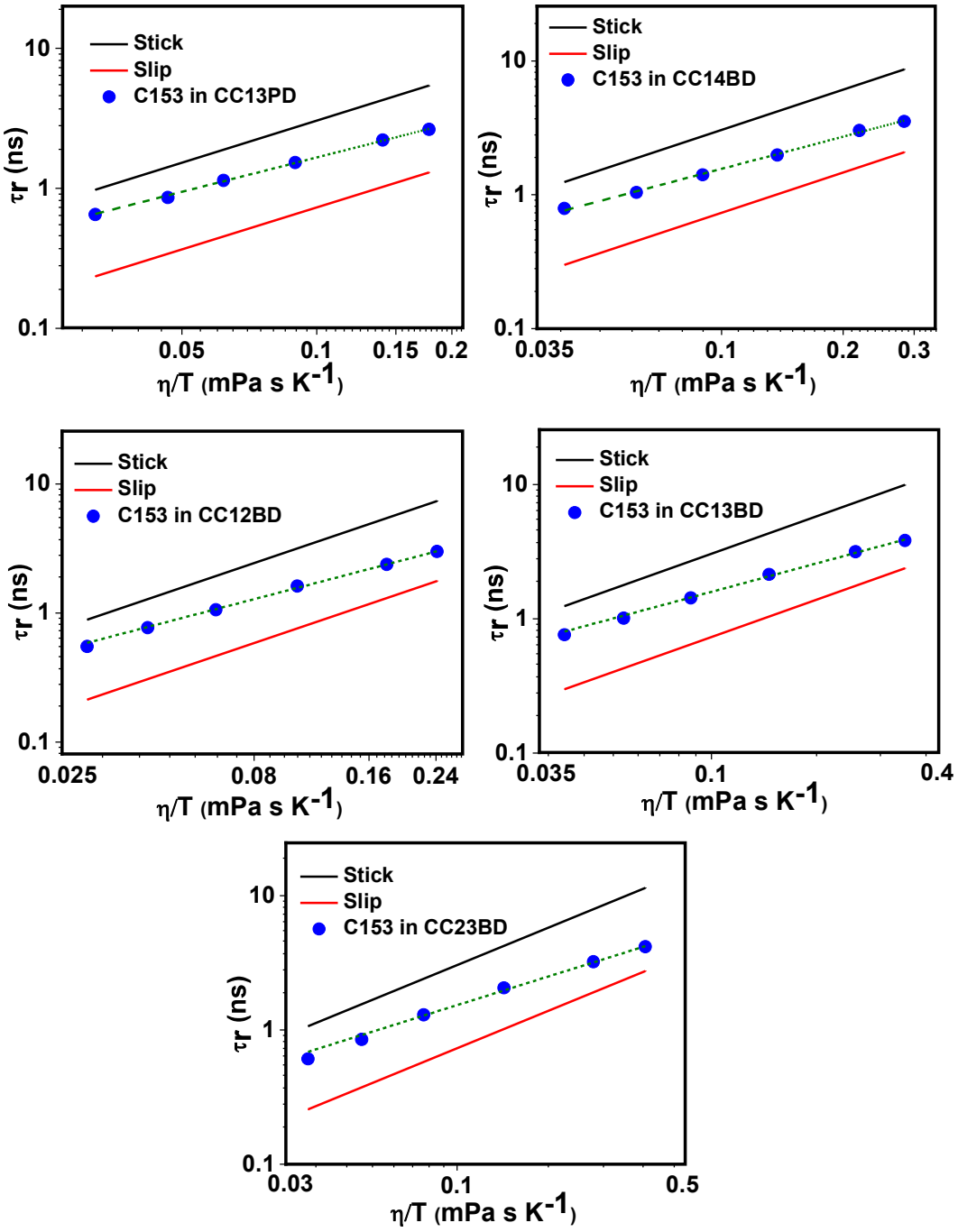

Figure A2.3. Plots of τ_r vs η/T for C153 in DESs. The solid circles indicate the experimental rotational times and the dashed lines represent fit to the data according to $\tau_r = A(\eta/T)^p$. Computed stick (black) and slip (red) lines using SED theory are also shown.

Table A2.1. Estimated Rotational Reorientation Times (τ_r) of the Solutes in DESs at Different Temperatures.

DESs	Temp. (K)	Viscosity (cP)	Rotational reorientation time (ns)		
			C153	AP	ANT
CC12ED	298	30.0	1.58	1.65	0.44
	303	24.5	1.30	1.37	0.36
	313	17.5	0.93	0.97	0.27
	323	13.5	0.69	0.71	0.19
	333	10.0	0.53	0.55	0.16
	343	08.0	0.43	0.44	0.13
CC13PD	298	53.0	2.64	3.14	0.66
	303	42.5	2.22	2.53	0.56
	313	28.0	1.53	1.83	0.39
	323	20.0	1.14	1.29	0.28
	333	15.5	0.86	0.96	0.21
	343	11.0	0.65	0.75	0.17
CC14BD	298	84.5	3.53	5.08	0.84
	303	66.5	3.02	4.00	0.70
	313	43.0	1.98	2.72	0.49
	323	29.0	1.41	1.87	0.35
	333	20.5	1.04	1.36	0.26
	343	14.0	0.79	1.00	0.19
CC12BD	298	72.0	2.99	5.30	0.64
	303	54.0	1.38	4.10	0.52
	313	32.5	1.62	2.50	0.32
	323	20.5	1.06	1.74	0.22
	333	14.0	0.77	1.18	0.17
	343	10.0	0.55	0.86	0.14
CC13BD	298	97.0	3.83	5.96	0.97
	303	73.0	3.16	4.75	0.76
	313	44.5	2.14	3.03	0.51
	323	28.5	1.43	2.02	0.34
	333	19.5	1.01	1.39	0.24
	343	14.0	0.76	1.05	0.18
CC23BD	298	112.0	4.17	7.20	0.99
	303	79.0	3.22	5.54	0.76
	313	43.5	2.06	3.09	0.47
	323	25.5	1.30	2.00	0.31
	333	17.0	0.85	1.33	0.22
	343	12.0	0.61	0.92	0.16

Appendix 3

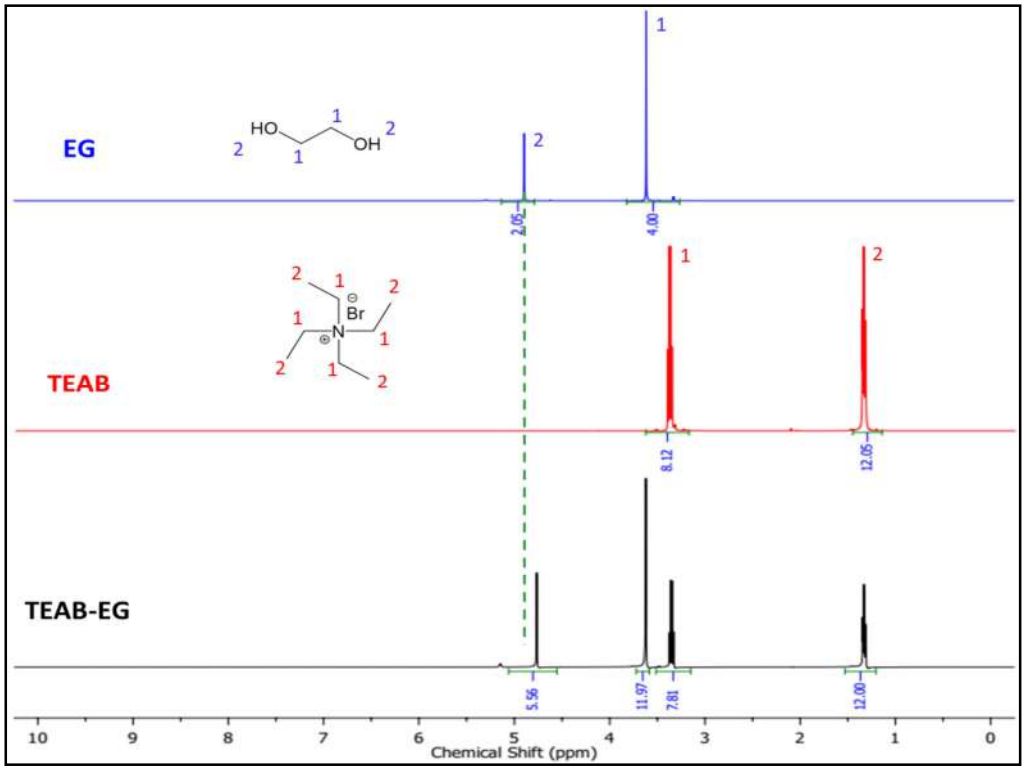
EG
TEAB
TEAB-EG
Chemical Shift (ppm)

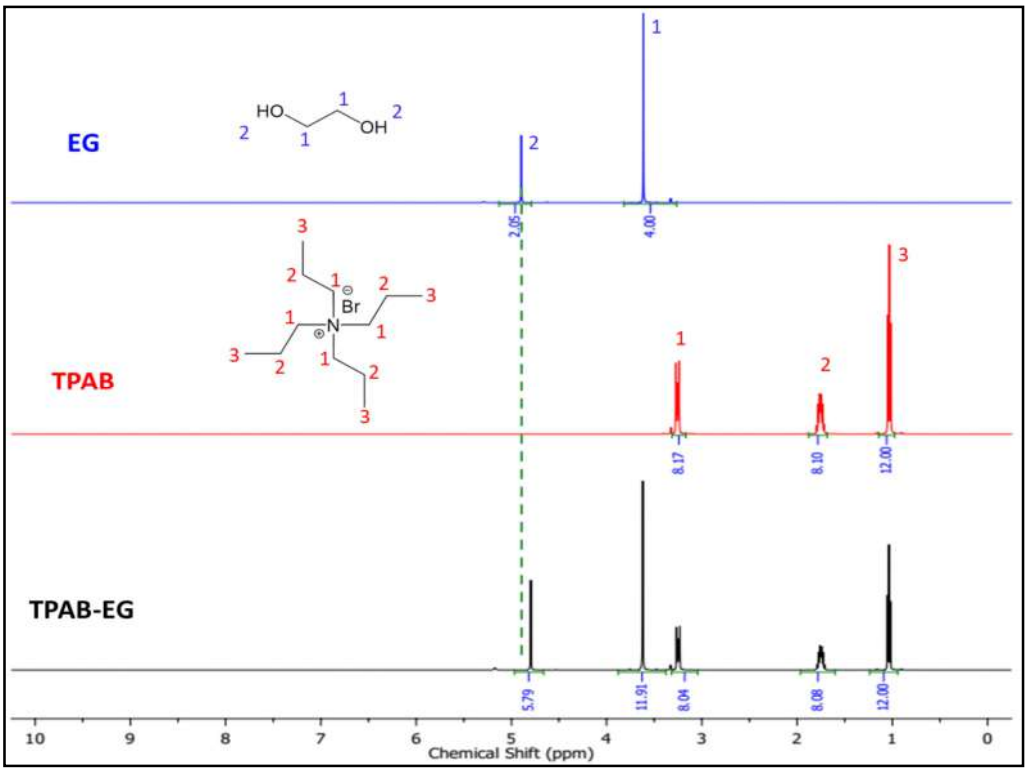
EG
TPAB
TPAB-EG
Chemical Shift (ppm)

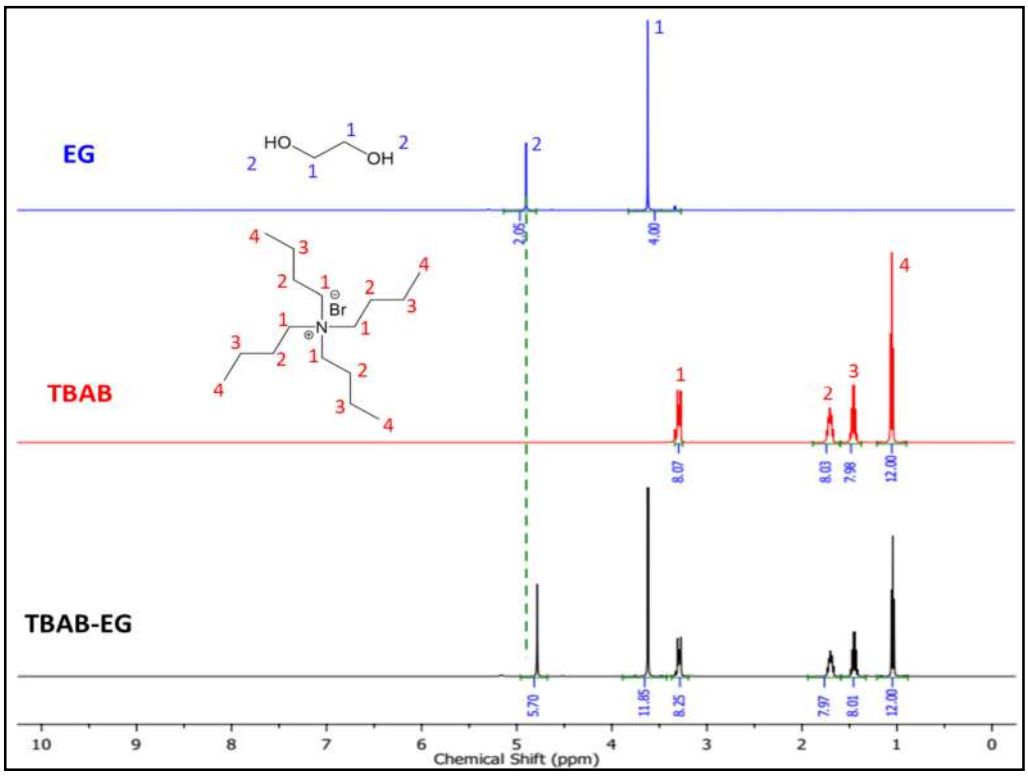

Figure A3.1. ^{1}H NMR spectra of the prepared DESs and their constituents in CD_3OD. The vertical dashed line in each panel shows shift of the OH peak on formation of the DESs through hydrogen-bonding between the two constituents.

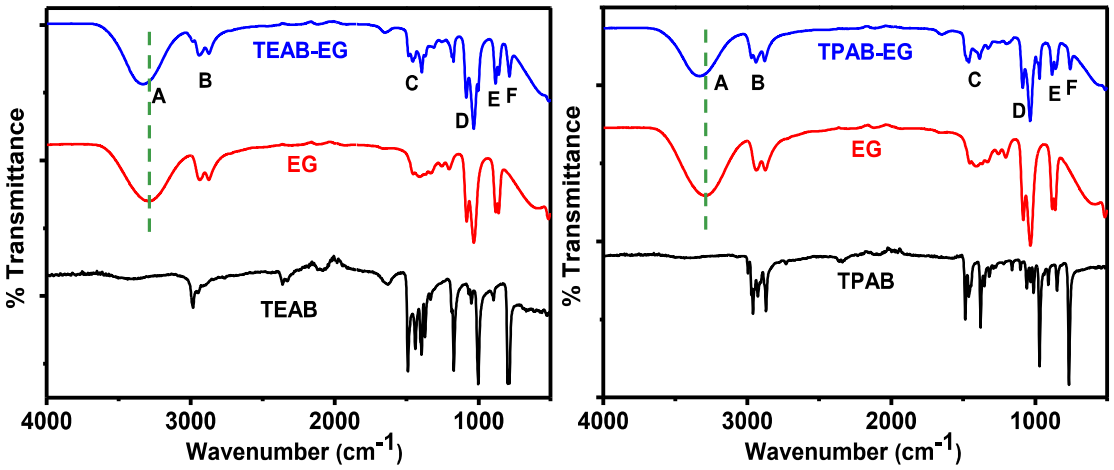

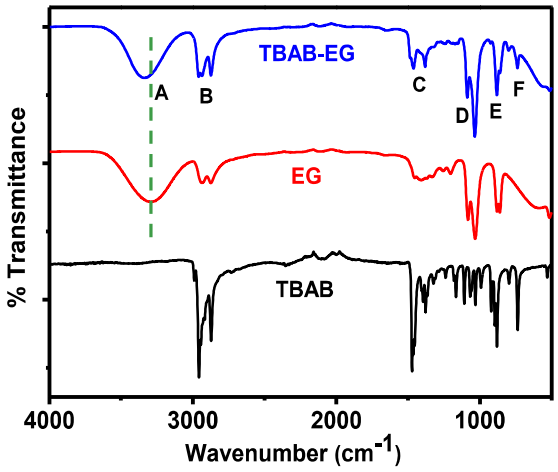

Figure A3.2. FTIR spectra of the prepared DESs and their constituents. The important bands are shown in each panel: (A) OH stretching, (B) C−H stretching, (C) C−OH bending, (D) C−O stretching, (E) OH wagging and (F) CH rocking. The vertical dashed line in each panel shows shift of the OH stretching band on formation of the DESs through hydrogen-bonding between the two constituents.

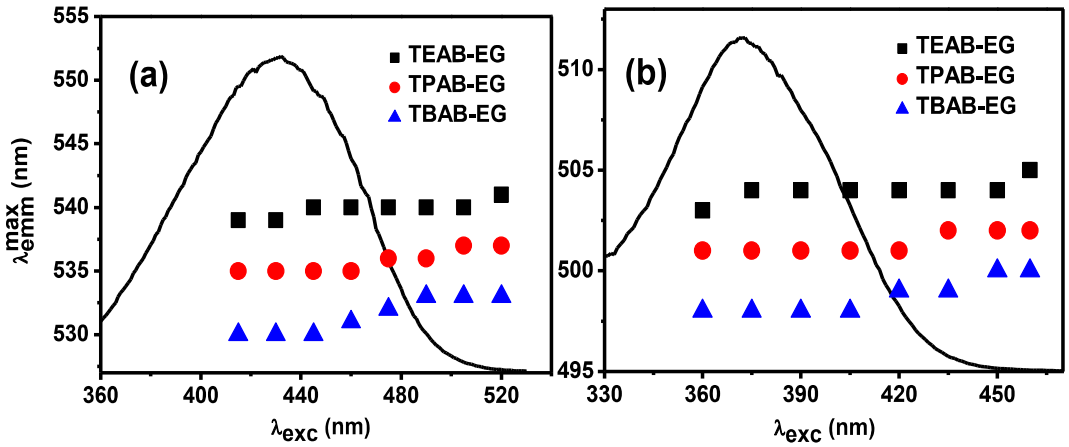

Figure A3.3. Dependence of the emission maximum (λ_{emm}^{max}) on the excitation wavelength (λ_{exc}) for C153 (a) and 4-AP (b) at 298 K in three DESs. Representative excitation spectra of the solutes are also shown.

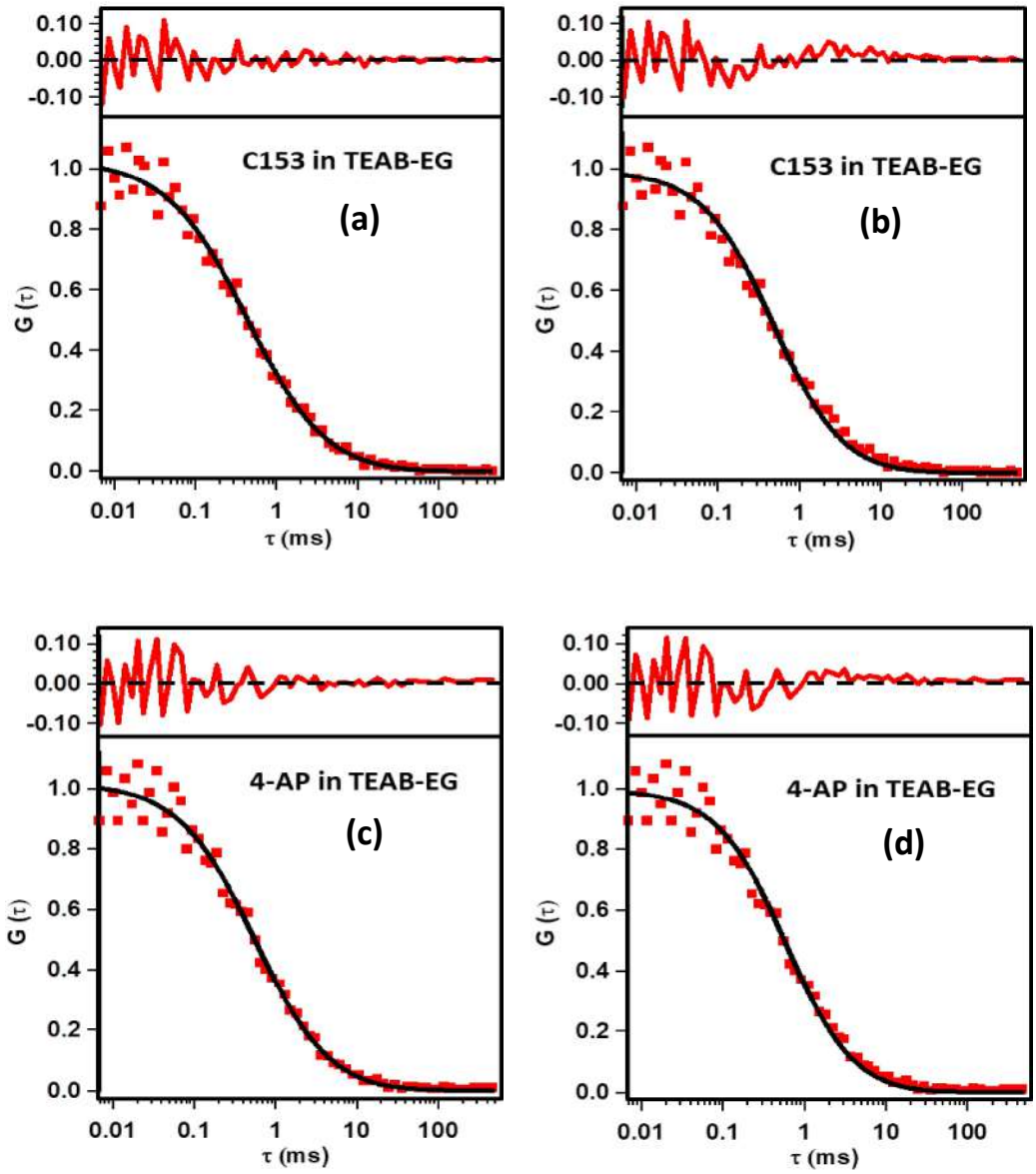

Figure A3.4. Normalized fluorescence correlation data of C153 and 4-AP in TEAB-EG. The solid lines represent fit to the data using anomalous diffusion model (left panel: a,c) and single-component diffusion model (right panel: b,d). The residuals showing the quality of the fits are also shown at the top of each panel.

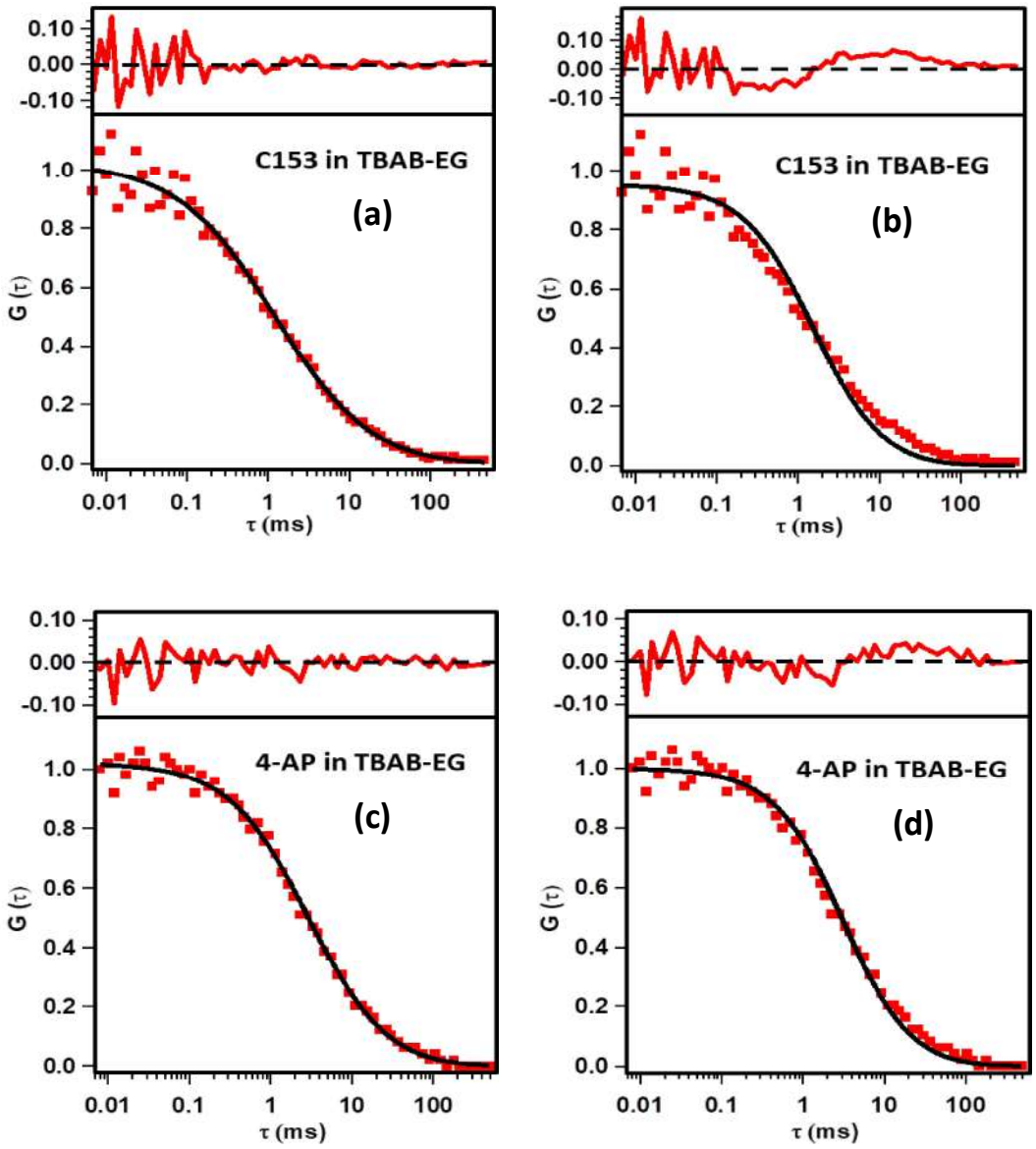

Figure A3.5. Normalized fluorescence correlation data of C153 and 4-AP in TBAB-EG. The solid lines represent fit to the data using anomalous diffusion model (left panel: a,c) and single-component diffusion model (right panel: b,d). The residuals showing the quality of the fits are also shown at the top of each panel.

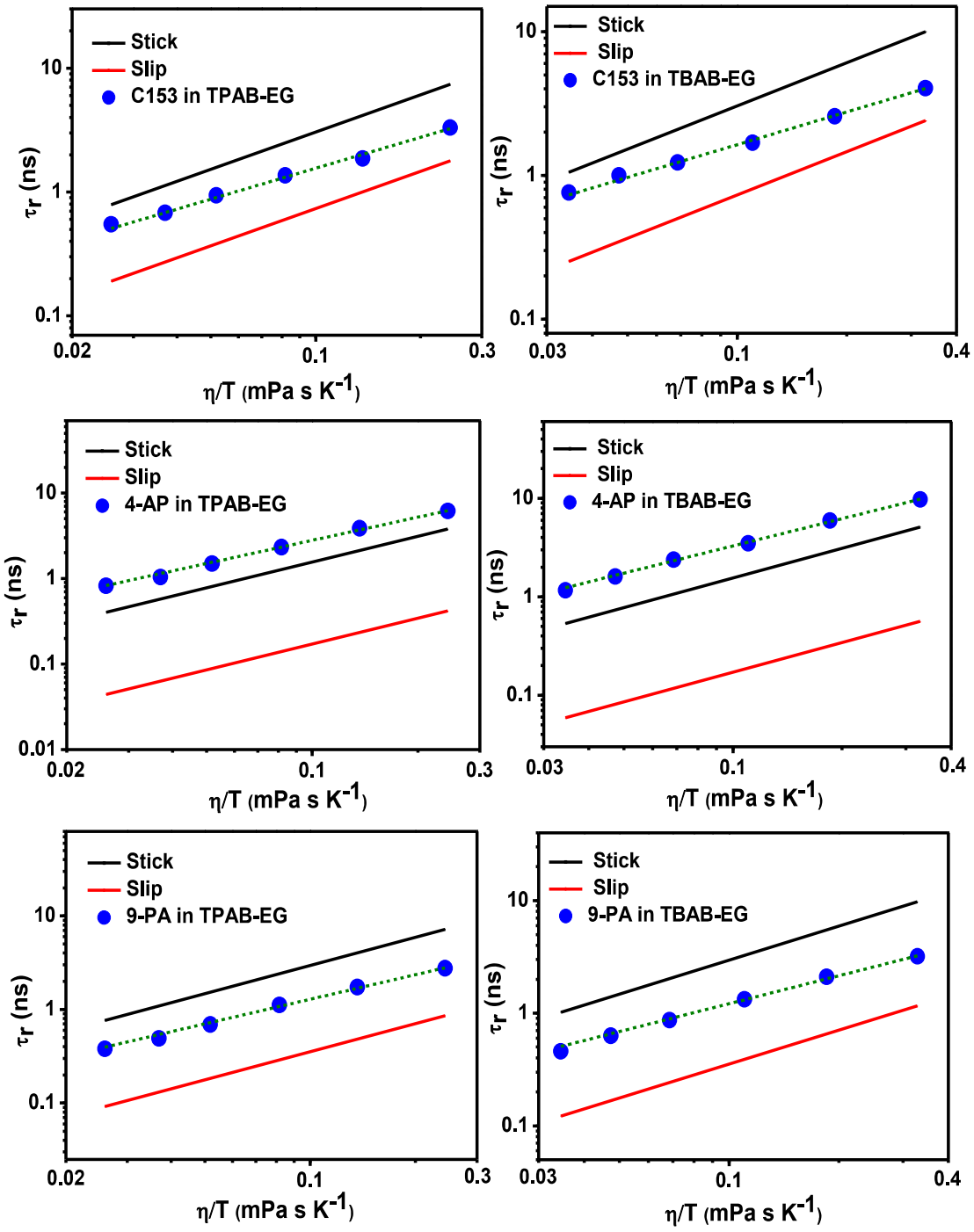

Figure A3.6. Plots of τ_r vs η/T for three solutes in TPAB-EG and TBAB-EG. The solid circles indicate the measured rotational times and the dashed lines represent fit to the data according to $\tau_r = A(\eta/T)^p$. The stick (black) and slip (red) lines, computed using SED theory, are also shown.

Table A3.1. Estimated rotational reorientation times (ns) of the solutes in three DESs at different temperatures.

DESs	Temp. (K)	Viscosity (cP)	Rotational reorientation time (ns)				
			C153			4-AP	9-PA
			τ_{r1} (a_1)	τ_{r2} (a_2)	$\langle\tau_r\rangle^{\#}$	τ_r	τ_r
TEAB-EG	298	28.0	0.16 (0.17)	1.86 (0.83)	1.57	2.10	1.27
	308	18.5	0.18 (0.18)	1.33 (0.82)	1.12	1.38	0.87
	318	13.0	0.20 (0.20)	0.94 (0.80)	0.79	1.03	0.61
	328	10.0	0.21 (0.19)	0.69 (0.81)	0.60	0.76	0.45
	338	8.0	0.11 (0.12)	0.52 (0.88)	0.47	0.58	0.33
	348	6.6	0.09 (0.14)	0.43 (0.86)	0.38	0.44	0.25
TPAB-EG	298	72.5	0.92 (0.26)	4.31 (0.74)	3.30	6.16	2.76
	308	42.0	0.17 (0.17)	2.22 (0.83)	1.87	3.87	1.74
	318	26.0	0.25 (0.24)	1.71 (0.76)	1.36	2.33	1.12
	328	17.0	0.18 (0.24)	1.18 (0.76)	0.94	1.50	0.69
	338	12.5	0.13 (0.24)	0.86 (0.76)	0.68	1.04	0.49
	348	9.0	0.09 (0.24)	0.70 (0.76)	0.55	0.82	0.38
TBAB-EG	298	98.0	0.95 (0.22)	4.92 (0.78)	4.05	9.75	3.20
	308	57.0	0.34 (0.25)	3.33 (0.75)	2.58	5.93	2.10
	318	35.0	0.23 (0.30)	2.32 (0.70)	1.69	3.49	1.33
	328	22.5	0.25 (0.31)	1.67 (0.69)	1.23	2.38	0.87
	338	16.0	0.20 (0.32)	1.36 (0.68)	1.00	1.61	0.63
	348	12.0	0.15 (0.26)	0.98 (0.74)	0.76	1.16	0.46

$^{\#}\langle\tau_r\rangle = \tau_{r1*} a_1 + \tau_{r2*} a_2$, where $a_{1+} a_2 = 1$.

Appendix 4

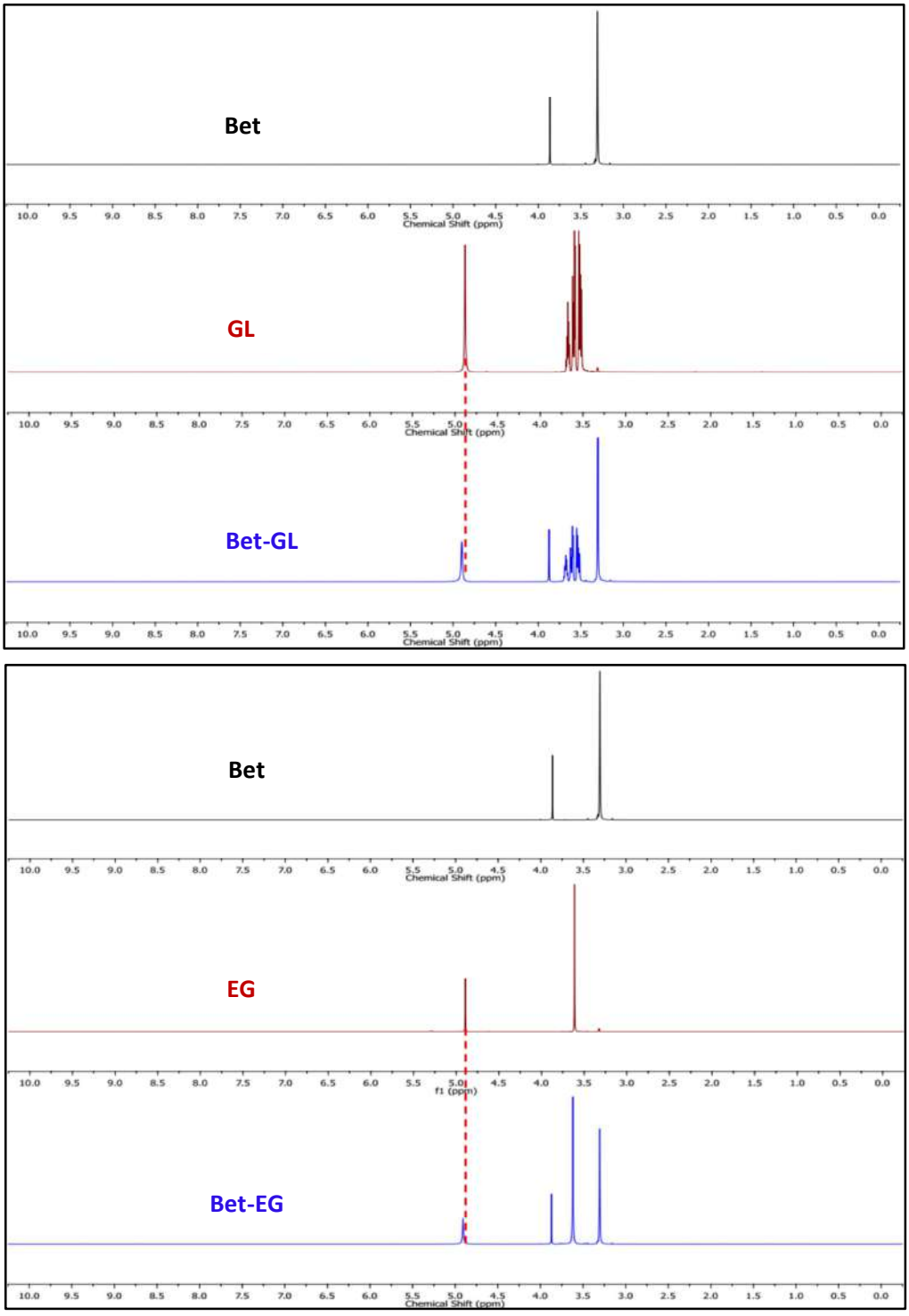

Figure A4.1. ^{1}H NMR spectra (in CD_3OD) of the prepared DESs and their constituents. The vertical dashed line in each panel is placed to monitor any shift of the OH peak following the formation of the DESs through hydrogen-bonding between the two constituents.

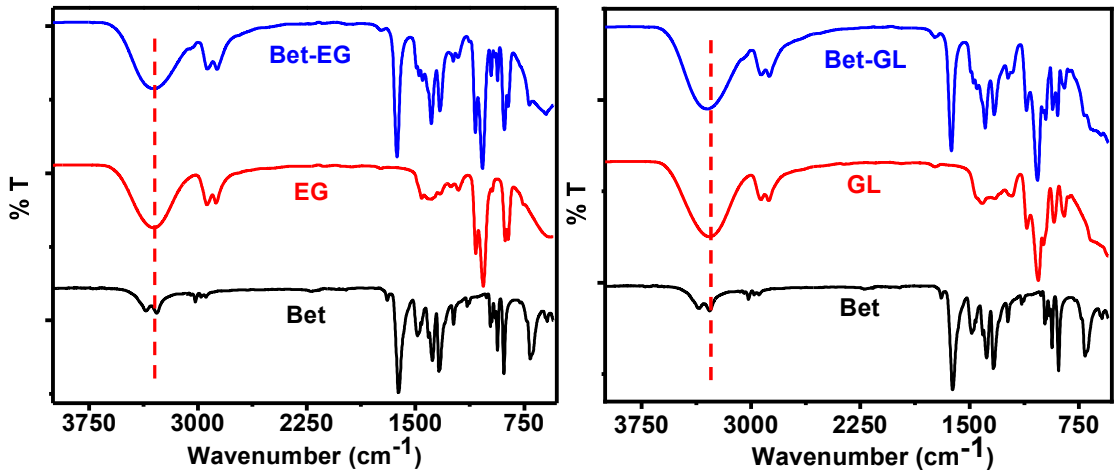

Figure A4.2. FTIR spectra of the prepared DESs and their constituents. The vertical dashed line in each panel is placed to monitor any shift of the OH peak following the formation of the DESs through hydrogen-bonding between the two constituents.

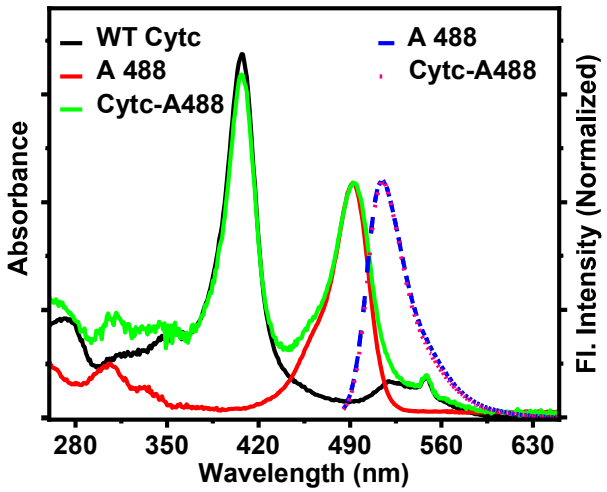

Figure A4.3. Steady-state absorption and fluorescence spectra of wild-type Cytc, A488 and Cytc-A488 in aqueous phosphate buffered solution (pH= 7).

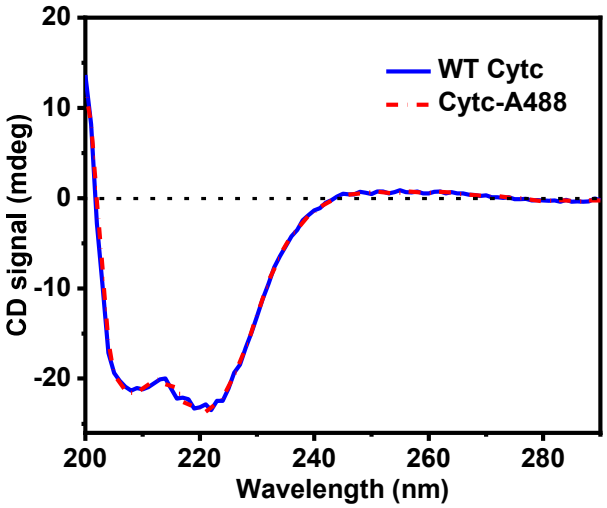

Figure A4.4. CD spectra of wild-type Cytc and Cytc-A488 in aqueous phosphate buffered solution (pH= 7).

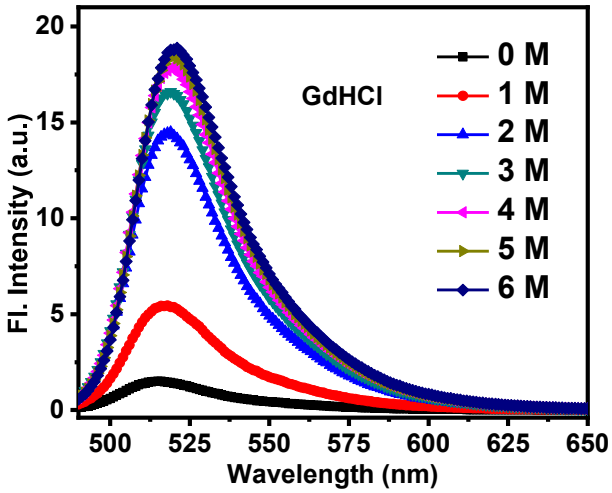

Figure A4.5. Fluorescence spectra of Cytc-A488 for different concentration of GdHCl in aqueous phosphate buffered solution (pH= 7) (λ_{exc} = 480 nm).

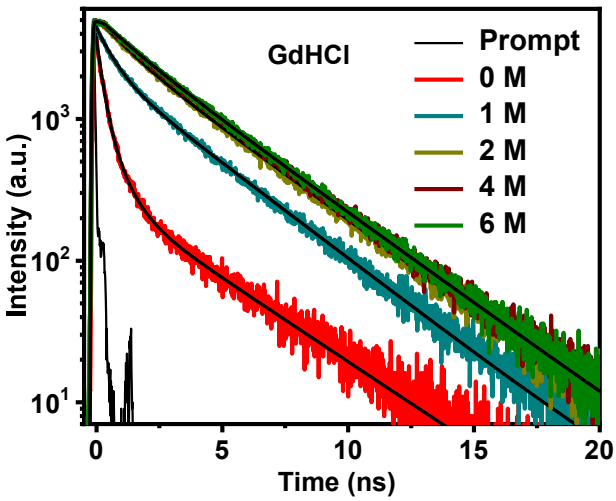

Figure A4.6. Fluorescence decay profiles of Cytc-A488 for different concentration of GdHCl in aqueous phosphate buffered solution (pH= 7) along with the fits to biexponential function (λ_{exc} = 481 nm, λ_{emm} = 515 nm).

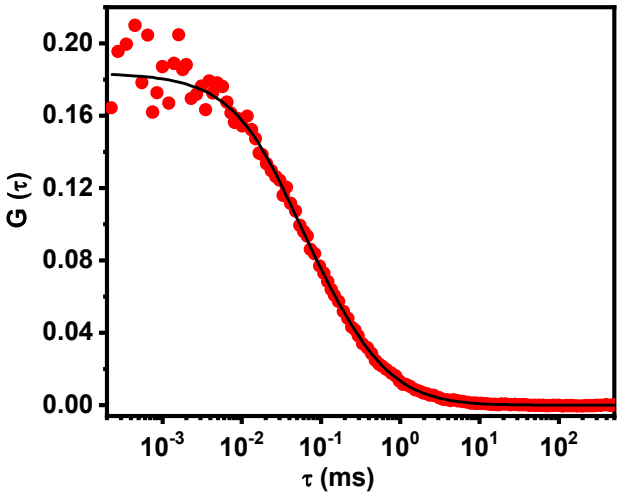

Figure A4.7. FCS data of free A488 in aqueous phosphate buffered solution (pH= 7) along with the fit to the simple single-component diffusion model (equation 2.7).

Reprints of Publications

THE JOURNAL OF PHYSICAL CHEMISTRY B

Article

Cite This: J. Phys. Chem. B 2017, 121, 10556-10565

pubs.acs.org/JPCB

Solute Rotation and Translation Dynamics in an Ionic Deep Eutectic Solvent Based on Choline Chloride

Sk Saddam Hossain and Anunay Samanta*

School of Chemistry, University of Hyderabad, Hyderabad 500 046, India

Supporting Information

ABSTRACT: Deep eutectic solvents (DESs) are an emerging class of environment-friendly media useful in a variety of applications. However, the microscopic structure of these liquids is quite unclear, and issues like whether spatial and dynamic heterogeneity is a generic feature of the ionic DESs and whether the solute molecules experience similar environment and interactions with the medium irrespective of their charge are still open. In this work, we have attempted to address some of these issues for ethaline, a less viscous and ionic DES consisting of a mixture of 1:2 mole ratio of choline chloride and ethylene glycol by monitoring the fluorescence response of a number of carefully chosen neutral and charged probe molecules in ensemble and single molecule conditions. Specifically, we have examined the liquid state structure of ethaline by studying the rotational and translational diffusion dynamics of the solutes measured by monitoring the time dependence of fluorescence anisotropy in ensemble condition and fluorescence correlation signal of extremely dilute samples diffusing through confocal volume. These studies clearly reveal dynamic heterogeneity of the medium, though no spatial heterogeneity is observable through excitation wavelength dependent fluorescence measurements. The insights obtained from this study will be helpful in understanding the nature of solute−solvent interactions in this type of complex media.

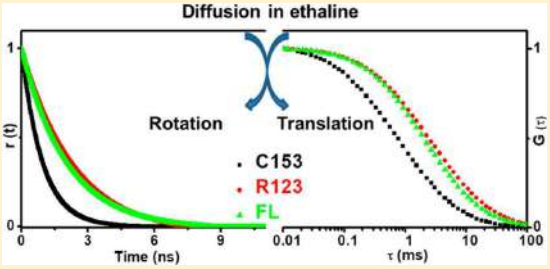

INTRODUCTION

The past two decades witnessed intense research activities on ionic liquids (ILs) in quest of environmentally benign alternatives to the conventional volatile organic compounds (VOCs), which are used as common solvents.[1−8] However, the potential of ILs in large-scale applications has not been realized as, in addition to the high cost of the raw materials, later developments have indicated considerable toxicity and poor biodegradability of these solvents.[9−11]

Deep eutectic solvents (DESs) are now widely considered as novel environmentally benign alternatives to the ILs because they not only exhibit many properties similar to the ILs but also present significant advantages over the conventional ILs, such as low toxicity, biodegradability, cheaper raw materials, and ease of preparation.[10−20] In addition, one can tune the properties of DESs over a wide range by adjusting the nature of the components as well as molar fraction of the constituents. These features of the DESs have garnered much recent attention as potential and useful media in numerous fields such as organic synthesis,[21−23] polymerizations,[20,24] biodiesel purification,[25] electrochemistry,[26,27] carbon dioxide adsorption,[28,29] nanotechnology,[30,31] and metal processing.[32−35] The DESs are systems composed of mixture of a salt/hydrogen-bond acceptor (HBA) and a hydrogen-bond donor (HBD) forming a eutectic system with a much lower melting point than either of the individual components.[12,19] Hydrogen-bonding interactions between salt/HBA and HBD are the main cause of large depression of freezing points of the mixtures.[15]

On the basis of the choice of constituents, one can obtain a large number of ionic and nonionic DESs. Ionic DESs can be formed by selecting one of the constituents as ionic,[15] whereas in nonionic DESs, both the constituents are nonionic in nature.[36] Though, in principle, a large number of DESs are possible by varying the combination of the components,[12] most extensively studied ones are those consisting of the quaternary ammonium salt, (2-hydroxyethyl)trimethylammonium chloride, commonly known as choline chloride (ChCl) and HBDs like amine, amide, alcohol, and carboxylic acid, etc. Since the first report on DES (1:2 molar mixture of ChCl and urea, commonly known as reline) by Abbott et al.,[18] several other combinations of HBDs and salts/HBAs have been explored, and many theoretical and experimental studies have been carried out on these novel media.[12,37−43] Edler and co-workers have studied the liquid structure of DES employing neutron diffraction experiment.[44] Very recently, Stefanovic et al.[45] and Kashyap and co-workers[46] have also investigated the nanostructure of some ChCl-based DESs theoretically, which reveal the nature of interactions between the constituents of DESs. Abbott and co-workers[47−50] investigated extensively diffusion

Received: August 24, 2017
Revised: October 3, 2017
Published: October 31, 2017

DOI: 10.1021/acs.jpcb.7b08472
J. Phys. Chem. B 2017, 121, 10556−10565

and dynamics in these solvents to understand the nature of intermolecular interactions in these media using ^{1}H pulsed field gradient NMR spectroscopy. Apart from these works, several fluorescence spectroscopic studies on different DESs have also been carried out.[36,51−59] Biswas and co-workers[36,51−56] have extensively studied (both theoretically and experimentally) a number of ionic and nonionic DESs to investigate the structural details of these liquids. These studies have revealed that most of the DESs are heterogeneous.[51,54−56] For example, mixtures of ChCl/urea and acetamide/electrolytes (ionic DESs) show both spatial and dynamic heterogeneity; in contrast, acetamide/urea (nonionic DES) does not show any heterogeneity. Thus, whether heterogeneity is a generic nature of all ionic DESs is unknown. Moreover, most of the fluorescence studies mentioned above have focused on probing the rotational diffusion in these media, and only neutral probe molecules have been used for this purpose. What is still lacking is the information on translational diffusion of solute molecules in these media. Fluorescence studies involving ionic solutes in DESs, which can help understanding whether different solute molecules experience similar solute−solvent interactions irrespective of their charge, are also missing. As understanding the solute−solvent interactions involving different solute molecules is key to the realization of the potential of these media as solvents, we undertake this work on a less viscous ChCl-based ionic DES, ethaline (mixture of 1:2 mole ratio of ChCl and ethylene glycol), wherein we have used several neutral and charged fluorescent probe molecules (Chart 1). Specifically, to understand the solvent environments in this medium, we have studied the excitation wavelength dependence of the steady-state fluorescence maximum of coumarin 153 (C153) and 2-amino-7-nitrofluorene (ANF) and the dynamics of rotational and translational diffusion of three carefully chosen fluorescent molecules of comparable sizes but differently charged—rhodamine 123 (R123, cationic), fluorescein (FL, anionic), and neutral C153 in ethaline—with the help of time-resolved fluorescence anisotropy and fluorescence correlation spectroscopy (FCS) measurements.

Chart 1. Chemical Structures and Abbreviations of the Constituents of Ethaline and Solute Molecules Used

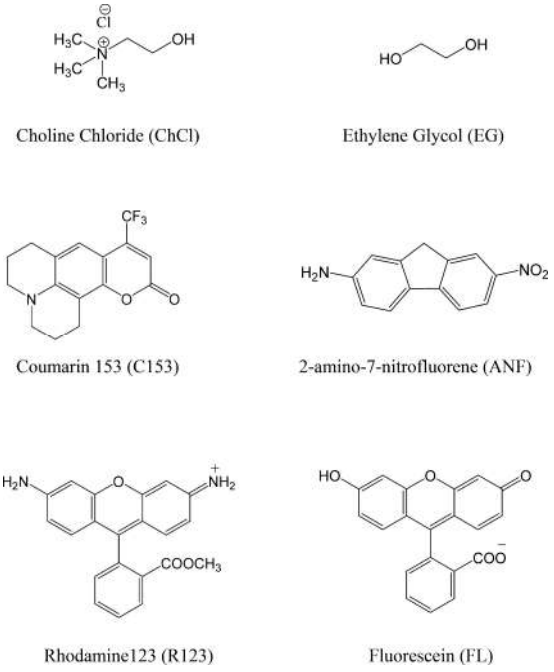

EXPERIMENTAL SECTION

Materials. Choline chloride (≥98%) and ethylene glycol (≥99%) were purchased from Sigma-Aldrich and dried under high vacuum for several hours prior to use. Laser grade C153 was obtained from Eastman Kodak. R123 and FL were obtained from Sigma-Aldrich. All three dyes were used as received. Ethanol was procured from Merck and purified by following a standard procedure before use.[60] Methanol-d_4 (CD_3OD) was purchased from Sigma-Aldrich and used as received. Milli-Q water was used in the present study.

Synthesis and Sample Preparation. Ethaline was synthesized by following a previously reported procedure[18] with slight modification of temperature. Briefly, choline chloride and ethylene glycol were mixed in 1:2 mole ratios under constant stirring and heated at 333 K until a homogeneous transparent liquid was formed. Then the liquid was allowed to cool to the room temperature. The resulting mixture was characterized through ^{1}H NMR spectra (in CD_3OD) (Figure S1 of Supporting Information) and comparison of the same with the literature data.[47] The viscosity (η) of ethaline was measured to be 42 cP at 298 K. The value is in good agreement with the previously reported value.[61]

A few microliters of a freshly prepared ethanol solution of solute was poured into a quartz cuvette of 1 cm optical path length. Ethanol was then evaporated by blowing a gentle flow of high purity nitrogen gas. Then, 2.5−3.0 mL of ethaline was added into the cuvette, which was tightly sealed with septum and parafilm, and the solution was slightly heated and stirred for some time to ensure complete dissolution of the solute. The solution was then allowed to cool slowly to the room temperature.

Instrumentation. A UV−vis spectrophotometer (Cary100, Varian) and a spectrofluorometer (FluoroLog, Horiba Jobin Yvon) were used for recording the absorption and steady-state emission spectra, respectively. Time-resolved fluorescence anisotropy decay measurements were performed using a time-correlated single-photon counting (TCSPC) fluorescence spectrometer (Horiba Jobin Yvon IBH). Diode lasers (405 and 481 nm) were used as the excitation sources, and an MCP photomultiplier (Hamamatsu R3809U-50) was used as the detector. The instrument response function (IRF) of the setup (60 and 80 ps for 405 and 481 nm excitation, respectively) was limited by the full width at half-maximum (fwhm) of the exciting laser pulse. The lamp profile was recorded by placing a scatterer (dilute solution of Ludox in water) in place of the sample. Decay curves were analyzed by nonlinear least-squares iteration procedure using IBH DAS6 (version 2.2) decay analysis software. The quality of the fits was assessed by the χ^2 values and distribution of the residuals. ^{1}H NMR spectra were recorded using a Bruker AVACE 400 MHz spectrometer. The viscosities of ethaline were measured by a LVDV-III Ultra Brookfield cone and plate viscometer (1% accuracy and 0.2% repeatability). The temperature-dependent studies were performed by using a Julabo (Model F32) water circulator.

The FCS measurements were performed on a time-resolved confocal fluorescence setup (MicroTime 200, PicoQuant),

DOI: 10.1021/acs.jpcb.7b08472
J. Phys. Chem. B 2017, 121, 10556−10565

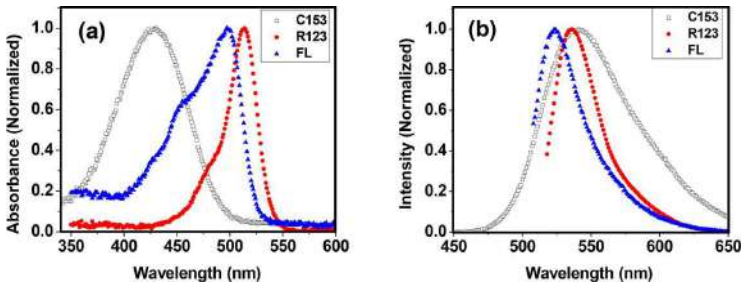

Figure 1. Normalized absorption (a) and emission (b) spectra of the solutes in ethaline at 298 K. The emission spectra are recorded by exciting the samples at their respective absorption peak.

which was equipped with an inverted microscope (Olympus IX 71) containing a water immersion objective (Olympus UPlansApo NA 1.2, 60×). Pulsed diode lasers (405 and 485 nm with fwhm 176 and 144 ps, respectively) with a stable repetition rate of 20 MHz were used as excitation sources. The laser output was coupled with the main optical unit through a polarization maintaining single-mode optical fiber, guided through a dichroic mirror, and focused onto the sample (which was placed on a coverslip) using the water immersion objective. Fluorescence from the samples was collected by the same objective and passed through the dichroic mirror, filtered by using 430 and 510 nm long-pass filters for 405 and 485 nm laser sources, respectively, to remove any exciting light. The signal was then focused onto a 50 μm diameter pinhole to remove the out-of-focus signal, recollimated, and directed onto a (50/50) beam splitter prior to entering two single-photon avalanche photodiodes (SPADs). The signals from the two SPAD detectors were cross-correlated to generate fluorescence correlation traces. The data acquisition was performed with a SymPhoTime software controlled PicoHarp300 TCSPC module in a time-tagged time-resolved (TTTR) mode. During all FCS measurements, the excitation power was kept at ~3 μW. Low excitation power was used in order to avoid any contribution of background noise from ethaline. The fluorescence intensity time traces of ethaline alone and R123 in ethaline are shown in Figure S2 (Supporting Information). All FCS experiments were carried out at room temperature (~298 K).

Method. The anisotropy measurements were performed by placing a polarizer in the excitation beam path and another one in front of the detector. The fluorescence intensity in parallel ($I_{\parallel}$) and perpendicular ($I_{\perp}$) polarization (with respect to the vertically polarized excitation laser beam) was collected alternatively for equal interval of time until the count difference between the two polarizations (at $t = 0$) was ~5000. The anisotropy measurements were performed at the respective fluorescence maxima of the probes using a monochromator with a band-pass of 2 nm. Time-resolved fluorescence anisotropy, $r(t)$, was calculated using the equation

$$r(t) = \frac{I_{\parallel}(t) - GI_{\perp}(t)}{I_{\parallel}(t) + 2GI_{\perp}(t)} \tag{1}$$

where G is the correction factor for the detector sensitivity to the polarization direction of the emission and was calculated following the same procedure as described above, but with only 5 cycles and horizontal polarization of the exciting laser beam. The anisotropy decay profiles could be reasonably well represented by a single-exponential decay from which the rotational time constants were estimated.

The translational diffusion (D) of the probe molecules was measured using the FCS technique, which is known to be an extremely sensitive and powerful technique for this purpose. In this technique, the fluctuations of fluorescence intensity of a highly dilute solution (~nM) were measured in a small detection volume (~1 fL) by using a pinhole and focused laser beam. These fluctuating fluorescence signals detected by two SPAD detectors were cross-correlated to generate the correlation curves $G(\tau)$. The decay of correlation function with respect to time was used for obtaining the dynamical information on translational diffusion. Data analysis of the individual correlation curves was performed by using the SymPhoTime software of PicoQuant. The correlation function $G(\tau)$ of the fluorescence intensity is given by[62]

$$G(\tau) = \frac{\langle \delta F(t)\delta F(t+\tau)\rangle}{\langle F(t)\rangle^2} \tag{2}$$

where $\langle F(t)\rangle$ is the average fluorescence intensity and $\delta F(t)$ and $\delta F(t+\tau)$ are the fluctuation in intensity around the mean value at time t and $(t + \tau)$, respectively, and are given by

$$\delta F(t) = F(t) - \langle F(t)\rangle$$
$$\delta F(t+\tau) = F(t+\tau) - \langle F(t)\rangle \tag{3}$$

The correlation data were fitted to both single-component diffusion ($\beta = 1$) and anomalous diffusion ($\beta < 1$) using the equation

$$G(\tau) = \frac{1}{N}\left[1 + \left(\frac{\tau}{\tau_D}\right)^{\beta}\right]^{-1}\left[1 + \left(\frac{r_0}{z_0}\right)^2\left(\frac{\tau}{\tau_D}\right)^{\beta}\right]^{-1/2} \tag{4}$$

However, as can be seen later, the anomalous diffusion model, which considers the mean-square displacement (MSD) of solute molecules to follow a power law,[63] $\langle r(\tau)^2\rangle \propto \tau^{\beta}$, fits our data much better compared to the simple single-component diffusion. In this equation, N is the average number of fluorescent molecules in the observation volume, τ_D is the time taken for the molecule to diffuse through this volume, τ is the delay or lag time, and β ($0 < \beta < 1$) is the stretching exponent representing the distribution of τ_D. k indicates the structure parameter of the observation volume and defined as $k = z_0/r_0$, where r_0 and z_0 are the transverse and longitudinal radii of the observation volume, respectively. Rhodamine 6G (R6G) was used for calibration of the excitation volume (diffusion coefficient of 426 μm^2 s^{-1} in water).[64] The estimated excitation

DOI: 10.1021/acs.jpcb.7b08472
J. Phys. Chem. B 2017, 121, 10556−10565

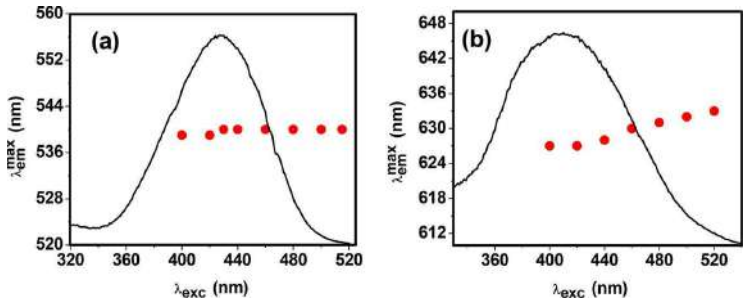

Figure 2. Dependence of the emission maximum (λ_{max}^{em}) on the excitation wavelength (λ_{exc}) for C153 (a) and ANF (b) at 298 K in ethaline. Red spheres represents the λ_{max}^{em} values for different λ_{exc}. The excitation spectra of the individual solutes are also shown.

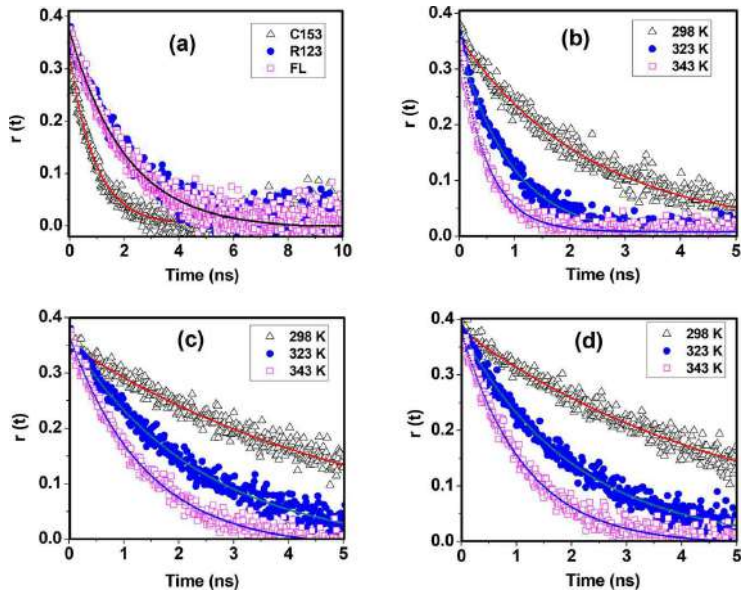

Figure 3. (a) Anisotropy decay profiles of the three solutes in ethaline at 323 K. Panels (b), (c), and (d) show the effect of temperature on the anisotropy decay profiles of C153, R123, and FL, respectively. The solid lines represent single-exponential fit to the experimental anisotropy data [$r(t) = r_0 \exp(-t/\tau_r)$]. The excitation and monitoring wavelengths for C153 are 405 and 540 nm, respectively, while for R123 and FL, the excitation wavelength is 481 nm and monitoring wavelengths are 535 and 524 nm, respectively.

volumes were ~0.4 and ~0.8 fL for 405 and 485 nm laser sources, respectively. The diffusion coefficient (D) was calculated by using

$$D = \frac{r_0^2}{4\tau_D} \quad (5)$$

RESULTS AND DISCUSSION

Steady-State Measurement. The steady-state absorption and emission spectra of C153, R123, and FL in ethaline at room temperature (298 K) are shown in Figure 1. The absorption maxima of C153, R123, and FL appear at 428, 513, and 497 nm, respectively and the corresponding emission maxima (λ_{max}^{em}) appear at 540, 535, and 524 nm. The large Stokes shift of C153 is consistent with its environment-sensitive fluorescence properties.[65] One can obtain an idea about the polarity of the microenvironment around C153 by comparing the measured λ_{max}^{em} values in ethaline and in other conventional solvents of known polarities. This comparison indicates that C153 experiences methanol-like environment in ethaline.

As the DESs are viscous media like the ILs, the dynamics of solvation in these media is much slower than that in conventional solvents like acetonitrile, water, or ethanol. Consequently, in these media, it is possible to observe emission, which does not originate from the fully solvent-equilibrated state of the solute molecule. If the microenvironments around the fluorescent molecules are not identical, then under this condition one observes an excitation wavelength-dependent shift of the fluorescence maximum of dipolar molecules reflecting the microheterogeneity of the medium.[66−70] As C153 has been used earlier for probing the heterogeneity in other DESs,[53,54] we have examined its dependence of λ_{max}^{em} on the excitation wavelength, λ_{exc}. However, unlike in other cases,[53,54] this dependence is found to be insignificant (Figure 2a). As fluorescence lifetime (τ_f) of a molecule is an important factor in determining whether it will

DOI: 10.1021/acs.jpcb.7b08472
J. Phys. Chem. B 2017, 121, 10556−10565

emit from an unrelaxed or fully equilibrated state and that molecules with shorter τ_f are more likely to exhibit excitation wavelength-dependent fluorescence behavior,[69] we have also examined the excitation wavelength dependence of λ_{max}^{em} of 2-amino-7-nitrofluorene (ANF), whose τ_f (τ_f < 50 ps in 2-propanol[71]) is much shorter than that of C153 (τ_f = 4.7 ns in ethanol). However, ANF also presents a very similar picture (Figure 2b) and does not indicate any spatial heterogeneity of the medium. This observation is interesting as Biswas and co-workers observed significant excitation wavelength dependence of C153 and *trans*-2-[4-(dimethylamino)styryl]benzothiazole (DMASBT) in other ionic DESs such as (CH_3CONH_2 + $LiNO_3$/Br/ClO_4) mixtures[53] and reline (ChCl + urea),[54] indicating their spatial heterogeneity. It is thus evident that spatial heterogeneity is not a generic feature of all ionic DESs; rather, it depends on the constituents of the DESs and interactions between them.

Time-Resolved Fluorescence Anisotropy Measurement. The rotational dynamics of a molecular system is determined by the friction experienced by it in a medium, and hence, it can provide valuable information on the microenvironments around the probe including solute−solvent interactions. To investigate the rotational motion, we studied time-resolved fluorescence anisotropy of C153, R123, and FL over a temperature range of 298−343 K. Representative anisotropy decay profiles of three solutes in ethaline at different temperatures are displayed in Figure 3. It is evident that at any given temperature (for example, 323 K, Figure 3a), anisotropy decay of the neutral solute, C153, is significantly faster compared to the ionic solutes R123 and FL (both show similar decay profiles). As the sizes of the solute molecules are comparable (vide later), the observation indicates that the ionic solutes experience more friction in ethaline compared to the neutral one.

It is also seen that the anisotropy decay becomes faster for all three solutes at higher temperature due to lowering of viscosity of the medium. The rotational reorientation times (τ_r) of the solutes, estimated from single-exponential fit to the experimental data, are shown in Table 1 along with the measured

Table 1. Estimated Rotational Reorientation Times (ns) of the Solutes in Ethaline at Different Temperatures

		rotational reorientation time (ns)		
temp (K)	viscosity (cP)	C153	R123	FL
298	42	2.25	5.62	5.10
313	23	1.28	3.40	2.78
323	16	0.93	2.38	2.08
333	12	0.70	1.79	1.49
343	08	0.51	1.39	1.15

viscosities of ethaline at different temperatures. The viscosity of the medium is found to follow the Vogel−Fulcher−Tamman (VFT) equation[61]

$$\eta = \eta_0 \exp\left(\frac{B}{T - T_0}\right) \tag{6}$$

where η is the viscosity at absolute temperature T, η_0 is the viscosity at infinite temperature, B is the fragility parameter, and T_0 is a characteristic temperature for which η diverges. Figure S3 shows the temperature dependence of the viscosity.

Careful inspection of the data collected in Table 1 reveals that at any given temperature the τ_r values of R123 and FL are higher than that of C153 by a factor of >2. As the sizes of three solutes are similar, the higher τ_r values for R123 and FL indicate their association with the solvent through electrostatic or hydrogen-bonding interaction.

We have analyzed the experimental results using Stokes−Einstein−Debye (SED) hydrodynamic theory,[72,73] which considers the solvent as a structureless continuum and according to which the rotational reorientation time (τ_r) of a solute in a solvent is given by

$$\tau_r = \frac{\eta V f C}{k_B T} \tag{7}$$

where V, f, and C are the van der Waals volume, shape factor, and boundary condition parameter of the solutes, respectively. η, k_B, and T are the solvent viscosity, Boltzmann constant, and absolute temperature of the system, respectively. The shape factor (f), which describes nonspherical nature of the solute, is a function of axial ratio of the semiaxes. C indicates the degree of solute−solvent coupling, which in two limiting cases are stick (C_{stick} = 1) and slip (0 < C_{slip} < 1). The axial radii, van der Waals volumes, boundary conditions, and shape factors for the probe molecules C153, FL, and R123 are collected in Table 2.

Table 2. Solute Dimension, van der Waals Volume, Shape Factor, and Boundary Condition Parameters Calculated from the SED Hydrodynamic Theory

solute	axial radii (Å^3)	van der Waals volume, V (Å^3)	shape factors (f)	C_{slip}
C153[a]	6.1 × 4.8 × 2.2	246	1.71	0.240
R123	7.0 × 5.5 × 1.8	289[c]	2.10[c]	0.155[c]
FL[b]	6.4 × 5.5 × 1.8	267	1.93	0.139

[a]Values are taken from ref 71. [b]Values are taken from ref 72. [c]Values are calculated using refs 70, 73, and 74.

While these parameters for C153 and FL were obtained from the literature,[74,75] for R123, the V value was calculated using Edward's volume increment method[76] and the shape factor and boundary conditions were calculated following reported procedure.[73,77] Briefly, the friction coefficients (ξ) for the stick and slip boundary conditions were obtained along three principal axes of rotation, treating each solute as an asymmetric ellipsoid.[78] The diffusion coefficients (D_i) were then computed along three axes using the Einstein relation[79]

$$D_i = \frac{k_B T}{\xi_i} \tag{8}$$

The rotational reorientation times (τ_r) were calculated from the D_i values along the *a*-, *b*-, and *c*-axis (assuming the transition dipole along the long axis of the solute) using the equation[80]

$$\tau_r = \frac{1}{12}\left(\frac{4D_a + D_b + D_c}{D_aD_b + D_bD_c + D_cD_a}\right) \tag{9}$$

The parameters f and C_{slip} were then estimated from the calculated τ_r value for stick and slip boundary conditions using eq 7.

The τ_r values are plotted against η/T for all three solutes, indicating the slip and stick lines in Figure 4. Table S1 (Supporting Information) summarizes the predicted slip and stick rotation times. Figure 4 shows that the rotational times of

DOI: 10.1021/acs.jpcb.7b08472
J. Phys. Chem. B 2017, 121, 10556−10565

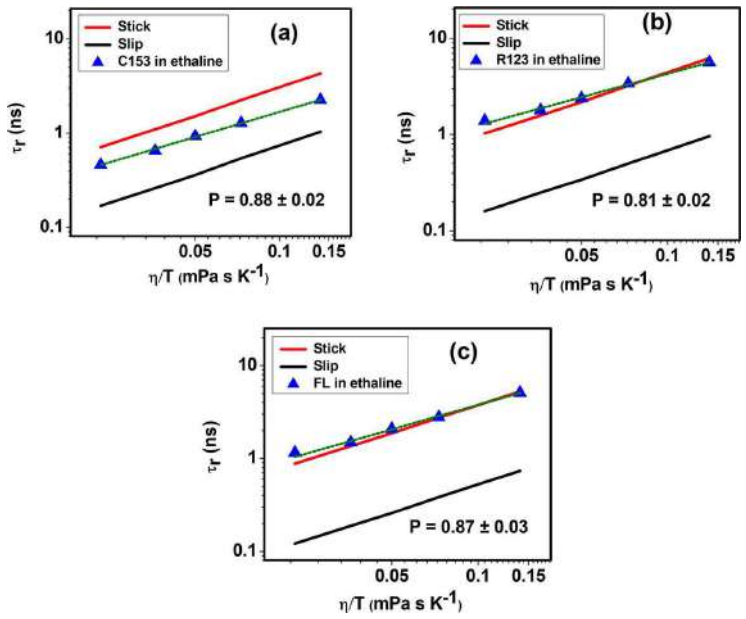

Figure 4. Plots of τ_r vs η/T for C153 (a), R123 (b), and FL(c) in ethaline. The solid triangles indicate the experimentally measured rotational times, and the dashed lines represent fit to the data according to $\tau_r = A(\eta/T)^P$. The P values obtained from the fits are shown in the figure. The stick (red) and slip (black) lines computed using SED theory are also shown.

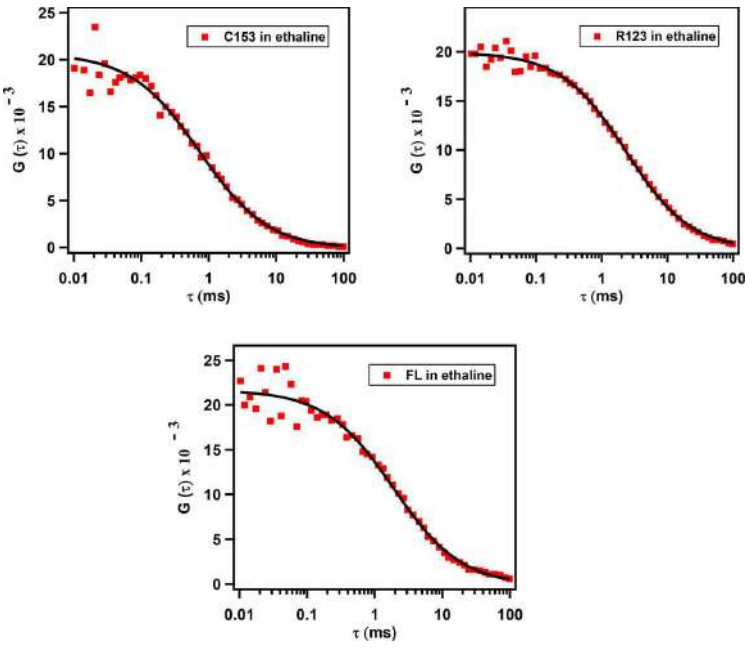

Figure 5. Fluorescence correlation curves for the diffusion of the solutes in ethaline. The points are the experimental data, and the solid lines represent best fit to the data using an anomalous diffusion model. The excitation wavelengths are 405 nm for C153 and 485 nm for R123 and FL.

neutral solute C153 lie between the slip and stick lines, whereas for positively charged R123 and negatively charged FL, the rotational behavior is very similar and the dynamics follows stick predictions of the SED theory, indicating strong association of these solutes with the solvent.[77] As these solutes are charged, this association is likely to be due to electrostatic interaction between the positively charged R123 and the chloride anion of the ethaline and between negatively charged FL and choline cation of ethaline. However, as hydrogen-bonding interaction of R110 (which is very similar to R123)

DOI: 10.1021/acs.jpcb.7b08472
J. Phys. Chem. B 2017, 121, 10556−10565

and FL is known to be the major reason for their stick behavior in ILs,[81] it is most likely that the stick behavior in ethaline is primarily due to the hydrogen-bonding interaction between R123 (or FL) and constituents of ethaline as both ChCl and ethylene glycol possess hydrogen-bond-forming functionalities.

A fit of the experimental data to $\tau_r = A(\eta/T)^P$ (dashed lines in Figure 4) shows significant nonlinearity, which is evident from the departure of the P value from unity, highlighting the deviation of τ_r from the SED hydrodynamic theory.

$$\tau_r = (13.38 \pm 0.66)(\eta/T)^{0.88\pm0.02} \quad (N = 5, R = 0.999) \text{ for C153}$$

$$\tau_r = (27.70 \pm 1.59)(\eta/T)^{0.81\pm0.02} \quad (N = 5, R = 0.998) \text{ for R123}$$

$$\tau_r = (28.45 \pm 1.87)(\eta/T)^{0.87\pm0.03} \quad (N = 5, R = 0.996) \text{ for FL}$$

The P values obtained from the fits lie between 0.81 and 0.88, indicating viscosity−diffusion decoupling in ethaline. As this P value is very close to 1 for common organic solvents, which are homogeneous in nature, this fractional viscosity dependence of rotational diffusion time (i.e., a breakdown of hydrodynamic behavior) is due to the dynamic heterogeneity of the medium, as found in recent studies.[53,54] This dynamic heterogeneity is shown to be the result of hydrogen-bond fluctuation and consequent motion of particles, which is very different from hydrodynamic diffusion[47] such as orientational jumps, and it can cause viscosity−diffusion decoupling.[82,83] We thus conclude that fluctuation of hydrogen-bond network in ethaline due to such orientational jumps contribute to this kind of observation. That dynamic heterogeneity of a medium does not require the presence of spatially distributed microenvironments (spatial heterogeneity) and is well documented for other systems.[84]

FCS Measurement. To further understand the nature of the medium, we have studied the translational diffusion of the molecules in single molecule condition using the FCS technique. To the best of our knowledge, no measurement based on FCS technique has been made so far to study the translational motion of a solute molecule in these media. Figure 5 shows the time dependence of fluorescence correlation of the three systems in ethaline. The data were analyzed using both single-component diffusion and the anomalous diffusion model (eq 4). However, the anomalous diffusion model, which considers stretching exponent, β (a parameter that quantifies the degree of deviation from normal diffusion), to describe the decay of fluorescence correlation, fits the data much better compared to the single-component diffusion model (as decided by the residuals and χ^2 values) for all three systems. This point is illustrated through single-component fits to the data and fit residuals using both models in Figures S4 and S5 (Supporting Information). In addition to these two models, one could have also fitted the data to two-component (bimodal) diffusion model, which considers diffusion of solutes in different subpopulations (spatially distributed microenvironments). However, as we could not observe such microenvironments through excitation wavelength dependence measurements, we did not fit the data to two-component diffusion model.

The diffusion coefficients of three solutes estimated from these fits are collected in Table 3 along with the β values. The latter, which lies between 0.84 and 0.86, indicates a distribution of translational diffusion time (τ_D) and suggests that the dynamics of translational diffusion of chosen molecules are diverse in nature. As these solute molecules exhibit single-component translational diffusion ($\beta = 1$) in conventional homogeneous solvents, the anomalous diffusion of solutes in ethaline can be attributed to the dynamic heterogeneity, which describes that the mean-square displacement (MSD) of solute molecules follows a subdiffusive behavior, $\langle r(\tau)^2 \rangle \propto \tau^\beta$ ($\beta < 1$), instead of the normal Brownian diffusion ($\beta = 1$). In this context, we note the recent observation of anomalous diffusion of Nile Red in ILs and its interpretation in terms of dynamic heterogeneity in ILs.[63]

Table 3. FCS Fittings Parameters Using the Anomalous Diffusion Model

solute	D (μm^2 s^{-1})	β
C153	17.8	0.84
R123	8.9	0.86
FL	10.9	0.86

Further, Table 3 shows that the observed diffusion coefficients (D) of the ionic solutes are significantly smaller than that of the neutral solute. It is evident that the translational diffusion of C153 is faster by a factor of almost 2 as compared to R123. These observations can be explained considering stronger association of the ionic solutes with ethaline due to electrostatic and hydrogen-bonding interactions between the ionic solutes and the constituents of ethaline. These findings are in good agreement with the results obtained in ensemble condition using time-resolved fluorescence anisotropy measurements. Thus, both translational and rotational motions of charged solutes in ethaline are significantly different than those of neutral one, and the formers are experiencing stronger solute−solvent interactions in this ionic medium.

CONCLUSION

The translational and rotational diffusion dynamics of the molecular systems reveal dynamic heterogeneity in ethaline though no static heterogeneity of the medium could be detected. Specifically, the dynamic heterogeneity in the medium is established from the departure of the reorientation times of the solutes from their hydrodynamic behavior and anomalous translational diffusion observed for solutes in FCS measurements. Furthermore, both translational and rotational diffusion dynamics show the charged solutes to experience stronger solute−solvent interactions in ethaline as a consequence of mutual effect of the electrostatic and hydrogen-bonding interactions between solutes and constituents of ethaline. The present findings are likely to be helpful toward the development and applications of this class of novel solvents.

ASSOCIATED CONTENT

Supporting Information

The Supporting Information is available free of charge on the ACS Publications website at DOI: 10.1021/acs.jpcb.7b08472.

^{1}H NMR spectra of ChCl, EG, and ethaline; fluorescence intensity time traces of ethaline alone and R123 in ethaline; temperature dependence of the viscosity of ethaline; correlation curves for the diffusion of C153, R123, and FL in ethaline along with the fits to single-component diffusion model; residuals of the fits to the correlation curves for single-component and anomalous diffusion model; calculated reorientation times of the three solutes for slip and stick boundary conditions at different temperatures using SED theory (PDF)

DOI: 10.1021/acs.jpcb.7b08472
J. Phys. Chem. B 2017, 121, 10556−10565

AUTHOR INFORMATION

Corresponding Author

*E-mail: anunay@uohyd.ac.in (A.S.).

ORCID

Sk Saddam Hossain: 0000-0002-5740-3703

Anunay Samanta: 0000-0003-1551-0209

Notes

The authors declare no competing financial interest.

ACKNOWLEDGMENTS

This work is supported by Grant EMR/2015/000582 and J. C. Bose Fellowship (to A.S.) of the Science and Engineering Research Board (SERB), Department of Science and Technology (DST), India. We also acknowledge the UGC-UPE and DST-PURSE support to our University. S.S.H. thanks UGC for a Fellowship.

REFERENCES

(1) Rogers, R. D.; R, S. K. Ionic Liquids—Solvents of the Future? *Science* **2003**, *302*, 792—793.

(2) Seddon, K. R. Ionic Liquids: A Taste of the Future. *Nat. Mater.* **2003**, *2*, 363—365.

(3) Welton, T. Room-Temperature Ionic Liquids-Solvents for Synthesis and Catalysis. *Chem. Rev.* **1999**, *99*, 2071—2083.

(4) Dupont, J. From Molten Salts to Ionic Liquids: A "Nano" Journey. *Acc. Chem. Res.* **2011**, *44*, 1223—1231.

(5) The Physical Chemistry of Ionic Liquids (Special issue on ionic liquids). *J. Phys. Chem. B* **2007**, *111*, 4639—5029.

(6) The Physical Chemistry of Ionic Liquids (Special issue on ionic liquids). *Phys. Chem. Chem. Phys.* **2010**, *12*, 1629—2032.

(7) Huddleston, J. G.; Willauer, H. D.; Swatloski, R. P.; Visser, A. E.; Rogers, R. D. Room Temperature Ionic Liquids As Novel Media for Clean Liquid—Liquid Extraction. *Chem. Commun.* **1998**, 1765—1766.

(8) Plechkova, N. V.; Seddon, K. R. Applications of Ionic Liquids in the Chemical Industry. *Chem. Soc. Rev.* **2008**, *37*, 123—150.

(9) Kareem, M. A.; Mjalli, F. S.; Hashim, M. A.; Al Nashef, I. M. Phosphonium-Based Ionic Liquids Analogues and Their Physical Properties. *J. Chem. Eng. Data* **2010**, *55*, 4632—4637.

(10) Romero, A.; Santos, A.; Tojo, J.; Rodríguez, A. Toxicity and Biodegradability of Imidazolium Ionic Liquids. *J. Hazard. Mater.* **2008**, *151*, 268—273.

(11) Wells, A. S.; Coombe, V. T. On the Freshwater Ecotoxicity and Biodegradation Properties of Some Common Ionic Liquids. *Org. Process Res. Dev.* **2006**, *10*, 794—798.

(12) Zhang, Q.; De Oliveira Vigier, K.; Royer, S.; Jé rôme, F. Deep Eutectic Solvents: Synthesis, Properties and Applications. *Chem. Soc. Rev.* **2012**, *41*, 7108—7146.

(13) Abbott, A. P.; Boothby, D.; Capper, G.; Davies, D. L.; Rasheed, R. K. Deep Eutectic Solvents Formed Between Choline Chloride and Carboxylic Acids: Versatile Alternatives to Ionic Liquids. *J. Am. Chem. Soc.* **2004**, *126*, 9142—9147.

(14) Abbott, A. P.; Davies, D. L.; Capper, G.; Rasheed, R. K.; Tambyrajah, V. Ionic Liquids and Their Use As Colvents U.S. Patent 7, **2007**, *183*, 433.

(15) Francisco, M.; van den Bruinhorst, A.; Kroon, M. C. LowTransition-Temperature Mixtures (LTTMs): A New Generation of Designer Solvents. *Angew. Chem., Int. Ed.* **2013**, *52*, 3074—3085.

(16) Dai, Y.; van Spronsen, J.; Witkamp, G. J.; Verpoorte, R.; Choi, Y. H. Natural Deep Eutectic Solvents as New Potential Media for Green Technology. *Anal. Chim. Acta* **2013**, *766*, 61—68.

(17) Paiva, A.; Craveiro, R.; Aroso, I.; Martins, M.; Reis, R. L.; Duarte, A. R. C. Natural Deep Eutectic Solvents-Solvents for the 21st Century. *ACS Sustainable Chem. Eng.* **2014**, *2*, 1063—1071.

(18) Abbott, A. P.; Capper, G.; Davies, D. L.; Rasheed, R. K.; Tambyrajah, V. Novel Solvent Properties of Choline Chloride/Urea Mixtures. *Chem. Commun.* **2003**, *1*, 70—71.

(19) Smith, E. L.; Abbott, A. P.; Ryder, K. S. Deep Eutectic Solvents (DESs) and Their Applications. *Chem. Rev.* **2014**, *114*, 11060—11082.

(20) Liao, J.-H.; Wu, P.-C.; Bai, Y.-H. Eutectic Mixture of Choline Chloride/Urea as a Green Solvent in Synthesis of a Coordination Polymer: [Zn(O3PCH2CO$_2$)]NH 4. *Inorg. Chem. Commun.* **2005**, *8*, 390—392.

(21) Ruβ, C.; Konig, B. Low Melting Mixtures in Organic Synthesis -An Alternative to Ionic Liquids? *Green Chem.* **2012**, *14*, 2969—2982.

(22) Ghosh, S. K.; Nagarajan, R. Deep Eutectic Solvent Mediated Synthesis of Quinazolinones and Dihydroquinazolinones: Synthesis of Natural Products and Drugs. *RSC Adv.* **2016**, *6*, 27378.

(23) Alonso, D. A.; Baeza, A.; Chinchilla, R.; Guillena, G.; Pastor, I. M.; Ramón, D. J. Deep Eutectic Solvents: The Organic Reaction Medium of the Century. *Eur. J. Org. Chem.* **2016**, *2016*, 612—632.

(24) Carriazo, D.; Serrano, M. C.; Gutiérrez, M. C.; Ferrer, M. L.; del Monte, F. Deep-Eutectic Solvents Playing Multiple Roles in the Synthesis of Polymers and Related Materials. *Chem. Soc. Rev.* **2012**, *41*, 4996—5014.

(25) Shahbaz, K.; Mjalli, F. S.; Hashim, M. A.; AlNashef, I. M. Using Deep Eutectic Solvents Based on Methyl Triphenyl Phosphunium Bromide for the Removal of Glycerol from Palm-Oil-Based Biodiesel. *Energy Fuels* **2011**, *25*, 2671—2678.

(26) Nkuku, C. A.; LeSuer, R. J. Electrochemistry in Deep Eutectic Solvents. *J. Phys. Chem. B* **2007**, *111*, 13271—13277.

(27) Jhong, H.-R.; Wong, D. S.-H.; Wan, C.-C.; Wang, Y.-Y.; Wei, T.-C. A Novel Deep Eutectic Solvent-Based Ionic Liquid Used As Electrolyte for Dye-Sensitized Solar Cells. *Electrochem. Commun.* **2009**, *11*, 209—211.

(28) Leron, R. B.; Li, M.-H. Solubility of Carbon Dioxide in a Choline Chloride—Ethylene Glycol Based Deep Eutectic Solvent. *Thermochim. Acta* **2013**, *551*, 14—19.

(29) Leron, R. B.; Li, M.-H. Solubility of Carbon Dioxide in a Eutectic Mixture of Choline Chloride and Glycerol at Moderate Pressures. *J. Chem. Thermodyn.* **2013**, *57*, 131—136.

(30) Wagle, D. V.; Zhao, H.; Baker, G. A. Deep Eutectic Solvents: Sustainable Media for Nanoscale and Functional Materials. *Acc. Chem. Res.* **2014**, *47*, 2299—2308.

(31) Liao, H.-G.; Jiang, Y.-X.; Zhou, Z.-Y.; Chen, S.-P.; Sun, S.-G. Shape-Controlled Synthesis of Gold Nanoparticles in Deep Eutectic Solvents for Studies of Structure—Functionality Relations in Electrocatalysis. *Angew. Chem.* **2008**, *120*, 9240—9243.

(32) Abbott, A. P.; McKenzie, K. J. Application of Ionic Liquids to the Electrodepsoition of Metals. *Phys. Chem. Chem. Phys.* **2006**, *8*, 4265—4279.

(33) Abbott, A. P.; Capper, G.; McKenzie, K. J.; Ryder, K. S. Voltammetric and Impedance Studies of the Electropolishing of Type 316 Stainless Steel in a Choline Chloride Based Ionic Liquid. *Electrochim. Acta* **2006**, *51*, 4420—4425.

(34) Abbott, A. P.; Capper, G.; Davies, D. L.; Rasheed, R. K.; Shikotra, P. Selective Extraction of Metals from Mixed Oxide Matrixes Using Choline-Based Ionic Liquids. *Inorg. Chem.* **2005**, *44*, 6497—6499.

(35) Abbott, A. P.; Capper, G.; Glidle, A.; Ryder, K. S. Electropolishing of Stainless Steels in a Choline Chloride Based Ionic Liquid: An Electrochemical Study With Surface Characterisation Using SEM and Atomic Force Microscopy. *Phys. Chem. Chem. Phys.* **2006**, *8*, 4214—4221.

(36) Das, A.; Das, S.; Biswas, R. Density Relaxation and Particle Motion Characteristics in a Non-Ionic Deep Eutectic Solvent (Acetamide + Urea): Time-resolved Fluorescence Measurements and All-atom Molecular Dynamics Simulations. *J. Chem. Phys.* **2015**, *142*, 034505.

(37) García, G.; Aparicio, S.; Ullah, R.; Atilhan, M. Deep Eutectic Solvents: Physicochemical Properties and Gas Separation Applications. *Energy Fuels* **2015**, *29*, 2616—2644.

(38) Yusof, R.; Abdulmalek, E.; Sirat, K.; Rahman, M. B. A. Tetrabutylammonium Bromide (TBABr)-Based Deep Eutectic Solvents (DESs) and Their Physical Properties. *Molecules* **2014**, *19*, 8011—8026.

DOI: 10.1021/acs.jpcb.7b08472
J. Phys. Chem. B 2017, 121, 10556—10565

(39) Florindo, C.; Oliveira, F. S.; Rebelo, L. P. N.; Fernandes, A. M.; Marrucho, I. M. Insights into the Synthesis and Properties of Deep Eutectic Solvents Based on Cholinium Chloride and Carboxylic Acids. *ACS Sustainable Chem. Eng.* **2014**, *2*, 2416−2425.
(40) Perkins, S. L.; Painter, P.; Colina, C. M. Experimental and Computational Studies of Choline Chloride-Based Deep Eutectic Solvents. *J. Chem. Eng. Data* **2014**, *59*, 3652−3662.
(41) Wagle, D. V.; Baker, G. A.; Mamontov, E. Differential Microscopic Mobility of Components within a Deep Eutectic Solvent. *J. Phys. Chem. Lett.* **2015**, *6*, 2924−2928.
(42) Yadav, A.; Pandey, S. Densities and Viscosities of (Choline Chloride + Urea) Deep Eutectic Solvent and Its Aqueous Mixtures in the Temperature Range 293.15 to 363.15 K. *J. Chem. Eng. Data* **2014**, *59*, 2221−2229.
(43) Yadav, A.; Kar, J. R.; Verma, M.; Naqvi, S.; Pandey, S. Densities of Aqueous Mixtures of (Choline Chloride + Ethylene Glycol) and (Choline Chloride + Malonic Acid) Deep Eutectic Solvents in Temperature Range 283.15 to 363.15 K. *Thermochim. Acta* **2015**, *600*, 95−101.
(44) Hammond, O. S.; Bowron, D. T.; Edler, K. J. Liquid Structure of the Choline Chloride-Urea Deep Eutectic Solvent (Reline) from Neutron Diffraction and Atomistic Modelling. *Green Chem.* **2016**, *18*, 2736−2744.
(45) Stefanovic, R.; Ludwig, M.; Webber, G. B.; Atkin, R.; Page, A. J. Nanostructure, Hydrogen Bonding and Rheology in Choline Chloride Deep Eutectic Solvents As a Function of the Hydrogen Bond Donor. *Phys. Chem. Chem. Phys.* **2017**, *19*, 3297−3306.
(46) Kaur, S.; Gupta, A.; Kashyap, H. K. Nanoscale Spatial Heterogeneity in Deep Eutectic Solvents. *J. Phys. Chem. B* **2016**, *120*, 6712−6720.
(47) D'Agostino, C.; Harris, R. C.; Abbott, A. P.; Gladden, L. F.; Mantle, M. D. Molecular Motion and Ion Diffusion in Choline Chloride Based Deep Eutectic Solvents Studied by 1H Pulsed Field Gradient NMR Spectroscopy. *Phys. Chem. Chem. Phys.* **2011**, *13*, 21383−21391.
(48) Abbott, A. P.; Harris, R. C.; Ryder, K. S.; D'Agostino, C.; Gladden, L. F.; Mantle, M. D. Glycerol Eutectics as Sustainable Solvent Systems. *Green Chem.* **2011**, *13*, 82−90.
(49) D'Agostino, C.; Gladden, L. F.; Mantle, M. D.; Abbott, A. P.; Essa, I. A.; Al-Murshedi, A. Y. M.; Harris, R. C. Molecular and Ionic Diffusion in Aqueous − Deep Eutectic Solvent Mixtures: Probing Inter Molecular Interactions Using PFG NMR. *Phys. Chem. Chem. Phys.* **2015**, *17*, 15297−15304.
(50) Abbott, A. P.; D'Agostino, C.; Davis, S. J.; Gladden, L. F.; Mantle, M. D. Do Group 1 Metal Salts Form Deep Eutectic Solvents? *Phys. Chem. Chem. Phys.* **2016**, *18*, 25528−25537.
(51) Guchhait, B.; Gazi, H. A. R.; Kashyap, H. K.; Biswas, R. Fluorescence Spectroscopic Studies of (Acetamide+Sodium/Potassium Thiocyanates) Molten Mixtures: Composition and Temperature Dependence. *J. Phys. Chem. B* **2010**, *114*, 5066−5081.
(52) Guchhait, B.; Daschakraborty, S.; Biswas, R. Medium Decoupling of Dynamics at Temperatures ∼ 100 K Above Glass-transition Temperature: A Case Study with (Acetamide + Lithium Bromide/Nitrate) Melts. *J. Chem. Phys.* **2012**, *136*, 174503.
(53) Guchhait, B.; Das, S.; Daschakraborty, S.; Biswas, R. Interaction and Dynamics of (Alkylamide + Electrolyte) Deep Eutectics: Dependence on Alkyl Chain-length, Temperature, and Anion Identity. *J. Chem. Phys.* **2014**, *140*, 104514.
(54) Das, A.; Biswas, R. Dynamic Solvent Control of a Reaction in Ionic Deep Eutectic Solvents: Time-Resolved Fluorescence Measurements of Reactive and Nonreactive Dynamics in (Choline Chloride + Urea) Melts. *J. Phys. Chem. B* **2015**, *119*, 10102−10113.
(55) Mukherjee, K.; Das, A.; Choudhury, S.; Barman, A.; Biswas, R. Dielectric Relaxations of (Acetamide + Electrolyte) Deep Eutectic Solvents in the Frequency Window, $0.2 \leq \nu/\mathrm{GHz} \leq 50$: Anion and Cation Dependence. *J. Phys. Chem. B* **2015**, *119*, 8063−8071.
(56) Pal, T.; Biswas, R. Heterogeneity and Viscosity Decoupling in (Acetamide + Electrolyte) Molten Mixtures: A Model Simulation Study. *Chem. Phys. Lett.* **2011**, *517*, 180−185.
(57) Pandey, A.; Rai, R.; Pal, M.; Pandey, S. How Polar are Choline Chloride-Based Deep Eutectic Solvents? *Phys. Chem. Chem. Phys.* **2014**, *16*, 1559−1568.
(58) Pandey, A.; Pandey, S. Solvatochromic Probe Behavior within Choline Chloride-Based Deep Eutectic Solvents: Effect of Temperature and Water. *J. Phys. Chem. B* **2014**, *118*, 14652−14661.
(59) Pandey, A.; Yadav, A.; Bhawna; Pandey, S. Fluorescence Quenching of Polycyclic Aromatic Hydrocarbons within Deep Eutectic Solvents and their Aqueous Mixtures. *J. Lumin.* **2017**, *183*, 494−506.
(60) Perrin, D. D.; Armarego, W. L. F.; Perrin, D. R. *Purification of Laboratory Chemicals*; Pergamon Press: New York, 1980.
(61) Mjalli, F. S.; Naser, J. Viscosity Model for Choline Chloride-Based Deep Eutectic Solvents. *Asia-Pac. J. Chem. Eng.* **2015**, *10*, 273−281.
(62) Lackowicz, J. R. *Principles of Fluorescence Spectroscopy*; Springer: New York, 2006; Chapter 24.
(63) Wu, E. C.; Kim, H. J.; Peteanu, L. A. Spectroscopic and MD Study of Dynamic and Structural Heterogeneities in Ionic Liquids. *J. Phys. Chem. B* **2017**, *121*, 1100−1107.
(64) Petrasek, Z.; Schwille, P. Precise Measurement of Diffusion Coefficients using Scanning Fluorescence Correlation Spectroscopy. *Biophys. J.* **2008**, *94*, 1437−1448.
(65) Baumann, R.; Ferrante, C.; Kneuper, E.; Deeg, F.-W.; Brauchle, C. Influence of Confinement on the Solvation and Rotational Dynamics of Coumarin 153 in Ethanol. *J. Phys. Chem. A* **2003**, *107*, 2422−2430.
(66) Rubinov, A. N.; Tomin, V. I. Bathochromic Luminescence of Organic Dyes at Low Temperatures. *Opt. Spektr.* **1970**, *29*, 1082−1086.
(67) Galley, W. C.; Purkey, R. M. Role of Heterogeneity of the Solvation Site in Electronic Spectra in Solution. *Proc. Natl. Acad. Sci. U. S. A.* **1970**, *67*, 1116.
(68) Weber, G.; Shinitzky, M. Failure of Energy Transfer between Identical Aromatic Molecules on Excitation at the Long Wave Edge of the Absorption Spectrum. *Proc. Natl. Acad. Sci. U. S. A.* **1970**, *65*, 823−830.
(69) Mandal, P. K.; Sarkar, M.; Samanta, A. Excitation-Wavelength-Dependent Fluorescence Behavior of Some Dipolar Molecules in Room-Temperature Ionic Liquids. *J. Phys. Chem. A* **2004**, *108*, 9048−9053.
(70) Demchenko, A. P. The red-edge effects: 30 years of exploration. *Luminescence* **2002**, *17*, 19−42.
(71) Hallidy, L. A.; Topp, M. R. Direct Time-Resolution of the Stokes Fluorescence Shift of a Polar Molecular in a Polar Solvent. *Chem. Phys. Lett.* **1977**, *48*, 40−45.
(72) Fleming, G. R. *Chemical Applications of Ultrafast Spectroscopy*; Oxford University Press: 1986.
(73) Ingram, J. A.; Moog, R. S.; Ito, N.; Biswas, R.; Maroncelli, M. Solute Rotation and Solvation Dynamics in a Room-Temperature Ionic Liquid. *J. Phys. Chem. B* **2003**, *107*, 5926−5932.
(74) Jin, H.; Baker, G. A.; Arzhantsev, S.; Dong, J.; Maroncelli, M. Solvation and Rotational Dynamics of Coumarin 153 in Ionic Liquids: Comparisons to Conventional Solvents. *J. Phys. Chem. B* **2007**, *111*, 7291−7302.
(75) Karve, L.; Dutt, G. B. Role of Specific Interactions on the Rotational Diffusion of Organic Solutes in a Protic Ionic Liquid−Propylammonium Nitrate. *J. Phys. Chem. B* **2012**, *116*, 9107−9113.
(76) Edward, J. T. Molecular volumes and the Stokes-Einstein equation. *J. Chem. Educ.* **1970**, *47*, 261−270.
(77) Khara, D. C.; Samanta, A. Rotational Dynamics of Positively and Negatively Charged Solutes in Ionic Liquid and Viscous Molecular Solvent Studied by Time-Resolved Fluorescence Anisotropy Measurements. *Phys. Chem. Chem. Phys.* **2010**, *12*, 7671−7677.
(78) Sension, R. J.; Hochstrasser, R. M. Comment on: Rotational Friction Coefficients for Ellipsoids and Chemical Molecules with Slip Boundary Conditions. *J. Chem. Phys.* **1993**, *98*, 2490.
(79) Einstein, A. *Investigations on the Theory of Brownian Movement*; Dover: New York, 1956.

DOI: 10.1021/acs.jpcb.7b08472
J. Phys. Chem. B 2017, 121, 10556−10565

(80) Hartman, R. S.; Alavi, D. S.; Waldeck, D. H. An Experimental Test of Dielectric Friction Models Using the Rotational Diffusion of Aminoanthraquinones. *J. Phys. Chem.* **1991**, *95*, 7872−7880.
(81) Gangamallaiah, V.; Dutt, G. B. Rotational Diffusion of Nonpolar and Ionic Solutes in 1-Alkyl-3-Methylimidazolium Bis-(trifluoromethylsulfonyl)imides: Is Solute Rotation Always Influenced by the Length of the Alkyl Chain on the Imidazolium Cation? *J. Phys. Chem. B* **2012**, *116*, 12819−12825.
(82) Das, S.; Biswas, R.; Mukherjee, B. Orientational Jump in (Acetamide + Electrolyte) Deep Eutectics: Anion Dependence. *J. Phys. Chem. B* **2015**, *119*, 11157−11168.
(83) Das, S.; Biswas, R.; Mukherjee, B. Reorientational Jump Dynamics and Its Connections to Hydrogen Bond Relaxation in Molten Acetamide: An All-Atom Molecular Dynamics Simulation Study. *J. Phys. Chem. B* **2015**, *119*, 274−283.
(84) Richert, R. Heterogeneous dynamics in liquids: fluctuations in space and time. *J. Phys.: Condens. Matter* **2002**, *14*, R703−R738.

DOI: 10.1021/acs.jpcb.7b08472
J. Phys. Chem. B 2017, 121, 10556−10565

PCCP

PAPER

View Article Online
View Journal | View Issue

Cite this: *Phys. Chem. Chem. Phys.*, 2018, **20**, 24613

How do the hydrocarbon chain length and hydroxyl group position influence the solute dynamics in alcohol-based deep eutectic solvents?†

Sk Saddam Hossain and Anunay Samanta *

Received 31st July 2018,
Accepted 11th September 2018

DOI: 10.1039/c8cp04859b

rsc.li/pccp

Deep eutectic solvents (DESs) have received considerable attention in recent years as new sustainable green media and some of their interesting properties have stimulated investigations on the microscopic solution structure, solute–solvent interactions and solute/solvation dynamics in these media. Even though the alcohol-based DESs, due to their low viscosity, serve as useful media in various applications, little is known about the structure and dynamics of these solvents. In order to obtain insight into the microscopic structure and interactions operating in these media, we have studied the rotational and translational diffusion dynamics of some carefully chosen molecular systems (both dipolar and nonpolar) using time-resolved fluorescence anisotropy and fluorescence correlation spectroscopy techniques in a series of choline chloride/alcohol based DESs differing in hydrocarbon chain length and positioning of the hydroxyl group on the hydrogen bond donor. The results reveal an increase of both spatial and dynamic heterogeneity upon an increase in chain length of one of the components of these solvents. No significant variation of heterogeneity, however, could be observed with the change in the hydroxyl group position. The analysis of the experimental results indicates that solute–solvent hydrogen-bonding interaction plays a dominant role in determining both rotational and translational diffusion dynamics of AP in these DESs.

Introduction

Deep eutectic solvents (DESs) have attracted considerable attention in recent years as new environmentally benign solvents with potential applications in diverse fields such as organic synthesis,[1,2] catalysis,[3] metal processing,[4–6] polymerizations,[7,8] biodiesel purification,[9] electrochemistry,[10,11] nanotechnology,[12,13] biotechnology[14] and carbon dioxide adsorption.[15,16] Due to several important features such as low toxicity, biodegradability, biocompatibility, ease of preparation from cheaper raw materials and wide tunability of properties, most of these novel media have emerged as better alternatives not only to common molecular solvents,[2,17,18] but also to ionic liquids (ILs).[19–23]

DESs generally consist of a salt or hydrogen bond acceptor (HBA) and a hydrogen bond donor (HBD). Mixing of two or more such components in a certain mole ratio forms a eutectic system, which shows large depression of the melting temperature (much lower than either of the individual pure constituents) owing to extensive interspecies hydrogen-bonding interactions.[19,24] A large numbers of DESs can be obtained by appropriate selection of individual components as well as by varying the molar ratio of the constituents.[23] This flexibility allows convenient solvent engineering yielding a large number of ionic and non-ionic DESs with desirable properties. The most common and popular DESs are composed of quaternary ammonium salts like choline chloride (ChCl) as the HBA and readily available materials like amides, alcohols, acids, sugars *etc.* as the HBD.[23]

Several theoretical and experimental studies have been performed in recent years to explore the structure, dynamics, and molecular level interactions of these media.[17,25–42] Abbott and co-workers have studied diffusion and dynamics in these media using ^{1}H pulsed field gradient NMR spectroscopy.[17,25,26] Biswas and co-workers have investigated structural as well as dynamical aspects of several DESs both theoretically and experimentally.[29–34,43] Even though a large number of DESs have been explored, most of the studies have focused on systems obtained by mixing of quaternary ammonium salts with amides and acids as HBDs. Not much is known, however, about the structure and dynamics of alcohol-based eutectic systems, which are quite useful as media in various applications[19,24,44–46] due to their significantly lower viscosity compared to the other DESs. As understanding of the physicochemical properties of a solvent

School of Chemistry, University of Hyderabad, Hyderabad-500 046, India.
E-mail: anunay@uohyd.ac.in

† Electronic supplementary information (ESI) available. See DOI: 10.1039/c8cp04859b

system is key to exploitation of its potential in applications, we recently studied the microscopic solution structure and solute–solvent interactions in one of the alcohol-based DESs, namely, ethaline.[47]

Recognizing the fact that a change of the hydrocarbon chain length and hydroxyl group position of the diols (one of the components of DESs) significantly influences the physical properties of the alcohol-based DESs,[48] we investigate how these factors influence the microscopic solution structure, diffusion dynamics of solute molecules and nature of solute–solvent interactions in this class of DESs. For this purpose, we have chosen three fluorescent systems, whose rotational diffusion dynamics are studied by monitoring the time-dependence of the fluorescence anisotropy and translational diffusion by fluorescence correlation spectroscopy measurements in a series of DESs comprising ChCl (as the HBA) and six different diols (as the HBD). The six diols chosen in this study (Chart 1) differ in their chain length or hydroxyl group position. The compositions of the DESs along with their abbreviations are presented in Table 1. The first three DESs contain diols of different chain length, whereas in the last four, the diols vary in their hydroxyl group position maintaining the same chain length. Dipolar solutes, coumarin 153 (C153) and 4-aminophthalimide (AP), and a nonpolar solute, anthracene (ANT), (Chart 1) are chosen as the fluorescent probe molecules. Of the two dipolar solutes, AP is chosen for high sensitivity of its fluorescence properties to hydrogen-bonding interactions.[49,50] ANT is chosen for its tendency to reside in relatively nonpolar regions of an organized assembly comprising regions with different polarities.[49,51]

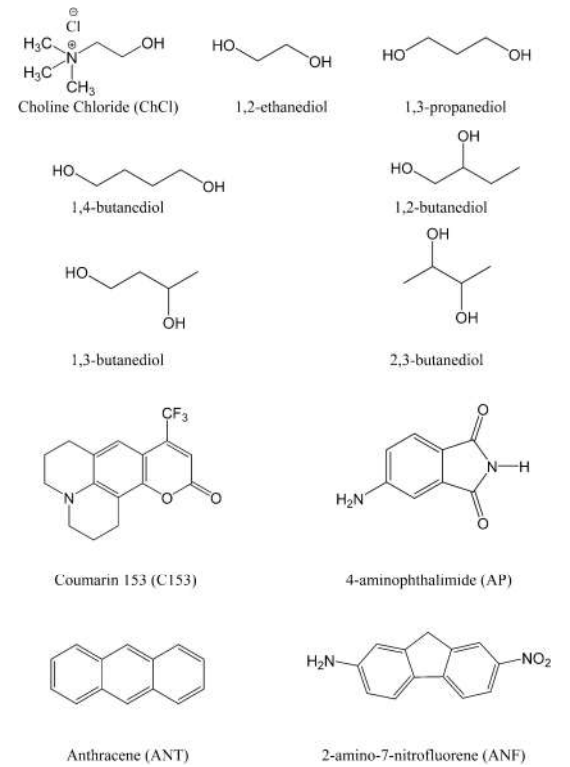

Chart 1 Molecular structures and abbreviations of the constituents of the DESs and solute molecules used in this study.

Table 1 Description of the DESs used in this study

Sl. no.	Salt	HBDs	Mole ratio (Salt : HBD)	Abbreviation	Water content (wt%)
1	ChCl	1,2-Ethanediol	1 : 3	CC12ED	0.160
2	ChCl	1,3-Propanediol	1 : 3	CC13PD	0.122
3	ChCl	1,4-Butanediol	1 : 3	CC14BD	0.133
4	ChCl	1,2-Butanediol	1 : 4	CC12BD	0.205
5	ChCl	1,3-Butanediol	1 : 4	CC13BD	0.218
6	ChCl	2,3-Butanediol	1 : 4	CC23BD	0.164

Experimental section

Materials

Choline chloride (≥98%), 1,2-ethanediol (≥99%), 1,3-propanediol (98%), 1,4-butanediol (99%), 1,2-butanediol (≥98%), 1,3-butanediol (98%), and 2,3-butanediol (98%) were purchased from Sigma-Aldrich and dried under high vacuum for several hours before use. The purity of these reagents was checked using ^{1}H NMR spectroscopy (Fig. S1, ESI†). C153, AP and ANT were procured from Eastman Kodak, TCI and Sigma-Aldrich, respectively, and used as received. Methanol and hexane were obtained from Merck, and purified by following a standard procedure prior to use.[52] Milli-Q water was used in this study.

Synthesis and sample preparation

Six DESs were synthesized by following a reported procedure.[48] Briefly, ChCl and respective diols were mixed in a molar ratio of 1 : 3/1 : 4 and heated at 333 K with constant stirring until a transparent liquid was formed. The liquids were then allowed to cool down to room temperature. The water contents of the liquids were determined by Karl Fischer titration after drying under high vacuum for several hours (Table 1) and the values are comparable with the other reported DESs.[53,54] A few μL of a freshly prepared solution of the solutes in methanol (except for ANT, which was prepared in hexane) was transferred into a quartz cuvette of 1 cm optical path length. Methanol/hexane was then evaporated by flowing ultra-high purity N_2 gas. Then, 3.0 mL of each DES was added into the cuvette, tightly sealed with a rubber septum and parafilm, and the solution was slightly heated and stirred for some time to ensure complete dissolution of the solutes. The solution was then allowed to cool down slowly to room temperature and stored in an inert atmosphere prior to experiments.

Instrumentation

^{1}H NMR spectra of the constituents of the DESs were recorded using a Bruker (AVANCE 500 MHz) spectrometer. The water contents of the DESs were measured using a Karl Fischer coulometer (METTLER TOLEDO DL39). The viscosities of DESs

were measured by a LVDV-III Ultra Brookfield cone and plate viscometer (0.2% repeatability and 1% accuracy). The steady-state absorption and emission/excitation spectra were recorded on a UV-vis spectrophotometer (Cary100, Varian) and spectrofluorometer (FluoroLog, Horiba Jobin Yvon), respectively. A time-correlated single-photon counting (TCSPC) fluorescence spectrometer (Horiba Jobin Yvon IBH) was used for time-resolved fluorescence anisotropy decay measurements. Pulsed diode lasers (375 and 405 nm) were used as the excitation sources and an MCP photomultiplier (Hamamatsu R3809U-50) was used as the detector. The instrument response function of the setup was measured by placing a dilute solution of Ludox in water as the scatterer, and the full-width at half-maximum (fwhm) was found to be 60 ps for both excitations. Fluorescence anisotropy decay curves were analyzed by a nonlinear least-squares iteration procedure using IBH DAS6 (version 2.2) decay analysis software. The temperature dependent studies were performed by using a Julabo water circulator (Model F32).

The FCS measurements were performed using a time-resolved confocal fluorescence microscope (MicroTime 200, PicoQuant). The details of the setup were described in our earlier publication.[47] A 405 nm pulsed diode laser (with fwhm 176 ps and repetition rate 20 MHz) was used as the excitation source. The laser output was focused onto the sample using a water immersion objective (Olympus UPlansApo, NA 1.2, 60×). Fluorescence from the samples was collected by the same objective and passed through the dichroic mirror, filtered by a 430 nm long-pass filter. A 50 μm pinhole was placed after the filter. Thereafter, a 50 : 50 beam splitter was used to divide the signal before entering the two single-photon avalanche photodiodes (SPADs). The data acquisition and analysis were performed using the SymPhoTime software package provided by PicoQuant. Rhodamine 6G (a diffusion coefficient of 426 $\mu m^2\ s^{-1}$ in water[55]) was used for calibration of the excitation volume and it was found to be ~0.45 fL for the 405 nm laser source. During all FCS measurements, the excitation power was kept at ~3 μW. All FCS experiments were carried out at room temperature (~298 K).

Method

To obtain the anisotropy decay profiles, fluorescence intensities in parallel ($I_{\parallel}$) and perpendicular ($I_{\perp}$) polarizations (with respect to the vertically polarized excitation laser beam) were collected alternatively using a monochromator with a band pass of 2 nm for equal intervals of time until the count difference between the two polarizations (at $t = 0$) was ~5000. The time-resolved fluorescence anisotropy, $r(t)$, was calculated using the equation

$$r(t) = \frac{I_{\parallel}(t) - GI_{\perp}(t)}{I_{\parallel}(t) + 2GI_{\perp}(t)} \quad (1)$$

where, G is the correction factor for the detector sensitivity to the polarization direction of the emission and was calculated following the same procedure as described above, but with only 5 cycles and horizontal polarization of the exciting laser beam.

The FCS measurements were performed by placing a highly dilute solution (~nM) on the coverslip which was placed on top of the objective. The fluctuations of fluorescence intensity were measured in a small detection volume (~1 fL) by using a focused laser beam and pinhole. These fluctuating fluorescence signals detected by two SPAD detectors were cross-correlated to obtain the correlation curves $G(\tau)$. The decay of the correlation function with respect to time was used for obtaining dynamical information on translational diffusion. The correlation function $G(\tau)$ of the fluorescence intensity is given by[56]

$$G(\tau) = \frac{\langle \delta F(t) \delta F(t+\tau) \rangle}{\langle F(t) \rangle^2} \quad (2)$$

where, $\langle F(t) \rangle$ is the average fluorescence intensity and $\delta F(t)$ and $\delta F(t + \tau)$ are the fluctuations in intensity around the average value at time t and $(t + \tau)$, respectively, and are given by

$$\delta F(t) = F(t) - \langle F(t) \rangle \quad (3a)$$

$$\delta F(t+\tau) = F(t+\tau) - \langle F(t) \rangle \quad (3b)$$

Table 2 Steady-state excitation and emission maxima of C153, AP and ANT in six DESs at room temperature (298 K)

	C153		AP		ANT	
DESs	λ_{ex}^{max} (nm)	λ_{em}^{max} (nm)	λ_{ex}^{max} (nm)	λ_{em}^{max} (nm)	λ_{ex}^{max} (nm)	λ_{em}^{max} (nm)
CC12ED	426	540	371	514	360	404
CC13PD	426	536	371	508	360	404
CC14BD	426	533	371	505	360	403
CC12BD	426	530	371	510	360	403
CC13BD	426	530	370	505	359	403
CC23BD	426	530	371	509	359	403

Results and discussion

Steady-state measurement

The steady-state excitation (λ_{ex}^{max}) and emission maxima (λ_{em}^{max}) of C153, AP and ANT in six DESs at room temperature (298 K) are collected in Table 2 (spectra in Fig. S2, ESI†). A comparison of the λ_{ex}^{max} and λ_{em}^{max} values of these solutes in six DESs is displayed in Fig. S3 (ESI†). It is evident that the λ_{ex}^{max} values of the solutes do not vary with the change of solvent. As far as the λ_{em}^{max} values are concerned, though ANT shows very similar emission behavior in all solvents, the λ_{em}^{max} values of C153 and AP show significant solvent dependence. A nearly 9–10 nm blue shift of λ_{em}^{max} is observed for these two systems with increasing hydrocarbon chain length. No effect of the hydroxyl group position is observed on the λ_{em}^{max} value of C153 except in CC14BD. The latter is presumably due to the different salt : HBD mole ratio (see Table 1) in this DES. For AP, a small variation of λ_{em}^{max} is observed with the change in the hydroxyl group position, but no clear trend could be identified. This small variation of λ_{em}^{max} is a reflection of the sensitivity of the fluorescence properties of AP on hydrogen-bonding interactions.[57] The blue shift of the λ_{em}^{max} values of C153 and AP with increasing hydrocarbon chain length of HBDs suggests these probes experience a less polar environment in DESs comprising longer alkyl chain length diols.

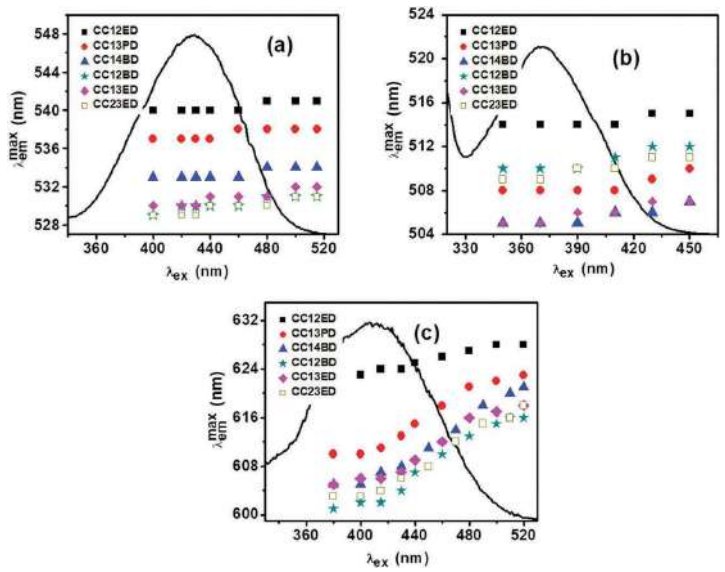

Fig. 1 Dependence of the emission maximum (λ_{em}^{max}) on the excitation wavelength (λ_{ex}) for C153 (a), AP (b) and ANF (c) at 298 K in DESs. Symbols represent the λ_{em}^{max} values at different λ_{ex}. Representative excitation spectra of the solutes are also shown by solid lines.

We also examined the excitation wavelength (λ_{ex}) dependence of λ_{em}^{max} of the dipolar molecules, C153 and AP, to find out whether any signature of the microheterogeneity of these media could be observed.[29,47,58] Biswas and co-workers indeed observed significant λ_{ex} dependence of C153 in other DESs.[29,31] Fig. 1 shows, however, that none of the two dipolar probes exhibits any λ_{ex} dependent emission behavior in any DESs. However, as it is well known that molecules with shorter τ_f are more likely to exhibit excitation wavelength dependent fluorescence behavior in viscous media,[58] we have also examined the λ_{ex} dependence of λ_{em}^{max} of 2-amino-7-nitrofluorene (ANF), whose τ_f (τ_f < 50 ps in 2-propanol[59]) is much shorter than that of C153 (τ_f = 4.1 ns in methanol) or AP (τ_f = 6.8 ns in methanol). Interestingly, as can be seen from Fig. 1c, ANF shows appreciable dependence of λ_{em}^{max} on the excitation wavelength. This increasing excitation wavelength dependent fluorescence behavior in DESs with longer chain length diols indicates spatial heterogeneity of the solvents arising from the formation of nanoscale heterogeneous structure through segregation of ionic and molecular domains/regions. A similar line of reasoning has been used for other eutectic systems.[31,37,38,60] However, DESs formed between ChCl and different isomers of butanediol (which differ in the position of the hydroxyl groups) show identical dependence indicating very similar heterogeneous structure perhaps due to their same chain length.

Time-resolved fluorescence anisotropy measurements

As stated earlier, in order to understand the microenvironments around the solute molecules and nature of solute–solvent interactions, we have studied the rotational diffusion of C153, AP and ANT in these media by monitoring the time-dependence of the fluorescence anisotropy of the systems over a temperature range of 298–343 K. Representative fluorescence anisotropy decay profiles of the solutes in six DESs at 298 K are shown in Fig. 2. The rotational reorientation times (τ_r) of the solutes in these DESs are obtained by fitting the anisotropy data to a single-exponential function, $r(t) = r_0 \exp(-t/\tau_r)$. The measured τ_r values of the solutes at 298 K are collected in Table 3, while those at other temperatures are provided in Table S1 of the ESI.† Table 3 shows that at 298 K, the τ_r values are very similar for AP and C153 in CC12ED. However, these values differ significantly with increasing chain length and the hydroxyl group position of the diols. As the size of AP is almost half that of C153 (*vide* later), the much higher τ_r value of AP compared to C153 in these solvents suggests hindrance of its rotational diffusion due to strong solute–solvent association/interactions. On the other hand, though the size of ANT is comparable with AP, its τ_r value is lowest in any given solvent indicating that it does not experience strong interaction (like that faced by AP) with the solvents. The above results clearly indicate that these solute molecules experience very different interactions in any given DES.

We have also examined the fluorescence anisotropy decay profiles of the solutes in iso-viscous conditions (30 cP) by adjusting the temperatures of the solvents (Fig. S4, ESI†). The τ_r values of C153 and ANT measured under this condition (Table 4) show small variation with increasing hydrocarbon chain length and remain almost constant with the change in hydroxyl group position; however, these values for AP differ more significantly in both situations. These are very interesting observations, and a more detailed and quantitative discussion on the rotational dynamics of the solutes in these media, therefore, is presented below using the Stokes–Einstein–Debye (SED) hydrodynamic theory.[61]

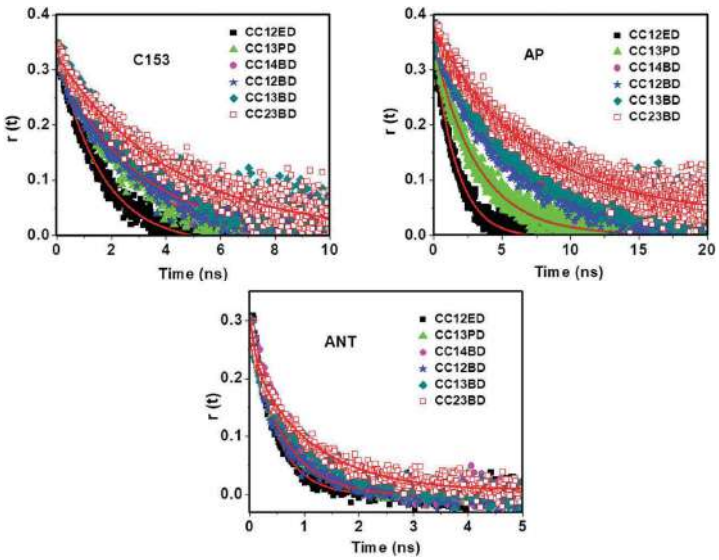

Fig. 2 Anisotropy decay profiles of the solutes in six DESs at isothermal (298 K) conditions. The solid lines represent single-exponential fits to the decay profiles. The excitation wavelengths for C153/AP and ANT are 405 and 375 nm, respectively. All the decay profiles are recorded by monitoring at respective emission maxima of solutes in the six DESs.

Table 3 Estimated rotational reorientation times (ns) of the solutes in various DESs at isothermal conditions (298 K)

		Rotational reorientation time (ns)		
DESs	Viscosity (cP)	C153	AP	ANT
CC12ED	30	1.58	1.65	0.44
CC13PD	53	2.64	3.14	0.66
CC14BD	84.5	3.53	5.08	0.84
CC12BD	72	2.99	5.30	0.64
CC13BD	97	3.83	5.96	0.97
CC23BD	112	4.17	7.20	0.99

Table 4 Estimated rotational reorientation times (ns) of the solutes in various DESs at isoviscous conditions (30 cP)

		Rotational reorientation time (ns)		
DESs	Viscosity (cP)	C153	AP	ANT
CC12ED		1.58	1.65	0.44
CC13PD		1.59	1.89	0.41
CC14BD	30	1.46	1.93	0.35
CC12BD		1.45	2.36	0.33
CC13BD		1.45	2.07	0.33
CC23BD		1.44	2.26	0.34

According to this theory, the τ_r value of a solute in a solvent continuum of viscosity η at temperature T is given by

$$\tau_r = \frac{\eta V f C}{k_B T} \quad (4)$$

where, V, f and C are respectively the van der Waals volume, shape factor and boundary condition parameter of the solutes and k_B is the Boltzmann constant. The shape factor (f), which is a function of the axial ratio of the semi axes, describes the nonspherical nature of the solutes, which are treated as asymmetric ellipsoids. C indicates the extent of coupling between the solute and the solvent; hydrodynamic slip ($0 < C_{slip} < 1$) and stick ($C_{stick} = 1$) are the two limiting cases. The V, f and C values for the three solutes are taken from the literature[49,62] and collected in Table 5.

Table 5 Solute dimensions, van der Waals volumes, shape factors and boundary condition parameters calculated from the SED hydrodynamic theory

Solute	Axial radii (Å^3)	van der Waals volume, V (Å^3)	Shape factors (f)	C_{slip}
C153[a]	6.1 × 4.8 × 2.2	246	1.71	0.24
AP[b]	5.0 × 3.5 × 1.8	134	1.60	0.11
ANT[b]	5.9 × 3.9 × 1.8	175	1.30	0.29

[a] Values are taken from ref. 62. [b] Values are taken from ref. 49.

Typical plots of the measured τ_r values of the solutes *versus* η/T in CC12ED are shown in Fig. 3 along with the slip and stick lines. The plots in other DESs are provided in the ESI† (Fig. S5–S7). Fig. 3 shows that C153 reorientation times lie between the slip and stick lines, AP exhibits superstick behavior and ANT shows slip behavior. The superstick behavior of AP is an indication of its strong association with the constituents of the solvent. This must be due to specific hydrogen-bonding interaction of AP with the hydroxyl groups of the eutectic solvent as this is well documented in both conventional solvents[57] and ionic liquids.[49,63] The slip behavior of ANT is because of its lack of interaction with the solvent due to its nonpolar nature and location in the hydrocarbon dominated molecular domain/region.

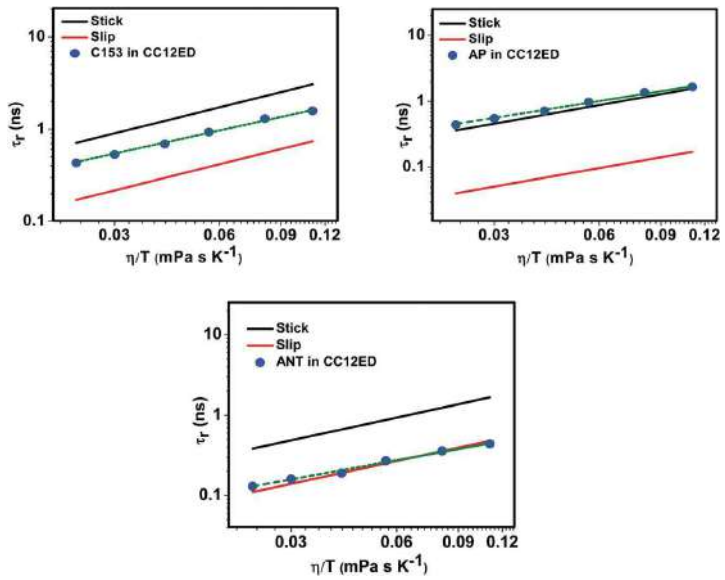

Fig. 3 Plots of τ_r *vs.* η/T for three solutes in the CC12ED system. The solid circles indicate the experimental rotational times and the dashed lines represent fits to the data according to $\tau_r = A(\eta/T)^p$. Computed stick (black) and slip (red) lines using SED theory are also shown.

A similar analysis in other DESs reveals that the superstick behavior of AP is more pronounced (Fig. S5, ESI†) with increasing chain length indicating stronger hydrogen-bonding interaction with the latter members of the series (leading to a slower rotation). On the other hand, the τ_r values of ANT change from slip to subslip behavior (Fig. S6, ESI†) with increasing chain length due to the lower friction experienced in larger solvents comprising a higher nonpolar fraction arising from the increasing hydrocarbon chain length of the diols. In this context, it may be noted that the subslip behavior of rotational dynamics is sometimes (like in ionic liquids[50]) considered to be due to void spaces created from the increasing chain length, which reduce the rotational friction. However, unlike the two other probes, the τ_r values of C153 change marginally towards the slip line with increasing chain length, that too only at low temperature. At higher temperature, it shows very similar behavior in all solvents (Fig. S7, ESI†).

The experimental τ_r values of the solutes are fitted to $\tau_r = A(\eta/T)^p$ in each DES (shown as dashed line in the τ_r *vs.* η/T plots). The A and p values obtained from these fits are presented in Table 6. The p values show significant departure from unity, indicating deviation of the rotational dynamics from the SED hydrodynamic behavior. This fractional viscosity dependence (or departure from the SED theory) is a reflection of the dynamic heterogeneity of the media,[29,31,47] which arises from fluctuations of the hydrogen-bonding network in these media and the consequent motion of its constituents.

As can be seen, the departure of the p values from unity for C153 and ANT increases with increasing hydrocarbon chain length. The p values, however, remain nearly constant upon the change of the hydroxyl group position. This suggests that dynamic heterogeneity is more pronounced in media comprising diols with longer chain length, but it does not vary with the change in the hydroxyl group position. Nearly constant (and high) p values for AP in all six DESs indicate that AP molecules experience relatively less and very similar dynamic heterogeneity in these media, perhaps due to its strong association with the constituents of the solvents, which does not allow much fluctuations of the hydrogen-bonding network. Further, Table 6 shows that the A (= VfC/k_B) values decrease marginally for C153 and ANT with the increase in the hydrocarbon chain length but remain almost constant upon the change of the hydroxyl group position. Considering that f/k_B is constant for a given solute and

Table 6 Parameters A [ns K (mPa s^{-1})] and p for the solutes obtained from least-squares fits of τ_r *vs.* η/T plots in DESs

	C153		AP		ANT	
DESs	A	p	A	p	A	p
CC12ED	10.8 ± 0.2	0.84 ± 0.02	10.9 ± 0.2	0.85 ± 0.02	2.6 ± 0.2	0.82 ± 0.03
CC13PD	11.0 ± 0.3	0.81 ± 0.01	13.4 ± 0.2	0.84 ± 0.02	2.5 ± 0.1	0.80 ± 0.02
CC14BD	9.3 ± 0.3	0.77 ± 0.02	14.8 ± 0.3	0.85 ± 0.01	2.2 ± 0.1	0.76 ± 0.01
CC12BD	9.0 ± 0.2	0.77 ± 0.01	17.9 ± 0.3	0.85 ± 0.01	2.0 ± 0.1	0.77 ± 0.02
CC13BD	9.1 ± 0.3	0.76 ± 0.02	15.3 ± 0.3	0.83 ± 0.01	2.2 ± 0.1	0.77 ± 0.01
CC23BD	8.9 ± 0.3	0.76 ± 0.02	16.6 ± 0.2	0.84 ± 0.02	2.1 ± 0.1	0.75 ± 0.01

Table 7 Calculated solute–solvent coupling constants (C_{obs})[a] of the solutes in the DESs

	C_{obs}		
DESs	C153	AP	ANT
CC12ED	0.55 ± 0.01	1.12 ± 0.02	0.30 ± 0.01
CC13PD	0.56 ± 0.005	1.29 ± 0.01	0.26 ± 0.01
CC14BD	0.51 ± 0.01	1.33 ± 0.01	0.23 ± 0.01
CC12BD	0.51 ± 0.01	1.64 ± 0.02	0.21 ± 0.02
CC13BD	0.50 ± 0.015	1.41 ± 0.02	0.22 ± 0.005
CC23BD	0.49 ± 0.02	1.51 ± 0.01	0.22 ± 0.01

[a] Average of the values measured at six temperatures between 298 and 343 K.

the volume of the solvents (V) increases with increasing chain length of HBDs, the decrease of the A values suggests a decrease of solute–solvent coupling with increasing chain length. Unlike C153 and ANT, the A values for AP increase significantly with increasing chain length suggesting stronger coupling in the latter media. Some variation of the A value with the change in the hydroxyl group position indicates a change in coupling with the hydroxyl group position too.

To corroborate these conclusions, we have calculated the solute–solvent coupling constants (C_{obs}) from the experimental τ_r values using $C_{obs} = \tau_r/\tau_{stick}$ (where, τ_{stick} is the rotational time calculated using SED hydrodynamic theory) and these are presented in Table 7. A careful inspection of the data reveals that the C_{obs} values decrease marginally for C153 and ANT with increasing chain length but show no significant variation with the hydroxyl group position. This trend is the same as seen for the A values in the previous section, indicating faster rotation of the solutes with increasing chain length. Interestingly, the C_{obs} values for AP increase significantly with the increase of chain length, suggesting slower rotational diffusion due to an enhanced hydrogen-bonding interaction between the solute and constituents of the solvents. These observations can be rationalized considering formation of a nanoheterogeneous domain-like structure[31,37,38,60] consisting of ionic and molecular regions in DESs containing longer chain length diols, where different solute molecules reside in different environments (Scheme 1). AP molecule resides in the ionic polar region, ANT resides specifically in the molecular region (relatively nonpolar region), and C153, being larger in size, locates itself at the boundary between the ionic and molecular regions. This heterogeneous structure becomes pronounced with increasing hydrocarbon chain length of diols, but does not change with the position of the hydroxyl groups. A similar picture also emerged from the steady-state measurements. With the increase in the hydrocarbon chain length of HBDs, the fraction of the molecular environment (nonpolar region) as well as the overall size of the solvent increases offering a lower friction to C153 and ANT leading to a decrease of the C_{obs} values. In contrast, as AP molecules reside in the ionic polar region of these solvents, an increase in the nonpolar fraction (or hydrocarbon chain length of HBDs) forces the AP molecules to come closer towards the hydroxyl groups of the diols offering stronger hydrogen-bonding interaction with the solvents resulting in an increase in C_{obs} values.

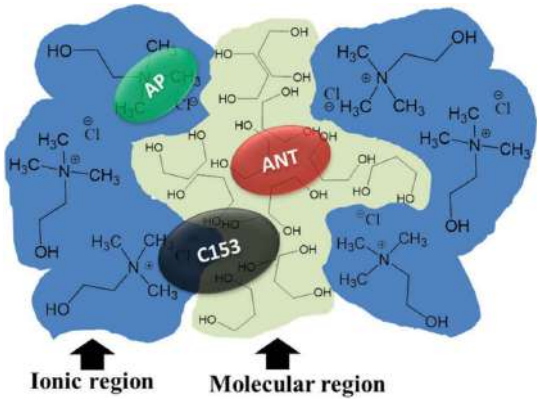

Scheme 1 A schematic representation showing different domains/regions in DESs and possible locations of various solutes in these regions.

Unlike the other two solutes, C_{obs} values for AP molecules vary significantly with the hydroxyl group position. A careful inspection of the data presented in Table 7 reveals a higher C_{obs} value and stronger solute–solvent association in solvents (CC12BD and CC23BD) where the hydroxyl groups are adjacent to each other.

FCS measurements

We have studied the translation diffusion dynamics of C153 and AP in these solvents by the single-molecule based FCS technique. ANT could not be studied due to its blue fluorescence and lack of a suitable excitation source. Representative fluorescence correlation curves of C153 and AP in CC12ED at 298 K are shown in Fig. 4. The correlation curves $G(\tau)$ of the solute molecules in all media were fitted to eqn (5) with both the single-component diffusion ($\beta = 1$) and the anomalous diffusion ($\beta < 1$) model, but, as judged by the distribution of the residuals and χ^2 values of the fits (*vide* ESI†), the anomalous diffusion model fits the data much better compared to the single-component diffusion model.

$$G(\tau) = \frac{1}{N}\left[1 + \left(\frac{\tau}{\tau_D}\right)^{\beta}\right]^{-1}\left[1 + \left(\frac{r_0}{z_0}\right)^2\left(\frac{\tau}{\tau_D}\right)^{\beta}\right]^{-1/2} \quad (5)$$

In eqn (5), N is the average number of fluorescent molecules present in the observation volume, τ_D is the time taken by the molecule to diffuse through this volume, τ is the delay or lag

$$D_t = \frac{r_0^2}{4\tau_D} \quad (6)$$

time and β ($0 < \beta < 1$) is the stretching exponent representing the distribution of τ_D. k indicates the structure parameter of the observation volume, which is defined as $k = z_0/r_0$, where, z_0 and r_0 are the longitudinal and transverse radii of the observation volume, respectively. Fig. 5 compares the fitted (to the anomalous diffusion model) correlation curves of the solutes in the DESs. The diffusion coefficients (D_t) of the solutes in the DESs, calculated using the τ_D values obtained from fits using eqn (6), are collected in Table 8 along with the β values.

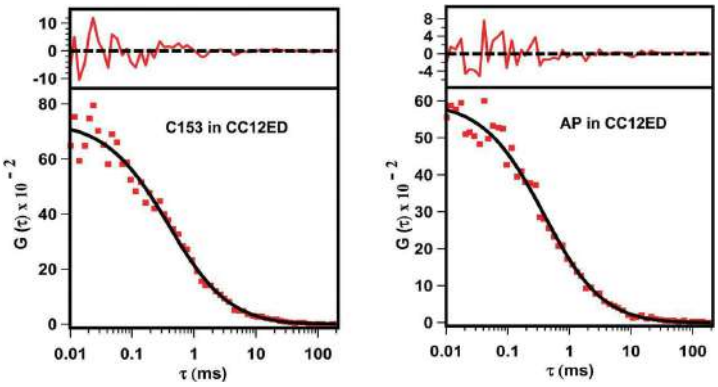

Fig. 4 Fluorescence correlation curves of the solutes in the CC12ED system. The points are the experimental data, and the solid lines represent fits to the data using an anomalous diffusion model. The residuals depicting the quality of the fits are also shown at the top of each curve.

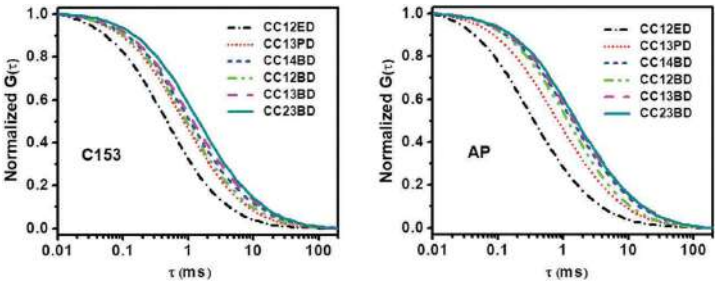

Fig. 5 The fitted correlation curves (normalized) of the solutes in six DESs using the anomalous diffusion model.

Table 8 Estimated diffusion coefficients (D_t in $\mu m^2\ s^{-1}$) and stretching exponents (β) obtained from the fits using the anomalous diffusion model for the solutes in DESs

	C153		AP	
DESs	D_t	β	D_t	β
CC12ED	32.9 ± 4.2	0.87 ± 0.02	35.4 ± 3.6	0.86 ± 0.02
CC13PD	18.2 ± 2.4	0.85 ± 0.01	16.9 ± 3.5	0.86 ± 0.03
CC14BD	15.6 ± 1.5	0.82 ± 0.02	10.5 ± 2.0	0.87 ± 0.02
CC12BD	16.1 ± 0.8	0.83 ± 0.02	12.9 ± 1.3	0.86 ± 0.03
CC13BD	12.0 ± 1.0	0.83 ± 0.03	9.8 ± 1.1	0.85 ± 0.03
CC23BD	10.1 ± 1.2	0.82 ± 0.03	7.7 ± 0.9	0.87 ± 0.01

It can be seen that the β values for both solutes deviate significantly from unity in these media. Considering the fact that these molecules show single-component diffusion in conventional solvents, this deviation of the β values from unity can be attributed to the dynamic heterogeneity of the media, as described in earlier reports.[47,64] The deviation of the stretching exponent β from unity suggests that the mean square displacement (MSD) of the probe molecules follows a sub-diffusive behavior, $\langle r(\tau)^2 \rangle \propto \tau^{\beta}$ (with $\beta < 1$), instead of the normal Brownian diffusion ($\beta = 1$) due to dynamic heterogeneity in these complex media.[25,47,64] Further, the data presented in Table 8 shows that the deviation of the β value of C153 from unity increases with the increase in chain length indicating greater dynamic heterogeneity in solvents containing HBDs with higher chain length. The near-constancy of the β value in solvents with different hydroxyl group positions indicates negligible variation of dynamic heterogeneity. On the other hand, these values for AP are very similar in both situations. These results are consistent with the trends observed for the rotational diffusion of the solutes.

In addition, we note that the D_t value of each solute correlates nicely with the viscosity of the media. However, there are two interesting points to note. First, even though AP is much smaller than C153, the D_t value of AP is comparable or lower than that of C153 in these solvents. Second, the D_t value of AP decreases more sharply compared to C153. These trends, which are similar to those observed for the rotational dynamics of the solutes in these media, confirm strong association of AP molecules with the constituents of the solvents due to strong solute–solvent hydrogen-bonding interaction.

Conclusion

In summary, we have studied the rotational and translational diffusion of some selected neutral fluorescent molecules in six ChCl-diol based DESs to find out the effect of the hydrocarbon chain length and hydroxyl group positioning (on HBDs) of the eutectic systems on the respective diffusion dynamics.

The results obtained from measurements in ensemble and single molecule conditions are in excellent agreement with each other and reveal several interesting outcomes. Specifically, the excitation wavelength dependent fluorescence studies reveal an evolution of spatial heterogeneity with the increase in the chain length of the HBDs in these solvents. The time-resolved fluorescence anisotropy and FCS studies show a significant increase of dynamic heterogeneity with increasing chain length of the HBDs. The variation of spatial and dynamic heterogeneity with the change in the hydroxyl group position is found to be insignificant. Additionally, this study shows that the solute molecules reside in different environments of the nanoheterogeneous structure of these solvents and specific solute–solvent hydrogen-bonding interaction plays a crucial role in determining both the rotational and translational diffusion dynamics of AP in these DESs.

Conflicts of interest

There are no conflicts to declare.

Acknowledgements

This work is supported by Research Grant No. EMR/2015/000582 and J. C. Bose Fellowship (to A. S.) of the Science and Engineering Research Board (SERB), Department of Science and Technology (DST), India. We also acknowledge the UGC-UPE and DST-PURSE support to our University. S. S. H. thanks UGC for a Fellowship.

References

1 C. Ruß and B. Konig, *Green Chem.*, 2012, **14**, 2969–2982.
2 D. A. Alonso, A. Baeza, R. Chinchilla, G. Guillena, I. M. Pastor and D. J. Ramón, *Eur. J. Org. Chem.*, 2016, 612–632.
3 Y. Gu and F. Jérôme, *Chem. Soc. Rev.*, 2013, **42**, 9550–9570.
4 A. P. Abbott, G. Capper, K. J. McKenzie and K. S. Ryder, *Electrochim. Acta*, 2006, **51**, 4420–4425.
5 A. P. Abbott, G. Capper, D. L. Davies, R. K. Rasheed and P. Shikotra, *Inorg. Chem.*, 2005, **44**, 6497–6499.
6 A. P. Abbott, G. Capper, A. Glidle and K. S. Ryder, *Phys. Chem. Chem. Phys.*, 2006, **8**, 4214–4221.
7 D. Carriazo, M. C. Serrano, M. C. Gutiérrez, M. L. Ferrer and F. D. Monte, *Chem. Soc. Rev.*, 2012, **41**, 4996–5014.
8 J.-H. Liao, P.-C. Wu and Y.-H. Bai, *Inorg. Chem. Commun.*, 2005, **8**, 390–392.
9 D. Z. Troter, Z. B. Todorović, D. R. Đokić-Stojanović, O. S. Stamenković and V. B. Veljković, *Renewable Sustainable Energy Rev.*, 2016, **61**, 473–500.
10 C. A. Nkuku and R. J. LeSuer, *J. Phys. Chem. B*, 2007, **111**, 13271–13277.
11 H.-R. Jhong, D. S.-H. Wong, C.-C. Wan, Y.-Y. Wang and T.-C. Wei, *Electrochem. Commun.*, 2009, **11**, 209–211.
12 D. V. Wagle, H. Zhao and G. A. Baker, *Acc. Chem. Res.*, 2014, **47**, 2299–2308.
13 H.-G. Liao, Y.-X. Jiang, Z.-Y. Zhou, S.-P. Chen and S.-G. Sun, *Angew. Chem.*, 2008, **120**, 9240–9243.
14 Y. P. Mbous, M. Hayyan, A. Hayyan, W. F. Wong, M. A. Hashima and C. Y. Looi, *Biotechnol. Adv.*, 2017, **35**, 105–134.
15 R. B. Leron and M.-H. Li, *Thermochim. Acta*, 2013, **551**, 14–19.
16 R. B. Leron and M.-H. Li, *J. Chem. Thermodyn.*, 2013, **57**, 131–136.
17 A. P. Abbott, R. C. Harris, K. S. Ryder, C. D'Agostino, L. F. Gladden and M. D. Mantle, *Green Chem.*, 2011, **13**, 82–90.
18 B. Tang and K. H. Row, *Monatsh. Chem.*, 2013, **144**, 1427–1454.
19 Q. Zhang, K. D. O. Vigier, S. Royer and F. Jérôme, *Chem. Soc. Rev.*, 2012, **41**, 7108–7146.
20 A. P. Abbott, D. Boothby, G. Capper, D. L. Davies and R. K. Rasheed, *J. Am. Chem. Soc.*, 2004, **126**, 9142–9147.
21 A. P. Abbott, G. Capper, D. L. Davies, R. K. Rasheed and V. Tambyrajah, *Chem. Commun.*, 2003, 70–71.
22 A. Paiva, R. Craveiro, I. Aroso, M. Martins, R. L. Reis and A. R. C. Duarte, *ACS Sustainable Chem. Eng.*, 2014, **2**, 1063–1071.
23 M. Francisco, A. van den Bruinhorst and M. C. Kroon, *Angew. Chem., Int. Ed.*, 2013, **52**, 3074–3085.
24 E. L. Smith, A. P. Abbott and K. S. Ryder, *Chem. Rev.*, 2014, **114**, 11060–11082.
25 C. D'Agostino, R. C. Harris, A. P. Abbott, L. F. Gladden and M. D. Mantle, *Phys. Chem. Chem. Phys.*, 2011, **13**, 21383–21391.
26 C. D'Agostino, L. F. Gladden, M. D. Mantle, A. P. Abbott, I. A. Essa, A. Y. M. Al-Murshedi and R. C. Harris, *Phys. Chem. Chem. Phys.*, 2015, **17**, 15297–15304.
27 O. S. Hammond, D. T. Bowron and K. J. Edler, *Green Chem.*, 2016, **18**, 2736–2744.
28 R. Stefanovic, M. Ludwig, G. B. Webber, R. Atkin and A. J. Page, *Phys. Chem. Chem. Phys.*, 2017, **19**, 3297–3306.
29 A. Das and R. Biswas, *J. Phys. Chem. B*, 2015, **119**, 10102–10113.
30 A. Das, S. Das and R. Biswas, *J. Chem. Phys.*, 2015, **142**, 034505.
31 B. Guchhait, S. Das, S. Daschakraborty and R. Biswas, *J. Chem. Phys.*, 2014, **140**, 104514.
32 B. Guchhait, S. Daschakraborty and R. Biswas, *J. Chem. Phys.*, 2012, **136**, 174503.
33 K. Mukherjee, A. Das, S. Choudhury, A. Barman and R. Biswas, *J. Phys. Chem. B*, 2015, **119**, 8063–8071.
34 T. Pal and R. Biswas, *Chem. Phys. Lett.*, 2011, **517**, 180–185.
35 S. Das, R. Biswas and B. Mukherjee, *J. Phys. Chem. B*, 2015, **119**, 11157–11168.
36 S. Das, R. Biswas and B. Mukherjee, *J. Phys. Chem. B*, 2015, **119**, 274–283.
37 S. Kaur, A. Gupta and H. K. Kashyap, *J. Phys. Chem. B*, 2016, **120**, 6712–6720.
38 A. Faraone, D. V. Wagle, G. A. Baker, E. C. Novak, M. Ohl, D. Reuter, P. Lunkenheimer, A. Loidl and E. Mamontov, *J. Phys. Chem. B*, 2018, **122**, 1261–1267.
39 E. O. Fetisov, D. B. Harwood, I. F. W. Kuo, S. E. E. Warrag, M. C. Kroon, C. J. Peters and J. I. Siepmann, *J. Phys. Chem. B*, 2018, **122**, 1245–1254.
40 A. Pandey, R. Rai, M. Pal and S. Pandey, *Phys. Chem. Chem. Phys.*, 2014, **16**, 1559–1568.
41 A. Pandey, A. Yadav, Bhawna and S. Pandey, *J. Lumin.*, 2017, **183**, 494–506.

42 A. Pandey, Bhawna, D. Dhingra and S. Pandey, *J. Phys. Chem. B*, 2017, **121**, 4202–4212.
43 B. Guchhait, H. A. R. Gazi, H. K. Kashyap and R. Biswas, *J. Phys. Chem. B*, 2010, **114**, 5066–5081.
44 W. Bi, M. Tian and K. H. Row, *J. Chromatogr. A*, 2013, **1285**, 22–30.
45 Z. S. Othman, N. H. Hassan and S. I. Zubairi, *AIP Conf. Proc.*, 2015, **1678**, 050004.
46 H. Cruz, N. Jordão and L. C. Branco, *Green Chem.*, 2017, **19**, 1653–1658.
47 S. S. Hossain and A. Samanta, *J. Phys. Chem. B*, 2017, **121**, 10556–10565.
48 R. M. Harris, PhD thesis, University of Leicester, 2008.
49 D. C. Khara, J. P. Kumar, N. Mondal and A. Samanta, *J. Phys. Chem. B*, 2013, **117**, 5156–5164.
50 S. K. Das and M. Sarkar, *J. Phys. Chem. B*, 2012, **116**, 194–202.
51 A. I. Zvaigzne, J. Wolfe and W. E. A. Jr., *J. Chem. Eng. Data*, 1994, **39**, 541–543.
52 D. D. Perrin, W. L. F. Armarego and D. R. Perrin, *Purification of Laboratory Chemicals*, Pergamon Press, New York, 1980.
53 W. Guo, Y. Hou, S. Ren, S. Tian and W. Wu, *J. Chem. Eng. Data*, 2013, **58**, 866–872.
54 C. Florindo, F. S. Oliveira, L. P. N. Rebelo, A. M. Fernandes and I. M. Marrucho, *ACS Sustainable Chem. Eng.*, 2014, **2**, 2416–2425.
55 Z. Petrasek and P. Schwille, *Biophys. J.*, 2008, **94**, 1437–1448.
56 J. R. Lackowicz, *Principles of Fluorescence Spectroscopy*, Springer, New York, 2006, ch. 24.
57 G. Saroja, T. Soujanya, B. Ramachandram and A. Samanta, *J. Fluoresc.*, 1998, **8**, 405–410.
58 P. K. Mandal, M. Sarkar and A. Samanta, *J. Phys. Chem. A*, 2004, **108**, 9048–9053.
59 L. A. Hallidy and M. R. Topp, *Chem. Phys. Lett.*, 1977, **48**, 40–45.
60 Y. Cui and D. G. Kuroda, *J. Phys. Chem. A*, 2018, **122**, 1185–1193.
61 G. R. Fleming, *Chemical Applications of Ultrafast Spectroscopy*, Oxford University Press, 1986.
62 H. Jin, G. A. Baker, S. Arzhantsev, J. Dong and M. Maroncelli, *J. Phys. Chem. B*, 2007, **111**, 7291–7302.
63 J. A. Ingram, R. S. Moog, N. Ito, R. Biswas and M. Maroncelli, *J. Phys. Chem. B*, 2003, **107**, 5926–5932.
64 E. C. Wu, H. J. Kim and L. A. Peteanu, *J. Phys. Chem. B*, 2017, **121**, 1100–1107.

THE JOURNAL OF PHYSICAL CHEMISTRY B

Article

Cite This: J. Phys. Chem. B 2019, 123, 6842−6850

pubs.acs.org/JPCB

Liquid Structure and Dynamics of Tetraalkylammonium Bromide-Based Deep Eutectic Solvents: Effect of Cation Chain Length

Sk Saddam Hossain, Sneha Paul, and Anunay Samanta*

School of Chemistry, University of Hyderabad, Hyderabad 500 046, India

Supporting Information

ABSTRACT: Deep eutectic solvents (DESs) have emerged in recent years as environmentally sustainable media across several fields. However, knowledge of liquid structure, dynamics, and solute−solvent interactions in many DESs that is essential for exploiting their potential is still lacking. In this work, we make an attempt to obtain some insight into these aspects of a set of less-explored DESs comprising tetraalkylammonium bromide salts and ethylene glycol (EG) by monitoring the fluorescence response of some carefully chosen dipolar (C153 and 4-AP) and nonpolar (9-PA) solutes in these media. Specifically, we have studied the translational and rotational diffusion dynamics of these molecular systems using single-molecule-based fluorescence correlation spectroscopy technique and ensemble-based time-resolved fluorescence anisotropy measurements. These results point to spatial and dynamic heterogeneity of these DESs, which becomes prominent in systems comprising cations with a longer alkyl chain length. This study reveals that diffusion dynamics of the probe molecules is determined not only by the solvent bulk viscosity but also dependent on their microenvironments and solute−solvent interactions experienced in these media.

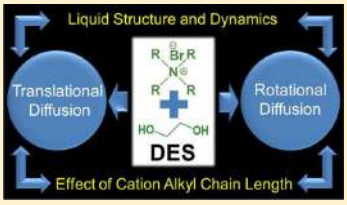

INTRODUCTION

DESs are an emerging class of environmentally sustainable solvents with a potential to overcome many limitations of the conventional organic solvents and ionic liquids (ILs).[1−7] Although similar in many ways to the ILs, these DESs are more favored green alternative to the organic solvents in a variety of applications because of relatively inexpensive starting materials, often made of natural and biodegradable constituents, ease of synthesis, and low toxicity.[1−4,6,8−10] These solvents are generally obtained by mixing a salt/hydrogen bond acceptor (HBA) and a hydrogen bond donor (HBD).[1] A large number of such mixtures with desirable properties can be prepared by judicious choice of the constituents and also by varying their stoichiometric molar ratio.[1,11]

A survey of literature shows that most of the works on DESs are application-oriented and fundamental studies directed toward understanding their physicochemical properties in terms of microscopic structure, dynamics, solute−solvent interactions, and so forth are rather limited.[1,2,5,8−10,12−21] These studies, most of which have been carried out in choline chloride (ChCl)-based DESs, have brought into light spatial and/or dynamic heterogeneity of these solvents, which contribute to some of the unique properties of these DESs. Several new but promising DESs based on various other salts are gaining attention recently.[22−34] However, little is known about the microscopic structural and dynamical features of these less-explored substances that are necessary for realization of the successful utility of these mixtures in different fields.

The objective of this study is to obtain an understanding of some of these promising but less-explored eutectic solvents through characterization of the microscopic structure, dynamics, and solute−solvent interactions. Additionally, we probe how the alkyl chain length attached to the cation of the salt influences these fundamental aspects. For this purpose, we have chosen three DESs[22,34] based on tetraalkylammonium bromide (TAAB) salts with different alkyl chain length and EG (Table 1) and examined their liquid-state structure and dynamics by probing the translation and rotation diffusion dynamics of dipolar molecules, coumarin 153 (C153) and 4-aminophthalimide (4-AP), and a nonpolar molecule, 9-phenylanthracene (9-PA), in these media. An identical salt/HBD molar ratio (1:3) in these DESs is chosen to ensure that the observed changes in the fluorescence properties of the probe molecules in different DESs are not due to any variation of the concentration of the salt or EG (HBD). The translation diffusion dynamics of the solutes is studied using fluorescence correlation spectroscopy (FCS) technique, whereas the rotational diffusion dynamics is investigated by monitoring

Table 1. Description of the DESs Used in This Study

sl. no.	salt[a]	HBD	mole ratio (salt/HBD)	abbreviation	water content (wt %)
1	TEAB	EG	1:3	TEAB−EG	0.09
2	TPAB	EG	1:3	TPAB−EG	0.07
3	TBAB	EG	1:3	TBAB−EG	0.08

[a]TEAB: tetraethylammonium bromide; TPAB: tetrapropylammonium bromide; and TBAB: tetrabutylammonium bromide.

Received: May 24, 2019
Revised: July 4, 2019
Published: July 16, 2019

DOI: 10.1021/acs.jpcb.9b04955
J. Phys. Chem. B 2019, 123, 6842−6850

time-dependent fluorescence anisotropy of the systems. Chart S1 (Supporting Information) depicts the molecular structures of the solutes and constituents of the DESs. The idea behind employing multiple probe molecules with different functional groups is that the chosen systems are expected to place themselves in different locations of a structured medium and together they will present a complete picture of all possible microenvironments and interactions operative in the media[35,36] and provide comprehensive insights into the structural and dynamical aspects of these less-explored DESs.

EXPERIMENTAL SECTION

Materials. Tetraethylammonium bromide (TEAB) (>98%, CAS no. 71-91-0), tetrapropylammonium bromide (TPAB) (>98%, CAS no. 1941-30-6), and tetrabutylammonium bromide (TBAB) (>99%, CAS no. 1643-19-2) were procured from TCI Chemicals. EG (≥99%, CAS no. 107-21-1) was obtained from Sigma-Aldrich. These chemicals were dried under high vacuum for 2 days before their use in synthesis. C153 (CAS no. 53518-18-6), 4-AP (CAS no. 3676-85-5), and 9-PA (CAS no. 602-55-1) were procured from Eastman Kodak, TCI Chemicals, and Sigma-Aldrich, respectively, and used as received. Methanol (CAS no. 67-56-1) and hexane (CAS no. 110-54-3) were obtained from Merck and purified following standard procedures prior to use. Methanol-d_4 (≥99.8 atom %D, CAS no. 811-98-3) was purchased from Sigma-Aldrich and used as received.

Synthesis and Characterization of DESs. Each DES was prepared according to the reported procedure.[22] Briefly, TAAB salt (1 mol) and EG (3 mol) were mixed in a conical flask and heated at 353 K in an oil bath with constant stirring until a transparent homogeneous liquid was obtained. The liquids were then slowly cooled down to room temperature and stored in an inert atmosphere prior to experiments. The purity of the synthesized DESs (and their constituents) was checked through ^{1}H NMR spectroscopy (Figure S1, Supporting Information). Fourier transform infrared (FTIR) spectra confirm the structural identity of the DESs (Figure S2). The NMR and IR spectra of the DESs match well with the other reported DESs[32,37,38] and indicate that no side reactions occurred during the synthesis of the DESs and the synthesized liquids were pure. The viscosities of the DESs at 298 K were measured to be 28.0, 72.5, and 98.0 cP for TEAB−EG, TPAB−EG, and TBAB−EG, respectively. These values are in agreement with previously reported values.[22,33] The water content in the liquids was determined after drying under high vacuum for several hours. The measured values (Table 1) are in good agreement with the other DESs.[39]

Sample Preparation. Solutions of individual solutes were prepared in methanol, except 9-PA, for which the solution was made in hexane. An aliquot of freshly prepared solution of the solutes was transferred into a reagent bottle and the solvent was subsequently evaporated by flowing a high-purity N_2 gas. Then, a measured amount of DES was added into the reagent bottle, tightly sealed with parafilm, and mixed thoroughly to ensure complete solubilization of the solutes. This solution was stored in an inert atmosphere prior to experiments and used as stock solution. A micromolar (μM) solution of the DESs was used for steady-state and time-resolved fluorescence measurements while nanomolar (nM) solution was used for the FCS measurements.

Instrumentation and Methods. ^{1}H NMR and FTIR spectra were recorded using an NMR spectrometer (Bruker AVANCE, 500 MHz) and an FTIR spectrometer (Bruker Tensor II), respectively. The viscosities of DESs were measured at different temperatures by employing a Brookfield (LVDV-III Ultra) cone and plate viscometer (0.2% repeatability and 1% accuracy), which was equipped with an external Julabo water circulator (model F32). The water contents of the DESs were measured using a Karl Fisher coulometer (METTLER TOLEDO DL39).

The steady-state absorption and emission/excitation spectra were recorded using a UV−vis spectrophotometer (Cary100, Varian) and spectrofluorometer (FluoroLog-3, HORIBA Jobin Yvon), respectively. Time-resolved fluorescence anisotropy measurements were performed using a time-correlated single-photon counting spectrometer (HORIBA Jobin Yvon IBH). The details of the setup were described elsewhere.[40] Briefly, diode lasers (375 and 405 nm, 60 ps pulse width) and an MCP photomultiplier (Hamamatsu R3809U-50) were employed as the excitation sources and detector, respectively. For time-resolved fluorescence anisotropy measurements, the fluorescence intensities of the solutes were collected alternatively in parallel ($I_{||}$) and perpendicular ($I_{\perp}$) polarizations (with respect to the vertically polarized excitation laser) for equal intervals of time until the count difference between the two polarizations (at $t = 0$) was ∼5000. The anisotropy decay, $r(t)$, was then calculated using the equation

$$r(t) = \frac{I_{||}(t) - GI_{\perp}(t)}{I_{||}(t) + 2GI_{\perp}(t)} \quad (1)$$

where G is the correction factor for the detector sensitivity to the polarization of the emission which was calculated following a procedure described elsewhere.[41] Fluorescence anisotropy decay curves were analyzed using IBH DAS6 (version 2.2) decay analysis software. The temperature-dependent anisotropy measurements were performed by using a water circulator described previously.

The FCS measurements were performed with an inverted confocal fluorescence microscope (MicroTime 200, PicoQuant). The details of the setup can be found elsewhere.[41] A pulsed diode laser (405 nm, fwhm 176 ps, and repetition rate 20 MHz) was used as the excitation source. The output of the laser was focused onto the sample placed on a coverslip using a water immersion objective (Olympus UPlansApo, NA 1.2, 60X). Fluorescence signal collected by the same objective was then passed through the dichroic mirror and 430 nm long-pass filter followed by a 50 μm pinhole. The signal was then directed onto a 50:50 beam splitter to divide the signal before entering the two single-photon avalanche photodiodes (SPADs). The FCS measurements were performed by placing a highly dilute solution (10−20 nM) on a coverslip placed on top of the objective. The fluctuations of fluorescence intensity were measured in a small detection volume (∼0.45 fL) by using focused laser beam and pinhole. These fluctuating fluorescence signals detected by two SPAD detectors were then cross-correlated to obtain the correlation function $G(\tau)$, which is given by

$$G(\tau) = \frac{\langle \delta F(t)\delta F(t+\tau)\rangle}{\langle F(t)\rangle^2} \quad (2)$$

where $\langle F(t)\rangle$, $\delta F(t)$, and $\delta F(t+\tau)$ are the average fluorescence intensity, the fluctuations in intensity from the average value at time t and $(t+\tau)$, respectively, and are given by

DOI: 10.1021/acs.jpcb.9b04955
J. Phys. Chem. B 2019, 123, 6842−6850

$$\delta F(t) = F(t) - \langle F(t)\rangle \quad (3a)$$

$$\delta F(t+\tau) = F(t+\tau) - \langle F(t)\rangle \quad (3b)$$

Calibration of the excitation volume (~0.45 fL) was done using Rhodamine 6G (diffusion coefficient of 426 $\mu m^2 \cdot s^{-1}$ in water).[42] The excitation power was kept at ~3 μW during all FCS measurements. The data were analyzed using SymPhoTime (PicoQuant) and Igor pro (Version 6.37, Wavemetrics) software.

RESULTS AND DISCUSSION

Steady-State Measurements: Microscopic Polarity and Liquid Structure. The steady-state excitation and emission spectra of the probe molecules in DESs were measured at room temperature (298 K). The spectral data, which are summarized in Table 2 (spectra in Figure S3), shows

Table 2. Steady-State Excitation and Emission Maxima of the Solutes in DESs at 298 K

	C153		4-AP		9-PA	
DESs	λ_{exc}^{max} (nm)	λ_{emm}^{max} (nm)	λ_{exc}^{max} (nm)	λ_{emm}^{max} (nm)	λ_{exc}^{max} (nm)	λ_{emm}^{max} (nm)
TEAB–EG	430	539	372	504	387	400
TPAB–EG	430	535	371	501	387	400
TBAB–EG	430	530	372	498	387	400

that the excitation maxima (λ_{exc}^{max}) of all solute molecules are independent of the solvents, whereas the emission maxima (λ_{emm}^{max}) of the dipolar solutes (C153 and 4-AP) show noticeable solvent dependence (a blue shift of 6–9 nm with an increase in alkyl chain length of the constituent cation of the DESs). The observed solvent dependence of λ_{exc}^{max} and λ_{emm}^{max} of the probe molecules is consistent with literature.[43,44] Only the λ_{emm}^{max} values of C153 and 4-AP are sensitive to the solvent as emission of these two dipolar systems originates from intramolecular charge-transfer state, whose position is dependent on both polarity of the media and hydrogen-bonding interaction with the solvent. The λ_{emm}^{max} values of these two indicate that these molecules experience a less polar environment with increase in alkyl chain length of the cation of the solvent.[45] A comparison of the measured λ_{emm}^{max} values of the two molecules with those in other conventional solvents and DESs reveals that the polarity of the microenvironment sensed by the two dipolar probes in the present DESs is similar to that of methanol and that experienced in ChCl-diol-based eutectic solvents.[15,40]

One of the approaches to examine whether a polar viscous medium such as DES is spatially heterogeneous or not is by studying dependence of the λ_{emm}^{max} value on λ_{exc} of dipolar molecules, which fulfill certain criteria.[46−48] A dipolar molecule can exhibit excitation-wavelength-dependent shift of its λ_{emm}^{max} in viscous polar environment, when excited at its long-wavelength absorption edge. The phenomenon, known as "red-edge effect", is observed in polar viscous media for molecules that exhibit a large change in dipole moment on excitation and are characterized by short fluorescence lifetime.[46,48] In order to explore the microscopic liquid structure of the present DESs in terms of the spatial heterogeneity, if any, we have examined λ_{exc} dependence of λ_{emm}^{max} of ANF, a molecule which exhibits a huge change in dipole moment ($\Delta\mu$ = 25 D[46]) on excitation and characterized by a very short excited-state lifetime (τ_f) (τ_f < 50 ps in 2-propanol[49]) compared to C153 (τ_f = 4.1 ns in methanol[40]) and 4-AP (τ_f = 6.8 ns in methanol[40]), which do not exhibit any excitation wavelength-dependent fluorescence behavior (Figure S4). Figure 1 shows that ANF exhibits

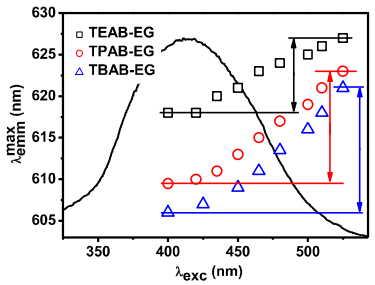

Figure 1. Dependence of the emission maximum (λ_{emm}^{max}) on the excitation wavelength (λ_{exc}) for ANF at 298 K in three DESs. Representative excitation spectrum of ANF is also shown.

significant excitation wavelength dependence of λ_{emm}^{max} in all three DESs, indicating the heterogeneous nature of these solvents. That C153 and 4-AP do not show any λ_{exc} dependence, but only ANF does, is primarily because τ_f of ANF is much shorter than the average solvent relaxation time (τ_s) of common DESs,[50,51] and hence, the emission, instead of originating from a fully solvent-equilibrated state, occurs from a state determined by the λ_{exc} value. A more prominent excitation wavelength-dependent emission behavior in longer alkyl chain length containing DESs indicates an enhanced spatial heterogeneity of these media. This enhanced spatial heterogeneity of the long alkyl chain length containing DESs is very similar to that observed for various ILs.[45,52−54] Hence, by drawing an analogy with the ILs, one can infer that the spatial heterogeneity of these DESs arises from the formation of hydrophobic and hydrophilic domain-like structure because of segregation of the alkyl chains from the ionic moieties of the cation and hydroxyl moieties of the HBD.[13,45,52−55]

FCS Measurements: Translational Diffusion Dynamics. As diffusion of a molecule depends on its surrounding environment and the interactions it experiences with the solvent, one can obtain an understanding of the nature of the medium by monitoring the diffusion dynamics of the probe molecules. Single-molecule-based FCS technique is a powerful and sensitive tool for studying diffusion and hence for the characterization of microscopic structural and dynamical features of complex media such as ILs and DESs.[40,41,52,56,57] We have studied the translation diffusion of C153 and 4-AP in the chosen DESs using this technique. Figure 2 shows representative time-dependence of the fluorescence correlation data of the two probe molecules in TPAB–EG at 298 K (data in other DESs are shown in Figures S5 and S6).

As the fits of the correlation data to a single-component diffusion model (eq 4 with β = 1) were found unsatisfactory, the data were fitted to anomalous diffusion model (β < 1), according to which mean square displacement of the solute molecules follows a subdiffusive behavior, $\langle r(\tau)^2\rangle \propto \tau^{\beta}$ (with β < 1), instead of normal Brownian diffusion (β = 1).[57]

$$G(\tau) = \frac{1}{N}\left[1 + \left(\frac{\tau}{\tau_D}\right)^{\beta}\right]^{-1}\left[1 + \left(\frac{r_0}{z_0}\right)^2\left(\frac{\tau}{\tau_D}\right)^{\beta}\right]^{-1/2} \quad (4)$$

DOI: 10.1021/acs.jpcb.9b04955
J. Phys. Chem. B 2019, 123, 6842−6850

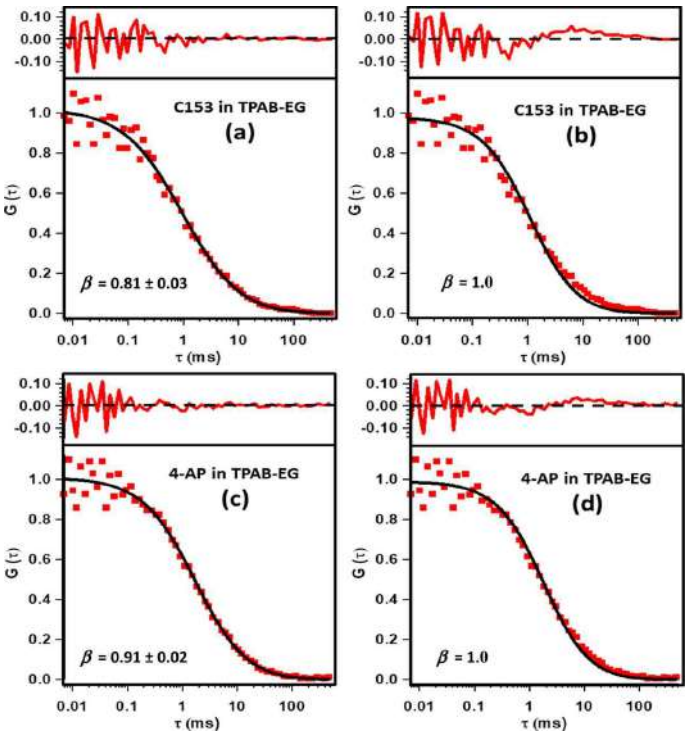

Figure 2. Normalized fluorescence correlation data of C153 and 4-AP in TPAB−EG. The solid lines represent fit to the data using anomalous diffusion model (left panel: a,c) and single-component diffusion model (right panel: b,d). The β values obtained from the fits are shown in the figure. The residuals showing the quality of the fits are also shown at the top of each panel.

Table 3. Estimated Diffusion Coefficients (D_t in $\mu m^2 \cdot s^{-1}$) and Stretching Exponents (β) for the Solutes in DESs

		C153		4-AP	
DESs	viscosity (cP)	D_t	β	D_t	β
TEAB−EG	28.0	31.6 ± 4.7	0.87 ± 0.02	25.0 ± 3.9	0.90 ± 0.03
TPAB−EG	72.5	14.5 ± 1.9	0.81 ± 0.03	8.1 ± 2.5	0.91 ± 0.02
TBAB−EG	98.0	11.4 ± 1.6	0.72 ± 0.03	4.8 ± 1.1	0.88 ± 0.02

Here, N is the average number of emissive molecules present in the observation volume, τ_D is the time taken by the molecule to diffuse through the observation volume (diffusion time), τ is the lag time, and β ($0 < \beta < 1$) is the stretching exponent representing the distribution of τ_D. k, given by z_0/r_0, represents the structural parameter of the observation volume (where z_0 and r_0 are the axial and lateral radii of the observation volume, respectively). The translation diffusion coefficients (D_t) of the probe molecules, calculated using the measured τ_D values employing eq 5, are collected in Table 3.

$$D_t = \frac{r_0^2}{4\tau_D} \tag{5}$$

It is seen that the D_t value of both solutes decreases substantially from TEAB−EG to TBAB−EG mainly because of increasing viscosity of the solvents. Another point to note is that the D_t value of 4-AP is smaller than that of C153 in all the solvents, even though the size of 4-AP (134 Å^3) is almost half than that of C153 (246 Å^3).[40] This observation clearly suggests strong association of 4-AP with the constituents of DESs, which must be through strong solute−solvent hydrogen-bonding interaction, as 4-AP is well known for such interaction both in molecular solvents[58] and ILs.[35,53] Another point to note is that the D_t value of 4-AP decreases more sharply compared to C153 with increasing cation chain length of the DESs (Figure 3). This indicates that the change in the D_t values is not solely due to solvent viscosity.

An important point to note here is that the stretching exponent β deviates notably from unity for both solutes in these solvents. As these solute molecules show single-component translational diffusion ($\beta = 1$) in homogeneous media,[54] the observed deviation in the present case indicates dynamic heterogeneity in these solvents, which results from the fluctuations of the hydrogen bond network and consequent motion of the constituents of these media.[50,59] It is pertinent to note here that FCS studies have been performed earlier to study the translation diffusion dynamics of several solute molecules in ILs and DESs.[40,52,54,60] Wu et al. observed anomalous diffusion dynamics of Nile Red in ILs, which they explained in terms of dynamic heterogeneity of the solvent.[60] We have also recently attributed similar anomalous diffusion dynamics of dipolar molecules in a series of ChCl-diol-based

DOI: 10.1021/acs.jpcb.9b04955
J. Phys. Chem. B 2019, 123, 6842−6850

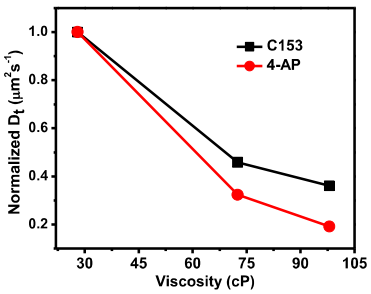

Figure 3. Viscosity dependence of the D_t values (normalized) of C153 and 4-AP in DESs.

DESs containing different hydrocarbon chain lengths of the HBD (diol) because of dynamic heterogeneity of the media.[40]

Further, Table 3 shows that, while the deviation of the β value for C153 is more prominent in solvents containing cation with longer alkyl chain length, for 4-AP, the β value is almost constant (and high) in all three DESs. These indicate that unlike C153, which experiences increasing dynamic heterogeneity in solvents containing larger cations, 4-AP experiences relatively less and very similar dynamic heterogeneity in these solvents because of its strong association with the constituents of the solvents. A similar trend was observed in ChCl-diol-based DESs as well.[40]

Time-Resolved Fluorescence Anisotropy Measurements: Rotational Diffusion Dynamics. To probe the microenvironments around the probe molecules in these solvents, we have also studied time-resolved fluorescence anisotropy of C153, 4-AP, and 9-PA in all three DESs over a temperature range from 298 to 348 K. Representative anisotropy decay profiles (Figure 4) of the solutes highlight the influence of solvents. The decay profiles are found to be biexponential for C153, but single-exponential for the other two systems in all DESs at all temperatures.

The measured rotational reorientation times (τ_r) of the solutes at six different temperatures are plotted in Figure 5 and Table S1. At any given temperature (e.g., 298 K, Table 4) in a given DES, the τ_r values of C153 and 9-PA are much smaller than that of 4-AP even though two former solutes are twice as large compared to the latter. The difference in the τ_r values of 4-AP from other two solutes is more prominent in longer alkyl chain length containing solvents, where it is more associated with the solvent. As expected, the τ_r values of the solutes decrease with increasing temperature in all DESs because of the decrease of solvent viscosity (Figure 5). We have also measured and compared the τ_r values of the solutes in isoviscous condition by adjusting the temperatures of the media to find out the difference in interactions between the probe molecules and solvents (Table 4). Under isoviscous condition, the τ_r values of C153 and 9-PA are lower in higher alkyl chain length containing solvent, but for 4-AP, the trend is quite opposite. This also indicates that the solute−solvent interactions experienced by the probe molecules are quite different.

We now analyze the measured rotational diffusion dynamics in terms of the Stokes−Einstein−Debye (SED) hydrodynamic theory,[56,61] according to which the reorientation time (τ_r) of a probe molecule in a solvent of viscosity η at temperature T is given by

$$\tau_r = \frac{\eta V f C}{k_B T} \tag{6}$$

where V and f are the van der Waals volume and shape factor of the molecule, respectively, and k_B is the Boltzmann constant. The shape factor (f) describes nonspherical nature of the probe molecules, which are treated as asymmetric ellipsoids. C is the boundary condition parameter that represents two limiting cases for the degree of solute−solvent interactions, where $C_{stick} = 1$ for stick condition and $0 < C_{slip} < 1$ for slip condition. The V, f, and C values for the probe molecules are taken from the literature[36,40] and collected in Table 5.

Figure 6 depicts plots of the measured τ_r values of the solutes against η/T in TEAB−EG along with the hydrodynamic stick and slip lines. Similar plots in other two solvents, TPAB−EG and TBAB−EG, are provided in Figure S8. It is evident that the τ_r values of both C153 and 9-PA lie between the slip and stick lines in TEAB−EG. They, however, gradually shift toward the slip boundary condition at low temperature, with increasing cation alkyl chain length of the DESs. In contrast, 4-AP exhibits a superstick behavior in TEAB−EG and the superstick nature increases with increasing alkyl chain length. This superstick behavior of 4-AP is reported previously both in conventional solvents and ILs and attributed to strong association of 4-AP with the solvents through hydrogen-bonding interactions.[35,53,56,62] A similar stick/superstick rotational dynamics of 4-AP is also observed in ChCl-diol-based DESs because of the same reason.[40] The other two systems (C153 and 9-PA), however, not associated like 4-AP and exhibit faster rotation. We have also estimated the solute−solvent coupling constant (C_{obs}) from the experimental τ_r value and calculated rotational reorientation time (τ_{stick}) for stick

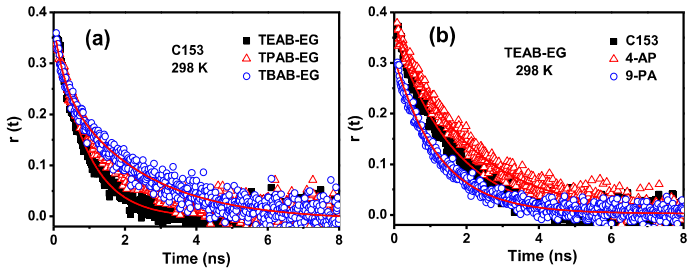

Figure 4. (a) Anisotropy decay profiles of C153 in DESs at 298 K. Panel (b) compares the anisotropy decay profiles of the three solutes in TEAB−EG. The solid lines represent fit to the experimental data. The excitation wavelength for C153 and 4-AP is 405, while for 9-PA, the excitation wavelength is 375 nm. In all cases, the monitoring wavelengths are steady-state emission peak maxima.

DOI: 10.1021/acs.jpcb.9b04955
J. Phys. Chem. B 2019, 123, 6842−6850

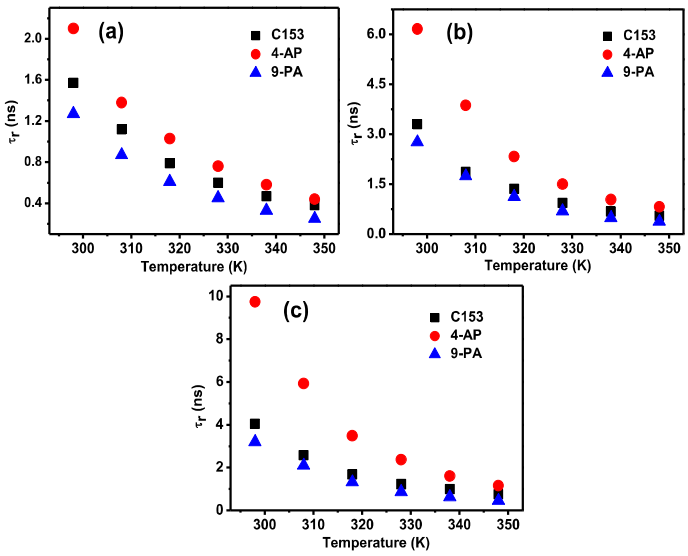

Figure 5. (a) Temperature dependence of the τ_r values of the solutes in TEAB–EG (a), TPAB–EG (b), and TBAB–EG (c).

Table 4. Estimated τ_r Values (ns) of the Solutes in DESs under Different Conditions

		isothermal (298 K)			isoviscous (28 cP)		
DESs	viscosity (cP)	C153[a]	4-AP	9-PA	C153[a]	4-AP	9-PA
TEAB–EG	28.0	1.57	2.10	1.27	1.57	2.10	1.27
TPAB–EG	72.5	3.30	6.16	2.76	1.46	2.51	1.18
TBAB–EG	98.0	4.05	9.75	3.20	1.39	2.90	1.11

[a]Average τ_r values (ns).

Table 5. Solute Size, Shape Parameters, and Boundary Condition Parameters (C_{slip}) of the Solutes Calculated from the SED Hydrodynamic Theory

solute	axial radii (Å^3)	van der Waals volume, V (Å^3)	shape factors (f)	C_{slip}
C153[a]	6.1 × 4.8 × 2.2	246	1.71	0.24
4-AP[a]	5.0 × 3.5 × 1.8	134	1.60	0.11
9-PA[b]	5.7 × 5.5 × 1.8	236	1.73	0.12

[a]Values from ref 40. [b]From ref 36.

boundary conditions using $C_{obs} = \tau_r/\tau_{stick}$. These values (Table 6) are lower for C153 and 9-PA in longer alkyl chain length containing solvents, but for 4-AP, the trend is very opposite. This observation is in agreement with the trend observed earlier.

Next, we check the linearity of the measured τ_r values with η/T by fitting the data to equation $\tau_r = A(\eta/T)^p$, where any deviation of the value of parameter (p) from unity would indicate a departure from the SED hydrodynamic behavior and the degree of viscosity–diffusion coupling.[41,50] The p values obtained from fits of the τ_r values using this equation (dashed lines in Figures 6 and S8) are presented in Table 7. The deviation of the p values from unity ($p < 1$) reflects viscosity–diffusion decoupling because of dynamic heterogeneity of the media.[50,55] A larger deviation of the p values from unity for both C153 and 9-PA with increase in cation alkyl chain length indicates an enhanced dynamic heterogeneity of these media. For 4-AP, the p values are high in all three DESs and they hardly vary with cation alkyl chain length, suggesting that it experiences relatively less and similar dynamic heterogeneity in these media because of strong interaction with the solvents. A similar increase of the heterogeneity in ChCl-diol-based DESs with increasing hydrocarbon chain length of the HBD is also reported recently.[40]

This steady change of the coupling constants as well as the degree of nonlinearity of the τ_r values on η/T with increasing cation alkyl chain length can be explained considering the existence of spatial heterogeneities in these DESs (which is indeed observed from the steady-state measurements) because of the formation of organized domain-like structure consisting of polar and nonpolar regions. The association of the alkyl chains attached to the cations induces formation of nonpolar domains, whereas the Coulombic interactions between the ionic moieties and hydrogen-bonding interactions with hydroxyl moieties of the HBD give rise to the ionic polar domains.[13,55] The formation of this type of domains owing to molecular-scale segregation in other DESs has already been established by neutron diffraction studies and simulations.[23] The experimental data presented here suggests that 4-AP molecules reside in the polar region, 9-PA resides specifically in nonpolar region, and C153 aligns itself at the interface of nonpolar and polar regions. As the cation alkyl chain length increases, the size of the nonpolar domain and excluded volume because of lower packing (void space) also increase. As a consequence, a reduced friction is experienced by C153 and 9-PA molecules and their rotational diffusion becomes faster. On the other hand, with increasing hydrophobic chain length,

DOI: 10.1021/acs.jpcb.9b04955
J. Phys. Chem. B 2019, 123, 6842–6850

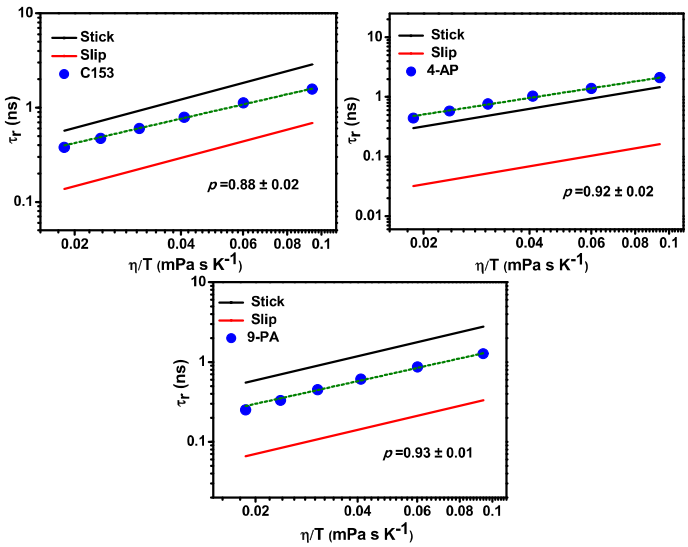

Figure 6. Plots of τ_r vs η/T for three solutes in TEAB−EG. The solid circles are the measured rotational times and the dashed lines represent fit to the data according to $\tau_r = A(\eta/T)^p$. The p values obtained from the fits are shown in the figure. The stick (black) and slip (red) lines, computed using SED theory, are also shown.

Table 6. Calculated C_{obs} Values of the Solutes in Six DESs at 298 K

	C_{obs}		
DESs	C153	4-AP	9-PA
TEAB−EG	0.55 ± 0.02	1.44 ± 0.02	0.46 ± 0.02
TPAB−EG	0.45 ± 0.01	1.63 ± 0.02	0.38 ± 0.015
TBAB−EG	0.41 ± 0.01	1.91 ± 0.03	0.33 ± 0.01

Table 7. p Values Obtained from Least-Squares Fits of τ_r vs η/T Plots in DESs

	C153	4-AP	9-PA
DESs	p	p	p
TEAB−EG	0.88 ± 0.02	0.92 ± 0.02	0.93 ± 0.01
TPAB−EG	0.83 ± 0.03	0.90 ± 0.03	0.87 ± 0.02
TBAB−EG	0.76 ± 0.02	0.91 ± 0.02	0.82 ± 0.02

as overall nonpolar fraction of the solvents increases, more 4-AP molecules move closer toward the −OH groups in the polar region and the solute rotation diffusion becomes slower because of enhanced hydrogen-bonding interaction. Similar effect of domain formation on rotational diffusion of probe molecules has already been described in ILs.[53]

CONCLUSIONS

We have studied translational and rotational diffusion dynamics of some selected solute molecules in a series of less-explored DESs by monitoring their fluorescence response to obtain an understanding of the liquid-state structure of these solvents. The results suggest both spatial and dynamic heterogeneity in these media, which becomes more pronounced in longer alkyl chain containing more viscous solvents. The spatial heterogeneity of these media, which arises from molecular-scale domain formation because of segregation of the ionic moieties (along with the hydroxyl moieties of the HBD) and the hydrophobic alkyl chain of the salt, becomes more pronounced in longer chain length containing solvents. As the probe molecules reside in the different regions of the solvents, they experience different solute−solvent interactions and exhibit translational and rotational dynamics. The present findings and recent results[40] show that the spatial and dynamic heterogeneity of the ionic DESs can be modified significantly by tuning the hydrocarbon chain length of both HBA and HBD of the solvents.

ASSOCIATED CONTENT

Supporting Information

The Supporting Information is available free of charge on the ACS Publications website at DOI: 10.1021/acs.jpcb.9b04955.

Molecular structures of the constituents of the DESs and solute molecules; 1H NMR and FTIR spectra of the DESs along with their constituents, excitation, and emission spectra of C153, 4-AP, and 9-PA in the DESs; excitation wavelength dependence of the emission maxima of C153 and 4-AP; FCS data of C153 and 4-AP in TEAB−EG and TBAB−EG; viscosity of the solvents at different temperatures; τ_r vs η/T plots of the solutes in TPAB−EG and TBAB−EG; and estimated τ_r values of C153, 4-AP, and 9-PA in various DESs at different temperatures (PDF)

AUTHOR INFORMATION

Corresponding Author

*E-mail: anunay@uohyd.ac.in.

ORCID

Sk Saddam Hossain: 0000-0002-5740-3703
Sneha Paul: 0000-0002-0631-1980
Anunay Samanta: 0000-0003-1551-0209

Notes

The authors declare no competing financial interest.

DOI: 10.1021/acs.jpcb.9b04955
J. Phys. Chem. B 2019, 123, 6842−6850

■ ACKNOWLEDGMENTS

This work is supported by Research grant no EMR/2015/000582 and J. C. Bose Fellowship (to A.S.) of the Science and Engineering Research Board (SERB), Department of Science and Technology (DST), India, and Mid-Career Award (to A.S.) of the University Grants Commission (UGC). The authors also acknowledge the UGC-UPE and DST-PURSE support to our University. S.S.H. and S.P. thank UGC for Fellowships.

■ REFERENCES

(1) Smith, E. L.; Abbott, A. P.; Ryder, K. S. Deep Eutectic Solvents (DESs) and Their Applications. *Chem. Rev.* **2014**, *114*, 11060−11082.
(2) Abbott, A. P.; Capper, G.; Davies, D. L.; Rasheed, R. K.; Tambyrajah, V. Novel Solvent Properties of Choline Chloride/Urea Mixtures. *Chem. Commun.* **2003**, *1*, 70−71.
(3) Alonso, D. A.; Baeza, A.; Chinchilla, R.; Guillena, G.; Pastor, I. M.; Ramón, D. J. Deep Eutectic Solvents: The Organic Reaction Medium of the Century. *Eur. J. Org. Chem.* **2016**, *2016*, 612−632.
(4) Paiva, A.; Craveiro, R.; Aroso, I.; Martins, M.; Reis, R. L.; Duarte, A. R. C. Natural Deep Eutectic Solvents-Solvents for the 21st Century. *ACS Sustainable Chem. Eng.* **2014**, *2*, 1063−1071.
(5) Zhang, Q.; De Oliveira Vigier, K.; Royer, S.; Jérôme, F. Deep Eutectic Solvents: Synthesis, Properties and Applications. *Chem. Soc. Rev.* **2012**, *41*, 7108−7146.
(6) Ruβ, C.; Konig, B. Low Melting Mixtures in Organic Synthesis -An Alternative to Ionic Liquids? *Green Chem.* **2012**, *14*, 2969−2982, DOI: 10.1039/c2gc36005e.
(7) Abbott, A. P.; Boothby, D.; Capper, G.; Davies, D. L.; Rasheed, R. K. Deep Eutectic Solvents Formed Between Choline Chloride and Carboxylic Acids: Versatile Alternatives to Ionic Liquids. *J. Am. Chem. Soc.* **2004**, *126*, 9142−9147.
(8) Abbott, A. P.; Capper, G.; McKenzie, K. J.; Glidle, A.; Ryder, K. S. Electropolishing of Stainless Steels in a Choline Chloride Based Ionic Liquid: An Electrochemical Study With Surface Characterisation Using SEM and Atomic Force Microscopy. *Phys. Chem. Chem. Phys.* **2006**, *8*, 4214−4221.
(9) Abbott, A. P.; Capper, G.; McKenzie, K. J.; Ryder, K. S. Voltammetric and Impedance Studies of the Electropolishing of Type 316 Stainless Steel in a Choline Chloride Based Ionic Liquid. *Electrochim. Acta* **2006**, *51*, 4420−4425.
(10) Cruz, H.; Jordão, N.; Branco, L. C. Deep Eutectic Solvents (DESs) as Low-Cost and Green Electrolytes for Electrochromic Devices. *Green Chem.* **2017**, *19*, 1653−1658.
(11) Francisco, M.; van den Bruinhorst, A.; Kroon, M. C. LowTransition-Temperature Mixtures (LTTMs): A New Generation of Designer Solvents. *Angew. Chem., Int. Ed.* **2013**, *52*, 3074−3085.
(12) Shahbaz, K.; Mjalli, F. S.; Hashim, M. A.; AlNashef, I. M. Using Deep Eutectic Solvents Based on Methyl Triphenyl Phosphunium Bromide for the Removal of Glycerol from Palm-Oil-Based Biodiesel. *Energy Fuels* **2011**, *25*, 2671−2678.
(13) Kaur, S.; Gupta, A.; Kashyap, H. K. Nanoscale Spatial Heterogeneity in Deep Eutectic Solvents. *J. Phys. Chem. B* **2016**, *120*, 6712−6720.
(14) Pandey, A.; Pandey, S. Solvatochromic Probe Behavior within Choline Chloride-Based Deep Eutectic Solvents: Effect of Temperature and Water. *J. Phys. Chem. B* **2014**, *118*, 14652−14661.
(15) Pandey, A.; Rai, R.; Pal, M.; Pandey, S. How Polar are Choline Chloride-Based Deep Eutectic Solvents? *Phys. Chem. Chem. Phys.* **2014**, *16*, 1559−1568.
(16) Stefanovic, R.; Ludwig, M.; Webber, G. B.; Atkin, R.; Page, A. J. Nanostructure, Hydrogen Bonding and Rheology in Choline Chloride Deep Eutectic Solvents As a Function of the Hydrogen Bond Donor. *Phys. Chem. Chem. Phys.* **2017**, *19*, 3297−3306.
(17) Wagle, D. V.; Baker, G. A.; Mamontov, E. Differential Microscopic Mobility of Components within a Deep Eutectic Solvent. *J. Phys. Chem. Lett.* **2015**, *6*, 2924−2928.
(18) Yadav, A.; Pandey, S. Densities and Viscosities of (Choline Chloride + Urea) Deep Eutectic Solvent and Its Aqueous Mixtures in the Temperature Range 293.15 to 363.15 K. *J. Chem. Eng. Data* **2014**, *59*, 2221−2229.
(19) Cui, Y.; Kuroda, D. G. Evidence of Molecular Heterogeneities in Amide-Based Deep Eutectic Solvents. *J. Phys. Chem. A* **2018**, *122*, 1185−1193.
(20) Faraone, A.; Wagle, D. V.; Baker, G. A.; Novak, E. C.; Ohl, M.; Reuter, D.; Lunkenheimer, P.; Loidl, A.; Mamontov, E. Glycerol Hydrogen-Bonding Network Dominates Structure and Collective Dynamics in a Deep Eutectic Solvent. *J. Phys. Chem. B* **2018**, *122*, 1261−1267.
(21) D'Agostino, C.; Harris, R. C.; Abbott, A. P.; Gladden, L. F.; Mantle, M. D. Molecular Motion and Ion Diffusion in Choline Chloride Based Deep Eutectic Solvents Studied by 1H Pulsed Field Gradient NMR Spectroscopy. *Phys. Chem. Chem. Phys.* **2011**, *13*, 21383−21391.
(22) Yusof, R.; Abdulmalek, E.; Sirat, K.; Rahman, M. Tetrabutylammonium Bromide (TBABr)-Based Deep Eutectic Solvents (DESs) and Their Physical Properties. *Molecules* **2014**, *19*, 8011−8026.
(23) McDonald, S.; Murphy, T.; Imberti, S.; Warr, G. G.; Atkin, R. Amphiphilically Nanostructured Deep Eutectic Solvents. *J. Phys. Chem. Lett.* **2018**, *9*, 3922−3927.
(24) Teles, A. R. R.; Capela, E. V.; Carmo, R. S.; Coutinho, J. A. P.; Silvestre, A. J. D.; Freire, M. G. Solvatochromic Parameters of Deep Eutectic Solvents Formed by Ammonium-Based Salts and Carboxylic Acids. *Fluid Phase Equilib.* **2017**, *448*, 15−21.
(25) Nkosi, N.; Tumba, K.; Ramsuroop, S. Activity Coefficients at Infinite Dilution of Various Solutes in Tetrapropylammonium Bromide + 1,6-Hexanediol Deep Eutectic Solvent. *J. Chem. Eng. Data* **2018**, *63*, 4502−4512.
(26) Mjalli, F. S.; Naser, J.; Jibril, B.; Alizadeh, V.; Gano, Z. Tetrabutylammonium Chloride Based Ionic Liquid Analogues and Their Physical Properties. *J. Chem. Eng. Data* **2014**, *59*, 2242−2251.
(27) Mohan, M.; Naik, P. K.; Banerjee, T.; Goud, V. V.; Paul, S. Solubility of Glucose in Tetrabutylammonium Bromide Based Deep Eutectic Solvents: Experimental and Molecular Dynamic Simulations. *Fluid Phase Equilib.* **2017**, *448*, 168−177.
(28) Dou, J.; Zhao, Y.; Yin, F.; Li, H.; Yu, J. Mechanistic Study of Selective Absorption of NO in Flue Gas Using EG-TBAB Deep Eutectic Solvents. *Environ. Sci. Technol.* **2019**, *53*, 1031−1038.
(29) Li, J.-j.; Xiao, H.; Tang, X.-d.; Zhou, M. Green Carboxylic Acid-Based Deep Eutectic Solvents as Solvents for Extractive Desulfurization. *Energy Fuels* **2016**, *30*, 5411−5418.
(30) Li, C.; Li, D.; Zou, S.; Li, Z.; Yin, J.; Wang, A.; Cui, Y.; Yao, Z.; Zhao, Q. Extraction Desulfurization Process of Fuels with Ammonium-Based Deep Eutectic Solvents. *Green Chem.* **2013**, *15*, 2793−2799.
(31) Shukla, S. K.; Mikkola, J.-P. Intermolecular Interactions upon Carbon Dioxide Capture in Deep-Eutectic Solvents. *Phys. Chem. Chem. Phys.* **2018**, *20*, 24591−24601.
(32) AlOmar, M. K.; Hayyan, M.; Alsaadi, M. A.; Akib, S.; Hayyan, A.; Hashim, M. A. Glycerol-Based Deep Eutectic Solvents: Physical Properties. *J. Mol. Liq.* **2016**, *215*, 98−103.
(33) Jibril, B.; Mjalli, F.; Naser, J.; Gano, Z. New Tetrapropylammonium Bromide-Based Deep Eutectic Solvents: Synthesis and Characterizations. *J. Mol. Liq.* **2014**, *199*, 462−469.
(34) García, G.; Aparicio, S.; Ullah, R.; Atilhan, M. Deep Eutectic Solvents: Physicochemical Properties and Gas Separation Applications. *Energy Fuels* **2015**, *29*, 2616−2644.
(35) Das, S. K.; Sarkar, M. Rotational Dynamics of Coumarin-153 and 4-Aminophthalimide in 1-Ethyl-3-methylimidazolium Alkylsulfate Ionic Liquids: Effect of Alkyl Chain Length on the Rotational Dynamics. *J. Phys. Chem. B* **2012**, *116*, 194−202.
(36) Mali, K. S.; Dutt, G. B.; Mukherjee, T. Rotational Diffusion of a Nonpolar and a Dipolar Solute in 1-Butyl-3-Methylimidazolium Hexafluorophosphate and Glycerol: Interplay of Size Effects and Specific Interactions. *J. Chem. Phys.* **2008**, *128*, 054504.

DOI: 10.1021/acs.jpcb.9b04955
J. Phys. Chem. B 2019, 123, 6842−6850

(37) Basaiahgari, A.; Panda, S.; Gardas, R. L. Effect of Ethylene, Diethylene, and Triethylene Glycols and Glycerol on the Physicochemical Properties and Phase Behavior of Benzyltrimethyl and Benzyltributylammonium Chloride Based Deep Eutectic Solvents at 283.15−343.15 K. *J. Chem. Eng. Data* **2018**, *63*, 2613−2627.
(38) Martins, M. A. R.; Crespo, E. A.; Pontes, P. V. A.; Silva, L. P.; Bülow, M.; Maximo, G. J.; Batista, E. A. C.; Held, C.; Pinho, S. P.; Coutinho, J. A. P. Tunable Hydrophobic Eutectic Solvents Based on Terpenes and Monocarboxylic Acids. *ACS Sustainable Chem. Eng.* **2018**, *6*, 8836−8846.
(39) Guo, W.; Hou, Y.; Ren, S.; Tian, S.; Wu, W. Formation of Deep Eutectic Solvents by Phenols and Choline Chloride and Their Physical Properties. *J. Chem. Eng. Data* **2013**, *58*, 866−872.
(40) Hossain, S. S.; Samanta, A. How Do the Hydrocarbon Chain Length and Hydroxyl Group Position Influence the Solute Dynamics in Alcohol-Based Deep Eutectic Solvents? *Phys. Chem. Chem. Phys.* **2018**, *20*, 24613−24622.
(41) Hossain, S. S.; Samanta, A. Solute Rotation and Translation Dynamics in an Ionic Deep Eutectic Solvent Based on Choline Chloride. *J. Phys. Chem. B* **2017**, *121*, 10556−10565.
(42) Petrásek, Z.; Schwille, P. Precise Measurement of Diffusion Coefficients using Scanning Fluorescence Correlation Spectroscopy. *Biophys J* **2008**, *94*, 1437−1448.
(43) Soujanya, T.; Fessenden, R. W.; Samanta, A. Role of Nonfluorescent Twisted Intramolecular Charge Transfer State on the Photophysical Behavior of Aminophthalimide Dyes. *J. Phys. Chem.* **1996**, *100*, 3507−3512.
(44) Samanta, A.; Fessenden, R. W. Excited-State Dipole Moment of 7-Aminocoumarins as Determined from Time-Resolved Microwave Dielectric Absorption Measurements. *J. Phys. Chem. A* **2000**, *104*, 8577−8582.
(45) Khara, D. C.; Samanta, A. Fluorescence Response of Coumarin-153 in N-Alkyl-N-methylmorpholinium Ionic Liquids: Are These Media More Structured than the Imidazolium Ionic Liquids? *J. Phys. Chem. B* **2012**, *116*, 13430−13438.
(46) Samanta, A. Dynamic Stokes Shift and Excitation Wavelength Dependent Fluorescence of Dipolar Molecules in Room Temperature Ionic Liquids. *J. Phys. Chem. B* **2006**, *110*, 13704−13716.
(47) Mandal, P. K.; Sarkar, M.; Samanta, A. Excitation-Wavelength-Dependent Fluorescence Behavior of Some Dipolar Molecules in Room-Temperature Ionic Liquids. *J. Phys. Chem. A* **2004**, *108*, 9048−9053.
(48) Demchenko, A. P. The Red-Edge Effects: 30 Years of Exploration. *Luminescence* **2002**, *17*, 19−42.
(49) Hallidy, L. A.; Topp, M. R. Direct Time-Resolution of the Stokes Fluorescence Shift of a Polar Molecular in a Polar Solvent. *Chem. Phys. Lett.* **1977**, *48*, 40−45.
(50) Das, A.; Biswas, R. Dynamic Solvent Control of a Reaction in Ionic Deep Eutectic Solvents: Time-Resolved Fluorescence Measurements of Reactive and Nonreactive Dynamics in (Choline Chloride + Urea) Melts. *J. Phys. Chem. B* **2015**, *119*, 10102−10113.
(51) Adam, H. T.; Kim, D. Rotation and Translation Dynamics of Coumarin 153 in Choline Chloride-Based Deep Eutectic Solvents. *J. Chem. Phys.* **2018**, *149*, 174503−174507.
(52) Patra, S.; Samanta, A. Microheterogeneity of Some Imidazolium Ionic Liquids As Revealed by Fluorescence Correlation Spectroscopy and Lifetime Studies. *J. Phys. Chem. B* **2012**, *116*, 12275−12283.
(53) Khara, D. C.; Kumar, J. P.; Mondal, N.; Samanta, A. Effect of the Alkyl Chain Length on the Rotational Dynamics of Nonpolar and Dipolar Solutes in a Series of N-Alkyl-N -Methylmorpholinium Ionic Liquids. *J. Phys. Chem. B* **2013**, *117*, 5156−5164.
(54) Sasmal, D. K.; Mandal, A. K.; Mondal, T.; Bhattacharyya, K. Diffusion of Organic Dyes in Ionic Liquid and Giant Micron Sized Ionic Liquid Mixed Micelle: Fluorescence Correlation Spectroscopy. *J. Phys. Chem. B* **2011**, *115*, 7781−7787.
(55) Guchhait, B.; Das, S.; Daschakraborty, S.; Biswas, R. Interaction and Dynamics of (Alkylamide + Electrolyte) Deep Eutectics: Dependence on Alkyl Chain-length, Temperature, and Anion Identity. *J. Chem. Phys.* **2014**, *140*, 104514.
(56) Lackowicz, J. R. *Principles of Fluorescence Spectroscopy*; Springer: New York, 2006.
(57) Sanabria, H.; Kubota, Y.; Waxham, M. N. Multiple Diffusion Mechanisms Due to Nanostructuring in Crowded Environments. *Biophys. J.* **2007**, *92*, 313−322.
(58) Saroja, G.; Soujanya, T.; Ramachandram, B.; Samanta, A. 4-Aminophthalimide Derivatives as Environment-Sensitive Probes. *J. Fluoresc.* **1998**, *8*, 405−410.
(59) Das, S.; Biswas, R.; Mukherjee, B. Reorientational Jump Dynamics and Its Connections to Hydrogen Bond Relaxation in Molten Acetamide: An All-Atom Molecular Dynamics SImulation Study. *J. Phys. Chem. B* **2015**, *119*, 274−283.
(60) Wu, E. C.; Kim, H. J.; Peteanu, L. A. Spectroscopic and MD Study of Dynamic and Structural Heterogeneities in Ionic Liquids. *J. Phys. Chem. B* **2017**, *121*, 1100−1107.
(61) Fleming, G. R. *Chemical Applications of Ultrafast Spectroscopy*; Oxford University Press, 1986.
(62) Ingram, J. A.; Moog, R. S.; Ito, N.; Biswas, R.; Maroncelli, M. Solute Rotation and Solvation Dynamics in a Room-Temperature Ionic Liquid. *J. Phys. Chem. B* **2003**, *107*, 5926−5932.

DOI: 10.1021/acs.jpcb.9b04955
J. Phys. Chem. B 2019, 123, 6842−6850

THE JOURNAL OF PHYSICAL CHEMISTRY B

pubs.acs.org/JPCB Article

Complete Solvation Dynamics of Coumarin 153 in Tetraalkylammonium Bromide-Based Deep Eutectic Solvents

Sk Saddam Hossain, Sneha Paul, and Anunay Samanta*

Cite This: J. Phys. Chem. B 2020, 124, 2473−2481 Read Online

ACCESS | Metrics & More | Article Recommendations

ABSTRACT: Deep eutectic solvents (DESs) are novel environment-friendly media for a variety of applications. In order to obtain insight into the structure and dynamics of some less-explored DESs comprising ethylene glycol and tetraalkylammonium bromide salts with variable alkyl chain length, we have captured complete dynamics occurring in these solvents in a timescale of few femtoseconds to several nanoseconds by monitoring the time-dependent fluorescence Stokes shift of coumarin 153 employing a combination of time-correlated single-photon counting and fluorescence upconversion techniques. The solvent response function constructed from the measured data reveals a sub-picosecond component (~0.8 ps, 20−35%) in addition to a slow component (180−475 ps) with a distribution of relaxation time. The slow time component is found to be strongly dependent on the viscosity of the medium, indicating that it arises from the diffusive motions of the solvent constituents into and out of the solvation shell, whereas the ultrafast time component, which is nearly independent of the solvent viscosity, arises from fast local motions of the constituents in the immediate vicinity of the solute molecule.

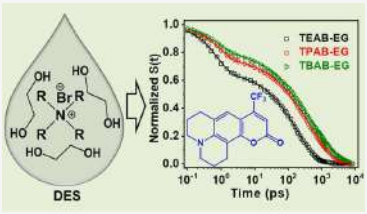

INTRODUCTION

Because of their attractive properties, deep eutectic solvents (DESs) have gained considerable attention in recent years as environment-friendly designer solvents in various fields.[1−6] These are composed of two or more components [usually a salt/hydrogen bond acceptor (HBA) and a hydrogen bond donor (HBD)], which self-associate through hydrogen-bonding interactions forming a stable liquid with melting point lower than that of the pure components.[4,5] A large number of eutectic mixtures can be obtained by varying the constituents and their molar ratios.[4,7] Because of the ease of preparation, relatively inexpensive starting materials, often natural and biodegradable constituents, and the possibility of designing task-specific solvents, the DESs can be a potential green alternative to the conventional volatile organic solvents and the ionic liquids (ILs).[1,4−6,8]

Notwithstanding their applications,[4,9−24] the structure and dynamics of the DESs are not very well understood from the studies made so far on the diffusion dynamics of constituents of the DESs[6,25−28] and translational and rotational diffusion dynamics of organic probe molecules in these media.[29−36] While Abbott and co-workers investigated molecular and ionic diffusion of the constituents in these solvents using pulsed field gradient NMR spectroscopy,[6,25,26] Biswas and co-workers studied rotational diffusion of several molecular systems in a number of DESs to understand the dynamics of these liquids.[33−36] We have recently investigated the translational and rotational diffusion dynamics of some probe molecules employing fluorescence correlation spectroscopy and time-resolved fluorescence anisotropy measurements.[29−31] These studies have revealed significant to moderate spatial and/or dynamic heterogeneity of these DESs, depending on the constituents.

As the dynamics of solvation often determines the fate of many chemical processes[37,38] and can uncover unique characteristics of a solvent such as its microheterogeneity, solvation dynamics has also been studied in some eutectic mixtures in recent years.[32−36,39−41] As solvation leads to a significant shift of the emission spectrum of a dipolar solute molecule in polar media, the dynamics of solvation is frequently studied by sudden perturbation of the charge distribution of a dipolar fluorescent molecule by a short optical pulse excitation and then monitoring the time-dependent fluorescence Stokes shift (TDFSS) of the system.[38,42−44] In addition to the studies based on this methodology,[32−36] Cui et al. and Chatterjee et al. have independently studied solvation dynamics of an ionic probe molecule recently in choline chloride (ChCl)-based DESs using Fourier transform infrared (FTIR) and two-dimensional infrared (2DIR) spectroscopy.[39,40] In another study, Subba et al. have examined solvation dynamics in a nonionic DES employing transient absorption (TA) spectroscopy.[41] These studies indicate that solvation in

Received: January 22, 2020
Revised: February 25, 2020
Published: March 5, 2020

https://dx.doi.org/10.1021/acs.jpcb.0c00594
J. Phys. Chem. B 2020, 124, 2473−2481

DESs is significantly slower than in common organic solvents and is quite similar to that in ILs. The time-resolved component of the dynamics is bimodal in nature and the average solvation time is dependent on the viscosity of the media. Although the slow nature of solvation dynamics in DESs is understood qualitatively, very little of the early part of the solvation dynamics has been explored till date. The TDFSS measurements carried out so far could not capture the fast solvation response due to limited time-resolution (typically 25−50 ps) of the technique.[42,44] On the other hand, the FTIR and 2DIR studies could not reliably estimate the slower component (occurring in a timescale ranging from hundreds of picoseconds to nanoseconds) of the solvation dynamics due to short vibrational lifetime of the probe used.[40,45] Another point to take note of in this context is that majority of the studies carried out so far were focused on ChCl-based DESs leaving many other salt-based DESs unexplored.

In view of the above, herein we focus on a set of less-explored DESs and attempt to capture the complete solvation dynamics (occurring between few femtoseconds and several nanoseconds) of coumarin 153 (C153) by monitoring its TDFSS using a combination of femtosecond fluorescence upconversion (UPC) and time-correlated single photon counting (TCSPC) techniques. We have chosen for this study a homologous series of DESs[29] comprising 3:1 molar mixture of ethylene glycol (EG) and tetraalkylammonium bromide (TAAB) salts with variable alkyl chain lengths. The choice of the molecular probe (C153) is guided by its rigid structure, large change of dipole moment upon electronic excitation ($\Delta\mu$ = ∼7.0 D), large shift of emission maximum as a function of the solvent polarity, relatively long fluorescence lifetime (∼4.5 ns), and its extensive use as a probe for the study of solvation dynamics in a variety of media including ILs and DESs.[43,44,46−48] Table 1 provides necessary details of the DESs along with their abbreviations, and Chart 1 provides chemical structures of the DES components and the probe molecule used in this study.

Table 1. Description of the DESs Used in This Study

Sl. no.	salt[a]	HBDs[a]	mole ratio (salt/HBD)	abbreviation
1	TEAB	EG	1:3	TEAB−EG
2	TPAB	EG	1:3	TPAB−EG
3	TBAB	EG	1:3	TBAB−EG

[a]TEAB: tetraethylammonium bromide; TPAB: tetrapropylammonium bromide; TBAB: tetrabutylammonium bromide; and EG: ethylene glycol.

Chart 1. Chemical Structures of the Components of DESs and Probe Molecule (C153) Used in This Study

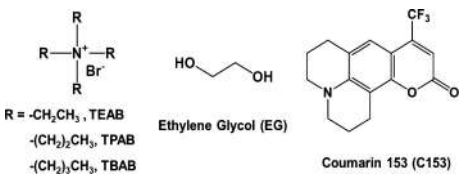

EXPERIMENTAL SECTION

Materials. Tetraethylammonium bromide (>98%), tetrapropylammonium bromide (>98%), and tetrabutylammonium bromide (>99%) were purchased from TCI Chemicals and ethylene glycol (≥99%) from Sigma-Aldrich. These chemicals were dried under high vacuum for 2 days before their use in synthesis. Laser grade C153 was procured from Eastman Kodak, and used as received. Methanol was obtained from Merck, and purified by following the standard procedure before use.[49]

Preparation and Characterization of DESs. The procedures for preparation of the DESs are described in an earlier report.[29] In brief, these were prepared by mixing the TAAB salt with EG in 1:3 molar ratio. The mixtures were heated at 353 K in an oil bath with constant stirring until transparent homogeneous liquids were formed. The resultant liquids were then slowly allowed to cool to room temperature (298 K) and stored in an inert atmosphere for the experiments. These DESs were characterized using both ^{1}H NMR and FTIR spectroscopy and also compared with the literature data.[29] The viscosities of the DESs at 298 K were measured to be 28, 72.5, and 98 cP for TEAB−EG, TPAB−EG, and TBAB−EG, respectively, and these values agree with the literature.[50,51] The water content of the DESs was estimated after drying the samples under high vacuum for several hours, and the values were found to be less than 0.1 wt % in all DESs, which is in agreement with the other DESs.[32,52]

Sample Preparation. Solution of C153 was prepared in methanol. An aliquot of this freshly prepared solution was transferred into a reagent bottle, and the solvent was fully evaporated by high purity N_2 gas flow. Then, a measured amount of the DES was added into the reagent bottle, tightly sealed with parafilm, and mixed thoroughly for complete dissolution of the solute. This solution was stored in an inert atmosphere prior to experiments, and used as stock solution. Finally, the solutions (C153 in DESs) were prepared by dilution such that the absorbance of the samples is maintained at around 0.1 and 1.5 at 400 nm for steady-state/TCSPC and UPC measurements, respectively, in a 1.0 cm sample cell.

Instrumentation. The steady-state absorption and emission spectra were recorded using a UV−vis spectrophotometer (Cary100, Varian) and spectrofluorometer (FluoroLog-3, Horiba Jobin Yvon), respectively. The emission spectra were corrected for the spectral sensitivity of the setup.

The picosecond/nanosecond fluorescence intensity decay measurements were performed using a TCSPC spectrometer (Horiba Jobin Yvon IBH). The details of the setup were described elsewhere.[31] In brief, a 405 nm diode laser and an MCP photomultiplier (Hamamatsu R3809U-50) were employed as the excitation source and detector, respectively. The instrument response function (IRF) of the setup, which is limited by the full-width at half-maximum (fwhm) of the excitation laser pulse, was recorded by placing a scatterer (dilute aqueous solution of LUDOX) in the sample cell and was found to be ∼60 ps. The decay curves were analyzed by a nonlinear least-squares iteration procedure using IBH DAS6 (Version 2.2) decay analysis software. The quality of the fits was assessed by the χ^2 values and distribution of the residuals.

The sub-picosecond fluorescence intensity decays were measured using a UPC setup (FOG 100, CDP systems, Russia).[53] The center wavelength of the mode-locked Ti:sapphire laser (Mai Tai), set at 800 nm, was directed to a β-barium borate (BBO) crystal to generate the second harmonic signal (400 nm). The output was then directed to a dichroic mirror, which reflected the 400 nm light (used as excitation beam) and transmitted the residual 800 nm light

https://dx.doi.org/10.1021/acs.jpcb.0c00594
J. Phys. Chem. B 2020, 124, 2473−2481

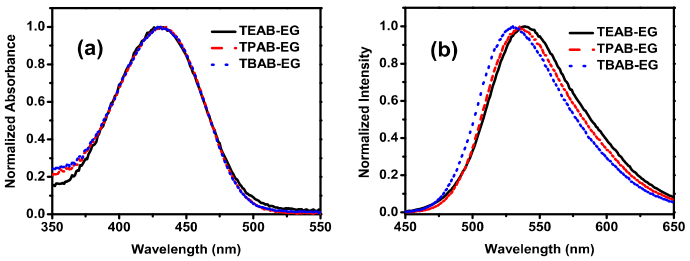

Figure 1. Steady-state absorption (a) and emission (b) spectra of C153 in chosen DESs at 298 K. The emission spectra are recorded by exciting the samples at 430 nm.

Table 2. Peak Positions, $\Delta_{sol}G$, and λ_{sol} Values of C153 in the DESs Used in This Study

DESs	ν_{abs} (10^3 cm^{-1})	ν_{emn} (10^3 cm^{-1})	$\nu_{cal}(0)^a$ (10^3 cm^{-1})	$\nu(\infty)^b$ (10^3 cm^{-1})	$-\Delta_{sol}G$ (kJ mol^{-1})	λ_{sol} (kJ mol^{-1})
TEAB−EG	23.26	18.52	20.37	18.49	46.30	11.20
TPAB−EG	23.23	18.69	20.34	18.61	45.60	10.50
TBAB−EG	23.26	18.87	20.37	18.72	44.90	9.80

[a]Estimated following ref 60. [b]Estimated from the time-resolved measurements.

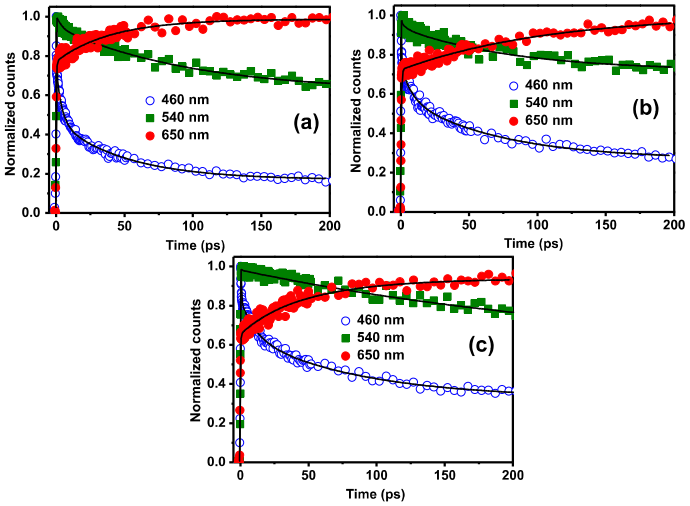

Figure 2. Representative wavelength-dependent fluorescence decay profiles of C153 (λ_{exc} = 400 nm) in the short time scale obtained from the UPC measurements in TEAB−EG (a), TPAB−EG (b), and TBAB−EG (c). The symbols denote the experimental data and the solid lines represent multiexponential fit to the data using eq 3.

(used as gate beam). The gate beam was passed through a motorized optical delay stage (4 ns) to introduce delay between the fluorescence signal and the gate beam. Fluorescence signal from the sample was upconverted in a sum-frequency generating BBO crystal using the gate beam. The upconverted signal was then directed to the photomultiplier tube through a monochromator. The IRF of the setup was estimated using the Raman scattering signal from water and was found to be ∼200 fs. The samples were kept in a rotating sample cell of 1.0 mm path length. The intensity decay curves were analyzed using Igor pro (Version 6.37, Wavemetrics) software.

RESULTS AND DISCUSSION

Steady-State Measurements. The steady-state absorption and emission spectra of C153 in the chosen DESs at room temperature (298 K) are shown in Figure 1 and the corresponding peak positions are collected in Table 2. The spectral shapes are found to be very similar in all three DESs, and they closely resemble those in conventional polar solvents[54,55] such as water and methanol or in ILs[56,57] and other DESs.[31,55] As far as the absorption and emission peak positions are concerned, they appear at wavelengths similar to those observed in ChCl-based DESs, indicating that the microenvironment around C153 in these solvents is comparable to that in ChCl/alcohol-based DESs.[31,55] Comparable absorption and emission maxima of C153 in these DESs and various commonly used ILs also suggest that a similar environment is experienced by the probe molecule in these two types of solvents.[48,58] Although the absorption maximum appears at ∼430 nm in all three DESs, the emission peak position shifts toward lower wavelength (from 540 to 530 nm) with increase in alkyl chain length of the cationic constituent of

https://dx.doi.org/10.1021/acs.jpcb.0c00594
J. Phys. Chem. B 2020, 124, 2473−2481

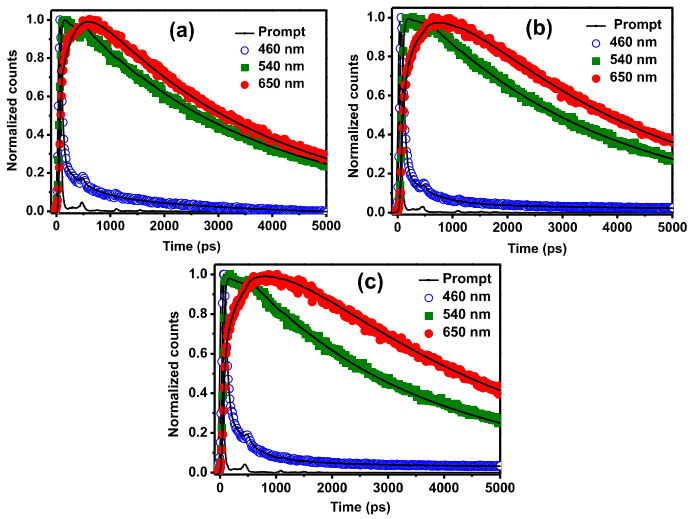

Figure 3. Representative wavelength-dependent fluorescence decay profiles of C153 (λ_{exc} = 405 nm) obtained from the TCSPC measurements in TEAB−EG (a), TPAB−EG (b), and TBAB−EG (c). The symbols denote the experimental data and the solid lines represent multiexponential fit to the data using eq 3.

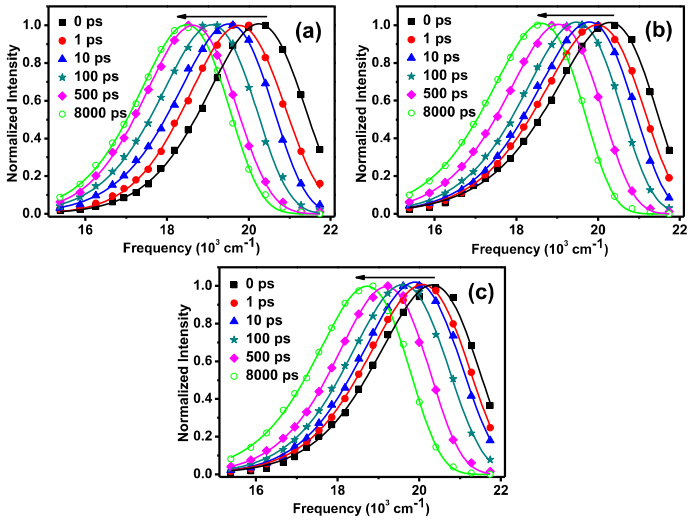

Figure 4. Representative TRES of C153 at different times in TEAB−EG (a), TPAB−EG (b), and TBAB−EG (c). The spectra up to 100 ps are reconstructed from the UPC data and the longer time spectra are reconstructed from the TCSPC data. The solid lines represent fit of the experimental data to log-normal function (eq 5).

the solvents. The enhanced sensitivity of the emission peak position on the solvent is consistent with a higher excited-state dipole moment of C153,[59] and the observed peak shift indicates a less polar nature of the solvent containing a longer alkyl chain length.[48,57,60]

Before studying the dynamics of solvation, we have estimated the static solvation parameters, solvation free-energy difference ($\Delta_{sol}G$), and solvent contribution to nuclear reorganization energy (λ_{sol}) associated with the $S_0 \leftrightarrow S_1$ transition of C153 in these solvents using[47,48]

$$\Delta_{sol}G = \frac{1}{2}h\{\nu_{abs} - \nu(\infty)\} - \Delta G_0 \quad (1)$$

$$\lambda_{sol} = \frac{1}{2}h\{\nu_{cal}(0) - \nu(\infty)\} \quad (2)$$

where, ν_{abs} is the absorption peak frequency (in cm^{-1}), $\nu_{cal}(0)$ and $\nu(\infty)$ are the emission peak frequencies immediately after excitation ($t = 0$) and at a sufficiently long time ($t = \infty$), when solvent relaxation is expected to be complete. The $\nu_{cal}(0)$ values are estimated following a procedure recommended by Fee and Maroncelli,[61] whereas the $\nu(\infty)$ values are obtained from the time-resolved fluorescence measurements (details in a later section). ΔG_0 is the gas-phase free-energy difference for C153 (296 kJ mol^{-1}).[48] The estimated $\Delta_{sol}G$ and λ_{sol} values for C153 in these DESs, which are presented in Table 2 along with

https://dx.doi.org/10.1021/acs.jpcb.0c00594
J. Phys. Chem. B 2020, 124, 2473−2481

Table 3. Parameters Obtained by Fitting of $S(t)$ to eq 6 in Different DESs Along with Observed Stokes Shift and Missing Percentage

DESs	τ_1 (ps)	f_1	τ_2 (ps)	f_2	α	τ_{st} (ps)[a]	$\Delta\nu$ (cm^{-1})[b]	$\Delta\nu_{miss}$[c] (%)
TEAB−EG	0.72	0.34	181	0.66	0.71	226	1766	6.10
TPAB−EG	0.80	0.23	424	0.77	0.60	638	1687	2.60
TBAB−EG	0.79	0.17	475	0.83	0.54	832	1602	2.60

[a]Calculated using eq 7. [b]$\Delta\nu = \nu(\infty) - \nu(0)$, is total observed dynamic fluorescence Stokes shift. [c]Calculated following ref 60.

the measured peak frequencies, are comparable to the respective values reported in various ILs.[47,48,58] This is understood, considering very similar values of the steady-state absorption and emission maxima of C153 in these DESs and various ILs.[48,58] A close inspection of the data reveals that both the parameters ($\Delta_{sol}G$ and λ_{sol}) change substantially with change in alkyl chain length of the cationic moiety, showing good correlation with the solvent polarity of these DESs and demonstrating its role in the solvation process in DESs.

TDFSS Measurements. As stated earlier, we have studied the dynamics of solvation of C153 by measuring its TDFSS in these DESs. As solvation takes a long time to complete in viscous media such as ILs and DESs and that solvation also has a fast component,[40,41,48,62] which was not time-resolved previously through TDFSS measurements, we have employed both UPC and TCSPC techniques to capture the complete dynamics ranging from few femtoseconds time scale to several nanoseconds. Figures 2 and 3 show that the fluorescence decay profiles of C153 are dependent on the monitoring wavelengths. The observation that at shorter wavelengths, fluorescence intensity decays steadily with time, but at longer wavelengths, the decay is preceded by a rise component, is indicative of solvation dynamics in these solvents. In each solvent, we have recorded the decay curves at several (18−20) wavelengths across the entire fluorescence spectrum of C153 (460−650 nm) using both UPC and TCSPC techniques. These decay curves are fitted independently to a multiexponential function of the form

$$I(t) = \sum_{i=1}^{n} a_i \exp(-t/\tau_i) \quad (3)$$

where, τ_i and a_i are the time constant and associated amplitude, respectively.

Time-resolved emission spectra (TRES) at various times are then constructed using the obtained decay parameters and the steady-state emission data following a standard procedure.[42,46] Figure 4, which displays representative TRES of C153 at few selected times in three DESs, shows a shift of the fluorescence spectra to lower energy with time, indicating stabilization of the emitting state of C153 through solvent reorganization/relaxation. In Figure 4, the spectra up to 100 ps were reconstructed from the UPC data and those beyond from the TCSPC data. A slight mismatch of the peak positions measured by the two techniques over 100−400 ps time range, as observed here, is not uncommon.[48,62] The spectra at the common time points (100−400 ps) obtained from the two techniques were matched by uniformly shifting the UPC data following reported procedures.[48,62] In order to parameterize the time-evolution of the reconstructed emission spectra and to estimate the peak frequencies at different times, the TRES are fitted to log-normal line shape function (eq 4), a commonly used representation of the emission spectra[62,63]

$$I(\nu) = I_0 \exp\{-\ln(2)[\ln(1+\alpha)/\gamma]^2\} \quad \text{for } \alpha > -1$$
$$= 0 \quad \text{for } \alpha \le -1 \quad (4)$$

where, $\alpha = 2\gamma(\nu - \nu_p)/\Delta$, and the four parameters, ν_p, I_0, Δ, and γ describe the peak frequency (in cm^{-1}), peak intensity, fwhm, and asymmetry of the band-shape, respectively. Figure 4 shows that the shapes of the reconstructed emission spectra are well described by this function (solid lines).

Important to note here is that total dynamic fluorescence Stokes shifts ($\Delta\nu = \nu(\infty) - \nu(0)$) observed for C153 in this study are 1766, 1687, and 1602 cm^{-1} in TEAB−EG, TPAB−EG, and TBAB−EG, respectively (Table 3). These values are significantly higher than the observed shift of C153 in other DESs.[32,33,35,36] This is not surprising as these TDFFS studies were based on the TCSPC technique, where a large portion of the early part of the total dynamics was missed due to limited time resolution (typically 25−50 ps).[32,33,35,36] It is important to note that the reported magnitude of the total shifts of C153 in the earlier studies of solvation dynamics in common ILs,[48] which captured the complete dynamics, are comparable to the present values. This indicates that we have been able to capture almost the entire solvation dynamics in the present case. This is also evident from the fact that the missing component ($\Delta\nu_{miss}$) of the dynamics, as estimated following the procedure recommended by Fee and Maroncelli,[61] is found to be only 3−6% (Table 3).

The normalized solvation response function, $S(t)$, which is commonly used to describe the solvation dynamics in a medium, is constructed from the estimated peak frequencies of the TRES at different times using[64,65]

$$S(t) = \frac{\nu(t) - \nu(\infty)}{\nu(0) - \nu(\infty)} \quad (5)$$

Figure 5 shows time-dependence of the normalized $S(t)$ of C153 in different DESs. To obtained quantitative information on the solvation dynamics, the data is fitted to eq 6, which

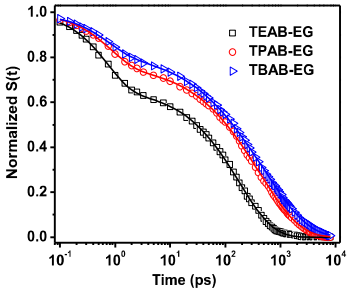

Figure 5. Time-dependence of $S(t)$ in different DESs. The symbols denote the experimental data and the solid lines represent fit to the data using eq 6.

https://dx.doi.org/10.1021/acs.jpcb.0c00594
J. Phys. Chem. B 2020, 124, 2473−2481

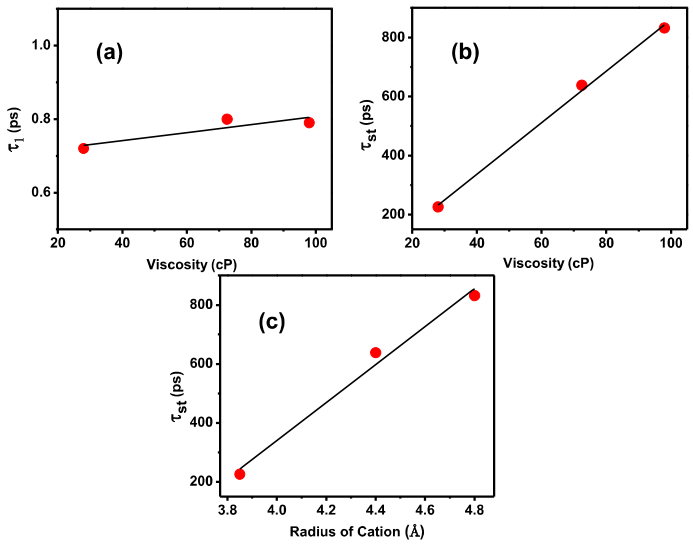

Figure 6. Dependence of the fast (a) and slow time components (b) of the solvation on viscosity of the DESs. The panel (c) shows the dependence of the slow time component on cationic radii of the DESs. The values of the cationic radii are taken from the previous literature.[68,69] The solid lines through the data represent the result of a linear fit.

contains sum of a single exponential function with relaxation time, τ_1 and a stretched exponential function with relaxation time, τ_2.[47,62]

$$S(t) = f_1 \exp(-t/\tau_1) + f_2 \exp(-t/\tau_2)^{\alpha} \quad (6)$$

where, f_1 and f_2 are the amplitudes associated with relaxation times τ_1 and τ_2, respectively, and α ($0 < \alpha < 1$) is the stretching exponent representing distribution of the relaxation time, τ_2. A simple biexponential fit (eq 6 with $\alpha = 1$) to the data, which described the time dependence of $S(t)$ in ChCl-based DESs,[32,33] is found unsatisfactory in the present case. This difference is not surprising because in previous studies a large portion of the early part of the total dynamics (as seen earlier) was missed.

The time components of the dynamic solvation response, estimated from the fits (eq 6 with $\alpha < 1$), are collected in Table 3. As can be seen, the solvation is characterized by a distinct ultrafast component, τ_1 of ~0.8 ps and a slower component, τ_2 (180−475 ps, depending on the DESs) with a distribution of the relaxation time. This kind of two solvation components of comparable values were also reported in ILs with similar viscosity.[47,48] The integral time corresponding to the slow stretched exponential component (τ_{st}) is calculated from the observed τ_2 values using eq 7 (where Γ is gamma function).

$$\tau_{st} = \frac{\tau_2}{\alpha}\Gamma(\alpha^{-1}) \quad (7)$$

It is clear from the table that this slow-stretched component of the relaxation time (τ_{st}) is strongly dependent on the solvent, unlike the ultrafast component (τ_1). The plots in Figure 6a,b show that the slow component is strongly dependent on the viscosity of the medium, much like that observed in ILs, suggesting that this component is associated with diffusional motions of the solvent constituents surrounding the probe molecule.[43,44,48] Furthermore, Table 3 suggests that the slow component is not single-exponential rather has a distribution of time constant, which is represented by a stretched-exponential relaxation with values of α less than unity. This broadly distributed time component may arise from heterogeneous diffusional motions present in the solvents. Another possible origin of this distribution could be the involvement of multiple processes arising from independent movements of each solvent constituent.[66] However, as heterogeneity in these DESs is well documented,[29] we suggest that it is the heterogeneous diffusional motions, which contribute to the slow component. This can be due to nonhydrodynamic diffusive motions involving center of mass movements such as rotation-translation coupling motions and/or jump moves of the solvent constituents into and out of the solvation shell leading to bulk structural reorganization.[33,40,67] Here, we note that such rotation-translation coupling motions and jump moves of the solvent constituents are already demonstrated in case of DESs.[27,33,34,67] One more interesting observation from Table 3 is that the α values associated with the slow component deviates further from unity (0.71 to 0.54) in solvents with longer alkyl chain lengths of the cation. The larger departure of the α values from unity, which indicates a wider distribution of the slow time component, suggests heterogeneous diffusional motions as the main origin of the slow component and corroborates our assignment. This finding is in accordance with that made in an earlier study based on fluorescence correlation spectroscopy and time-resolved fluorescence anisotropy measurements, which indicated a greater heterogeneity for DESs comprising cations with longer alkyl chain lengths.[29]

In contrast, the ultrafast sub-picosecond component, which is nearly independent of the solvent viscosity, can be attributed to fast relaxation of the local environment created by DES constituents that arises because of only minor readjustments of the intermolecular hydrogen-bonding, positions, and orientations of the constituents present in immediate vicinity of the probe molecule within the solvation shell.[33,39,40]

In order to understand the influence of alkyl chain length (or ionic radius) of the cation on the individual solvation

https://dx.doi.org/10.1021/acs.jpcb.0c00594
J. Phys. Chem. B 2020, 124, 2473−2481

component, we have examined the dependence of the slow solvation time (τ_{st}) with the cation radius (i.e., size) in Figure 6c. A linear relationship between the two suggests that this slow solvation component, which arises from the diffusive movements in DESs, strongly depends on the size of cationic constituent of these solvents. As far as the ultrafast solvation component is concerned, Table 3 shows that even though this time constant does not vary significantly, the weightage (amplitude) associated with this component (f_1) decreases significantly from 0.34 to 0.17 upon increasing the cation alkyl chain length (i.e., size). The decrease in weightage of this component with increase in the chain length suggests reduction in contribution of the fast local motions of the constituents in DESs comprising longer alkyl chain cations; a similar observation is reported in ILs as well.[48] A recent MD simulation and ab initio computational study in ChCl-based DESs also indicates that in-plane local motions in the first solvation shell and translational motions into and out of the solvation shell of the cation influence the fast and slow components of the solvation, respectively.[40] Hence, we conclude that the fast and slow components of the solvation response in these DESs arise, respectively, from the local motions and heterogeneous diffusive motions of the constituents, and the cationic moiety plays a significant role in defining the solvation dynamics in these DESs.

CONCLUSIONS

In summary, we have been able to capture the complete solvation dynamics of C153 by monitoring its time-dependence of the fluorescence Stokes shift using a combination of UPC and TCSPC techniques in a series of relatively less-explored DESs comprising ethylene glycol and TAAB salts with variable alkyl chain length. The study reveals temporally diverse nature of the solvation in these DESs, characterized by a distinct fast sub-picosecond component and a slow component with a distribution of the relaxation time. The ultrafast sub-picosecond component arises from rapid local structural relaxation in the immediate vicinity of the solute molecule within the solvation shell, whereas the broadly distributed slow component arises from heterogeneous dynamical processes due to nonhydrodynamic diffusive motions of the solvent constituents into and out of the solvation shell that cause bulk structural relaxation. It is also found that the length of the alkyl chain and hence, the size of the cationic component greatly influences the solvation dynamics in these solvents.

AUTHOR INFORMATION

Corresponding Author

Anunay Samanta − *School of Chemistry, University of Hyderabad, Hyderabad 500 046, India;* orcid.org/0000-0003-1551-0209; Email: anunay@uohyd.ac.in

Authors

Sk Saddam Hossain − *School of Chemistry, University of Hyderabad, Hyderabad 500 046, India;* orcid.org/0000-0002-5740-3703

Sneha Paul − *School of Chemistry, University of Hyderabad, Hyderabad 500 046, India;* orcid.org/0000-0002-0631-1980

Complete contact information is available at: https://pubs.acs.org/10.1021/acs.jpcb.0c00594

Notes

The authors declare no competing financial interest.

ACKNOWLEDGMENTS

This work is supported by the J. C. Bose Fellowship (to A.S.) of the Science and Engineering Research Board (SERB), Department of Science and Technology (DST), India. Financial and infrastructural support received from the University Grants Commission (UGC, through the UPE and CAS programs) and DST (through the PURSE and FIST programs) are also gratefully acknowledged. S.S.H. and S.P. thank UGC for Fellowships.

REFERENCES

(1) Abbott, A. P.; Boothby, D.; Capper, G.; Davies, D. L.; Rasheed, R. K. Deep Eutectic Solvents Formed Between Choline Chloride and Carboxylic Acids: Versatile Alternatives to Ionic Liquids. *J. Am. Chem. Soc.* **2004**, *126*, 9142−9147.

(2) Abbott, A. P.; Capper, G.; Davies, D. L.; Rasheed, R. K.; Tambyrajah, V. Novel Solvent Properties of Choline Chloride/Urea Mixtures. *Chem. Commun.* **2003**, *1*, 70−71.

(3) Alonso, D. A.; Baeza, A.; Chinchilla, R.; Guillena, G.; Pastor, I. M.; Ramón, D. J. Deep Eutectic Solvents: The Organic Reaction Medium of the Century. *Eur. J. Org. Chem.* **2016**, *2016*, 612−632.

(4) Smith, E. L.; Abbott, A. P.; Ryder, K. S. Deep Eutectic Solvents (DESs) and Their Applications. *Chem. Rev.* **2014**, *114*, 11060−11082.

(5) Zhang, Q.; De Oliveira Vigier, K.; Royer, S.; Jérôme, F. Deep eutectic solvents: syntheses, properties and applications. *Chem. Soc. Rev.* **2012**, *41*, 7108−7146.

(6) Abbott, A. P.; Harris, R. C.; Ryder, K. S.; D'Agostino, C.; Gladden, L. F.; Mantle, M. D. Glycerol Eutectics as Sustainable Solvent Systems. *Green Chem.* **2011**, *13*, 82−90.

(7) Francisco, M.; van den Bruinhorst, A.; Kroon, M. C. Low-Transition-Temperature Mixtures (LTTMs): A New Generation of Designer Solvents. *Angew. Chem., Int. Ed.* **2013**, *52*, 3074−3085.

(8) Ruß, C.; Konig, B. Low Melting Mixtures in Organic Synthesis -An Alternative to Ionic Liquids? *Green Chem.* **2012**, *14*, 2969−2982.

(9) Abbott, A. P.; Capper, G.; McKenzie, K. J.; Glidle, A.; Ryder, K. S. Electropolishing of Stainless Steels in a Choline Chloride Based Ionic Liquid: An Electrochemical Study With Surface Characterisation Using SEM and Atomic Force Microscopy. *Phys. Chem. Chem. Phys.* **2006**, *8*, 4214−4221.

(10) Cruz, H.; Jordão, N.; Branco, L. C. Deep Eutectic Solvents (DESs) as Low-Cost and Green Electrolytes for Electrochromic Devices. *Green Chem.* **2017**, *19*, 1653−1658.

(11) Shahbaz, K.; Mjalli, F. S.; Hashim, M. A.; AlNashef, I. M. Using Deep Eutectic Solvents Based on Methyl Triphenyl Phosphunium Bromide for the Removal of Glycerol from Palm-Oil-Based Biodiesel. *Energy Fuels* **2011**, *25*, 2671−2678.

(12) García, G.; Aparicio, S.; Ullah, R.; Atilhan, M. Deep Eutectic Solvents: Physicochemical Properties and Gas Separation Applications. *Energy Fuels* **2015**, *29*, 2616−2644.

(13) Gu, Y.; Jérôme, F. Bio-Based Solvents: An Emerging Generation of Fluids for the Design of Eco-Efficient Processes in Catalysis and Organic Chemistry. *Chem. Soc. Rev.* **2013**, *42*, 9550−9570.

(14) Gorke, J. T.; Srienc, F.; Kazlauskas, R. J. Hydrolase-Catalyzed Biotransformations in Deep Eutectic Solvents. *Chem. Commun.* **2008**, 1235−1237.

(15) Leron, R. B.; Li, M.-H. Solubility of carbon dioxide in a choline chloride-ethylene glycol based deep eutectic solvent. *Thermochim. Acta* **2013**, *551*, 14−19.

(16) Li, C.; Li, D.; Zou, S.; Li, Z.; Yin, J.; Wang, A.; Cui, Y.; Yao, Z.; Zhao, Q. Extraction Desulfurization Process of Fuels with Ammonium-Based Deep Eutectic Solvents. *Green Chem.* **2013**, *15*, 2793−2799.

(17) Li, J.-j.; Xiao, H.; Tang, X.-d.; Zhou, M. Green Carboxylic Acid-Based Deep Eutectic Solvents as Solvents for Extractive Desulfurization. *Energy Fuels* **2016**, *30*, 5411−5418.
(18) Liao, H.-G.; Jiang, Y.-X.; Zhou, Z.-Y.; Chen, S.-P.; Sun, S.-G. Shape-Controlled Synthesis of Gold Nanoparticles in Deep Eutectic Solvents for Studies of Structure-Functionality Relationships in Electrocatalysis. *Angew. Chem.* **2008**, *120*, 9240−9243.
(19) Jhong, H.-R.; Wong, D. S.-H.; Wan, C.-C.; Wang, Y.-Y.; Wei, T.-C. A Novel Deep Eutectic Solvent-Based Ionic Liquid Used As Electrolyte for Dye-Sensitized Solar Cells. *Electrochem. Commun.* **2009**, *11*, 209−211.
(20) Li, X.; Hou, M.; Han, B.; Wang, X.; Zou, L. Solubility of CO_2in a Choline Chloride + Urea Eutectic Mixture. *J. Chem. Eng. Data* **2008**, *53*, 548−550.
(21) Carriazo, D.; Serrano, M. C.; Gutiérrez, M. C.; Ferrer, M. L.; del Monte, F. Deep-Eutectic Solvents Playing Multiple Roles in the Synthesis of Polymers and Related Materials. *Chem. Soc. Rev.* **2012**, *41*, 4996−5014.
(22) Boldrini, C. L.; Manfredi, N.; Perna, F. M.; Trifiletti, V.; Capriati, V.; Abbotto, A. Dye-Sensitized Solar Cells that use an Aqueous Choline Chloride-Based Deep Eutectic Solvent as Effective Electrolyte Solution. *Energy Technol.* **2017**, *5*, 345−353.
(23) Troter, D. Z.; Todorović, Z. B.; Đokić-Stojanović, D. R.; Stamenković, O. S.; Veljković, V. B. Application of Ionic Liquids and Deep Eutectic Solvents in Biodiesel Production: A Review. *Renewable Sustainable Energy Rev.* **2016**, *61*, 473−500.
(24) Zhao, B.-Y.; Xu, P.; Yang, F.-X.; Wu, H.; Zong, M.-H.; Lou, W.-Y. Biocompatible Deep Eutectic Solvents Based on Choline Chloride: Characterization and Application to the Extraction of Rutin from Sophora japonica. *ACS Sustainable Chem. Eng.* **2015**, *3*, 2746−2755.
(25) D'Agostino, C.; Gladden, L. F.; Mantle, M. D.; Abbott, A. P.; Essa, I. A.; Al-Murshedi, A. Y. M.; Harris, R. C. Molecular and Ionic Diffusion in Aqueous − Deep Eutectic Solvent Mixtures: Probing Inter Molecular Interactions Using PFG NMR. *Phys. Chem. Chem. Phys.* **2015**, *17*, 15297−15304.
(26) D'Agostino, C.; Harris, R. C.; Abbott, A. P.; Gladden, L. F.; Mantle, M. D. Molecular Motion and Ion Diffusion in Choline Chloride Based Deep Eutectic Solvents Studied by 1H Pulsed Field Gradient NMR Spectroscopy. *Phys. Chem. Chem. Phys.* **2011**, *13*, 21383−21391.
(27) Das, S.; Biswas, R.; Mukherjee, B. Orientational Jumps in (Acetamide + Electrolyte) Deep Eutectics: Anion Dependence. *J. Phys. Chem. B* **2015**, *119*, 11157−11168.
(28) Wagle, D. V.; Baker, G. A.; Mamontov, E. Differential Microscopic Mobility of Components within a Deep Eutectic Solvent. *J. Phys. Chem. Lett.* **2015**, *6*, 2924−2928.
(29) Hossain, S. S.; Paul, S.; Samanta, A. Liquid Structure and Dynamics of Tetraalkylammonium Bromide-Based Deep Eutectic Solvents: Effect of Cation Chain Length. *J. Phys. Chem. B* **2019**, *123*, 6842−6850.
(30) Hossain, S. S.; Samanta, A. Solute Rotation and Translation Dynamics in an Ionic Deep Eutectic Solvent Based on Choline Chloride. *J. Phys. Chem. B* **2017**, *121*, 10556−10565.
(31) Hossain, S. S.; Samanta, A. How Do the Hydrocarbon Chain Length and Hydroxyl Group Position Influence the Solute Dynamics in Alcohol-Based Deep Eutectic Solvents? *Phys. Chem. Chem. Phys.* **2018**, *20*, 24613−24622.
(32) Turner, A. H.; Kim, D. Rotation and Translation Dynamics of Coumarin 153 in Choline Chloride-Based Deep Eutectic Solvents. *J. Chem. Phys.* **2018**, *149*, 174503−174507.
(33) Das, A.; Biswas, R. Dynamic Solvent Control of a Reaction in Ionic Deep Eutectic Solvents: Time-Resolved Fluorescence Measurements of Reactive and Nonreactive Dynamics in (Choline Chloride + Urea) Melts. *J. Phys. Chem. B* **2015**, *119*, 10102−10113.
(34) Guchhait, B.; Das, S.; Daschakraborty, S.; Biswas, R. Interaction and Dynamics of (Alkylamide + Electrolyte) Deep Eutectics: Dependence on Alkyl Chain-length, Temperature, and Anion Identity. *J. Chem. Phys.* **2014**, *140*, 104514.
(35) Mukherjee, K.; Tarif, E.; Barman, A.; Biswas, R. Dynamics of a PEG Based Non-Ionic Deep Eutectic Solvent: Temperature Dependence. *Fluid Phase Equilib.* **2017**, *448*, 22−29.
(36) Tarif, E.; Mondal, J.; Biswas, R. Interaction and Dynamics in a Fully Biodegradable Glucose-Containing Naturally Abundant Deep Eutectic Solvent: Temperature-Dependent Time-Resolved Fluorescence Measurements. *J. Phys. Chem. B* **2019**, *123*, 9378−9387.
(37) Nitzan, A. *Chemical Dynamics in Condensed Phases*; Oxford University Press: New York, 2006.
(38) Bagchi, B.; Jana, B. Solvation Dynamics in Dipolar Liquids. *Chem. Soc. Rev.* **2010**, *39*, 1936−1954.
(39) Chatterjee, S.; Ghosh, D.; Haldar, T.; Deb, P.; Sakpal, S. S.; Deshmukh, S. H.; Kashid, S. M.; Bagchi, S. Hydrocarbon Chain-Length Dependence of Solvation Dynamics in Alcohol-based Deep Eutectic Solvents: A Two-Dimensional Infrared Spectroscopic Investigation. *J. Phys. Chem. B* **2019**, *123*, 9355−9363.
(40) Cui, Y.; Fulfer, K. D.; Ma, J.; Weldeghiorghis, T. K.; Kuroda, D. G. Solvation Dynamics of an Ionic Probe in Choline Chloride-Based Deep Eutectic Solvents. *Phys. Chem. Chem. Phys.* **2016**, *18*, 31471−31479.
(41) Subba, N.; Polok, K.; Piatkowski, P.; Ratajska-Gadomska, B.; Biswas, R.; Gadomski, W.; Sen, P. Temperature-Dependent Ultrafast Solvation Response and Solute Diffusion in Acetamide-Urea Deep Eutectic Solvent. *J. Phys. Chem. B* **2019**, *123*, 9212−9221.
(42) Lackowicz, J. R. *Principles of Fluorescence Spectroscopy*; Springer: New York, 2006.
(43) Samanta, A. Dynamic Stokes Shift and Excitation Wavelength Dependent Fluorescence of Dipolar Molecules in Room Temperature Ionic Liquids. *J. Phys. Chem. B* **2006**, *110*, 13704−13716.
(44) Samanta, A. Solvation Dynamics in Ionic Liquids: What We Have Learned from the Dynamic Fluorescence Stokes Shift Studies. *J. Phys. Chem. Lett.* **2010**, *1*, 1557−1562.
(45) Ren, Z.; Ivanova, A. S.; Couchot-Vore, D.; Garrett-Roe, S. Ultrafast Structure and Dynamics in Ionic Liquids: 2D-IR Spectroscopy Probes the Molecular Origin of Viscosity. *J. Phys. Chem. Lett.* **2014**, *5*, 1541−1546.
(46) Karmakar, R.; Samanta, A. Solvation Dynamics of Coumarin-153 in a Room-Temperature Ionic Liquid. *J. Phys. Chem. A* **2002**, *106*, 4447−4452.
(47) Arzhantsev, S.; Jin, H.; Baker, G. A.; Maroncelli, M. Measurements of the Complete Solvation Response in Ionic Liquids. *J. Phys. Chem. B* **2007**, *111*, 4978−4989.
(48) Zhang, X.-X.; Liang, M.; Ernsting, N. P.; Maroncelli, M. Complete Solvation Response of Coumarin 153 in Ionic Liquids. *J. Phys. Chem. B* **2013**, *117*, 4291−4304.
(49) Perrin, D. D.; Armarego, W. L. F.; Perrin, D. R. *Purification of Laboratory Chemicals*; Pergamon Press: New York, 1980.
(50) Jibril, B.; Mjalli, F.; Naser, J.; Gano, Z. New Tetrapropylammonium Bromide-Based Deep Eutectic Solvents: Synthesis and Characterizations. *J. Mol. Liq.* **2014**, *199*, 462−469.
(51) Yusof, R.; Abdulmalek, E.; Sirat, K.; Rahman, M. Tetrabutylammonium Bromide (TBABr)-Based Deep Eutectic Solvents (DESs) and Their Physical Properties. *Molecules* **2014**, *19*, 8011−8026.
(52) Guo, W.; Hou, Y.; Ren, S.; Tian, S.; Wu, W. Formation of Deep Eutectic Solvents by Phenols and Choline Chloride and Their Physical Properties. *J. Chem. Eng. Data* **2013**, *58*, 866−872.
(53) Paul, S.; Ahmed, T.; Samanta, A. Influence of Divalent Counterions on the Dynamics in DNA Probed by a Minor Groove Binder. *ChemPhysChem* **2017**, *18*, 2058.
(54) Eom, I.; Joo, T. Polar Solvation Dynamics of Coumarin 153 by Ultrafast Time-Resolved Fluorescence. *J. Chem. Phys.* **2009**, *131*, 244507.
(55) Pandey, A.; Rai, R.; Pal, M.; Pandey, S. How Polar are Choline Chloride-Based Deep Eutectic Solvents? *Phys. Chem. Chem. Phys.* **2014**, *16*, 1559−1568.
(56) Chowdhury, P. K.; Halder, M.; Sanders, L.; Calhoun, T.; Anderson, J. L.; Armstrong, D. W.; Song, X.; Petrich, J. W. Dynamic

https://dx.doi.org/10.1021/acs.jpcb.0c00594
J. Phys. Chem. B 2020, 124, 2473−2481

Solvation in Room-Temperature Ionic Liquids. *J. Phys. Chem. B* **2004**, *108*, 10245−10255.
(57) Khara, D. C.; Samanta, A. Fluorescence Response of Coumarin-153 in N-Alkyl-N-methylmorpholinium Ionic Liquids: Are These Media More Structured than the Imidazolium Ionic Liquids? *J. Phys. Chem. B* **2012**, *116*, 13430−13438.
(58) Jin, H.; Baker, G. A.; Arzhantsev, S.; Dong, J.; Maroncelli, M. Solvation and Rotational Dynamics of Coumarin 153 in Ionic Liquids: Comparisons to Conventional Solvents. *J. Phys. Chem. B* **2007**, *111*, 7291−7302.
(59) Samanta, A.; Fessenden, R. W. Excited-State Dipole Moment of 7-Aminocoumarins as Determined from Time-Resolved Microwave Dielectric Absorption Measurements. *J. Phys. Chem. A* **2000**, *104*, 8577−8582.
(60) Das, S. K.; Majhi, D.; Sahu, P. K.; Sarkar, M. Investigation of the Influence of Alkyl Side Chain Length on the Fluorescence Response of C153 in a Series of Room Temperature Ionic Liquids. *RSC Adv.* **2015**, *5*, 41585−41594.
(61) Fee, R. S.; Maroncelli, M. Estimating the time-zero spectrum in time-resolved emmsion measurements of solvation dynamics. *Chem. Phys.* **1994**, *183*, 235−247.
(62) Kimura, Y.; Kobayashi, A.; Demizu, M.; Terazima, M. Solvation Dynamics of Coumarin 153 in Mixtures of Carbon Dioxide and Room Temperature Ionic Liquids. *Chem. Phys. Lett.* **2011**, *513*, 53−58.
(63) Siano, D. B.; Metzler, D. E. Band Shapes of the Electronic Spectra of Complex Molecules. *J. Chem. Phys.* **1969**, *51*, 1856−1861.
(64) Bagchi, B.; Oxtoby, D. W.; Fleming, G. R. Theory of the Time Development of the Stokes Shift in Polar Media. *Chem. Phys.* **1984**, *86*, 257−267.
(65) Van der Zwan, G.; Hynes, J. T. Time-Dependent Fluorescence Solvent Shifts, Dielectric Friction, and Nonequilibrium Solvation In Polar Solvents. *J. Phys. Chem.* **1985**, *89*, 4181−4188.
(66) Verma, S. D.; Corcelli, S. A.; Berg, M. A. Rate and Amplitude Heterogeneity in the Solvation Response of an Ionic Liquid. *J. Phys. Chem. Lett.* **2016**, *7*, 504−508.
(67) Mukherjee, K.; Das, A.; Choudhury, S.; Barman, A.; Biswas, R. Dielectric Relaxations of (Acetamide + Electrolyte) Deep Eutectic Solvents in the Frequency Window, $0.2 \lesssim \nu/\mathrm{GHz} \lesssim 50$: Anion and Cation Dependence. *J. Phys. Chem. B* **2015**, *119*, 8063−8071.
(68) Bart, E.; Meltsin, A.; Huppert, D. Solvation Dynamics of Coumarin 153 in Molten Salts. *J. Phys. Chem.* **1994**, *98*, 3295−3299.
(69) Aue, D. H.; Webb, H. M.; Bowers, M. T. A Thermodynamic Analysis of Solvation Effects on the Basicities of Alkylamines. An Electrostatic Analysis of Substituent Effects. *J. Am. Chem. Soc.* **1976**, *98*, 318−329.

https://dx.doi.org/10.1021/acs.jpcb.0c00594
J. Phys. Chem. B 2020, 124, 2473−2481

Photophysical Behaviour of Some Molecular Systems and a Protein in Deep Eutectic Solvents

by Sk Saddam Hossain

Photophysical Behaviour of Some Molecular Systems and a Protein in Deep Eutectic Solvents

ORIGINALITY REPORT

21%	7%	20%	2%
SIMILARITY INDEX	INTERNET SOURCES	PUBLICATIONS	STUDENT PAPERS

PRIMARY SOURCES

1	Sk Saddam Hossain, Sneha Paul, Anunay Samanta. "Liquid Structure and Dynamics of Tetraalkylammonium Bromide-Based Deep Eutectic Solvents: Effect of Cation Chain Length", The Journal of Physical Chemistry B, 2019 Publication	11% Own publication
2	Sk Saddam Hossain, Anunay Samanta. "Solute Rotation and Translation Dynamics in an Ionic Deep Eutectic Solvent Based on Choline Chloride", The Journal of Physical Chemistry B, 2017 Publication	2% Own publication
3	pubs.rsc.org Internet Source	Own publication 2%
4	Sk Saddam Hossain, Sneha Paul, Anunay Samanta. "Complete Solvation Dynamics of Coumarin 153 in Tetraalkylammonium Bromide-Based Deep Eutectic Solvents", The Journal of Physical Chemistry B, 2020	1% Own publication

Dynamics in (Choline Chloride + Urea) Melts", The Journal of Physical Chemistry B, 2015
Publication

55 Manjari Chakraborty, Tasnim Ahmed, Ranu Satish Dhale, Debashis Majhi, Moloy Sarkar. "Understanding the Microscopic Behavior of Binary Mixtures of Ionic Liquids through Various Spectroscopic Techniques", The Journal of Physical Chemistry B, 2018 <1%
Publication

Exclude quotes	On	Exclude matches	< 14 words
Exclude bibliography	On		

Photophysical Behaviour of Some Molecular Systems and a Protein in Deep Eutectic Solvents

ORIGINALITY REPORT

49%	19%	47%	3%
SIMILARITY INDEX	INTERNET SOURCES	PUBLICATIONS	STUDENT PAPERS

PRIMARY SOURCES

1	Sk Saddam Hossain, Sneha Paul, Anunay Samanta. "Liquid Structure and Dynamics of Tetraalkylammonium Bromide-Based Deep Eutectic Solvents: Effect of Cation Chain Length", The Journal of Physical Chemistry B, 2019 Publication	11%
2	pubs.rsc.org Internet Source	10%
3	Sk Saddam Hossain, Sneha Paul, Anunay Samanta. "Complete Solvation Dynamics of Coumarin 153 in Tetraalkylammonium Bromide-Based Deep Eutectic Solvents", The Journal of Physical Chemistry B, 2020 Publication	10%
4	Sk Saddam Hossain, Anunay Samanta. "Solute Rotation and Translation Dynamics in an Ionic Deep Eutectic Solvent Based on Choline Chloride", The Journal of Physical Chemistry B, 2017	10%

Own publication.

Own publication.

Own publication.

Own publication.

Liquids", The Journal of Physical Chemistry B, 2013
Publication

57	Submitted to University of Georgia Student Paper	<1%
58	Anuradha Das, Ranjit Biswas. "Dynamic Solvent Control of a Reaction in Ionic Deep Eutectic Solvents: Time-Resolved Fluorescence Measurements of Reactive and Nonreactive Dynamics in (Choline Chloride + Urea) Melts", The Journal of Physical Chemistry B, 2015 Publication	<1%
59	Manjari Chakraborty, Tasnim Ahmed, Ranu Satish Dhale, Debashis Majhi, Moloy Sarkar. "Understanding the Microscopic Behavior of Binary Mixtures of Ionic Liquids through Various Spectroscopic Techniques", The Journal of Physical Chemistry B, 2018 Publication	<1%

Exclude quotes	Off	Exclude matches	< 14 words
Exclude bibliography	On		